University College London
Division of Medicine

Exercise-Induced 4-Hydroxynonenal Alters Myotube Cellular Redox Homeostasis and Mitochondrial Metabolism

A Thesis Submitted to **University College London**
For the Degree of **Doctor of Philosophy**

Afnan Saleh Al-Menhali

Principal Supervisor: **Prof. Andrey Abramov**
Subsidiary Supervisor: **Dr. Morana Jaganjac**

February 2019

To my beloved parents,

Every success in my life is because of you ♥

DECLARATION

I, Afnan Saleh Al-Menhali confirm that the work presented in this thesis, **Exercise-induced 4-hydroxynonenal alters myotube cellular redox homeostasis and mitochondrial metabolism**, is entirely my own under the supervision of Prof. Andrey Abramov and Dr. Morana Jaganjac. Where information has been derived from other sources, I confirm that this has been indicated in the thesis.

Signature:

Date:

ABSTRACT

Regular physical exercise is associated with numerous health benefits and physiological adaptations. Mild and reversible oxidative stress induced by skeletal muscle contractions during exercise can result in long-term systemic redox adaptations. However, strenuous exercise can alter redox homeostasis and induce oxidative damage to macromolecules triggering a chain reaction of lipid peroxidation. Lipid peroxidation, yields formation of reactive aldehydes among which is biologically active 4-hydroxynonenal (4-HNE). 4-HNE can easily diffuse through membranes and covalently binds to macromolecules, such as proteins, altering cellular functions. Still little is known about the possible pathophysiological role of exercise induced 4-HNE on mitochondrial performance. In this work the effect of a caffeine, frequently used as an effective ergogenic aid by athletes, on the myotube mitochondrial metabolism, signaling and cellular redox homeostasis was studied using mouse C2C12, rat L6 and human HSMM skeletal muscle cells. Furthermore, the role of 4-HNE on myotube redox homeostasis, mitochondrial energy metabolism, mitochondrial transcriptome and mitochondrial density was investigated. Finally, the effect of physical exercise on 4-HNE post-translational modifications of proteins was studied using skeletal muscle samples from exercised animals by genuine mass spectrometry method.

Obtained data indicate that short and long-term stimulation of myotubes with caffeine promotes reactive oxygen species formation and peroxidation of lipids leading to formation of 4-HNE protein adducts. 4-HNE further altered cellular redox homeostasis, mitochondrial metabolism and significantly increased mitochondrial density. Both caffeine and 4-HNE were found to regulate mitochondrial respiration and biogenesis gene expression. Finally, proteomics analysis of tissue samples from exercised mice revealed modifications of proteins susceptible to

oxidative stress. In conclusion, the findings signify the importance of skeletal muscle cells hormesis in response to acute stress and also suggest an important role of caffeine and 4-HNE on regulation of myotube's metabolism and cellular energy production.

IMPACT STATEMENT

When 4-hydroxynonenal (4-HNE) was first discovered it was identified as a cytotoxic product formed by microsomal lipid peroxidation. A decade later it became evident that it has an important role in pathogenesis and progression of numerous human diseases but also a crucial physiological role in the modulation of cell growth, differentiation, apoptosis, and cell signaling. This thesis shows, for the first time, the potential physiological and pathological effects of 4-HNE in mitochondrial energy metabolism, mitochondrial transcriptome and mitochondrial biogenesis. The obtained results, using state-of-the art technologies in cellomics, proteomics and genomics, highlight the significant physiological role of 4-HNE in mitochondrial functions.

Furthermore, this thesis provides a novel method developed for rapid and sensitive identification of 4-HNE-modified proteins. The significance of this method lies in its ability to identify the specific amino acid sites that are modified by 4-HNE. This can give a clear understanding of the exact role of 4-HNE in post-translational modification of proteins that can result in either physiological changes or pathological changes, which alter proteins function or structure and can impact cellular functions. Understanding the cellular changes at a molecular level helps to develop pharmacological solutions.

LIST OF PUBLICATIONS

Original publications arising from this thesis:

- **Al-Menhali A.S.**, Banu S., Angelova, P.R., Barcaru A., Horvatovich P., Abramov A. and Jaganjac M. Calcium and contracting dependent upregulation of mitochondrial metabolism in skeletal muscle is orchestrated by lipid peroxidation. (*Submitted*)
- **Al-Menhali A.S.,** Gourine A., Abramov A. and Jaganjac M. Detection of Exercise-induced 4-hydroxynonenal protein adducts by nanoLC-MS/MS (*in preparation*)
- **Al-Menhali A.S.,** Banu S., Jaganjac M. and Abramov A.Y. The effect of caffeine on myotube mitochondria metabolism (*in preparation*)
- **Al-Menhali A.S.,** Abramov A. and Jaganjac M. Implications of exercise-induced lipid peroxidation (*Review Paper, in preparation*)

Added value publications:

- Al-Thani A.M., Voss S.C., **Al-Menhali A.S.**, Barcaru A., Horvatovich P.L., Al Jaber H., Nikolovski Z., Latiff A., Georgakopoulos C., Merenkov Z., Segura J., Alsayrafi M. and Jaganjac M. (2018). Whole blood storage in CPDA1 blood bags alters erythrocyte membrane proteome. *Oxidative Medicine and Cellular Longevity*. 2018:6375379. doi: 10.1155/2018/6375379.
- Ludtmann M.H., Angelova P.R., Horrocks M.H., Choi M.L., Rodrigues M., Baev A.Y., Berezhnov A.V., Yao Z., Little D., Banushi B., **Al-Menhali A.S.**, Ranasinghe R.T., Whiten D.R., Yapom R., Dolt K.S., Devine M.J., Gissen P., Kunath T., Jaganjac M., Pavlov E.V., Klenerman D., Abramov A.Y. and Gandhi S. (2018). α-synuclein oligomers

interact with ATP synthase and open the permeability transition pore in Parkinson's disease. *Nature Communications*. 9(1):2293. doi: 10.1038/s41467-018-04422-2.

- **Al-Menhali A.,** Jameela S., Latiff A., El-Rayess M., Al-Sayrafi M. and Jaganjac M. (2017). *Cistanche tubulosa* induces reactive oxygen species-mediated apoptosis of primary and metastatic human colon cancer cells. *Journal of Applied Pharmaceutical Science.* 7(5):39-45
- Elrayess M., Al-Muraikhy S., Kafienah W., **Al-Menhali A.**, Al-Khalaifi F., Bashah M., Zarkovic K., Zarkovic N., Waeg G., Alsayrafi M. and Jaganjac M. (2017) 4-hydroxynonenal causes impairment of human subcutaneous adipogenesis and induction of adipocyte insulin resistance. *Free Radical Biology and Medicine*. 104:129-137. doi: 10.1016/j.freeradbiomed.2017.01.015.
- Voss S., Jaganjac M., Al-Thani A., Grivel J., Raynaud C., Al-Jaber H., **Al-Menhali A.**, Merenkov Z., Alsayrafi M., Latiff A., and Georgakopoulos C. (2017). Analysis of RBC-Microparticles in stored whole blood bags – a promising marker to detect blood doping in sports?. *Drug Testing and Analysis*. 9(11-12):1794-1798. DOI: 10.1002/dta.2212

CONFERENCE PROCEEDINGS

1. **Al-Menhali, A.S.**, Banu, S., Angelova, P.R., Barcaru, A., Horvatovich, P., Gourine, A., Abramov, A.Y. and Jaganjac, M. (2018). Physiological role of exercise-induced 4-hydroxynonenal in myotube mitochondrial function. Poster in the *ADLQ 6th Junior Symposium, December 11, Doha, Qatar.*
2. Jaganjac, M., **Al-Menhali, A.S.** and Abramov, A. (2018). The effect of caffeine on mitochondria metabolism and myotube redox homeostasis. Oral presentation in *ADLQ 8th Annual Symposium: Dietary Supplements: Strength, Weaknesses, Opportunities and Threats, May 1–2, Doha, Qatar.*
3. **Al-Menhali, A.S.**, Banu, S., Barcaru, A., Horvatovich, P., Abramov, A. and Jaganjac, M. (2018). Central role of exercise induced 4-hydroxynonenal in myotube mitochondrial metabolism. Poster in *The 16th Annual Society of Free Radical Research-India (SFRR-India) Meeting, February 18–20, New Delhi, India.*
4. **Al-Menhali, A.S.**, Abramov, A. and Jaganjac, M. (2017). Exercise Induced 4-hydroxynonenal Alters Myotube Cellular Redox Homeostasis and Mitochondrial Metabolism. Oral presentation in *5th Annual ADLQ Junior Symposium, December 19, Doha, Qatar.*
5. **Al-Menhali, A.S.**, Abramov, A. and Jaganjac, M. (2017). The impact of 4-Hydroxynonenal on C2C12 myotubes. Poster in *Gordon Research Conference: Oxidative Stress and Disease. March 19–24, Renaissance Tuscany Il Ciocco, Italy.*
6. **Al-Menhali, A.S.**, Banu, S., Barcaru, A., Horvatovich, P., Abramov, A. and Jaganjac, M. (2016). The Effect of Mild, Moderate and Extensive Stress on Mitochondrial

Performance. Oral presentation in *4th Annual ADLQ Junior Symposium, December 5, Doha, Qatar.*

7. **Al-Menhali, A.S.**, Jaganjac, M. and Abramov, A. (2016). 4-Hydroxynonenal alters myotube cellular redox homeostasis and affects mitochondrial performance. Poster in *7th Targeting Mitochondria World Congress, October 24–26, Berlin, Germany.*
8. Elrayess M., Al-Muraikhy S., **Al-Menhali A.**, Al-Khalaifi F., Bashah M. and Jaganjac M. (2016). The Role of 4-hydroxynonenal in Human Preadipocyte Proliferation and Differentiation. Poster in *Qatar Foundation Annual Research Conference Proceedings.* Vol. 1, HBOP1500. DOI: 10.5339/qfarc.2016.HBOP1500
9. **Al-Menhali, A.S.**, Abramov, A. and Jaganjac, M. (2015). Influence of 4-Hydroxynonenal on Mitochondrial Performance. Oral presentation in *3rd Annual ADLQ Junior Symposium, December 7, Doha, Qatar*
10. **Al-Menhali, A.S.**, Al-Thani, A.M., Abramov, A. and Jaganjac, M. (2015). Rapid and sensitive identification of protein site specific 4-HNE-modifications using nanoLC Hybrid Orbitrap mass spectrometer. Poster in *Keystone Symposia: The human Proteome, April 24–29, Stockholm, Sweden.*
11. **Al-Menhali A.S.**, Jameela S., Latiff A., Al-Sayrafi M. and Jaganjac M. (2014). Anticancer properties of Cistanche tubulosa extract on four colon cancer cell lines. Oral presentation *2nd Annual ADLQ Junior Symposium, October 27, Doha, Qatar.*
12. Jameela S.A., **Al-Menhali A.S.**, Mustafa K.M., Hashim Mahmoud F.E., Gawadi A.E., Mahmoud N., Harvey T.M., Latiff A.A., Jaganjac M. (2014). Phenolic content and antioxidant activity of selected local plants. Poster in *2nd Annual ADLQ Junior Symposium, October 27, Doha, Qatar.*

13. Jaganjac, M., **Al-Menhali, A.S.**, Jameela, S.A., Lobigs, L., Harvey, T.M., Nikolovski, Z., Voss, S.C., Schumacher, Y.O., Reverter, G., Segura, J., Latiff, A.A. (2014). Exercise-Mediated Redox Adaptations in Erythrocyte Membrane Proteome. Poster presentation in *Free Radical Biology and Medicine* 76:S105. DOI: 10.1016/j.freeradbiomed.2014.10.259
14. Jameela S.A., **Al-Menhali A.S.**, Banu S., Harvey T.M., Latiff A.A., Jaganjac M. (2014). Cucumis Sativus Prevents Oxidative Stress Induced Protein Modifications in Human Keratinocytes. Poster in *Free Radical Biology and Medicine* 76:S82. DOI:. 10.1016/j.freeradbiomed.2014.10.291
15. **Al-Menhali A.S.**, Jameela S.A., Alnoor A., Alzahra F., Muzamil K., Mahmoud N., Latiff A., AlSayrafi M. and Jaganjac M. (2014). Anticancer properties of cistanche tubulosa extract tested on four colon cancer cell lines. Poster in *Free Radical Biology and Medicine* 76:S120. DOI: 10.1016/j.freeradbiomed.2014.10.177
16. **Al-Menhali A**, Jameela S.A., Latiff A.A., Jaganjac M. (2014). Influence Of Qatar Agricultural Products On Human Cell Redox Homeostasis. Poster *Qatar Foundation Annual Research Conference Proceedings.* Vol. 1, HBPP0261. DOI: 10.5339/qfarc.2014.HBPP0261
17. Jameela S.A., **Al-Menhali A.S.**, Banu S., Harvey T.M., Latiff A.A., Jaganjac M. (2014). Qatar Cultivated Vegetables Enhance Resistance To Protein Modifications Induced By Altered Redox Homeostasis. Poster in *Qatar Foundation Annual Research Conference Proceedings.* Vol. 1, HBPP0412. DOI: 10.5339/qfarc.2014.HBPP0412
18. Jaganjac, M., **Al-Menhali, A.S.**, Jameela, S.A., Lobigs, L., Harvey, T.M., Nikolovski, Z., Voss, S.C., Schumacher, Y.O., Reverter, G., Segura, J., Latiff, A.A. (2014). Exercise

Induced Changes In Erythrocyte Membrane Proteome. Poster in *Qatar Foundation Annual Research Conference Proceedings.* Vol. 1, HBOP0311. DOI: 10.5339/qfarc.2014.HBOP0311

ACKNOWLEDGEMENT

I would like to express my gratitude to everyone who helped me to conduct this project by providing me with all needed support. I am deeply thankful to my supervisors: Prof. Andrey Abramov and Dr. Morana Jaganjac for directing, advising, and motivating me to present my effort in the best image.

Furthermore, I have to thank UCL Division of Medicine for providing me the opportunity to conduct such a project and the Institute of Neurology for allowing me to work in their laboratories during my visits to UCL. I wish to thank Prof. Alexander Gourine for kindly offering the tissues samples, Dr. Plamena R. Angelova for her help with NADH experiment, Dr. Noemi Gallego for her continuous help in lab and everyone who assist my work in UCL the labs.

Moreover, I would like to express my deepest appreciation to Anti-Doping Lab Qatar (ADLQ) for funding the project and for providing laboratories equipped with the most advanced technologies for a suitable research environment. I wish to thank Ms. Noor Al-Motawa for her support in administration and registration. I am also obliged to acknowledge Toxicology and Multipurpose lab's ADLQ staff for their continuous help, motivation and guidance in the laboratory; their inputs certainly contributed to my knowledge. I thank Ms. Sameem Banu for her help with PCR experiments, Amna Al-Thani for her help in proteomic and the soldiers behind the scene the facility and the IT departments for their continuous support.

I would like to give my special thanks to my mother, father, brothers and sisters, all my family and friends for all their help and their appreciation to my work; they guided me and supported me to achieve my goals and to do my best.

CONTENTS

LIST OF TABLES

LIST OF EQUATIONS

LIST OF FIGURES

LIST OF ABBREVIATIONS

$^{\bullet}O_2^-$	Superoxide
[Ca2+]c	Cytosolic calcium concentration
13-HPODE	13-hydroperoxyoctadecadienoic acid
15-HPETE	15- hydroperoxyeicosatetraenoic acids
4-HNE	4-hydroxynonenal
AA	Arachidonic acid
AGC	Automatic gain control
AICAR	5-Aminoimidazole-4-carboxamide ribonucleotide
AMP	Adenosine monophosphate
AMPK	adenosine monophosphate-activated protein kinase
ATP	Adenosine triphosphate
BSA	Bovine serum albumin
Ca^{2+}	Calcium ion
CaMK	Calmodulin-dependent protein kinase
cAMP	Cyclic adenosine monophosphate
$CH{=}CH_2$	Vinyl group
CH_2	Methylene group
CID	Collision-induced dissociation
Ct	Threshold cycle
CYP450	Cytochrome P450
DCFH-DA	Dichloro-dihydro-fluorescein diacetate

DDA	Data dependent acquisition
DHE	Dihydroethidium
DMEM	Dulbecco's Modified Eagle's Medium
DNA	Deoxyribonucleic acid
DTT	Dithiothreitol
DUOX	Dual oxidase
ECAR	Extracellular acidification rates
ERK1	Extracellular signal-regulated kinases 1
ERK2	Extracellular signal-regulated kinases 2
ETC	Electron transport chain
ETD	Electron transfer dissociation
FBS	Fetal bovine serum
FCCP	Carbonylcyanide-p-trifluoromethoxyphenyl hydrazone
Fura 2AM	Fura-2-acetoxymethyl
GPX	Glutathione peroxidase
GSH	Glutathione
H_2O_2	Hydrogen peroxide
HBSS	Hank's buffered salt solution
HCD	Higher energy collision-induced dissociation
$HO^{\bullet}_2$	Hydroperoxyl
HPLC	High performance liquid chromatography
HS	Horse serum
IκB	Inhibitor-kappa B

L•	Lipid radical
LA	linoleic acid
LC-MS	Liquid chromatography-mass spectrometry
LH	Polyunsaturated lipid
LOO•	Lipid peroxy radical
LOOH	Lipid hydroperoxide
LOX	Lipoxygenases
MAPK	Mitogen-activated protein kinases
MHC	Myosin heavy chain
MIPS	Monoisotopic precursor selection
MnSOD	Manganese superoxide dismutase or mitochondria-specific superoxide dismutase
mtDNA	Mitochondrial DNA
MTT	3-(4,5-dimethylthiazol-2-yl)-2,5-diphenyltetrazolium bromide
mtTFA	Mitochondrial transcription factor A
NADPH	Nicotinamide adenine dinucleotide phosphate
NCD	Non-communicable diseases
NF-κB	Nuclear factor-kappa B
NIS	Nanoelectrospray ionization
NOX	NADPH oxidase
NRF-1	Nuclear respiratory factor 1
NRF-2	Nuclear respiratory factor 2
Nrf2	Nuclear factor E2 related factor 2

NSI	Nanoelectrospray ionization
NUGEMP	Nuclear genes encoding mitochondrial proteins
OCR	Oxygen consumption rates
PBS	Phosphate-buffered saline
PCR	Polymerase chain reaction
PGC-1α	PPAR- gamma coactivator-1α
PKC	Protein Kinase C
PLA2	Phospholipase A2
PPAR	Peroxisome proliferator-activated receptor
PPARδ	Peroxisome proliferator-activated receptor delta
PUFAs	Polyunsaturated fatty acids
RCC	Reactive carbonyl compounds
RIPA	Radioimmunoprecipitation assay
ROS	Reactive oxygen species
RT	Real-Time
RyR	Ryanodine receptor
SD	Standard deviation
SDS-PAGE	Sodium dodecyl sulfate polyacrylamide gel electrophoresis
SERCA	Sarcoplasmic/endoplasmic reticulum calcium ATPase
SkGM-2	Skeletal Muscle Growth Media-2
SOD	Superoxide dismutase
SR	Sarcoplasmic reticulum
TFAM	Mitochondrial transcription factor A

XF24	Extracellular Flux 24
XO	Xanthine oxidase

1. INTRODUCTION

1.1. Physical inactivity a leading cause of death

Physical inactivity is associated with an increased prevalence of non-communicable diseases (NCDs) such as cardiovascular diseases, hypertension, type 2 diabetes, musculoskeletal disorders and some cancers like colorectal and breast cancer (Knight, 2012). All those diseases are estimated to contribute to more than 71% of global deaths (WHO, 2018). Furthermore, the natural aging process leads to sarcopenia, which is loss of muscle mass. It is estimated that by the age of 80 years an average of 40% of muscle mass will be lost (Saini, *et al.*, 2009). Increasing scientific evidences support the need of improved life quality to combat NCDs.

1.2. Exercise to combat the increasing prevalence of non-communicable diseases

Since the early 1950s, Morris and colleagues showed the association between physical activity and reduced deaths by coronary heart disease, which led to increased scientific interest in the potential of physical activity to combat diseases (Morris, *et. al.*, 1953). Current scientific knowledge shows a clear link between active lifestyle and overall health. Increasing scientific evidence shows that physical exercise can enhance the cardiovascular system (Villella and Villella, 2014), manage diabetes (Lumb, 2014), manage neurodegenerative disorders (Svensson, et al., 2015), regulate the immune system (Simpson, et al., 2015), and induce many adaptational responses such as controlling apoptosis and autophagy (Mooren and Krüger, 2015).

1.3. Exercise mimetic, stimulants and ergogenic substances

Even though physical exercise is proven to be a very effective method to combat non-communicable diseases, current sedentary lifestyle has been an obstacle. As a result, a new interest has emerged, which attempts to adapt to the current lifestyle, to defeat the global epidemic of obesity by exploiting the benefits of physical exercise through using stimulants and ergogenic substances. Exercise mimetics initiate the biochemical cascade of a contracting muscle or induce genes involved in muscles remodeling. For example, 5-Aminoimidazole-4-carboxamide ribonucleotide (AICAR) is one of the early and widely known exercise mimetics that directly activates adenosine monophosphate-activated protein kinase (AMPK), which initiates the process of mitochondrial biogenesis (Merrill, *et. al.*, 1997). Another commonly used exercise mimetic is GW501516, which is a synthetic peroxisome proliferator-activated receptor delta (PPARδ) ligand that can induce fatty acid oxidation and muscle fatigue resistance. The use of those two drugs as exercise mimetics was first investigated by Prof. Ronald Evans and his team in 2008, when AICAR and GW501516 were tested on the endurance capacities of sedentary mice. Both drugs enhanced muscle metabolism through mitochondrial biogenesis, glucose and fatty acid oxidation and also promoted muscle remodeling to more oxidative fiber type (Narkar, *et. al.*, 2008). In fact, a study in mice compared the effect of running and the use of AICAR over a period of time and both showed similar response in skeletal muscle, i.e. AMPK activation and an increase in muscle metabolism over time. The same study showed that long-term AICAR treatment had inverted effects compared to exercise on brain tissues, where it increased the expression of proapoptotic genes, as well as, inflammatory cytokines level compared to reduced levels by exercise (Guerrieri and van Praag, 2015). Both AICAR and GW501516 drugs are prohibited by the World Anti-Doping Agency (WADA), due to their proven ability to enhance

athlete performance (WADA prohibited list 2018). Prohibited substances are those with proven ability to stimulating the central nervous system (CNS), alertness, reduce fatigue, locomotion and affecting cardiovascular actions. There is a detailed list of substances and methods prohibited by the WADA (WADA prohibited list 2018). The WADA prohibited list is updated annually, in order to include new substances produced and discovered to mimic physical exercise through different mechanisms. Some substances are added to WADA monitoring list, with the possibility to detect patterns of misuse in sport. Caffeine is another compound that was on WADA prohibited list from 1984 to 2004. But lately it was shifted to the monitoring program (del Coso, *et. al.*, 2011).

1.3.1. Caffeine

Caffeine is commonly present in consumed food and due to its intensive use in everyday life (Table 1) different scientific studies are conducted to unravel all possible effects of caffeine in human body. Of a particular interest is the use of caffeine as an exercise mimetic. Early findings proved that caffeine can increase time to physical exhaustion, increase intuition and alertness, improve muscle contractibility, reduce tiredness, improve mood and accelerate reaction time (Sokmen, *et. al.*, 2008). These characteristics of caffeine have made it an increasingly popular ergogenic supplement. But the exact mechanisms on how caffeine improves the athletic performance still needs to be elucidated.

Table 1: Concentration of caffeine in some of the common beverages. (Heckman, *et. al.*, 2010)

Caffeine Source		Caffeine (mg)/ 8 oz
Coffee	Decaffeinated	3 to 12
	Instant	27 to 173
	Plain, brewed	102 to 200
	Espresso	240 to 720
Tea	Tea, brewed	40 to 120
	Green	30 to 50
	Black	25 to 110

1.3.1.1. Caffeine chemical structure and metabolism

Caffeine (1,3,7-trimethylpurine-2,6-dion, Figure 1) is an alkaloid found naturally in coffee beans, cocoa beans, tea leaves and kola nuts. Caffeine is the most consumed pharmacologic substance. The major route to caffeine exposure is through direct or indirect ingestion of caffeine containing food, although other routes such as dermal and inhalation routes are also possible (Herman and Herman, 2013; Galvalisi, *et. al.*, 2017). A daily caffeine intake of ≤ 400 mg for a healthy adult is considered to be safe and is not associated with adverse health effects (Mejia and Ramirez-Mares, 2014). After oral administration of caffeine, 90% is absorbed by the stomach and small intestine. Then, it gets transferred to blood, where it can reach a peak concentration in plasma within 20 to 40 minutes after ingestion. A human exposure study demonstrated that out of 130 mg of ingested caffeine a peak concentration of 3.6 mg/L in plasma was reached in less than 40 minutes (O'Connell and Zurzola, 1984). The half-life of caffeine in the plasma is estimated to be, on average, 4 hours (Kerrigan and Lindsey, 2005). In the liver, caffeine is metabolized mainly by the enzymatic reaction of cytochrome P450 (CYP450) within 3 to 5 hours after ingestion (Martinez-Lopez, *et. al.*, 2014). Its major metabolites are:

paraxanthine (80 %) metabolized by CYP1A2, theobromine (12 %) and theophylline (7 %) both metabolized mainly by CYP1A2 and partially by CYP2E1. Since the majority of caffeine is metabolized in the body; only around 2% is excreted unchanged in urine (Atia, *et. al.*, 2009; Nehlig, 2018). Finally, in a healthy individual caffeine half-life is on average of 4 to 5 hours, and around 85% of caffeine dose is metabolized and excreted within 48 hours in urine (Kerrigan and Lindsey, 2005; Begas, *et. al.*, 2007).

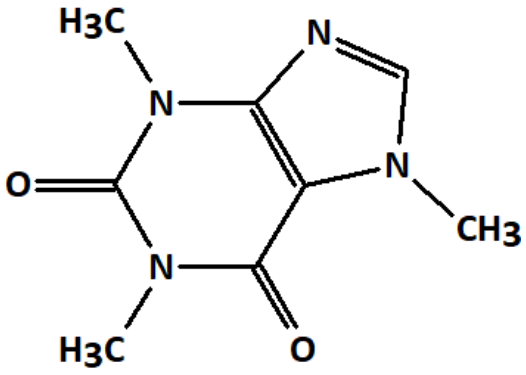

Figure 1: Caffeine chemical structure

1.3.1.2. Caffeine mechanisms of action and athletic performance

Caffeine's main mechanisms of actions include: adenosine receptors antagonism, phosphodiesterases inhibition and calcium signaling (Herrmann-Frank, *et. al.*, 1999). Caffeine can cross the blood-brain barrier and bind to adenosine receptors in brain due to having similar chemical structure to the adenosine, acting as an adenosine-receptor antagonist. Adenosine is a central nervous system neuromodulator that normally binds to its receptor and leads to several effects leading eventually to a reduction in neural activity, that are shown by the feeling of exhaustion and tiredness. However, when caffeine binds to the adenosine receptor it blocks those reactions and stimulates the production of adrenaline as well. As a result, the central nervous system keeps alerted with enhanced performance, along with an extra burst of energy and

increased attention (Meeusen and Decroix, 2018). In addition to the adenosine receptor antagonism mechanism of caffeine, it is also well established that high doses of caffeine inhibit phosphodiesterases activity. Phosphodiesterases are group of enzymes that degrade the phosphodiester bond in second messengers, such as cyclic adenosine monophosphate (cAMP). Thus, inhibition of phosphodiesterase activity enhances or prolong the activities mediated by cAMP. cAMP regulate several biological processes such as: activation of protein kinase A and stimulation of lipolysis (Cappelletti, *et. al.*, 2015). Many experiments focus on the ability of caffeine to act as a stimulant of the central nervous system (Tarnopolsky, 2008). The ergogenic effect of caffeine is proved to enhance both short-duration and long-duration exercise including several types of physical exercises, such as: running (3 mg·kg-1), cycling (3 mg·kg-1), sprint swimming (3 mg·kg-1) and rowing (2, 4, or 6 mg·kg-1) (Bridge and Jones, 2006; Lane, *et. al.*, 2014; Lara, *et. al*., 2010; Skinner, *et. al*., 2010). This is due to the ability of caffeine to target physiological responses that leads to an enhanced physical performance. For example; an improved physical performance in athletes after caffeine ingestion is found to be associated with increased work intensity, oxygen consumption, heart rate, adrenaline level and blood lactate accumulation. However, this improved performance was also associated with higher muscular pain (Stadheim, *et. al.,* 2013). Caffeine also results in increased post-exercise muscle glycogen accumulation, which can help with faster recovery after intensive exercise, as well as increased fatty acid oxidation, by stimulating hormone sensitive lipase activity and inhibiting glycogen phosphorylase activity increasing lipid substrate metabolism instead of glycogen (Cappelletti, *et. al.*, 2015). All those evidences of the significant improvements of caffeine on physical performance, along with it being legal drug, and most importantly with minimum side effects, have made it a popular chemical for scientific experiments. The interindividual differences in

caffeine metabolism, exercise intensity, diet and other limitations are inevitable when conducting such a study. Thus, *in-vitro* experiments involving studying the direct effect of caffeine in an isolated skeletal muscles can give more a controlled environment. An early study by Weber and Herz, demonstrated the direct effect of caffeine on calcium release, which is the main muscle contraction regulator, of a sarcoplasmic reticulum isolated from skeletal muscles of rabbit and frogs using 1 mM to 10 mM of caffeine concentration (1968).

1.3.1.3. Mechanism of caffeine-induced contraction in skeletal muscle

Excitation-contraction coupling of skeletal muscles is regulated by the release of calcium ions (Ca^{2+}) from the sarcoplasmic reticulum (SR) to the cytosol through the ryanodine receptor (RyR) channel, mainly by RyR1 which is the dominant Ca^{2+} releasing channel in mammalian skeletal muscles. Contraction is initiated when Ca^{2+} binds to troponin C in the actin. Binding of Ca^{2+} removes the acto-myosin ATPase inhibition that exposes the active site of troponin, in actin, for the binding of myosin. Binding of actin to myosin cause contraction of muscle (Gailly, 2002). Then, the released Ca^{2+} is removed back to SR by ATP-dependent process through sarcoplasmic/endoplasmic reticulum calcium ATPase (SERCA) pump (Gehlert, *et al.*, 2015). Caffeine is found to induce the release of Ca^{2+} from RyR. This is achieved by increasing the number and duration of open calcium channels by caffeine (Rousseau, *et. al.*, 1988). That eventually triggers contraction of muscle. Therefore, measuring calcium oscillations in skeletal muscle cells to study the release of calcium from SR is considered an accepted method used in scientific experiments as indirect measure of muscle contractions. Even though the maximum intake limit of caffeine that does not have adverse health effects for human is estimated to be approximately 1 mM (400 mg), it is estimated that concentrations between 1 mM to 10 mM are

needed for *in-vitro* experiments to trigger muscle contraction (Mejia and Ramirez-Mares, 2014; Weber and Herz, 1968)

1.4. Skeletal muscle in physical fitness

Skeletal muscle cells, being one of the main energy generators in the body, are involved in many crucial physiological adaptations. The ability of physical exercise to combat metabolic diseases is associated with the fact that skeletal muscle is a secretory organ. It releases myokines that interact with adipose tissue, liver, pancreas, bones and brain (Pedersen and Febbraio, 2008). The exquisite structure of the skeletal muscles enables them to perform their specific functions and activities. The different types of skeletal muscle fibers, which are classified based on their metabolic and contractile activity and myosin heavy chain (MHC) structure, include: MHC type I fibers, which contract with slow velocity but are characterized of being harder to fatigue. MHC type II, which contract with high velocity and characterized of being easier to fatigue. Fibers types can be further classified based on metabolic activity: oxidative slow-twitch fibers (Type I), mixed oxidative and glycolytic fast-twitch fibers (Type IIa) and glycolytic fast-twitch myofibers (Type IIb) with different metabolic and mechanical characteristics (Fan and Evans, 2016). All the different fibers types are found in all skeletal muscles in the body but with different distribution, depending on genetic composition as well as environmental factors. In humans, it is difficult to change between MHC fiber types, but it is common for metabolic activity to change in each fiber type (Pattanakuhar, *et. al.*, 2017).

1.4.1. Plasticity of skeletal muscle

Skeletal muscles are characterized by the high adaptation ability to some events and stimuli such as: aging, degenerative disorders, starvation and physical exercise due to their high

plasticity. It is well recognized that physical activity is substantial for the preconditioning of skeletal muscle that can prepare the muscles to upcoming challenges (Mounier, *et. al.*, 2015). This plasticity is derived by changing muscle metabolism, phenotype, size, and/or protein contents and activities (Remels *et al.*, 2010). The type and duration of exercise, even single bout of exercise, can result in some adaptational changes that involve the regulation of gene expression in skeletal muscle (Booth and Thomason, 1991). The major stressors during physical exercise that are known to induce functional and structural adaptations in skeletal muscle are: mechanical load, metabolic disturbances, neuronal activation and hormonal adjustments. It was found that the type of exercise can define the kind of stressors the skeletal muscle experience. For example, muscle experiences mainly mechanical stress with strength exercise. While with endurance exercise it experiences mainly metabolic stress. The neuronal activation and hormonal adjustments accompany all different types of exercise (Hoppeler, 2016). In particular, the mitochondrial role in the plasticity of skeletal muscle is becoming the focus of many current studies. Mitochondria have the flexibility to adapt to numerous different stimuli, and upon response to contractile activity associated with exercising.

1.4.2. Energy metabolism in skeletal muscle

Energy metabolism is basically the balance between energy production and energy expenditure. The main energy production pathways are glycolysis and oxidative phosphorylation. Glucose levels in plasma are maintained at a specific range that is regulated by different signaling activity, such as insulin or contraction. Glucose transporters (GLUT1, GLUT4) play the key role in mediating glucose uptake. During basal condition (fasting), glucose is transported to cells mainly by GLUT1 (Ciaraldi, *et. al.*, 2005), while the major glucose transport in skeletal muscle is GLUT4. During muscle contraction, Ca^{2+} released from SR

triggers signaling mechanisms that leads to increased glucose uptake by muscle cells through regulating intracellular vesicles containing GLUT4 to skeletal muscle cells surface. This results in increased glucose uptake by transporting glucose into the cells through plasma membrane, which goes into glycolysis process, shown in Figure 2 (Jensen, *et. al.*, 2014). Basically, the glycolysis process catalyzes glucose into two pyruvates, with a net yield of two ATP and electron donor nicotinamide adenine dinucleotide (NADH). Pyruvate can be further oxidized to yield the acetyl group of acetyl-coenzyme A, acetyl-coenzyme A is then oxidized completely by citric acid cycle yielding CO_2 and two electron carriers NADH and flavin adenine dinucleotide ($FADH_2$). Alternatively, glucose can be catalyzed to glucose-6-phosphate that is converted to glycogen for storage (Jensen and Richter, 2012). Skeletal muscle catalyzes glucose to produce energy based on demand level, once energy exceeds the demand excess glucose is converted to lipid by lipogenesis. Electron carriers transfer electron in oxidative phosphorylation pathway. NADH transfers electrons to complex I, while $FADH_2$ transfers electrons to complex II in the electron transport chain (ETC) where electrons goes into series of reactions through mitochondrial complexes, located in inner mitochondrial membrane. The movement of electrons through complexes pumps H^+ into mitochondrial intermembrane space, which creates an electrochemical gradient that pumps H^+ back to mitochondrial matrix through ATP synthase and generates ATP. The oxidative phosphorylation produces the majority of ATP in cells (du Plessis, *et. al.*, 2014).

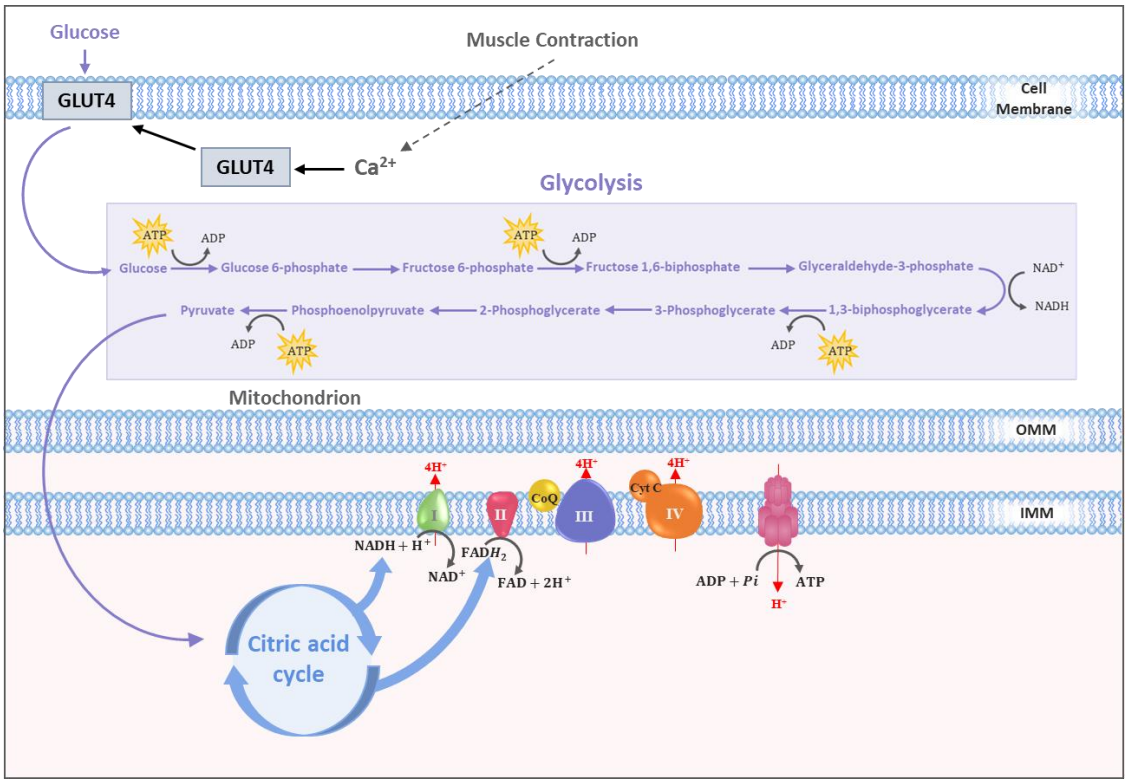

Figure 2 : Energy metabolism in skeltal muscle through glycolysis and oxidative phosphorylation pathway. Muscle contraction trigger the transport of glucose into the cell through GLUT4. Glocuse is catalyzed by glycolysis to generate 2 ATP, 2 pyruvate and NADH. Pyruvate is further oxidized in citric acid cylce generating NADH and $FADH_2$ that transfer electrons to ETC to generate more energy though oxidative phosphorylation pathway.

1.4.3. Mitochondrion – a key component of skeletal muscle

Mitochondria, the powerhouse of the cell, are the main source of energy production in the body, providing energy needed for the majority of cellular activities. Mitochondria have a substantial role that can influence cell survival or death. On the one hand, mitochondria are essential for energy production, cellular signaling, cell growth and apoptosis (Shadel and Horvath, 2015). On the other hand, mitochondrial dysfunction due to for example mutations of mitochondrial DNA (mtDNA) or nuclear DNA genes, dysfunction in bioenergetic, mutation of

proteins associated with mitochondria, or alteration in mitochondrial dynamics all are implicated in several diseases such as: Parkinson's disease (Bose and Beal, 2016), type 2 diabetes (Rovira-Llopis, *et. al.*, 2017), cardiovascular diseases (Hoppel, *et. al.*, 2017), insulin resistance (Wang and Wei, 2017) and others. The structure of mitochondria includes: outer membrane (OMM), the intermembrane space (IMS), the inner membrane (IMM) and the matrix. The IMM is highly folded to increase surface area, holding the complexes that makeup the electron transport chain where oxidative phosphorylation takes place. ETC complexes are: complex I (NADH dehydrogenase), complex II (succinate dehydrogenase), complex III (cytochrome bc1 complex), complex IV (cytochrome c oxidase) and complex V (ATP synthase). In the matrix is the mtDNA, which is circular double-stranded DNA. The mtDNA has approximately 16.5 kilobases coding for 37 genes. Those genes encode for ETC subunits, ribosomal RNA, transfer RNA and mitochondrial proteins synthesis (Theilen, *et. al.*, 2017). Maintaining physiological activities of mitochondria is essential for healthy cellular processes and energy production. Some factors affecting mitochondria function include aging and diseases. The natural aging process is associated with mitochondrial degradation, however, this can be retained with physical exercise (Carter, 2015).

1.4.4. Contractile activity-induced mitochondrial biogenesis

In early studies, endurance exercise in tested subjects over six weeks was found to increase the total mitochondrial volume density by 40% and the maximal oxygen uptake capacity by 14% (Hoppeler *et al.*, 1985). This is due to the influence of contractile activity on many signaling pathways that lead to mitochondrial biogenesis, shown in Figure 3. When cytosolic Ca^{2+} increase it triggers myofibril contraction that activates many signals including but not limited to: production of reactive oxygen species (ROS), increases in adenosine triphosphate

(ATP) turnover, activation of p38 mitogen-activated protein kinases (p38 MAPK) and AMPK. Increasing cytosolic Ca^{2+} activates calcium calmodulin-dependent protein kinase II (CaMKII). All those signaling cascades promote the transcription of PPAR gamma coactivator-1α (PGC-1α). PGC-1α is of a great interest in the process of mitochondrial biogenesis, because it can promote the transcription of specific genes that drive mitochondrial biogenesis (Ljubicic *et al.*, 2010). Thus, activation of PGC-1α in skeletal muscles is used to mimic endurance exercise, such as inducing calcium oscillations through caffeine treatment (Craig *et al.*, 2015). When PGC-1α is transcribed, it can auto-regulate its own transcription and regulate nuclear genes encoding mitochondrial proteins (NGEMP). Especially it promotes the transcription of nuclear respiratory factor 1 (NRF-1) and 2 (NRF-2). These two factors, specifically NRF-1 can stimulate the genes to transcribe respiratory chain proteins and mtDNA transcription factors such as mitochondrial transcription factor A (TFAM), which is a key activator of mtDNA replication (Viña *et al.*, 2009). Proteins produced from both nuclear DNA and mtDNA are then assembled to form the ETC. Skeletal muscle adaptation can be developed by the accumulation of those signaling cascades, which increase the amount of cellular proteins that are involved in mitochondrial biogenesis and ATP production. Interestingly, regular exercise was found to accumulate and elevate the protein levels of PGC-1α, NRF-1 and TFAM, which creates an adaptive response to exercise (Irrcher, *et al*., 2003).

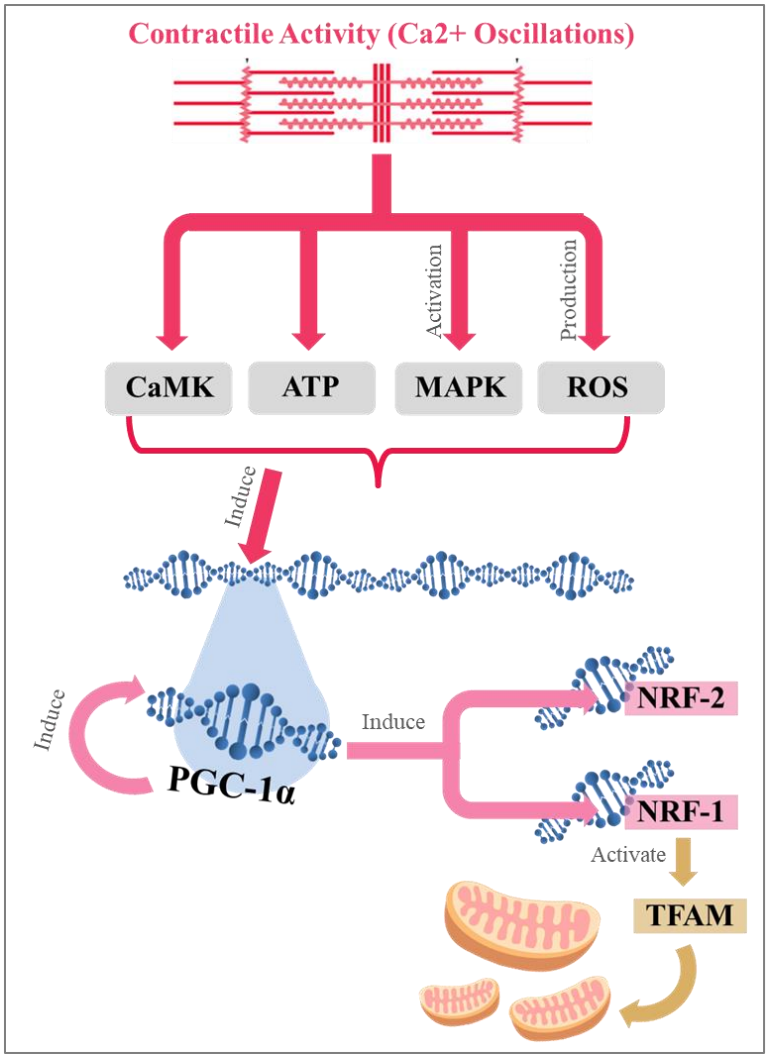

Figure 3: Contractile activity-induced mitochondrial biogenesis. Calcium oscillations trigger muscle contraction that increases adenosine triphosphate (ATP) turnover, activates calcium calmodulin-dependent protein kinase II (CaMKII), p38 mitogen-activated protein kinases (p38 MAPK), and reactive oxygen species (ROS) production. Those signaling cascades promote the transcription of PPAR gamma coactivator-1α (PGC-1α). PGC-1α auto-regulates its own transcription and regulates nuclear genes encoding mitochondrial proteins through activation of nuclear respiratory factor 1 and 2 (NRF-1 and NRF-2). NRF-1 also stimulates mitochondrial transcription factor A (TFAM) that is involved in mtDNA replication. All those signals, among others, lead to mitochondrial biogenesis.

1.5. Exercise-induced ROS

It is well established that regular moderate exercise is beneficial for skeletal muscle and overall health whereas aggressive exercise tends to result in skeletal muscle damage or fatigue (Di Meo and Venditti, 2001). ROS are continuously formed in skeletal muscle but their generation increases with physical activity.

1.5.1. Sources of ROS during exercise

Exercise triggers the production of ROS in many different tissues. The major source of ROS during exercise is not yet defined, due to limitations of experimental methods to measure exact source of ROS in *in-vivo* models. Some of the sources of exercise-induced ROS include: blood (Turner, *et al.*, 2011), lungs, brain, skeletal muscle and heart (Powers and Jackson, 2008). The role of skeletal muscle in the generation of ROS is gaining much interest in many scientific experiments. In the early 1980s, the relationship between exercise and generation of free radicals in skeletal muscle was first discovered (Davies, *et al.*, 1982). Skeletal muscle generates ROS during contraction and even at rest (Powers and Jackson, 2008), as ROS are involved in many signaling pathways. Previously, due to the intensive research on mitochondrial ROS, it was thought that mitochondria are the main source of ROS generated during exercise, but recent evidence proved that other non-mitochondrial sources are important intracellular ROS sources during exercise. It is suggested that Nicotinamide adenine dinucleotide phosphate (NADPH) oxidases could be the major source of ROS during exercise (Michaelson, *et al.*, 2010). The main cellular sources of exercise-induced ROS are described below:

- Mitochondrial respiratory chain (Electron transport chain, ETC)

Cellular respiration was previously classified as the major contributor of ROS generation during exercise. Current scientific evidences disprove this hypothesis as it was found that majority of ROS produced during exercise were generated by non-mitochondrial sources. Although, ETC contains many different sites for superoxide ($^{\bullet}O_2^-$) and hydrogen peroxide (H_2O_2) production, there is a lack of scientific knowledge to reveal the major *in-vivo* site of $^{\bullet}O_2^-$ and H_2O_2 generation. However, many *in-vitro* studies showed that the overall rate could vary with different substrates used (Goncalves, *et al.*, 2015). To date, a total of 11 sites for the production of $^{\bullet}O_2^-$ and H_2O_2 are known in mammalian mitochondria. Those sites are linked to electron transport and substrate catabolism (Brand, 2016). Measuring both $^{\bullet}O_2^-$ and H_2O_2 is a popular method to assess ROS production. Even though $^{\bullet}O_2^-$ is found to be the main reactive species produced in mitochondria, due to its chemical structure with negative charge, the $^{\bullet}O_2^-$ is unable to permeate easily through mitochondrial membrane, thus, cannot travel long distances. However, $^{\bullet}O_2^-$ is immediately converted in mitochondria by manganese-dependent superoxide dismutase (MnSOD) into H_2O_2, which can eventually form a more aggressive radical which is the hydroxyl radical (Starkov, 2010). Mitochondria can generate H_2O_2 both at rest and exercise. The major sites for H_2O_2 production during rest were found to be complex I (NADH dehydrogenase) and complex II (succinate dehydrogenase). While during mild and intense aerobic exercise complex I and complex III (cytochrome c oxidoreductase) generate the majority of H_2O_2. Interestingly, it was found that the H_2O_2 generated during exercise is lower than that at rest (Goncalves, *et al.*, 2015). Increasing physical activity demands more ATP hydrolysis to generate energy, resulting in increased concentrations of ADP. An early study on isolated mitochondria from rat liver showed that increasing ADP concentration results in lower H_2O_2

generation, which initiated the notion that mitochondria generate free radicals at rest (Boveris, *et. al.*, 1972). However, a more recent study also on mitochondria isolated from liver, shows increase in H_2O_2 with ADP in the presence of rotenone/succinate (Nègre-Salvayre, *et. al.*, 1999).

- NADPH oxidases

NADPH oxidase (NOX) is an enzyme complex that is bound to the cellular membranes, such as: cell membrane, nucleus, mitochondria, endoplasmic reticulum, endosomes and phagosomes. Basically, NOX transfers electrons from inside the cell to the extracellular space, where it couples with molecular oxygen to form the free radical $^{\bullet}O_2^-$. The produced $^{\bullet}O_2^-$radical anion is a precursor of many other ROS species (Filip-Ciubotaru, *et al.*, 2016). ROS generated by NOX induce the signal that activates calcium release through RyR (Cherednichenko, *et. al.*, 2004). The contribution of mitochondria to the overall ROS generated during exercise is well established, while NOX's role is yet to be explored. As previously mentioned, recent studies indicate that NOX is possibly the major source of ROS in skeletal muscle during exercise. In fact, it was suggested that NOX2 is the predominant contributor of $^{\bullet}O_2^-$ production among the NOX family in skeletal muscle cells (Sakellariou, *et al.*, 2013). The mechanism of NOX2 activation was found to be through extracellular ATP produced during muscle contraction. It was found to induce the activation of protein kinase C-NOX2 (PKC-NOX2), which mediates ROS production in cells (Díaz-Vegas, *et al.*, 2015). Other NOXs with different isoforms are: NOX1, NOX3, NOX4 and NOX5. In addition to two dual oxidase enzymes: Dual oxidase (DUOX) 1 and DUOX2. The distribution in tissues and the activation mechanisms differ for each member of the NOX family (Sakellariou, *et. al.*, 2014). Based on mRNA sequencing skeletal muscle contains NOX4 and a small amount of NOX2 (Bedard and Krause, 2007). NOX4 is involved in the enhanced contractility mechanism, where O_2-coupled H_2O_2 produced by NOX4 leads to

oxidation of RyR1 thiols, which activates RyR1 channel to release Ca^{2+}, and hence, enhances the contractility of skeletal muscles (Sun, *et. al.*, 2011).

- Xanthine oxidase

Xanthine oxidase (XO) is an intracellular enzyme that catalyzes hypoxanthine to xanthine and then to uric acid and H_2O_2, shown in Equation 1: Xanthine oxidase catalytic reaction, along many purines metabolism reactions. This enzyme is an important source of ROS (Kostic, *et al.*, 2015). XO-induced ROS are suggested to be important in adaptation mechanisms during exercise. ROS produced by XO were found to activate MAPKs: p38 MAPK, extracellular signal regulated kinase 1 and 2 (ERK 1 and ERK 2). Those MAPKs then activate nuclear factor-kappa B (NF-κB), which upregulates the transcription of superoxide dismutase (SOD), a major antioxidant enzyme. All those pathways were attenuated when XO was inhibited (Gomez-Cabrera, *et al.*, 2005). Another study showed that inhibiting XO activity can decrease physical performance. The exact mechanism is not fully understood, however, it is suggested to be due to reactive species produced during physiological activity, which are important to maintain the function of muscle (Veskoukis, *et al.*, 2008). Although XO was found to be important in signaling pathways, it was also found to be associated with increased lipid peroxidation level during exercise (Judge and Dodd, 2004). This is most likely due to the location of XO in the sarcolemma which is composed mainly of lipids (Ibrahim and Stoward, 1978).

Equation 1: Xanthine oxidase catalytic reaction

$$Hypoxanthine + O_2 + H_2O \rightarrow Xanthine + H_2O_2$$

$$Xanthine + O_2 + H_2O \rightarrow Uric\ acid + H_2O_2$$

- Phospholipase A2

Phospholipase A2 (PLA2) is a membrane lipolytic enzyme that catalyzes the hydrolysis of the phospholipids at the second position resulting in the release of fatty acids and lysophospholipids as products (Shridas and Webb, 2014). Early findings demonstrated the increase in PLA2 activity with contracting muscle (Federspil, *et al.*, 1987). H_2O_2 was found to trigger the activity of PLA2 along with a presence of increased lipid peroxidation. Thus, it was suggested that changes in membrane composition due to lipid peroxidation might trigger the activation of PLA2 to produce the fatty acid arachidonic acid (AA) (Balboa and Balsinde, 2002). AA can then further induce the generation of ROS through the stimulation of mitochondrial ETC (Nethery, *et al.*, 2000) and NOX (Zhao, *et al.*, 2002).

- Other enzymatic sources of ROS

Other sources of ROS produced by mitochondria can be formed by enzymatic activity. These enzymes include: cytochrome b5 reductase, monoamine oxidase, glycerol-3-phosphate dehydrogenase, pyruvate dehydrogenase, α-ketoglutarate dehydrogenase and aconitase (Angelova and Abramov, 2016).

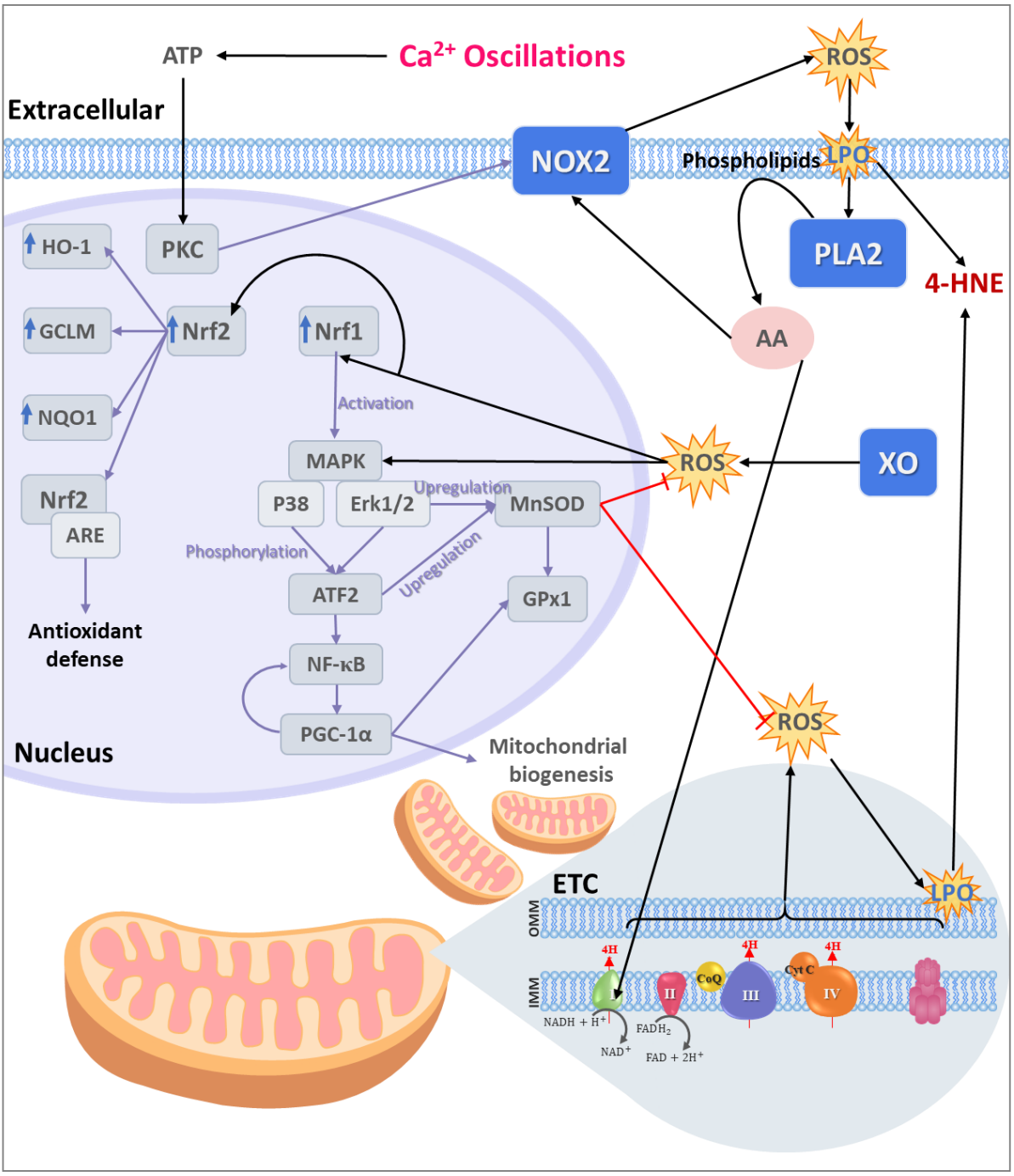

Figure 4: Major sources of ROS in skeletal muscle during contraction. Muscle contraction induces the production of ROS from different sources including: Electron transport chain (ETC), NADPH oxidase (NOX), xanthine oxidase (XO) and phospholipase A2 (PLA2) that can trigger several signaling pathways. ROS produced by XO activate MAPKs: p38 MAPK, extracellular

signal regulated kinase 1 and 2 (ERK 1 and ERK 2). Once they are activated, they induce the upregulation of nuclear factor-kappa B (NF-κB), which upregulates PGC-1α through the phosphorylation of activating transcription factor 2. The activation of MAPKs was found to mediate the transcription of manganese-dependent superoxide dismutase (MnSOD). Lipid peroxidation (LPO) trigger the activation of PLA2 to produce the fatty acid arachidonic acid (AA). AA can then further induce the generation of ROS through the stimulation of mitochondrial ETC and NOX.

1.5.2. ROS-induced adaptive responses during exercise

Regular exercise induces various adaptational responses in skeletal muscles ranging from gene expression up to morphological changes, such as mitochondrial biogenesis and enhanced antioxidant defense system. ROS have an important role in numerous exercise induced adaptations of skeletal muscle cells. Some of the ROS-induced adaptive responses include:

- **Mitogen-activated protein kinases (MAPK):** ROS were found to be important signaling molecules for the activation of MAPKs (Gomez-Cabrera, *et al.*, 2005). Erk1, Erk2 and p38 MAPK are activated by exercise (Yu, *et al.*, 2001). Once they are activated, they induce the upregulation of PGC-1α through the phosphorylation of activating transcription factor 2 (Morton, *et al.*, 2004). Moreover, the activation of MAPKs was found to mediate the transcription of MnSOD, which is a critical antioxidant enzyme that maintains $^{\bullet}O_2^-$ at physiological levels (JI, *et al.*, 2006).

- **Nuclear factor-kappa B (NF-κB):** is a transcription factor that is involved in the regulation of many genes. The activation pathway of NF-κB was found to be redox-sensitive through XO-derived ROS during exercise (Gomez-Cabrera, *et al.*, 2006).

Activation of NF-κB up regulates the expression of MnSOD (Hollander, *et al.*, 2001). The exact upstream mechanism of ROS-activation of protein kinases to activate NF-κB is not yet identified. NF-κB is found in cytosol bound to the inhibitor-kappa B (IκB), which is the dimeric and inactive form of NF-κB. Under oxidative stress condition NF-κB gets activated through phosphorylation and translocates from cytoplasm to the nucleus (Galter, *et. al.*, 1994; Poljak-Blazi, *et. al.*, 2009). Treatment of human monocytes with 4-hydroxynonenal (4-HNE), a very reactive aldehyde, inhibited the phosphorylation of IκB, and subsequent activation of NF-κB (Page, *et. al.*, 1999), providing evidence that lipid peroxidation aldehyde product is involved in the regulation of NF-κB.

- **Nuclear factor E2 related factor 2 (Nrf2):** Nrf2 is a transcription factor shown to be redox sensitive. Nrf2, known as the master regulator of cellular redox homeostasis, gets activated by oxidative stress and translocates to the nucleus. It is linked to the regulation of transcription of many antioxidant enzymes such as: glutathione S-transferases, glutathione disulfide reductase, glutathione peroxidase and others (Hansen, *et. al.*, 2004). Moreover, it regulates the transcription of glutathione reductase 1, which reduces oxidized glutathione by using NADPH as an electron donor. Nrf2 is also partially involved in the regulation of the transcription of NADPH-generating enzymes (Dinkova-Kostova and Abramov, 2015).

- **Antioxidant system activated by exercise:** The increase in ROS production in a contractile muscle is also accompanied with increased antioxidant activity. Muscle contraction is found to be involved in the regulation of enzymatic antioxidants, such as: glutathione peroxidase (GPX), copper-zinc superoxide dismutase (Cu, Zn-SOD, SOD1)

in cytosol, MnSOD (SOD2) in mitochondria, and catalase as well as nonenzymatic antioxidants, such as: glutathione (GSH) (Steinbacher and Eckl, 2015).

1.6. Exercise-induced oxidative stress

There are many studies that suggests the beneficial effects of free radicals induced by exercise. The effect of free radical depends on type and duration of exercise, which can either be involved in enhanced bioenergetics pathways or improved antioxidant systems. Still, the direct association between exercise and oxidative stress is not clear (Radak, *et al.*, 2001). The term "oxidative stress" was first used in 1985 (Sies and Cadenas, 1985). With the advancements and continuous changes of science, the definition of oxidative stress has continuously changed. The most recent and widely accepted definition by Jones and colleagues states that oxidative stress is "an imbalance between oxidants and antioxidants in favor of the oxidants, leading to a disruption of redox signaling and control and/or molecular damage" (Jones, *et. al.*, 2017). In skeletal muscle the pathological effect of uncontrolled and accumulated production of oxidants is suggested to be involved in sarcopenia, which is in a simple term muscle senescence. Sarcopenia is associated with loss of muscle mass, strength and contraction velocity (Meng and Yu, 2010). At a molecular level, excess oxidants can damage macromolecules, including DNA, proteins and lipids, altering their chemical structure and function. The severity of oxidative damage is a function of concentration and duration of ROS production. This determines the cellular response that can range from activation of some signaling transcriptional factors to triggering apoptosis.

1.7. Membrane damage through lipid peroxidation

Lipids are one of the target sites of ROS-induced damage in skeletal muscles and all cells in general. Some studies demonstrate that endurance exercise and contractile activity can lower lipid peroxidation, along with an increase in mitochondria-specific isoform of MnSOD activity, which is a major enzyme in antioxidant defense system (Vincent *et al.*, 1999). Others have shown that maximal and supra-maximal exercise can significantly increase lipid peroxidation (Mohamed, *et. al.*, 2016).

1.7.1. Lipid peroxidation process

Lipid peroxidation is considered to be one of the most important mechanisms of cell injury under conditions of oxidative stress, and was shown to be involved in the pathology of numerous diseases.

Polyunsaturated fatty acids (PUFAs), with one or more carbon-carbon double bonds, were found to be more susceptible to ROS induced damage compared with saturated and mono-olefinic fatty acids (Cosgrove *et al.*, 1987). Lipid peroxidation process, shown in Figure 5, can be initiated by the reaction of a ROS, like hydroxyl radical, which abstract the allylic or bis-allylic hydrogen. The allylic or bis-allylic site is saturated carbon in the methylene group ($-CH_2-$), which is attached to the vinyl group ($-CH=CH_2$), shown in Figure 6. The abstraction of hydrogen from polyunsaturated lipid (LH) will result in a carbon-centered lipid radical (L•). In the propagation stage, the L• reacts with oxygen molecule forming a lipid peroxyl radical (LOO•) that abstracts a hydrogen from another polyunsaturated lipid producing L• and lipid hydroperoxide (LOOH) continuing the chain reaction of lipid peroxidation. This single electron rearrangement can result in the production of degraded lipid peroxide and lipid peroxidation end

products such as 4-hydroxynonenal. Finally, the chain reaction can be terminated in the presence of a termination factor. Usually the termination factor is an antioxidant, such as vitamin E that donates a hydrogen (an electron) to the LOO• to become non-radical (Halliwell and Gutteridge, 2007; Ayala *et al.*, 2014).

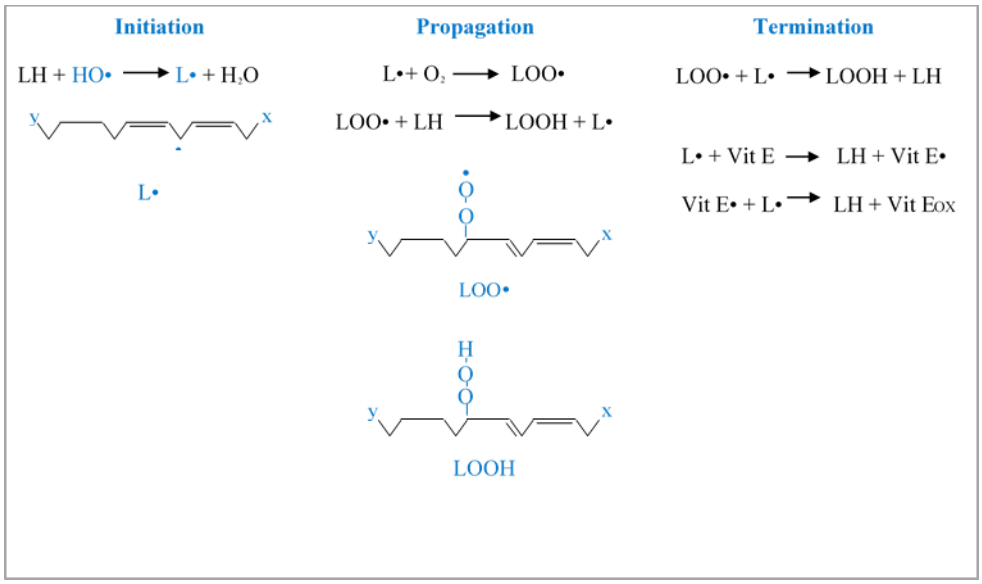

Figure 5: The process of lipid peroxidation starts with initiation stage when a reactive species abstract the allylic hydrogen from unsaturated lipid forming a lipid radical. Then, propagation reaction continues reacting with oxygen and forming lipid peroxy radical and lipid hydroperoxide. Finally, the reaction comes to an end in the termination stage by donation of an electron from an antioxidant such as vitamin E.

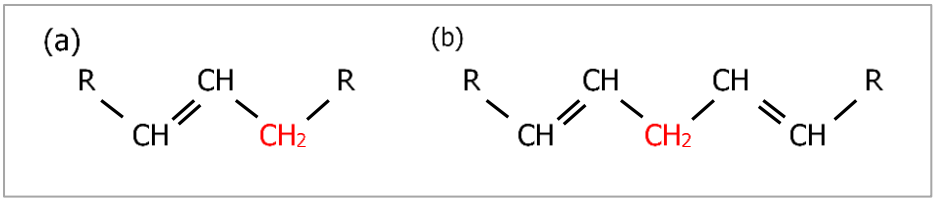

Figure 6: Hydrogen atoms on methylene groups at the allylic or bis-allylic sites of lipids are readily abstracted by reactive radical species. A. Shows the allylic site, which is the saturated carbon in the methylene group (-CH_2-) that is attached to a vinyl group (-CH=CH_2), R is the rest of the chain. **B.** When a methylene group is attached to two vinyl groups from both sides it is called bis-allylic site.

1.7.2. Lipid peroxidation products

Lipid peroxidation process results in the formation of LOOH as a primary product. It also can result in the formation of many reactive species as secondary products, known as reactive carbonyl compounds (RCC) due to the highly reactive carbonyl group. The accumulation of lipid peroxides can change the membrane's fluidity and permeability (Dobretsov *et al.*, 1977). Furthermore, the secondary products from PUFAs-induced oxidation have high stability with an average half-life of minutes or even hours, compared to the short half-life of ROS, which can only last for nanoseconds or milliseconds. As a result, RCC can diffuse through cellular membranes and attack biomolecules that are far away from the site of origin, compared to ROS that can only attack biomolecules that are located within few nanometers of site of origin (Jaganjac *et al.*, 2016). Some of those reactive aldehydes are: glyoxal, acrolein, methylglyoxal, and malonic dialdehyde (Negre-Salvayre *et al.*, 2008). Among all secondary products studied, of particular biochemical and biomedical relevance is the α,β-unsaturated aldehyde 4-hydroxynonenal (4-HNE) (Esterbauer *et al.*, 1990). A stable lipoxidation (ALEs) end product can evolve from the reaction of initial adducts with a second aldehyde molecule (the same or

different) by oxidation, dehydration, cyclization, tautomerization and sometimes condensation. Proteins modified by 4-HNE can be detected by using the 4-HNE specific enzyme-linked immunosorbent assay (Borovic, *et. al.*, 2006), immuno-cytochemical, immuno-histochemical and immuno-electronmicroscopical analyses (Živković, *et. al.*, 2005), immuno-blotting (Cipak, *et. al.*, 2005), MALDI-TOF-MS (Sayre, *et. al.*, 2006), neutral loss-triggered electron capture dissociation tandem mass spectrometry (Rauniyar, *et. al.*, 2009), Collision-induced dissociation (CID) and electron transfer dissociation (ETD) MS/MS (Fritz, *et. al.*, 2012) and others.

1.8. 4-Hydroxynonenal (4-HNE)

1.8.1. Milestones in the history of 4-HNE

In the 60s, 4-HNE (Figure 7) was first discovered by Esterbauer and his colleagues (Schauenstein *et al.*, 1964). Later in the 80s, Esterbauer and his colleagues identified 4-HNE as a cytotoxic product formed by microsomal lipid peroxidation in rat liver (Benedetti *et al.*, 1980). Although in the 90s, 4-HNE started as a "toxic product of lipid peroxidation" and "second toxic messenger of free radicals", a decade later it became evident that it has an important role in pathogenesis and progression of numerous human diseases but also a crucial physiological role in the modulation of cell growth, differentiation, apoptosis, and cell signaling. This will be discussed in section 1.8.3.

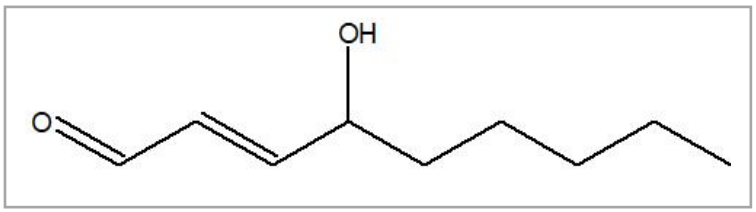

Figure 7: Chemical structure of 4-hydroxy-nonenal (4-HNE). Chemical structure showing the functional groups: carbonyl group, carbon-carbon double bond, and the hydroxyl group.

1.8.2. Chemical mechanisms for 4-HNE formation

4-HNE can be formed by the decomposition of lipid hydroperoxide by enzymatic and non-enzymatic reactions (Figure 8).

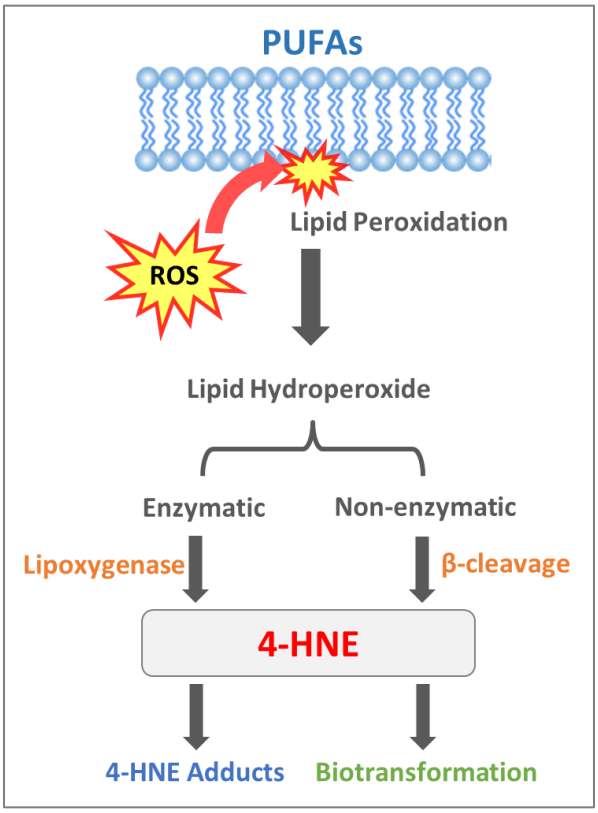

Figure 8: Formation of 4-HNE by enzymatic and non-enzymatic reactions. Through enzymatic and non-enzymatic reaction the lipid hydroxide produced from lipid peroxidation goes into several processes that eventually generate 4-HNE or other RCCs. If 4-HNE is not detoxified through biotransformation, it can lead to the formation of 4-HNE adducts with macromolecules.

In the enzymatic reaction, the hydroperoxide with ω-6 PUFAs or higher ω number, which has the carbon-carbon double bond in carbon number 6 or higher, such as linoleic acid (LA) and AA, goes under oxidation by lipoxygenases (LOX) forming 4-HNE main precursors. LA is

oxidized by LOX to form 13-hydroperoxyoctadecadienoic acid (13-HPODE) and AA is oxidized by LOX to form 15- hydroperoxyeicosatetraenoic acids (15-HPETE) (Ayala *et al.*, 2014; Zhong and Yin, 2015). In the non-enzymatic reaction 4-HNE is formed by the β-cleavage of hydroperoxides, namely the hydroxyalkoxy-radicals. This process will result in the formation of hexanal that goes into further reactions to eventually form 4-HNE (Esterbauer *et al.*, 1991; Schneider *et al.*, 2001).

1.8.3. 4-HNE: a double edged sword

The cellular level of 4-HNE varies between different cells types. For example, it was found that 4-HNE basic concentration in human blood serum ranges from 0.05 to 0.15 μM (Gil *et al.*, 2006). Moreover, it is important to point out that the contributing factors in determining the half-life of 4-HNE, include: the site of production, amount produced, and the detoxification rate by antioxidants. Siems and his co-workers found that 100 μM of 4-HNE has a half-life of only 5 minutes in hepatocytes (Siems *et al.*, 1997). More evidence showed that different cells have different abilities to detoxify 4-HNE. For example; endothelial cells were able to metabolize 50% of 25 μM 4-HNE after 6 hours (Whitsett *et al.*, 2007), while smooth muscle cells were found to be more resistant with the ability to metabolize 50 μM 4-HNE completely within 8 hours (Hill *et al.*, 2008). It is crucial for cells to control 4-HNE concentrations, as low concentrations, which are estimated to be between 0.5 to 5.0 μM, are needed for normal physiological processes such as promoting differentiation and proliferation, and activating antioxidant cell defense mechanism through activation of Nrf2 (Chapple *et al.*, 2013). However, high concentrations may cause cellular stress and loss of function. Chronic exposure and accumulation of high concentrations, which are estimated to be between 10 to 20 μM, were found to ultimately trigger apoptosis and necrosis through activation of caspase enzymes, cytochrome

C, and other cytotoxic pathways (Chapple *et al.*, 2013). Thus, 4-HNE concentration is the accepted biomarker for numerous pathologies such as cataract, atherosclerosis, Alzheimer's disease, diabetes and cancer (Negre-Salvayre *et al.*, 2010; Chapple *et al.*, 2013).

1.8.4. 4-HNE modification of proteins

Hydrophobic species, such as 4-HNE, are confined to lipid membranes mostly affecting membrane proteins. The high reactivity of 4-HNE is due to its chemical structure, shown in Fig. 7, which consists of three functional groups:

- C=C double bond: that can form Michael additions to thiol
- C=O carbonyl group: that gives a partial positive charge to carbon 3 and can form Schiff-base oxidation, reduction, or formation
- Hydroxyl group: at carbon 4 that increases the positivity on carbon 3 making C3 more susceptible to nucleophilic attack, such as thiol or amino groups

This makes biological nucleophile groups such as cysteine, histidine and lysine liable to 4-HNE attack (Zarkovic *et al.*, 2013; Schaur *et al.*, 2015). Formation of 4-HNE adducts by Michael additions and Schiff-base are shown in Figure 9.

The common effect of protein carbonylation is enzyme inactivation i.e. loss of function, however protein carbonylation may also result in a gain of function (Grimsrud *et al.*, 2008; Suzuki *et al.*, 2010). Modifications of metabolic and structural proteins play a significant role in protein dysfunctions, altering trafficking, processing of proteins, generating tissue damage and pathogenesis of numerous human diseases (Zarkovic *et al.*, 2013).

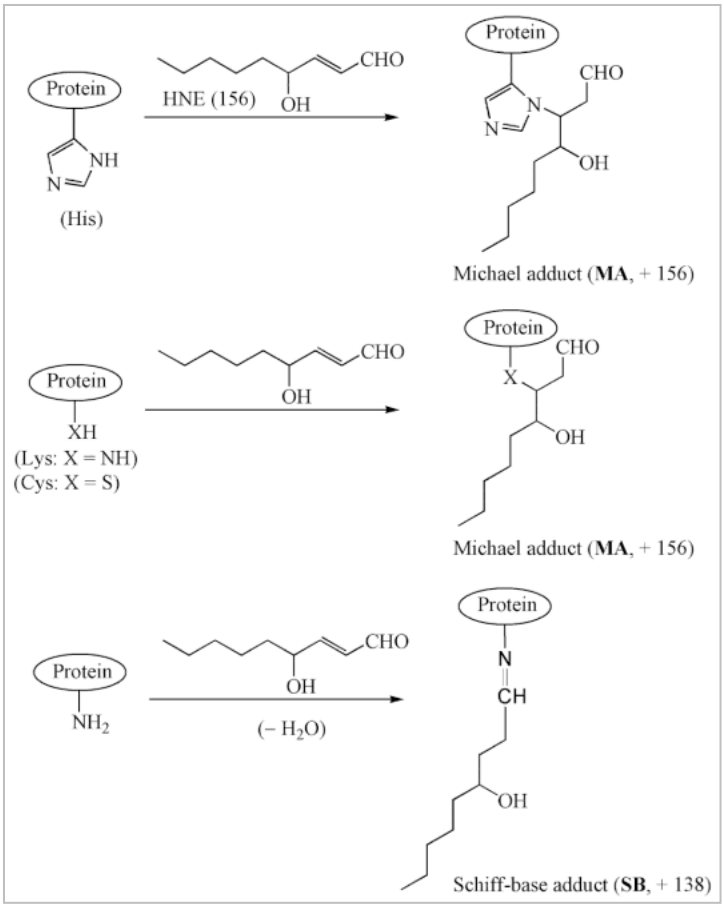

Figure 9: Formation of 4-HNE post-translational modifications of proteins by Michael additions and Schiff-base (Rauniyar and Prokai, 2009).

For the last few decades researchers have been developing methods to detect 4-HNE-protein adducts. Early methods include immunochemical methods with chromogens for light microscopy detection of 4-HNE protein adducts presence (Uchida *et al*., 1993) and immunogold method for subcellular localization of 4-HNE-modified proteins by electron microscopy (Zivkovic *et al.*, 2005). Recent methods are aiming to identify proteins modified by 4-HNE and are utilizing mass spectrometry methodology (Tanito *et al*., 2006; Chavez *et al.*, 2011).

1.9. Hypothesis

Exercise induced oxidative stress affects body redox homeostasis leading to training mediated redox adaptations. However, excessive ROS formation will lead to disturbance of redox homeostasis and peroxidation of lipids yielding formation of reactive aldehydes such as 4-HNE. Due to numerous known bioactive properties of 4-HNE we hypothesize that the formation of 4-HNE adducted proteins has an important role on mitochondrial function affecting mitochondrial biogenesis, cellular energy production and cell metabolism. Recently some efforts have been made to investigate the 4-HNE role in modification of mitochondria proteins (Andringa *et al.*, 2014; Zhao *et al.*, 2014), using conventional techniques. However, till today the pathophysiological role of 4-HNE on mitochondrial function has not been studied in details. Therefore, in the proposed project we are aiming to investigate the effects of caffeine, which can act as an exercise mimetic by inducing calcium stimulation, on mitochondrial metabolism and cellular redox homeostasis that could lead to induction of LPO and the impact of LPO product 4-HNE on physiology and pathology of skeletal muscles.

1.10. Specific aims and objectives

1. Study the effect of caffeine, used as exercise mimetic, on mitochondrial function in skeletal muscle cells by measuring caffeine-induced: calcium signaling, mitochondrial bioenergetics, rate of lipid peroxidation and 4-HNE adducts formation.
2. Study the role of 4-HNE in skeletal muscle specifically identifying and focusing on: redox homeostasis, mitochondrial energy metabolism, mitochondrial transcriptome and mitochondrial density
3. Develop a method for rapid and sensitive identification of 4-HNE-modified proteins
4. Identify *in-vivo* 4-HNE post-translational modification of proteins induced by exercise.

2. METHODOLOGY

2.1. Cell culture

Mouse C2C12 and rat L6 skeletal muscle cells were purchased from American type culture collection (ATCC, CRL-1772 and CRL-1458) while human skeletal muscle myoblasts (HSMM) were purchased from Lonza (CC-2580). C2C12 and L6 myoblasts were maintained in the Dulbecco's Modified Eagle's Medium (DMEM, SIGMA) supplemented with 10% fetal bovine serum (FBS, SIGMA), 2 mM L-glutamine (SIGMA), 100 U/ml penicillin (SIGMA) and 100 μg/ml streptomycin (SIGMA), while HSMM were grown in Skeletal Muscle Growth Media-2 (SkGM-2 Medium, Lonza) supplemented with SkGM-2 singleQuots kit according to the manufacture's protocol. All cells were maintained at 37ºC in a humidified atmosphere with 5% CO_2.

C2C12 and L6 cell lines are useful rodent cell lines extensively used to unravel the underlining mechanisms of muscle function. C2C12 and L6 cell lines have high growth rates, ease of use and theoretically replicate indefinitely. However, as immortalized cell lines it is possible that they do not resemble normal muscle function. On the other hand, HSMM cells are primary human skeletal muscle myotubes that preserve metabolic characteristics of the donor, thus have higher clinical relevance. C2C12 and L6, selected for this project, as mammals skeletal muscle cells were able to provide some reflection on biological processes of human skeletal muscle cells. All experimental methods were optimized using C2C12 and L6 cell lines. Then, optimized methods were used in HSMM. The obtained results from using C2C12, L6 and HSMM can provide indication on the physiological functions and responses of the different species.

2.1.1. Cell growth assessment

C2C12, L6 and HSMM myoblasts characteristics including: cell cycle, volume and diameter were assessed using Scepter handheld automated cell counter (Millipore). Cells were seeded in 12 well plates with density of 2×10^5 cells per well. Cells were detached from the surface by the action of trypsin, the number of cells was counted in triplicates at day 0, 1, and 2 and Scepter Software Pro 2.1 (Millipore) used to analyze the data. Figure 10 shows the cell growth rate of each cell type. Both C2C12 and L6 double in number within the first 24 h, while HSMM number increased by approximately 39% in the same time. After 48 h the number of C2C12, L6 and HSMM cells increased by 4, 6 and 2 times, respectively. The histogram of measured diameter and volume of each cell type is shown on Figure 11 C2C12 had an average diameter of 14.04 ± 0.47 µm and an average volume of 1.46 ± 0.14 pL, while L6 had an average diameter of 12.99 ± 0.69 µm and average volume of 1.16 ± 0.18 pL. HSMM had an average diameter of 13.73 ± 0.29 µm and average volume of 1.36 ± 0.10 pL

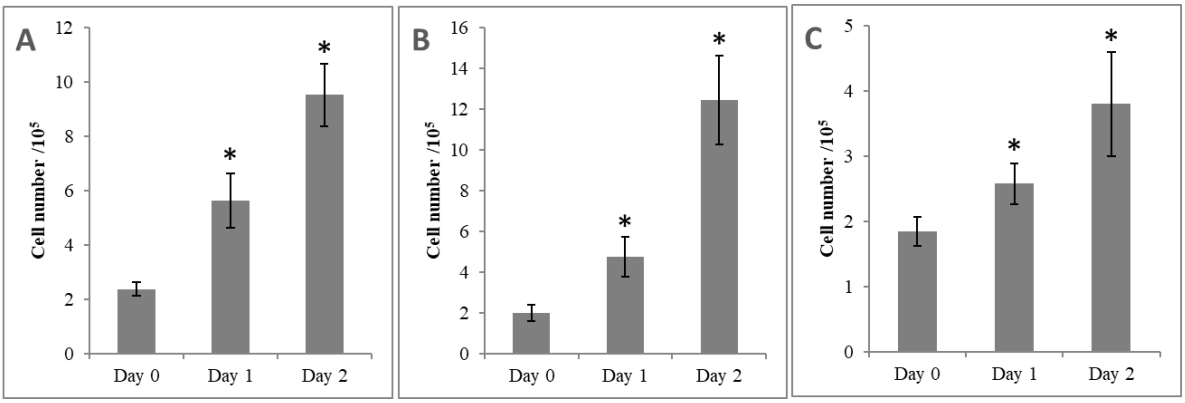

Figure 10: Growth rate assessment. Growth speed for the selected cell lines was assessed. **A.** C2C12 **B.** L6 and **C.** HSMM myoblasts. Mean values of triplicates ± *SD* are given ($p < 0.01$).

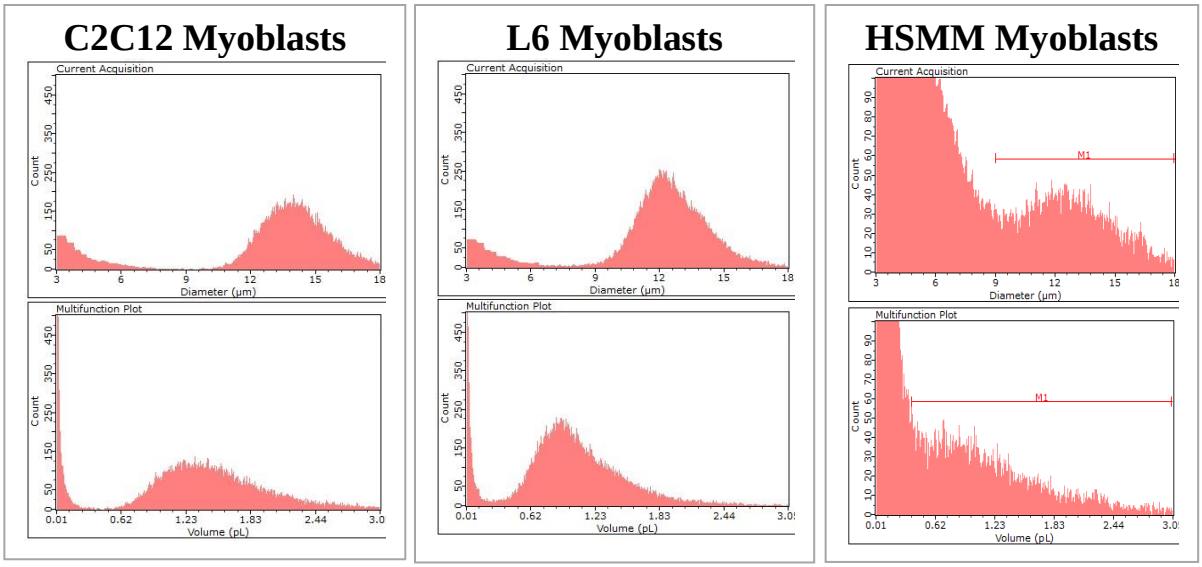

Figure 11: Assessment of cells diameter and volume. Representative histograms of C2C12, L6 and HSMM myoblasts showing the average diameter and volume measured using Scepter handheld automated cell counter in Scepter Software Pro (2.1). (*N* =3)

2.1.2. Myoblasts differentiation into myotubes

To induce differentiation of mono-nucleated myoblasts into multi-nucleated myotubes, when cells reach 70% to 80% confluence, cell maintenance media with 10% FBS was replaced with complete DMEM supplemented with 2% horse serum (HS, SIGMA). The differentiation media (DMEM with 2%HS) was changed every 24 hours. The cells reached full differentiation by the fourth day of differentiation and hence all experiments were carried between the fifth and eighth day of differentiation. Figure 12 shows myoblast images and differentiated myotubes.

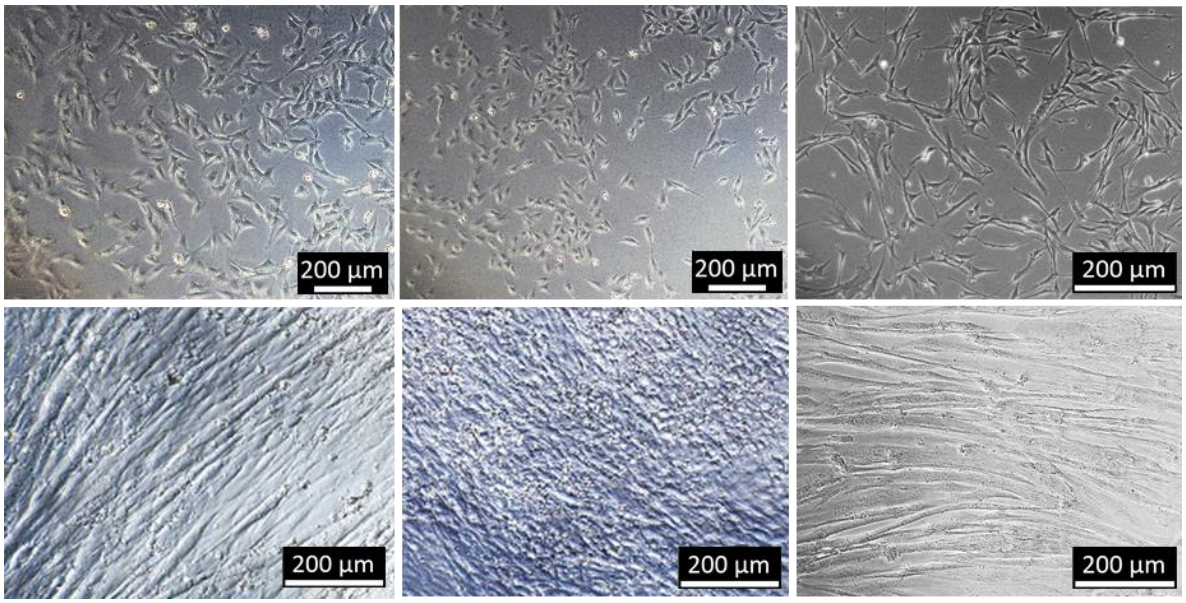

Figure 12: Light microscopy images of myoblasts and myotubes. Myoblasts (on top) differentiated into myotubes (down) of C2C12 on the left, L6 in the middle and HSMM on right.

2.2. Measuring mitochondrial bioenergetics using XFe24 Seahorse analyzer

2.2.1. Optimizing cell density for XFe24 Seahorse analyzer using glycolysis stress test

Glycolytic reserve is determined by measuring the glycolytic capacity and the glycolysis rate using glycolysis stress test kit on Seahorse Extracellular Flux (XFe24) Analyzer (Billerica, MA, USA). Figure 13 shows the standard assay profile of the key parameters of glycolytic function for the XF glycolysis stress test. Myoblasts were seeded at different densities: 8000 and 16000 cell per well, in Seahorse XF 24-well culture microplates and differentiated into myotubes as described above. One hour prior to experiment, differentiation media was replaced with the Seahorse XF Base medium supplemented with 1 mM glutamine and incubated at 37ºC in non-

CO_2 incubator. Glycolysis was tested according to manufacturer instructions. Briefly, first injection is glucose (10 mM), which represents the rate of glycolysis under basal conditions. Second injection is oligomycin (1.0 µM), which inhibits mitochondrial ATP production to shift all energy to glycolysis production revealing the maximal glycolytic capacity. Third and final injection is 2-deoxy-glucose (2-DG, 50 mM), which inhibits glycolysis by binding to glucose hexokinase. Extracellular acidification rates (ECAR, mpH/min) and oxygen consumption rates (OCR, pmol/min) are measured three times in multiple wells. For each cell density 10 replicates were analyzed. To optimize best seeding density, different number of cells needed to be tested. However, working with myoblasts differentiated to myotubes requires the cells to reach 70% to 80% confluency. Thus, different seeding densities that were tested, 8000 and 16000 cell per well, did not show significant difference in glycolysis parameters in all cell lines as shown in Figure 14. Based on results, 8000 cells per well is used for all Seahorse experiments.

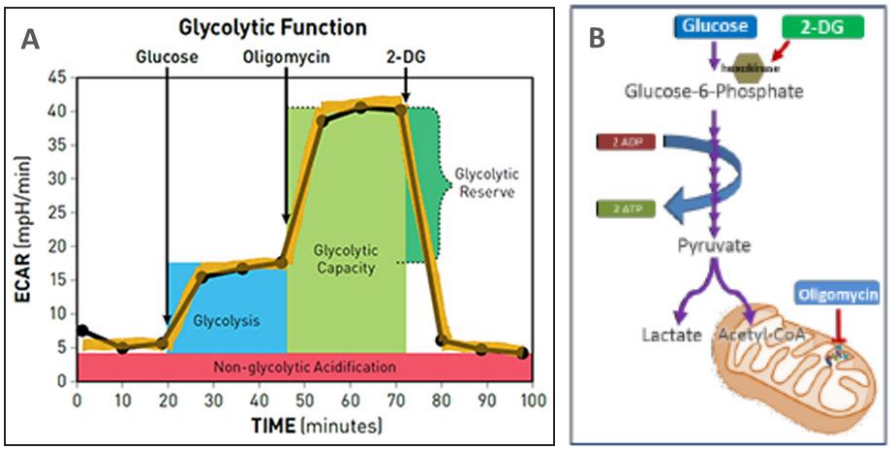

Figure 13: Glycolysis stress test illustration. A. Standard profile of the key parameters of glycolytic function, where it measures glycolysis, maximum glycolytic capacity, glycolytic reserve and non-glycolytic acidification. **B.** Illustration where glucose fuel the cell, oligomycin inhibit ATP synthase and 2-DG is competitive inhibitor of glucose to inhibit glycolysis. *Source:* Seahorse XF Glycolysis Stress Test Kit user guide.

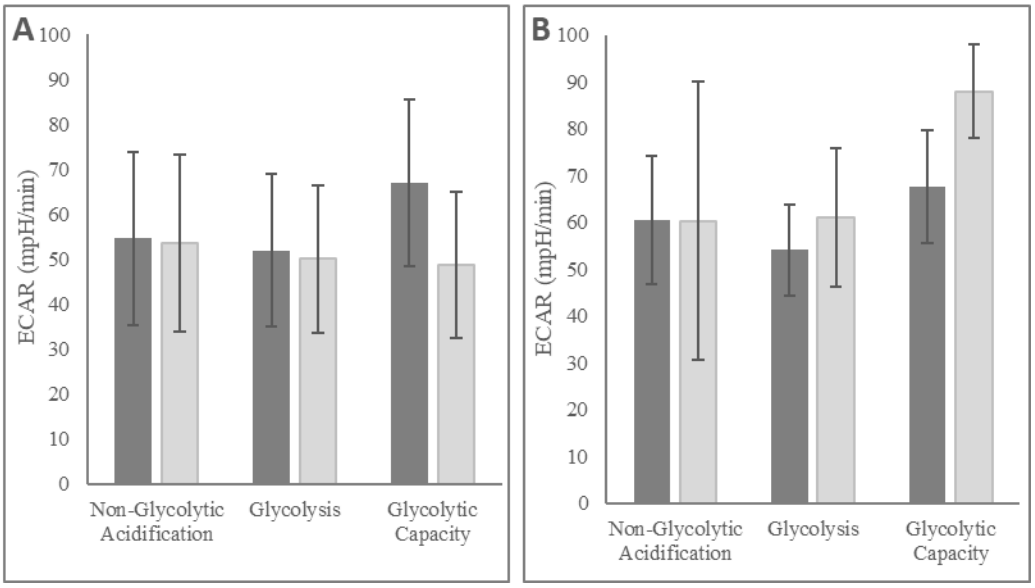

Figure 14 Extracellular acidification rate (ECAR) for seeding density optimization. Two seeding densities are tested: 8000 and 16000 cell/well dark grey bars and light grey bars, respectively. **A.** Glycolysis of C2C12 myotubes. **B.** Glycolysis of L6 myotubes. Both results show no significant difference between seeding densities. (*N* =10, mean ± *SD*)

2.2.2. Mitochondrial respiration using mitochondrial stress test

Cells were seeded in XFe24 cell culture microplates at a density of 8000 cell/well and differentiated into myotubes as described in section 2.1.2. Cellular respiration was assessed by using cell mitochondrial stress test kit and oxygen consumption rate (OCR, pmol/min) was measured by Seahorse XFe24 Analyzer (Agilent, USA). Mitochondrial stress test standard profile of the key parameters of mitochondrial respiration is illustrated on Figure 15 and Figure 16. Prior to experiment, the myotubes were serum starved for 1 hour in Seahorse XF Base Medium supplemented with 2 mM glutamine, 1 mM pyruvate and 10 mM glucose at 37ºC in a humidified atmosphere without CO_2. First injection port contained an ATP synthase (complex V) inhibitor oligomycin (1.0 µM) causing the decrease in OCR. The decrease in OCR directly

correlates with ATP production. Second injection port contained uncoupler of oxygen consumption from ATP production FCCP (0.5 µM), the injection of which will collapse the proton gradient and alter mitochondrial membrane potential allowing maximal oxygen consumption by complex IV. In the final, third injection port is a mixture of rotenone and antimycin A (0.5 µM) an inhibitors of complex I and III, and injection of which will shut down mitochondrial respiration enabling the calculation of the non-mitochondrial respiration. Extracellular acidification rates (ECAR, mpH/min) and oxygen consumption rates (OCR, pmol/min) are measured three times in 5-replicate wells.

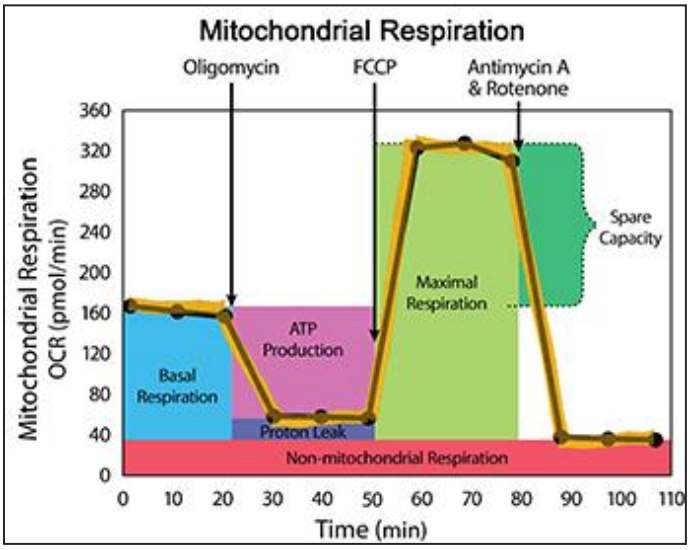

Figure 15: Mitochondrial stress test standard profile. Mito. Stress test allowing measurement of basal respiration, ATP production, proton leak, maximal respiration, spare respiratory capacity, and non-mitochondrial respiration. *Source:* Seahorse XF Cell Mito Stress Test Kit user guide.

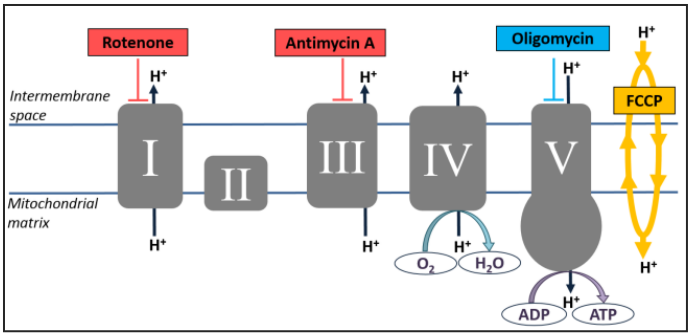

Figure 16: Illustration of the effects of compounds used in mitochondrial stress test on mitochondrial electron transport chain. Oligomycin inhibits complex V (ATP synthase), FCCP uncouples oxygen consumption from ATP production, and rotenone and antimycin A inhibit complexes I and III, respectively. *Source:* Seahorse XF Cell Mito Stress Test Kit user guide.

	1	2	3	4	5	6
A	●	T1	T1	T1	T1	T1
B	T2	T2	T2	●	T2	T2
C	T3	T3	●	T3	T3	T3
D	T4	T4	T4	T4	T4	●

Figure 17: XF24 cell culture microplate scheme. Different concentrations of caffeine or 4-HNE treatment were added according to the above scheme, where T1, T2, T3 and T4 each represent replicates of same concentration treatment. Treatment is added either in the port to test immediate response or in the well for the overnight response. Black wells (A1, B4, C3 and D6) are background correction wells where only media and no cells were added.

2.3. RNA extraction and real-time PCR

RT² Profiler PCR arrays were used to determine the effect of caffeine or 4-HNE on the expression of mitochondrial genes. Myoblasts were seeded in 24 well plates with a density of 40×10^3 cells per well. When cells reached 70-80% confluency they were differentiated into myotubes. Myotubes were treated with caffeine (0, 1, 5 and 10 mM) for 2 hours over three consecutive days or treated overnight with 4-HNE (0, 2.5, 5 and 10 µM). Total RNA was isolated using RNeasy Mini Kit (Qiagen). Followed by measuring RNA quantity using NanoDrop 2000 spectrophotometer (Thermo Scientific). RNA was normalized based on concentration (500 ng). For the reverse transcription of cDNA, RT² First Strand Kit (Qiagen) was used. Then, for the RNA extracted from C2C12 myotubes, real-time PCR was performed using The Mouse Mitochondrial Energy Metabolism RT² Profiler PCR Array (PAMM-008ZC, Qiagen). On the other hand, RNA extracted from L6 myotubes was analyzed by real-time PCR using Rat Mitochondria RT² Profiler PCR Array (PARN-087ZC, Qiagen). Real time PCR used was ABI StepOnePlus (Applied Biosystems). The mitochondrial energy metabolism array profiles the expression of 84 genes involved in mitochondrial respiration, i.e. genes involved in Complex I (NADH-Coenzyme Q Reductase), Complex II (Succinate-Coenzyme Q Reductase), Complex III (Coenzyme Q-Cytochrome c Reductase), Complex IV (Cytochrome c Oxidase) and Complex V (ATP Synthase). The mitochondrial array profiles the expression of genes involved in the mitochondrial membrane potential and polarization, mitochondrial transport, mitochondrial membrane translocation genes, genes involved in mitochondrial fission and fusion, mitochondrial localization and genes involved in apoptosis. The list of genes with their description is included in supplementary Table 14 and Table 15 Values are expressed in fold-regulation threshold of 3 and p <0.01. Results are grouped as control compared to each treated

group with 4-HNE (2.5 µM is Group 1, 5 µM is Group 2 and 10 µM is Group 3). The scatter plot shows the upregulated, unchanged and downregulated genes of each 4-HNE concentration compared to control results.

2.4. Statistical analysis

All experiments are presented as mean ± standard deviation (*SD*) of a minimum of 4 biological replicates (represented as *N*). ArrayScan and CCD camera results are presented as mean of minimum of 20 fields per replicate. The significance of differences between groups was assessed using Student's *t*-test or one-way ANOVA with appropriate post hoc testing to compare treated with non-treated groups and different treatments with each other. The IBM SPSS Statistics 25 for Microsoft Windows and Thermo Scientific™ HCS Studio™ Cell Analysis Software were used for cell culture experiments. Differences are considered significant if $p < 0.01$. Proteomics results were analyzed by Thermo Proteome Discoverer 1.4 and 2.2 software and the details of data analysis are described in 5.2.1.3 and 5.2.2.3.

For RT² Profiler PCR arrays data analysis were performed using QIAGEN's The GeneGlobe Data Analysis Center. It is a web resource that transform the threshold cycle (Ct) values to gene expression level as fold-regulation. Basically, average Ct values were grouped, triplicate experiments of each sample in one group, based on treatment and collected in the custom file. The 4-HNE treatment groups were: 0 µM is Control group, 2.5 µM is Group 1, 5 µM is Group 2, and 10 µM is Group 3. The caffeine treatment groups were: 0 mM is Control group, 1 mM is Group 1, 5 mM is Group 2, and 10 mM is Group 3. Then, data were normalized manually using housekeeping genes. Housekeeping genes selection was based on genes with smallest changes in their expression across different sample groups. Table 13 in the appendices

shows the selected housekeeping genes for each experiment. Results are presented in a log-transformed format. Equation 2 shows the calculation of fold-change.

Equation 2: Calculating fold-change for RT² Profiler PCR arrays results

$$2^{\Delta\Delta C_T} = (2^{-\Delta C_T \, of \; Group})/(2^{-\Delta C_T \, of \; Control})$$

3. CAFFEINE-INDUCED MUSCLE CONTRACTION ALTERS MITOCHONDRIAL BIOENERGETICS, TRANSCRIPTOME, AND PRODUCES 4-HNE ADDUCTS

3.1. Introduction

Caffeine controls several well-known biological processes including: adenosine receptors antagonism, phosphodiesterases inhibition and calcium signaling (Herrmann-Frank, *et. al.*, 1999). In skeletal muscle, it is known to induce contraction of muscle through calcium signaling. Muscle contraction promotes mitochondrial biogenesis, energy metabolism and ROS production. Prolonged or high intensity muscle contraction leads to oxidative damage to macromolecules. Selected caffeine concentrations were chosen (1 mM, 5 mM and 10 mM) to mimic low, moderate and intensive exercise respectively. Selection of caffeine concentrations is based on previous studies, where concentrations between 1 mM to 10 mM were found to induce Ca^{2+} release from reticulum to trigger contractions of skeletal muscles (Weber and Herz, 1968). Our key aim is to study the effect of caffeine-induced calcium signaling on redox homeostasis and how this can lead to lipids peroxidation and eventually to the formation of protein adducts by lipid peroxidation byproduct (4-HNE).

3.2. Methodology

3.2.2. Effect of caffeine on mitochondrial biochemical activities

3.2.1.1 Effect of repetitive caffeine treatment on the viability of myotubes

AlamarBlue assay is used to measure the viability of myotubes. The active ingredient of AlamarBlue is Resazurin a redox indicator that is non-toxic to cells. Resazurin is reduced to resorufin in viable cells by enzymatic activity (O'Brien *et. al.*, 2000). Cells were seeded in 96-well plates at a density of 6×10^3 cells per well and differentiated into myotubes. Myotubes were treated with 0, 1, 5 and 10 mM caffeine for 2 hours, washed with PBS and new media was added to myotubes. Treatment was added for three consecutive days, where replicates of day 1, 2 and 3 treatments were carried in the same plate. Viability was measured after 1 day, 2 days and 3 days of treatment. Media was replaced with transparent DMEM media supplemented with 2% HS and 10% (v/v) AlamarBlue (Molecular Probes). Cells were incubated with AlamarBlue in the dark for 1.5 hours at 37ºC in a humidified atmosphere with 5% CO_2. The absorbance was measured at 570 nm wavelength with a reference wavelength at 600 nm using TECAN Infinite M200 PRO plate reader.

3.2.1.2. Measuring the effect of caffeine on cytosolic Ca^{2+} signaling

Fura-2-acetoxymethyl (fura-2, AM, Molecular Probes) ester, a fluorescence calcium indicator was used to measure the impact of caffeine on cellular calcium concentration in C2C12 myotubes similarly as previously described (Domijan and Abramov, 2011). Cells were seeded at a density of 2×10^5 cells on glass 22 mm coverslip in 6 well plates and differentiated into myotubes. Prior to the experiment, cells were loaded with fura-2, AM (5 μM) and pluronic (0.005%) for 30 min followed by wash with HEPES-buffered salt solution (HBSS, in mM: 156 NaCl, 3 KCl, 2 $MgSO_4$, 1.25 KH_2PO_4, 2 $CaCl_2$, 10 glucose, and 10 HEPES, pH adjusted to 7.35

with NaOH). Fluorescence was measured using an epifluorescence inverted microscope equipped with a 20× fluorite objective, where cytosolic calcium concentration $[Ca^{2+}]_c$ was monitored in single cells using excitation light provided by a xenon arc lamp, the beam passing monochromator at 340 nm and 380 nm with bandwidth of 10 nm (Cairn Research, Kent, UK). Fluorescence light was reflected through a 510 nm long-pass filter to a cooled CCD camera (Retiga, QImaging, Canada) and digitized to a 12-bit resolution. Data are analyzed using software from Andor (Belfast, UK). Fura-2, AM is a ratiometric dye that can provide an accurate measurement of the $[Ca^{2+}]_c$ independent of loading variations due its high affinity for Ca^{2+}. Data were recorded with 10 s time interval for 2 min to measure baseline. Myotubes were then treated with ranging concentrations of caffeine followed by a continuous measurement for 18 min to measure caffeine-induced cytosolic Ca^{2+} signal. Then, a maximum signal is generated with carbonylcyanide-p-trifluoromethoxyphenyl hydrazone (FCCP, 1 μM) and recorded for 5 min to enable normalizing the signal between baseline level and maximum level. Data are presented as ratio of excitations 340 nm (high, bound Ca^{2+}) and 380 nm (low, free Ca^{2+}). Fura-2, AM was not calibrated in form of $[Ca^{2+}]_c$ due to inaccuracies arising from different calibration methods.

The impact of caffeine on intracellular calcium concentration in L6 myotubes was assessed by the ArrayScan XTI reader using fura-2AM probe similarly as described above. Briefly, cells were seeded in 96-well transparent plates with density of 6×10^3 cells per well, differentiated into myotubes and loaded with fura 2AM. Then, caffeine treatment (0, 1, 5 and 10 mM) was added and the myotube response immediately imaged, measured by ArrayScan VTI HCS Reader using 386_23 nm excitation filter. Ratio of Ca^{2+} was not measured due to unavailability of required filters in the used instrument. Finally, the total intensity was calculated

using Thermo Scientific™ HCS Studio™ Cell Analysis Software and statistical differences measured using t-test ($p < 0.01$).

3.2.1.3. Measuring effect of caffeine on cellular redox homeostasis

Cells were seeded in 96-well black plates at a density of 6×10^3 cells per well and differentiated into myotubes. The dichloro-dihydro-fluorescein diacetate (DCFH-DA, SIGMA) redox sensitive probe was used to assess the impact of caffeine on intracellular ROS production similarly as described before (Poljak-Blazi *et al.*, 2011). Briefly, differentiated myotubes were treated with 0, 1, 5 and 10 mM caffeine for 2 hours, caffeine treatment was washed with PBS and new media was added to myotubes. Treatment was added for three consecutive days, where replicates of day 1, 2 and 3 treatments were carried in the same plate. After each day of treatment, cells were loaded with 10 µM DCFH-DA for 30 min at 37^0C in the dark in a humidified atmosphere with 5% CO_2. Cells were then washed twice with phosphate-buffered saline (PBS), 100 µL/well of fresh transparent media (DMEM + 2% horse serum) added and fluorescence recorded using Tecan M200 Pro reader with excitation/emission of 500/529 nm. Results are presented as mean ± *SD* of 4 replicates in percent of control.

To measure caffeine-induced superoxide production; dihydroethidium (DHE) was used. DHE in cytosol exhibits a blue fluorescence, but when it gets oxidized it is converted to ethidium bromide, which intercalates with DNA that results in the formation of red fluorescence. Myotubes were loaded with 10 µM DHE probe (Molecular Probes) in transparent DMEM + 2% HS followed by addition of caffeine treatment (0, 1, 5 and 10 mM). Fluorescence was measured continuously for 4 hours with 10 min interval using Tecan M200 Pro reader at excitation/emission of 530/ 580 nm.

3.2.1.4. Detection of caffeine-induced lipid peroxidation

Lipid peroxidation was assessed using a ratiometric fluorescent dye C11-BODIPY$^{581/591}$ (Molecular Probes). Due to its lipophilic moiety, BODIPY$^{581/591}$ is distributed into membranes and upon oxidation its fluorescence emission peak shifts from red (~590nm) to green (~510 nm). Cells were seeded in 96-well black plates with density of 6×10^3 cells per well and differentiated into myotubes. Myotubes were treated with 0, 1, 5 and 10 mM caffeine for 2 hours, for two consecutive days to study the effect of chronic caffeine doses. Lipid peroxidation was measured after 1 day and 2 days of treatment. Upon treatment, cells were loaded with 1 μM BODIPY$^{581/591}$ for 30 minutes in the dark. The excess dye was then washed with PBS, replaced with fresh media and samples analyzed immediately using Tecan Infinite M200 PRO with excitation/emission of 495/521 nm for the green signal (oxidized) and 575/600 nm for the red signal (non-oxidized). Results are in ratio of green/red in percent of control. The effect of caffeine was also imaged using ArrayScan VTI HCS Reader with 485-20 filter for green signal.

3.2.1.5. Measuring effect of caffeine on 4-HNE protein adducts formation

One of the widely accepted methods to assess for oxidative damage is to measure the formation of end products of lipid peroxidation. End products of lipid peroxidation, such as 4-HNE can readily modify proteins to form stable protein adducts. The effect of caffeine on the production of 4-HNE protein adducts was measured using HNE Adduct Competitive ELISA kit (Cell Biolabs). Myoblasts were seeded in 24-well plates with density of 2×10^5 , differentiated into myotubes and treated with caffeine (0, 1, 5 and 10 mM) for 2 hours for three consecutive days. Then cells were washed with PBS, and proteins isolated using Radioimmunoprecipitation assay (RIPA) buffer (50 mM Trizma base, 150 mM NaCl, 1% Triton X-100, 0.05% Na-deoxycholate, 0.01% SDS, pH adjusted to 7.5). To prepare complete RIPA buffer, immediately

prior cell lysis the protease inhibitor, 100 mM phenylmethylsulfonyl fluoride (PMSF, 1mM final concentration), was added. Cells were detached from surface by using cell scraper and transferred to Protein LoBind eppendorf tubes. Samples were incubated on ice for 60min, centrifuged for 10 min at 15000 rpm at $+4^0$C, supernatants collected and protein concentrations measured using BCA Protein Assay Kit (Pierce). Samples were normalized to equal protein concentrations and analyzed by ELISA using bovine serum albumin modified with 4-HNE (HNE-BSA, Cell Biolabs) as a standard. Each experiment consisted of a calibration curve. A calibration curve from a representative experiment is shown in Figure 18.

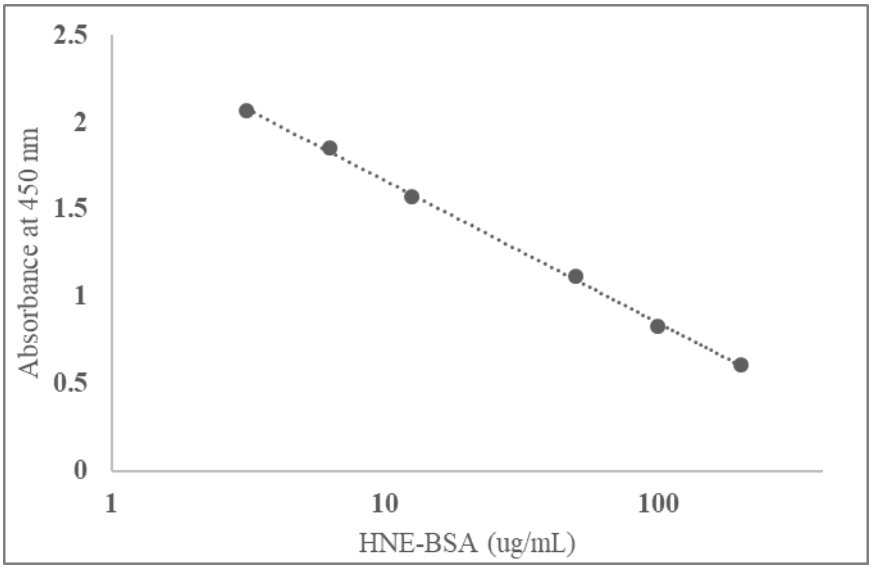

Figure 18: A representative HNE-BSA competitive ELISA calibration curve.

3.2.3. Measuring mitochondrial bioenergetics using XFe24 Seahorse analyzer

3.2.3.1. Acute effect of caffeine on glycolysis

Glycolysis stress test directly measures extracellular acidification rate (ECAR, mpH/min) the change of which is dependent on the protons excreted extracellularly. The amount of protons excreted in the extracellular media is directly related to the glycolysis process; as the

protons are produced and excreted during the conversion of glucose into pyruvate, and eventually to lactate. Glycolysis was measured using cell glycolysis stress test similarly as described in section 2.2.1 with minor modifications. To evaluate the acute effect of caffeine on glycolysis, ranging concentrations of caffeine were added in the first injection port (0, 1, 5 and 10 mM). Second, third and fourth injection ports were loaded with glucose (10 mM), oligomycin (1.0 µM) and 2-DG (50 mM), respectively. The injection volume from each port varied in order to deliver the specified final concentration of each compound. The effect of each injection on ECAR was continuously measured by Seahorse XFe24 Extracellular Flux Analyzer (Agilent, USA).

3.2.3.2. Acute effect of caffeine on mitochondrial respiration using mitochondrial stress test

Same method as in section 2.2.2 is used to measure mitochondrial respiration. The mitochondrial stress test protocol was modified by adding caffeine treatment as first injection in order to record the immediate response. The following injections were according to recommended protocol. In the first injection port, different caffeine concentrations were loaded (0, 1, 5, and 10 mM). Second injection port contained oligomycin (1.0 µM). Third injection port contained FCCP (0.5 µM). In the final, fourth injection port is a mixture of rotenone and antimycin A (0.5 µM). Extracellular acidification rates (ECAR, mpH/min) and oxygen consumption rates (OCR, pmol/min) are measured three times in 5-replicate wells.

3.2.4. Effect of caffeine on mitochondrial gene expression

The effect of caffeine on the mitochondrial gene expression was carried out as described in section 2.3.

3.3. Results

3.3.2. Effect of caffeine on mitochondrial biochemical activities

3.3.2.1. Caffeine-induced Ca^{2+} signal

Physical activity induces Ca^{2+} release from sarcoplasmic reticular (SR) initiating muscle contraction. In this work caffeine was used as an exercise mimetic as it induces Ca^{2+} release. The selection of caffeine concentrations was based on preliminary screening of caffeine-induced Ca^{2+} signal using concentrations ranging between 0.5 mM to 12 mM, results are not shown. Selected concentrations 1, 5 and 10 mM are used to reflect low, moderate and intensive exercise respectively. Figure 19 shows the immediate effect of caffeine on Ca^{2+} signaling of C2C12 myotubes. At 1 mM caffeine treatment, myotubes showed a slight increase in $[Ca^{2+}]_c$ from 0.6 ± 0.1 to 0.8 ± 0.1 fura ratio (n = 75 cells). Myotube treated with 5 mM caffeine responded to the stimulation with increased $[Ca^{2+}]_c$ from 0.8 ± 0.1 to 1.5 ± 0.3 fura ratio (n = 75 cells) and then recovered to baseline within short time. However, although 10 mM caffeine treatment stimulated the highest increase in $[Ca^{2+}]_c$ from 0.8 ± 0.1 to 1.6 ± 0.1 fura ratio (n = 75 cells) the cells took longer time to recover or did not recover at all after the stimulation. The effect of three days doses of caffeine on Ca^{2+} signaling is measured for L6 myotubes. Automated analysis using HCS Studio Software based on total intensity signal and presented on Figure 20 showed that caffeine induced a dose-dependent Ca^{2+} changes in L6 myotubes, with a significant increase (p <0.01) in cells treated with all caffeine concentrations 1 mM, 5 mM and 10 mM by 30% ± 9%, 50% ± 3% and by 65% ± 12%, respectively compared to control.

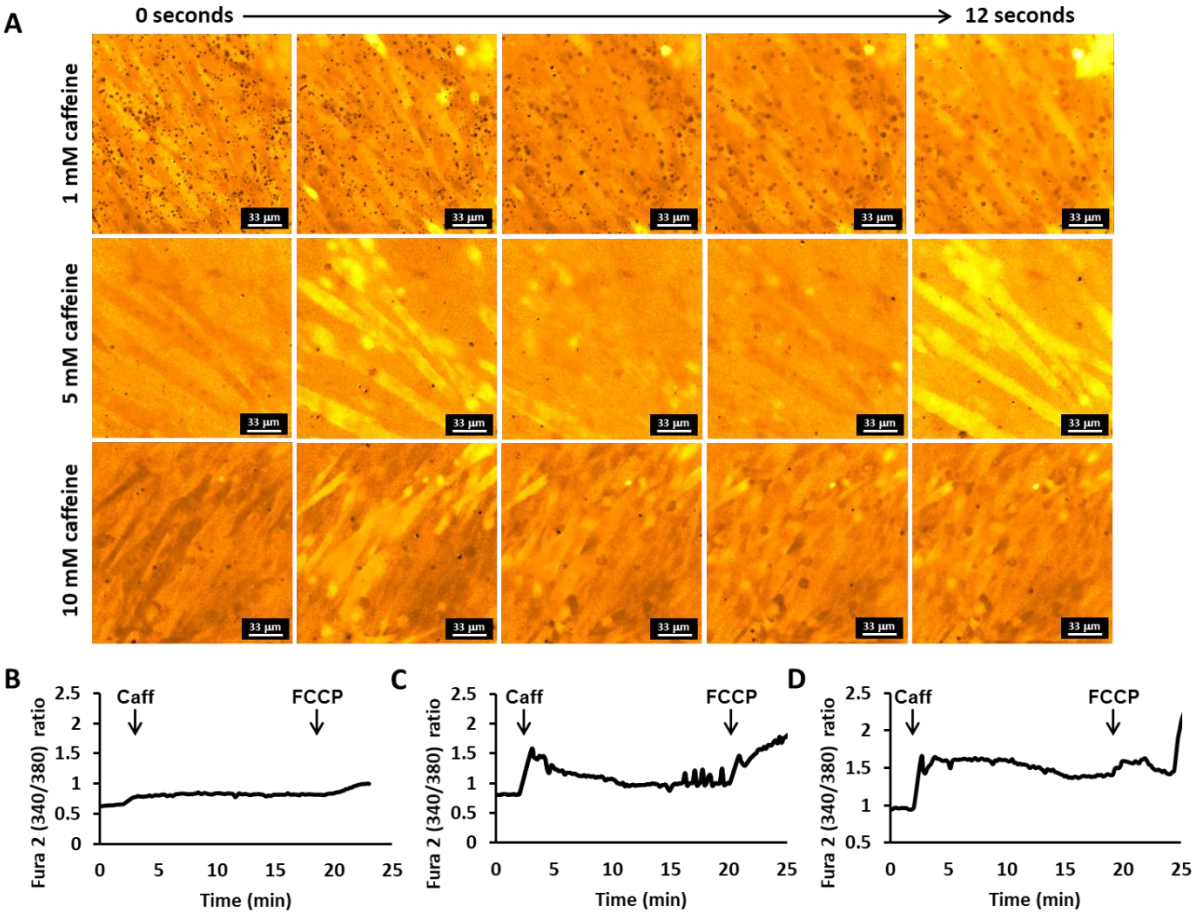

Figure 19: The continuous measurement of caffeine effect on $[Ca^{2+}]_c$ level measured by Fura 2AM in C2C12 myotubes. A. Impact of 1 mM, 5 mM and 10 mM caffeine on $[Ca^{2+}]_c$ release within the first 12 seconds of exposure. **B.** The kinetic profile of $[Ca^{2+}]_c$ release in myotubes when exposed to 1 mM caffeine, **C.** 5 mM caffeine and **D.** 10 mM caffeine. (B., C and D. are representative data from a response of one cell, *N*= 3 of 25 cells measured /replicate)

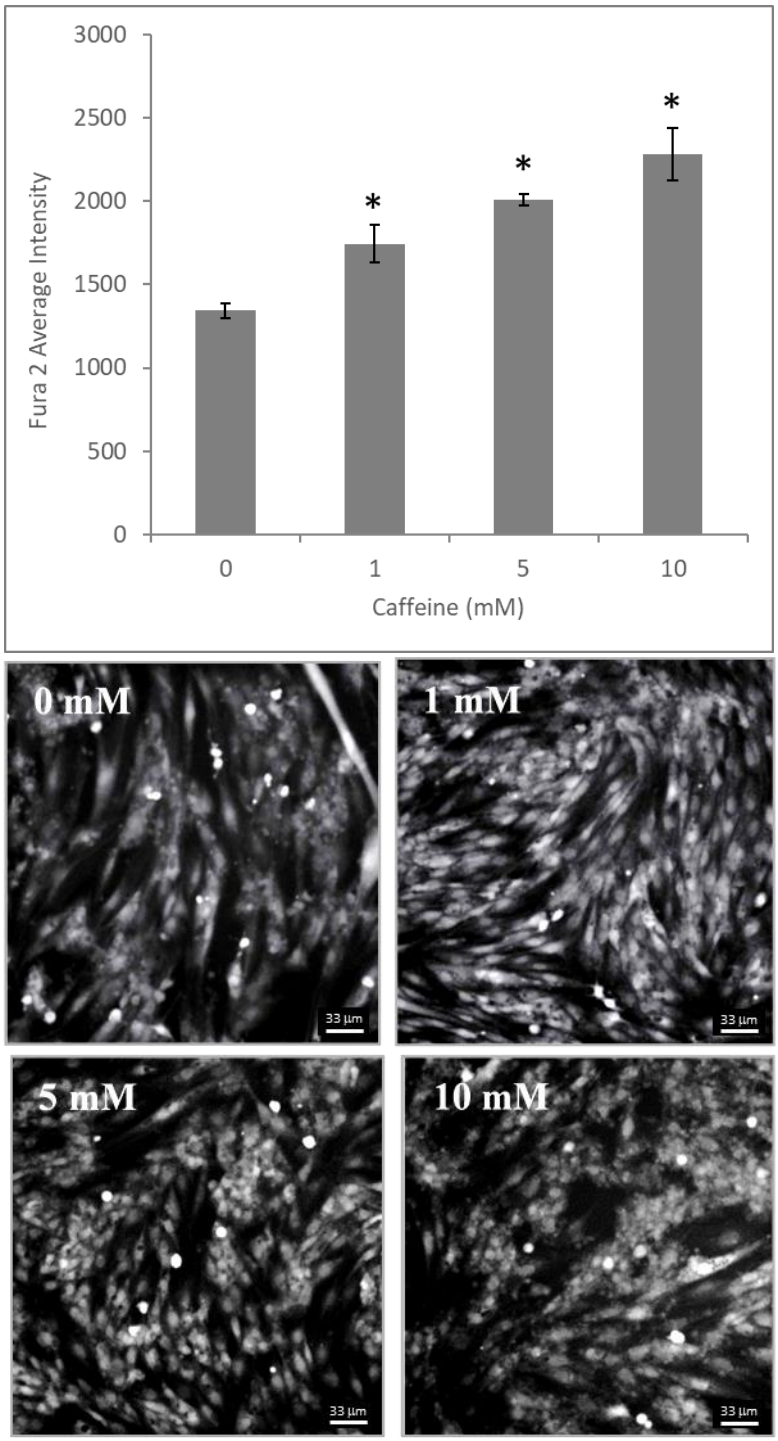

Figure 20: Caffeine-induced Ca^{2+} signal in L6. Fura 2 intensity (340nm) on L6 myotubes treated with different caffeine concentrations measured by ArrayScan VTI HCS Reader. Results presented are mean ± *SD* of *N* = 4 where 25 field were scanned/replicate, representative image is shown for each concentration. * p <0.01 compared to the control.

3.3.2.2. Effect of caffeine on the viability of cells

Based on the caffeine ability to induce Ca^{2+} release, caffeine concentrations were selected to mimic low exercise (1 mM), moderate exercise (5 mM) and extensive exercise (10 mM). Selected caffeine concentrations were tested for their ability to impact myotube viability Figure 21, Figure 22 and Figure 23 shows that selected caffeine concentrations have no significant effect on the myotube viability on all cell lines tested (p >0.01) compared to the control over the three days treatment.

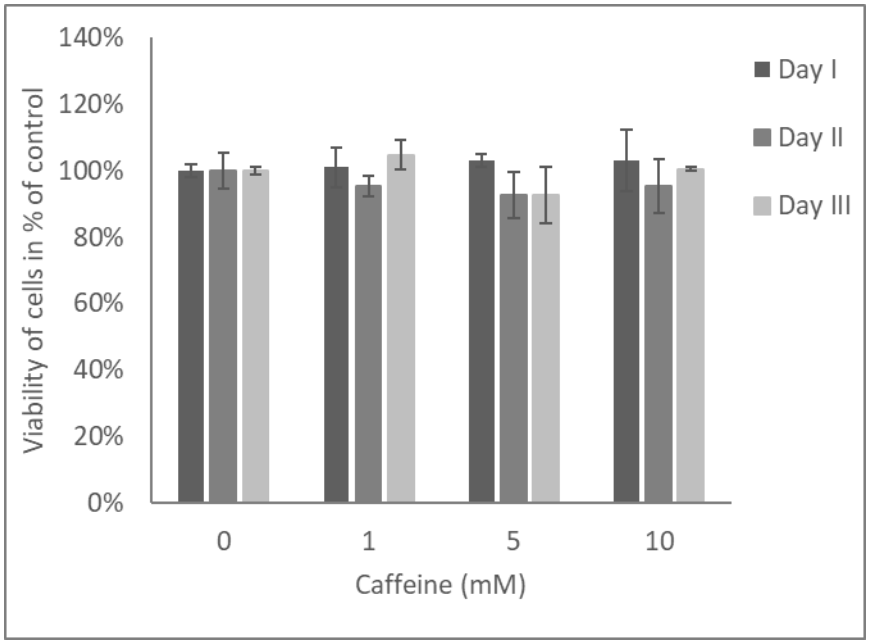

Figure 21: Effect of caffeine on viability of C2C12. No significant effect (p >0.01) of three days doses of caffeine on C2C12 myotubes viability measured by AlamarBlue. Results are presented are mean ± *SD*. (N =5)

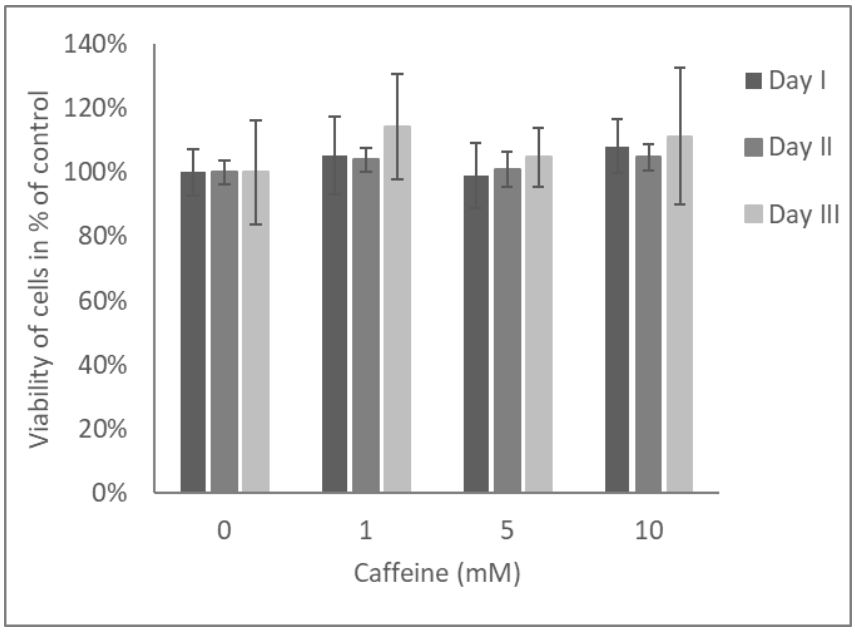

Figure 22: Effect of caffeine on viability of L6. No significant effect (p >0.01) of three days doses of caffeine on L6 myotubes viability measured by AlamarBlue. Results are presented are mean ± *SD*. (N =5)

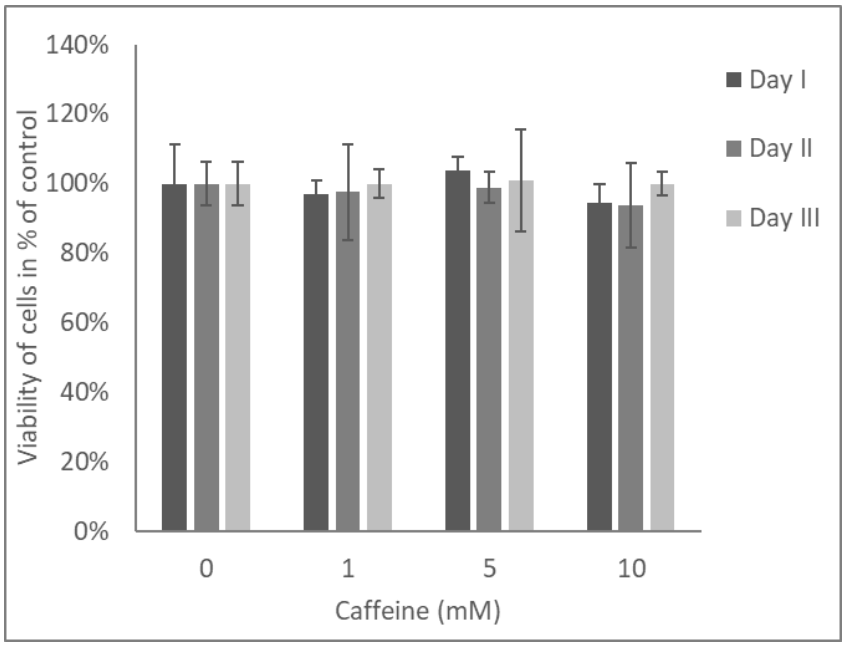

Figure 23: Effect of caffeine on viability of HSMM. No significant effect (p > 0.01) of three days doses of caffeine on HSMM myotubes viability measured by AlamarBlue. Results are presented are mean ± *SD*. (N =5)

3.3.2.3. Effect of caffeine on myotubes bioenergetics

Skeletal muscle cells are designed to manage energy metabolism between mitochondrial respiration and glycolysis systems to cover energy demand, depending on the work load exerted on them. Therefore, the effect of caffeine on both systems was tested and shown in Figure 24 and Figure 25. All caffeine concentrations used (1 mM, 5 mM and 10 mM) did not show any significant changes in mitochondrial respiration for both C2C12 and L6 (p >0.01, using *t*-test). Only, 5 mM caffeine, significantly decreased the maximum respiration and relative ATP level in C2C12 myotubes (p <0.01 using *t*-test). The significance was confirmed using one-way ANOVA.

Although no significant impact on mitochondrial bioenergetics was observed, caffeine affected the myotube glycolysis. Caffeine treatment showed a dose-dependent decrease in both relative glycolytic capacity and glycolytic reserve for both C2C12 and L6 myotubes, reaching significance at higher caffeine concentrations (p <0.01), as shown in Figure 26 and Figure 27. Same results were found using both *t*-test and one-way ANOVA.

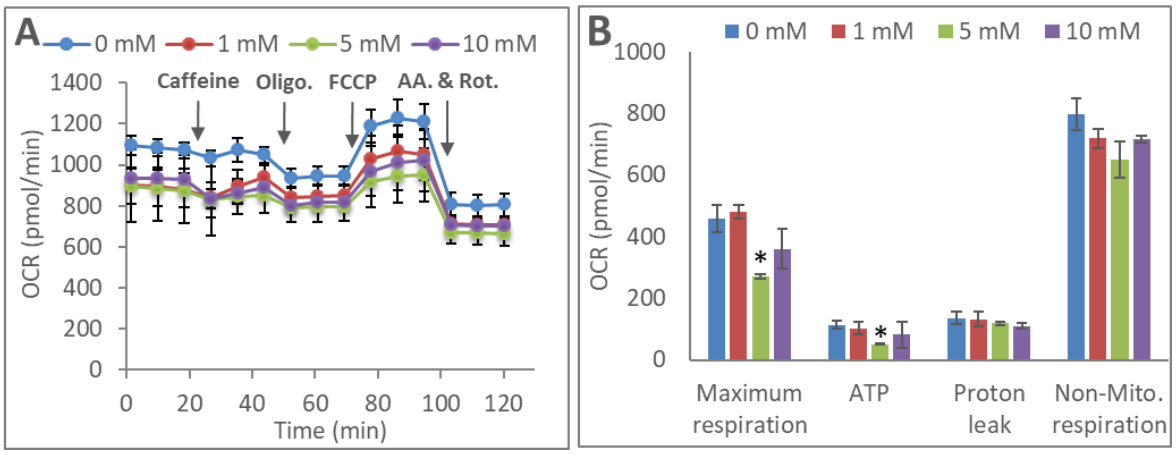

Figure 24: Effect of caffeine on mitochondrial respiration of C2C12 myotubes. A. A representative experiment graph output from XF24 showing (OCR, pmol/min) response to caffeine, oligomycin, FCCP and rotenone and antimycin A; **B.** The effect of caffeine on maximum respiration, ATP production, proton leak and non-mito. respiration. C2C12 treated with 5 mM significantly reduced maximum respiration and relative ATP production when compared to control. (* p <0.01, Mean ± SD of N = 5)

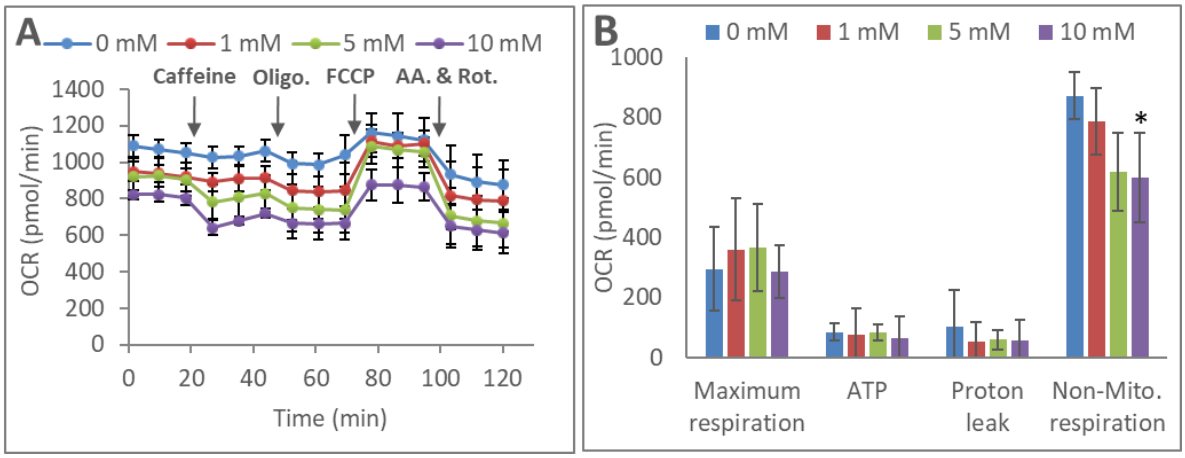

Figure 25: Effect of caffeine on mitochondrial respiration of L6 myotubes. A. A representative experiment graph output from XF24 showing (OCR, pmol/min) response to caffeine, oligomycin, FCCP and rotenone and antimycin A; **B.** The effect of caffeine on

maximum respiration, ATP production, proton leak and non-mito. respiration. Caffeine did not show significant changes on mitochondrial respiration. (* p <0.01, Mean ± *SD* of N = 5)

Table 2: Effect of immediate caffeine treatment on mitochondrial respiratory parameters in C2C12 myotubes. Results are presented as mean of 5 replicates ± *SD* measured in pmol (O_2)/min.

Parameter	0 mM	1 mM	5 mM	10 mM
Proton Leak	131 ± 23	134 ± 20	125 ± 14	98 ± 12
Maximal Respiration	427 ± 63	357 ± 103	284 ± 72	318 ± 124
Spare Respiratory Capacity	181 ± 74	123 ± 84	95 ± 48	132 ± 95
Non Mito Respiration	802 ± 51	708 ± 37	664 ± 61	703 ± 32
ATP Production	113 ± 13	99 ± 18	63 ± 20	87 ± 44

Table 3: Effect of immediate caffeine treatment on mitochondrial respiratory parameters in L6 myotubes. Results are presented as mean of 5 replicates ± *SD* measured in pmol (O_2)/min.

Parameter	0 mM	1 mM	5 mM	10 mM
Proton Leak	108 ± 123	51 ± 66	72 ± 25	50 ± 80
Maximal Respiration	284 ± 96	328 ± 141	419 ± 85	263 ± 174
Spare Respiratory Capacity	98 ± 95	203 ± 48	258 ± 66	155 ± 88
Non Mito Respiration	875 ± 136	787 ± 169	666 ± 134	613 ± 112
ATP Production	77 ± 23	73 ± 88	88 ± 31	58 ± 75

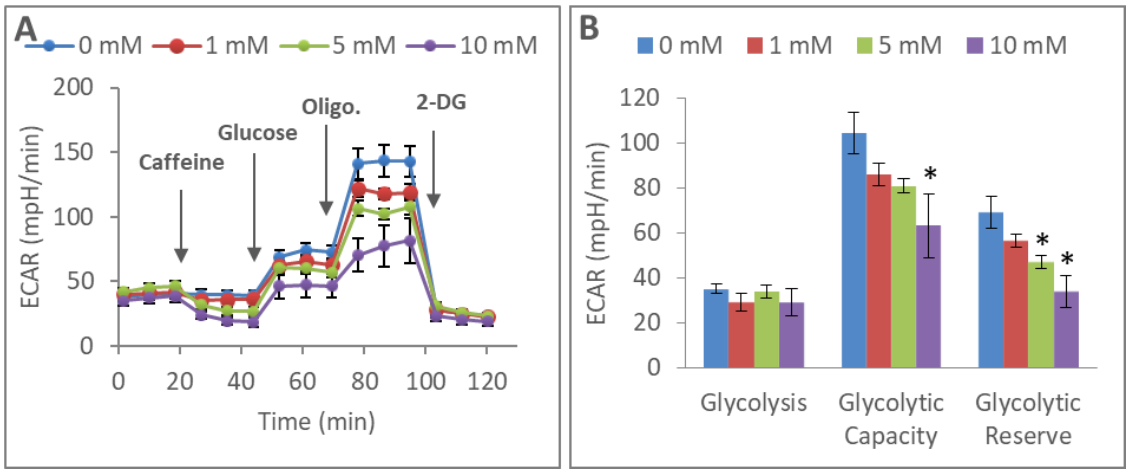

Figure 26: Immediate caffeine treatment affect glycolysis of C2C12 myotubes. A. A representative graph from XF24 showing the ECAR (mpH/min) response to caffeine, glucose, oligomycin and 2-DG; **B.** The effect of caffeine on glycolysis, glycolytic capacity and glycolytic reserve. Glycolytic capacity and reserve significantly decreased with higher caffeine concentrations when compared to control. (* p <0.01, mean ± SD of N =5)

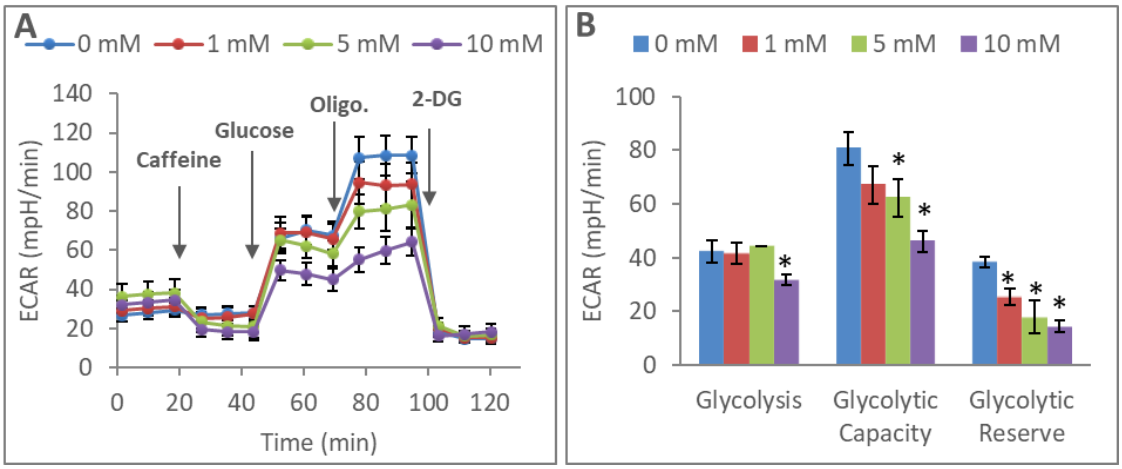

Figure 27: Caffeine showed dose dependent decrease in Glycolysis stress test of L6 myotubes. A. A representative graph from XF24 showing the ECAR (mpH/min) response to caffeine, glucose, oligomycin and 2-DG; **B.** The effect of caffeine on Glycolysis, Glycolytic capacity and Glycolytic reserve. 10 mM significantly decreased glycolysis, and both glycolytic capacity and reserve significantly decreased with higher caffeine concentrations compared to control. (* p <0.01, mean ± SD of N =5)

3.3.2.4. Caffeine induces intracellular ROS production in skeletal muscle cells measured by DCFH assay

Myotubes were treated with caffeine for 2 hours for 3 consecutive days. After each day, the ability of caffeine treatment to induce intracellular ROS was measured using DCFH assay, results shown on Figure 28-A and B. In both C2C12 and L6 myotubes, treatment with 1 mM caffeine did not affect cellular redox homeostasis compared to control ($p > 0.01$) throughout the three days, except for HSMM. Even though treatment with 1 mM did not affect ROS signal in HSMM after 24 hours, on the second and third day of treatment ROS signal significantly increased ($p < 0.01$) compared to control and compared to ROS signal after treatment with 1 mM on the first day. L6 myotubes were found to be more susceptible to caffeine induced oxidative stress compared to C2C12 myotubes, as there was a significant increase ($p < 0.01$) in ROS signal after second day of treatment with highest concentration (10 mM), and after the third day with both 5 mM and 10 mM compared to the control as well as compared to the same treatment on the first day. Similarly, caffeine induced dose and time dependent increase in intracellular ROS in C2C12 myotubes but it reached significance only after the third day of treatment with the highest caffeine concentration, by approximately 300% increase. On the other hand, HSMM myotubes showed slightly different response Figure 28-C. Higher concentrations 5 mM and 10 mM of caffeine did not show significant changes on ROS level in all three days of treatment.

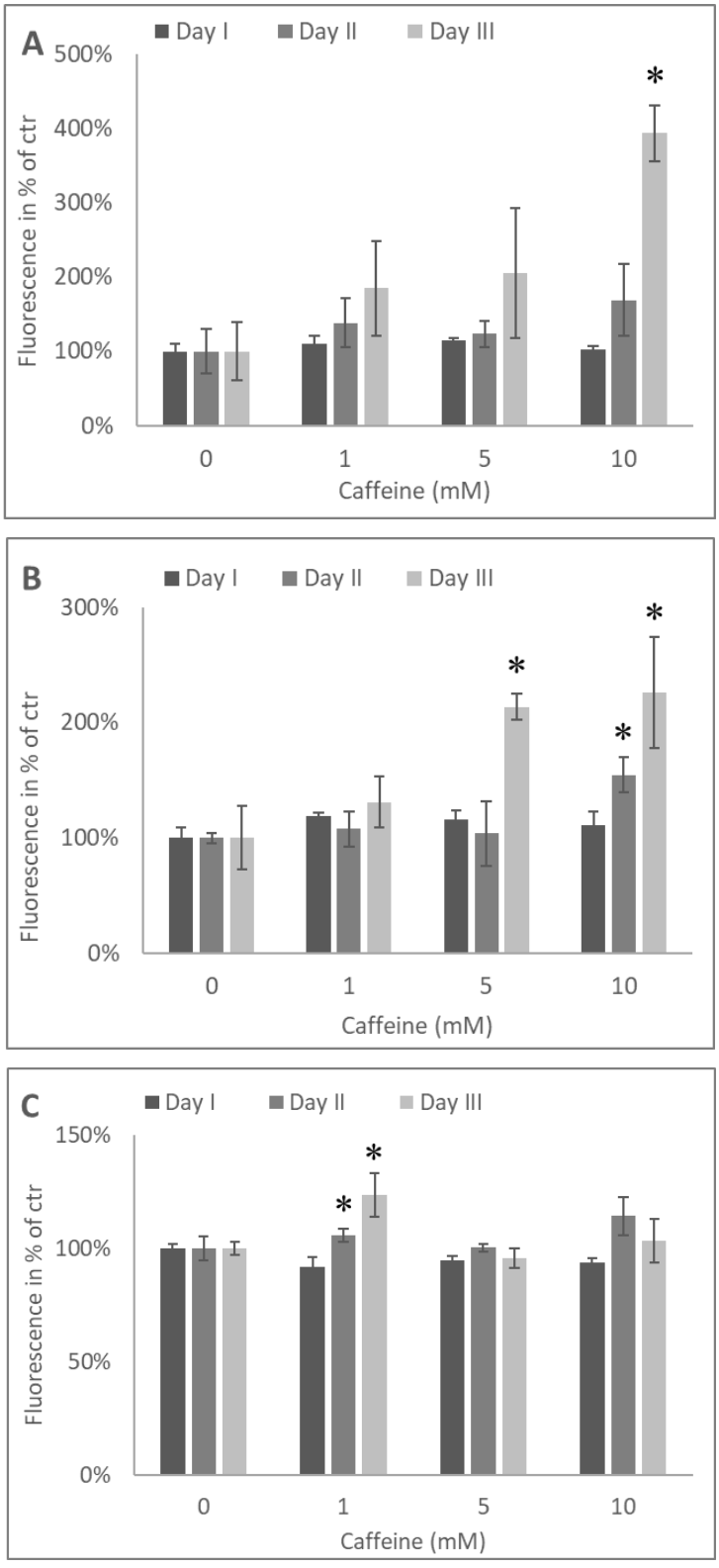

Figure 28: Caffeine induces intracellular ROS production in skeletal muscle myotubes measured by DCFH.

A. C2C12 myotubes induced by caffeine showed significant increase in ROS production only on after third day of treatment with the highest caffeine concentration 10 mM.

B. L6 treated with caffeine significantly increased ROS signal with 10 mM after second day. As well as with 5 mM and 10 mM caffeine treatments after third day. **C.** HSMM significantly increased ROS signal with 1 mM caffeine in second and third day compared to day I. (* p <0.01) (Results are presented as percentage of control myotubes, mean ± *SD* of N =4).

3.3.2.5.Caffeine induces superoxide production in myotubes measured by DHE

The immediate effect of caffeine on myotube superoxide production was measured continuously for 4 hours using DHE redox sensitive fluorescent probe. The first point measurement is the base line before addition of caffeine, followed by immediate addition of caffeine. The lowest 1 mM caffeine concentration, significantly (p <0.01) increased the superoxide production in the C2C12 myotubes after the 4 hours of incubation, when compared to control myotubes (Figure 29). The same concentration did not have significant increase on superoxide production in L6 (Figure 30) and HSMM (Figure 31) myotubes (p >0.01 for both). Higher caffeine concentrations, 5 mM and 10 mM, stimulated superoxide production in a time and dose dependent manner and were significantly increased after 4 hours of the treatment (p <0.01) in all three, C2C12, L6 and HSMM myotubes tested.

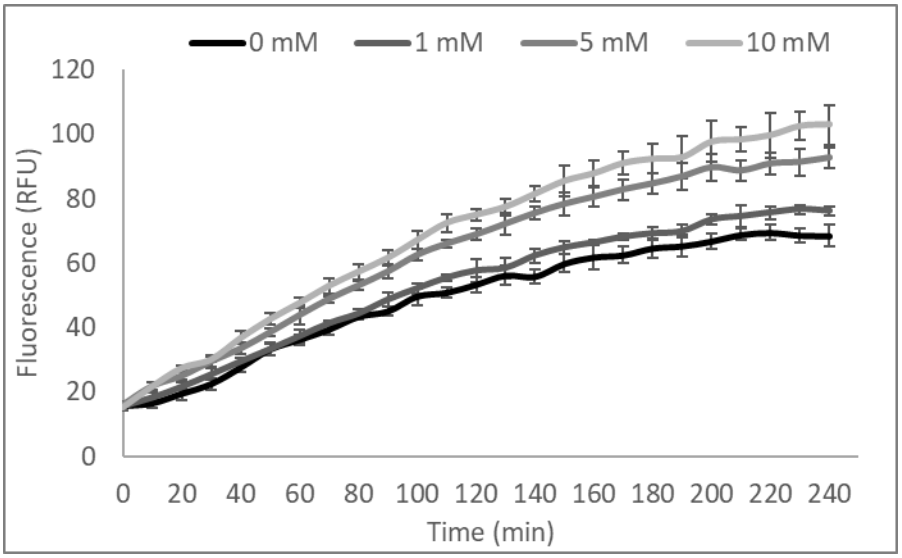

Figure 29: Caffeine induces superoxide production in C2C12 myotubes. All caffeine concentrations (1 , 5 and 10 mM) significantly increased superoxide production over 4 hours of treatment when compared to control myotubes. (p <0.01) (Results are mean ± *SD* of N =4).

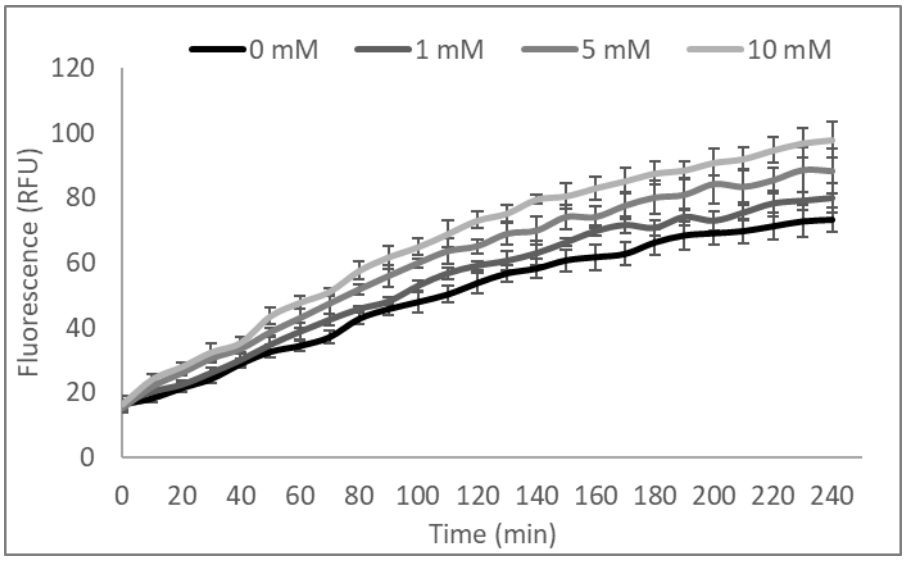

Figure 30: Caffeine induces superoxide production in L6 myotubes. Kinetic measurement of the immediate effect of caffeine on superoxide production over 4 hours showed a significant increase in superoxide production with 5 mM and 10 mM. (p <0.01) (Results are mean ± *SD* of N =4).

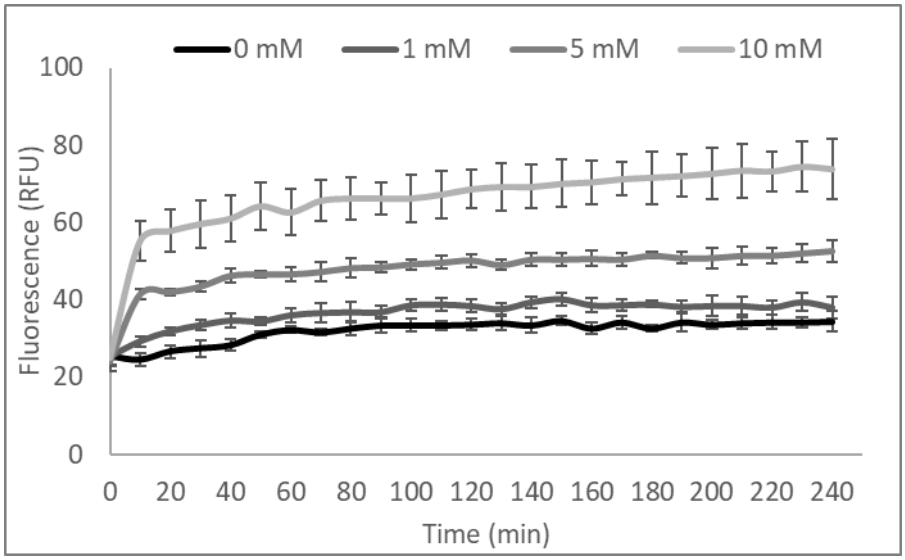

Figure 31: Caffeine induces superoxide production in HSMM myotubes. Higher caffeine concentrations 5 mM and 10 mM significantly increased superoxide production measured over 4 hours. (p <0.01) (Results are mean ± *SD* of N =4).

3.3.2.6. Caffeine induces lipid peroxides formation in myotubes

The effect of caffeine on the induction of lipids peroxidation measured by ratio of oxidized/ non-oxidized signal using BODIPY$^{581/591}$ was examined. After the first day of treatment, C2C12 myotubes were found to be more susceptible to caffeine treatment, where 5 mM and 10 mM significantly (p <0.01) increased lipid peroxidation level (Figure 32). There was no effect on L6 myotube lipid peroxidation level after first day of caffeine treatment compared to control myotubes, (Figure 33, p >0.01). Results of HSMM showed a significant increase in lipid peroxidation only with 10 mM caffeine after first day of treatment, (Figure 34**,** p >0.01). On the second day of the treatment similar trend was found for both C2C12 and L6 myotubes, where higher caffeine concentrations (5 and 10 mM) significantly increased (p <0.01) lipid peroxidation by more than 20% compared to the control on the same day and compared to the same concentration on the first day of treatment.

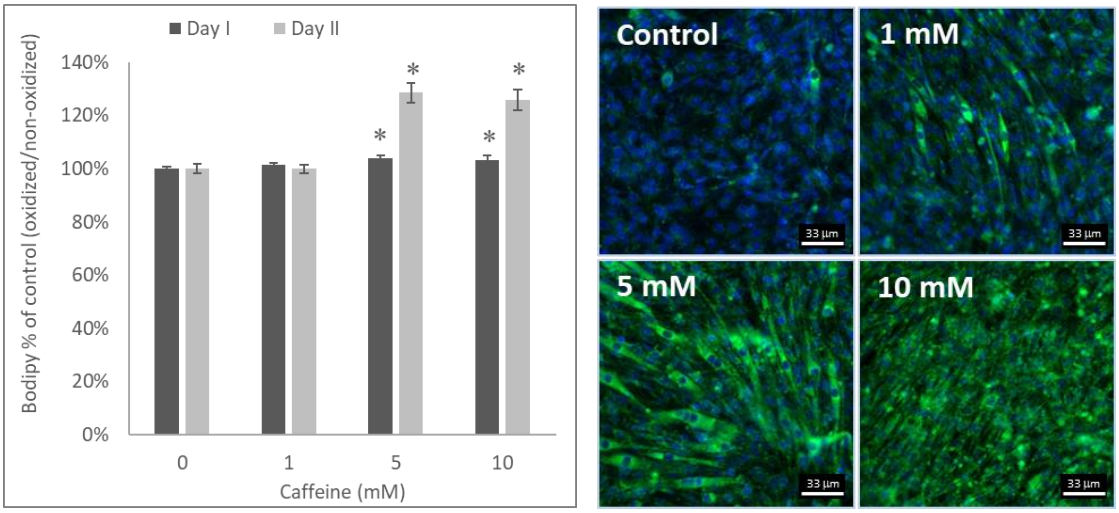

Figure 32: Caffeine induces lipid peroxidation in C2C12 myotubes. Myotubes treated with 5 mM and 10 mM significantly increased LPO in first and second day treatment compared to control of the same day. ArrayScan images are taken after second day of treatment shows a clear increases in oxidized lipids (green signal) with increasing caffeine concentrations. (* p <0.01) (Results are mean ± *SD* of N =4).

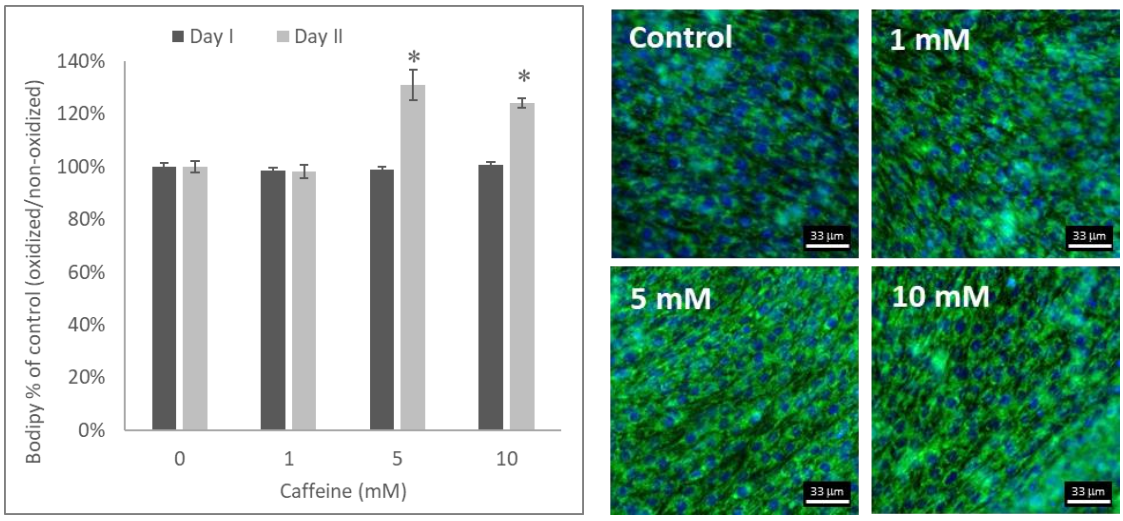

Figure 33: Caffeine induces lipid peroxidation in L6 myotubes. Concentrations 5 and 10 mM significantly increased LPO after second day treatment compared to control. Images taken after second day shows the oxidized lipid (green color). (* p <0.01) (Results are mean ± *SD* of N =4).

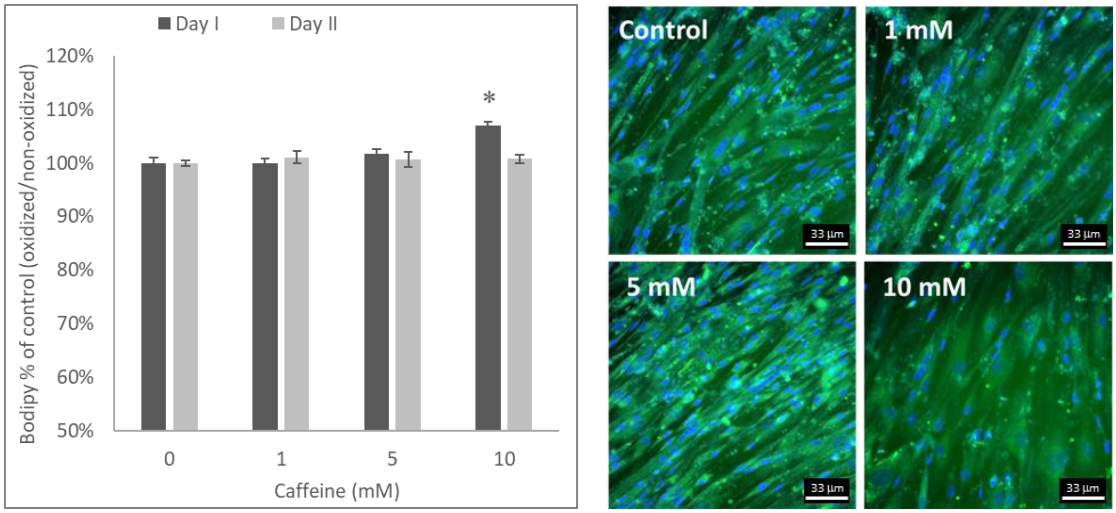

Figure 34: Effect of caffeine on lipid peroxides production in HSMM myotubes. Caffeine induces lipid peroxidation significantly with 10 mM after first day of treatment compared to control. in myotubes. Images are showing myotubes treated with different caffeine concentrations taken after the first day of treatment. (* p <0.01) (Results are mean ± *SD* of N =4).

3.3.2.7. Caffeine induced 4-HNE modification of protein

The direct effect of caffeine on 4-HNE formation is identified by measuring the effect of caffeine on 4-HNE protein adducts, shown in Figure 35. The lowest caffeine concentration (1mM) had no significant effect on the formation of 4-HNE-protein adducts ($p > 0.05$, compared to control cells). Contrary, higher concentrations of caffeine (5 and 10 mM) significantly increased ($p < 0.05$) 4-HNE protein adducts formation in both C2C12 and L6 myotubes when compared to control cells.

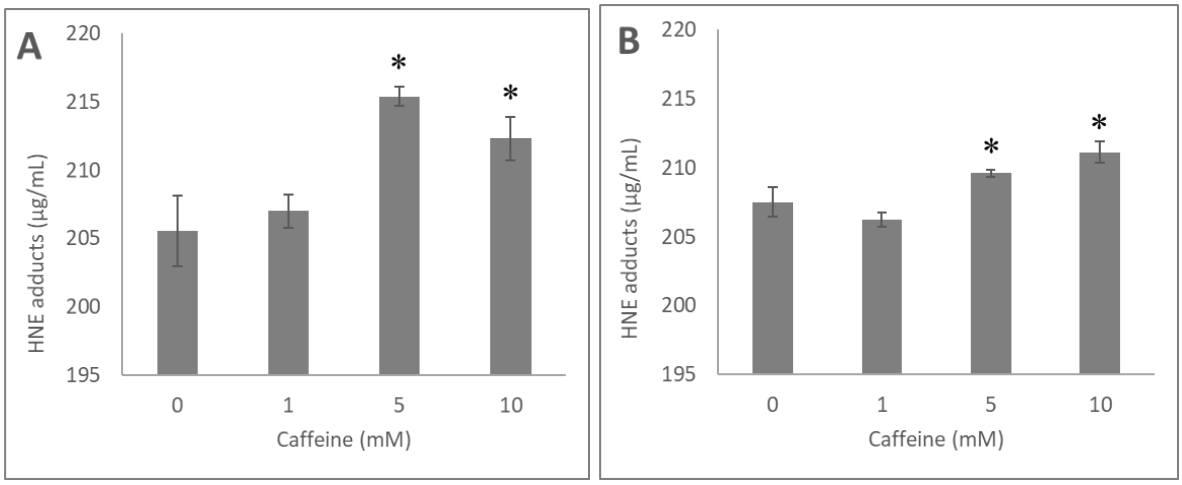

Figure 35: Measuring effect of caffeine on the formation of 4-HNE protein adducts. Both cell lines **A.** C2C12 myotubes and **B.** L6 myotubes had significantly increased levels of 4-HNE adducts when treated with higher caffeine concentrations (5 and 10 mM) compared to control myotubes. ($p < 0.05$) (The results presented are mean ± *SD* of $N = 9$).

3.3.3. Effect of caffeine on mitochondrial genes

The ability of caffeine to induce mitochondrial genes regulation was tested. Myotubes were treated with caffeine for three consecutive days, 2 hours per day. Upregulated and downregulated genes in the treated groups are compared with those of control group. Results showed that treatment with 1 mM caffeine had the major effect on regulation of genes, with 33 genes downregulated, and had no effect on upregulating any gene (Figure 37). Treating myotubes with 5 mM and 10 mM caffeine had minor changes in regulation of mitochondrial genes. Where 5 mM upregulated one gene that is involved in mitochondrial proteins import (Cav2), and downregulated 5 genes (Grpel1, Pmaip1, Aip, Aifm2 and Rnf135) (Figure 38). Treating myotubes with 10 mM upregulated 4 genes (Cav2, Mipep, and Timm10b that are involved in mitochondrial proteins import and Slc25a12 that is involved in small molecules transport) and downregulated 3 genes (Aip, Grpel1 and Pmaip) (Figure 39). Gene that was commonly upregulated with both 5 mM and 10 mM is one gene that is involved in coding mitochondrion protein import (Cav2). Genes that were commonly downregulated in all treatments (1 mM, 5 mM and 10 mM) are genes involved in mitochondrial transport, targeting proteins to mitochondria and mitochondria protein import (Aip and Grpel1), and a gene involved in apoptosis (Pmaip). Genes that were commonly downregulated in 1 mM and 5 mM were two genes: one involved in apoptosis (Aifm2) and one involved in mitochondrial localization (Rnf135).

Furthermore, treating myotubes with 1 mM caffeine had minor changes in regulation of mitochondrial metabolism genes, with only two downregulated genes that are involved in complex III (Uqcrq and Uqcr11) (Figure 41). Both 5 mM and 10 mM upregulated one gene that is involved in complex III (Uqcrc2). Treatment of myotubes with 5 mM caffeine downregulated

a total of 12 mitochondrial metabolism genes (Figure 42), and 10 mM downregulated a total of 16 genes (Figure 43). The genes that were commonly downregulated in both treatments were 8 genes that are involved in complex V (Atp5f1, Atp5b, Atp5d, Atp5g3, Atp5g1, and Atp5c1) and in complex IV (Cox4i1 and Cox6c).

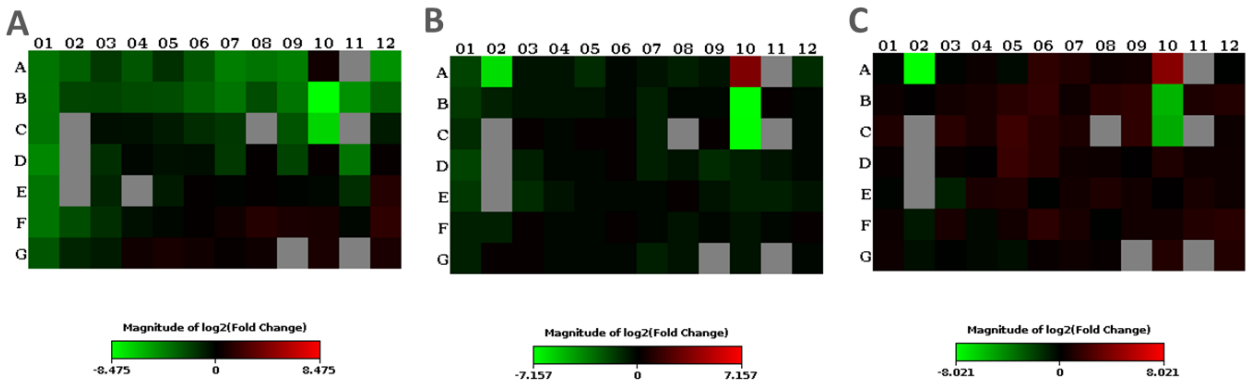

	1	2	3	4	5	6	7	8	9	10	11	12
A	Aifm2	Aip	Akt1	Bak1	Bbc3	Bcl2	Bcl2l1	Bid	Bnip3	Cav2	Cdkn2a	Cln8
B	Cox18	Cpt1b	Cpt2	Dnm1l	Fis1	Timm10b	Gclc	Gclm	Gpx1	Grpel1	Hsp90aa1	Hspd1
C	Immp1l	LOC6918	Mfn1	Mfn2	Mipep	Msto1	Mtx2	Nefl	Opa1	Pmaip1	Ppargc1a	Rhot2
D	Rnf135	Sfn	Sh3glb1	Slc25a10	Slc25a12	Slc25a13	Slc25a14	Slc25a15	Slc25a16	Slc25a17	Slc25a19	Slc25a2
E	Slc25a20	Slc25a21	Slc25a22	Slc25a23	Slc25a24	Slc25a25	Slc25a27	Slc25a3	Slc25a30	Slc25a36	Slc25a37	Slc25a4
F	Slc25a5	Sod1	Sod2	Stard3	Taz	Timm10	Timm17a	Timm17b	Timm22	Timm44	Timm8a1	Timm8b
G	Timm9	Tomm22	Tomm34	Tomm40	Tomm40l	Tomm70a	Tp53	Tspo	Ucp1	Ucp2	Ucp3	Uxt

Figure 36: Effect of 4-HNE on the gene expression of mitochondrial genes in L6 myotubes. Heat map showing downregulated genes in green, unchanged in black and upregulated in red. The symbol and location of each gene in the heat map is shown in the table under the heat maps, which is the plate layout. The effect of caffeine **A.** 1 mM vs. control, **B.** 5 mM vs. control and **C.** 10 mM vs. control on the regulation of genes expression. (Results are in averages of triplicates)

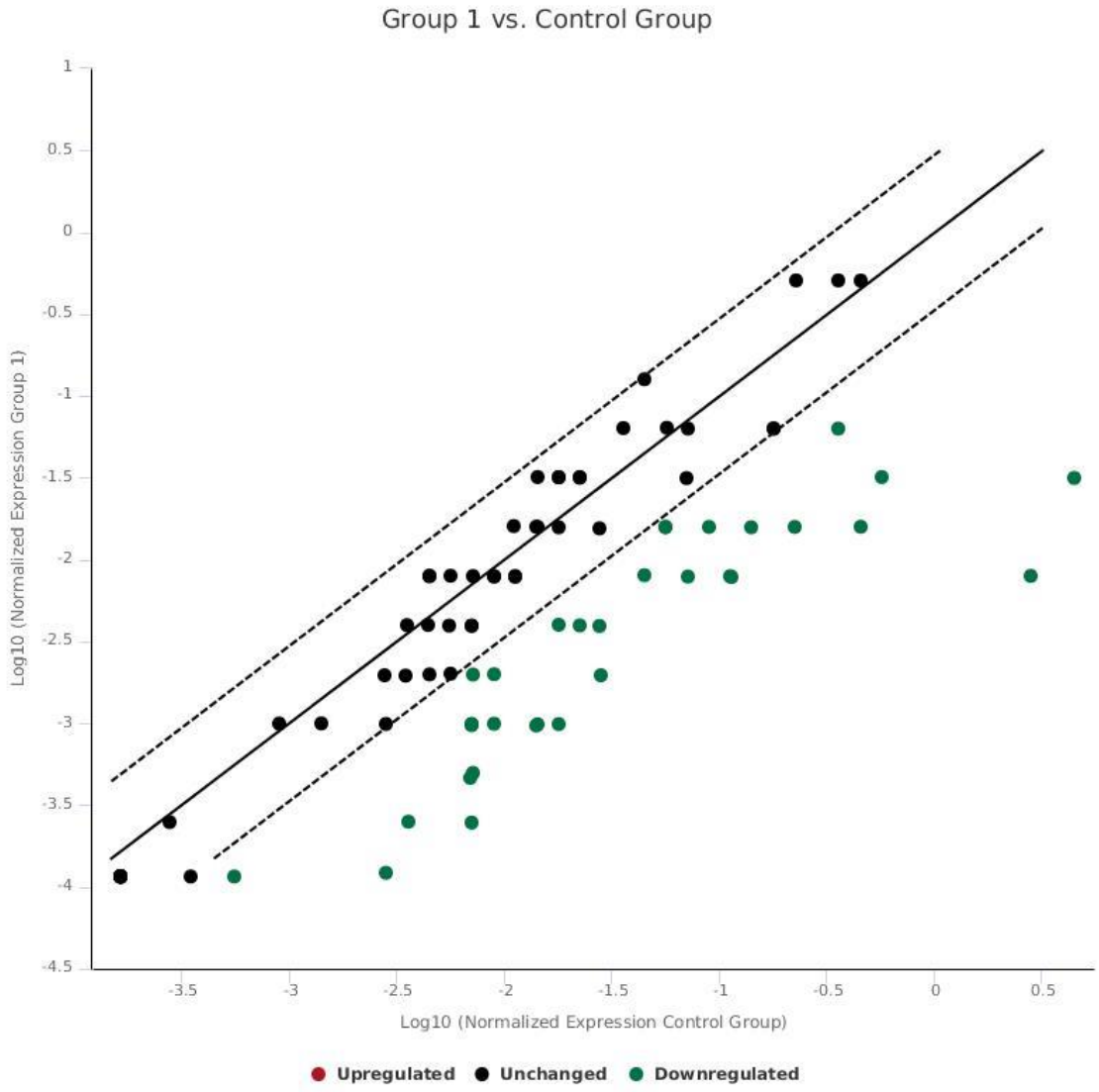

Figure 37: Expression of mitochondria genes in control L6 myotubes compared to treated with 1 mM caffeine. Scatter plot shows the treatment group 1 in y-axis against the control group in x-axis. The dotted line indicate 3 fold-regulation. Green dots are downregulated genes.

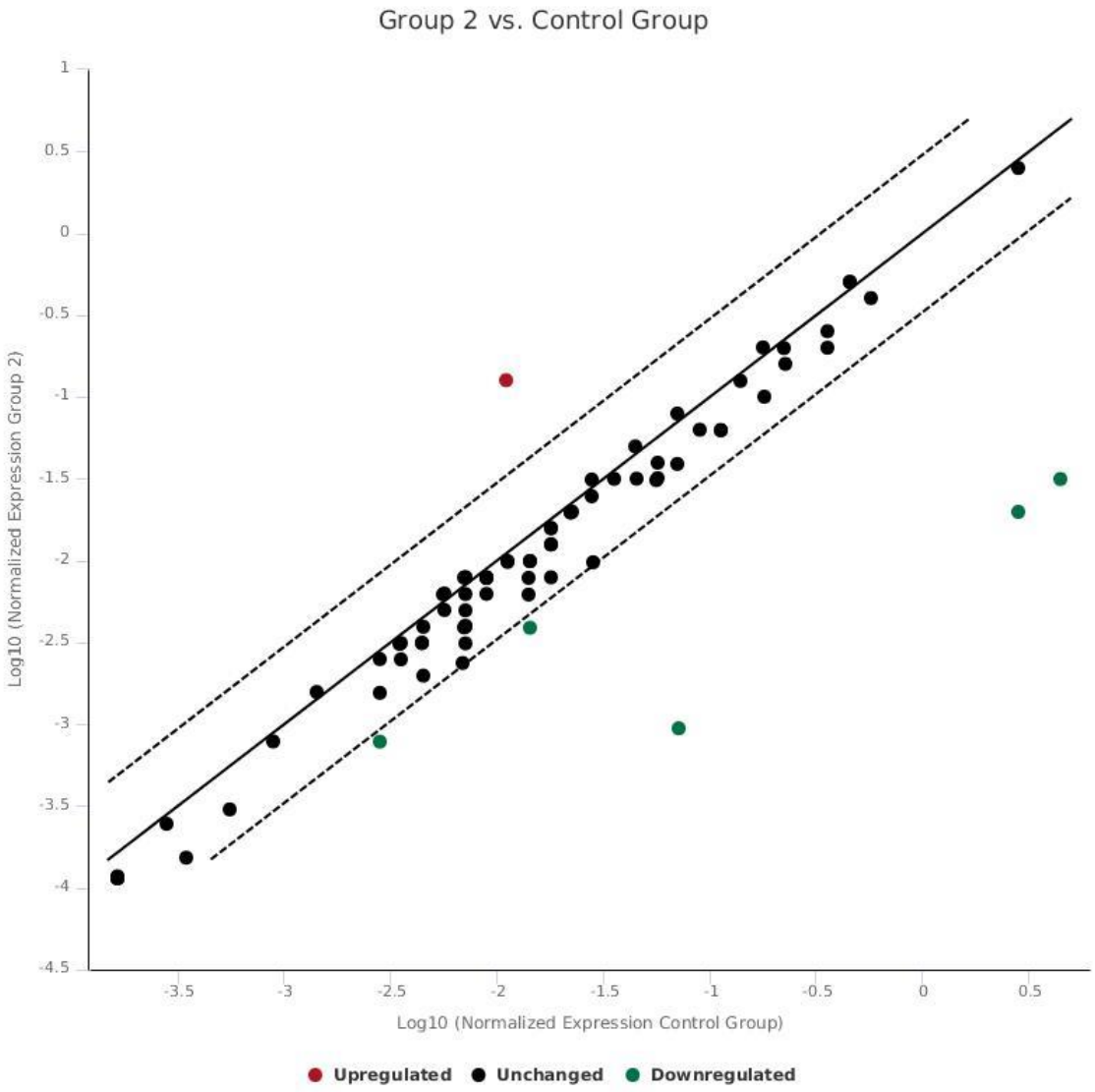

Figure 38: Expression of mitochondria genes in control L6 myotubes compared to treated with 5 mM caffeine. Scatter plot shows the treatment group 2 in y-axis against the control group in x-axis. The dotted line indicate 3 fold-regulation. Green dots are downregulated genes and red dots are upregulated genes.

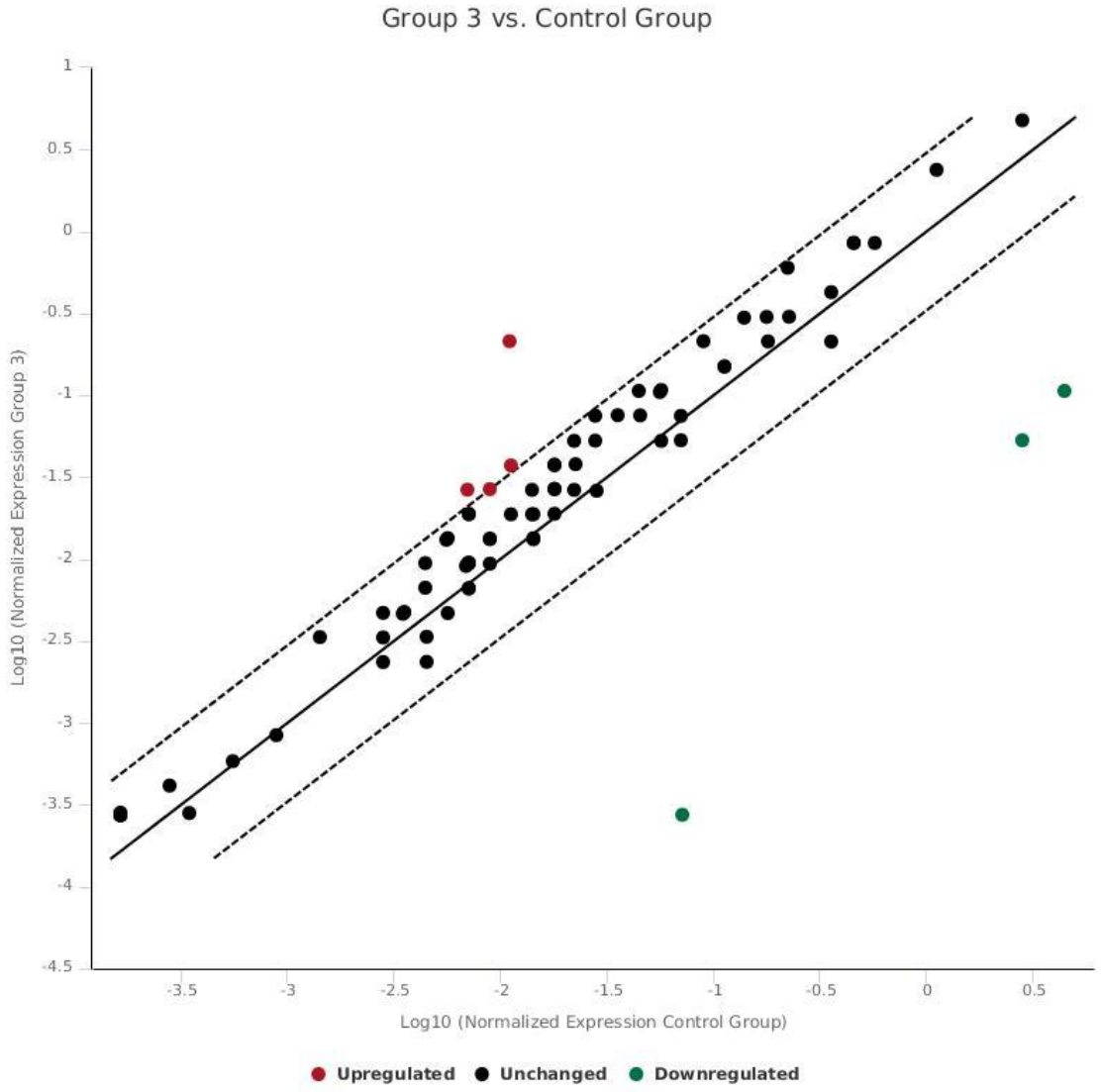

Figure 39: Expression of mitochondria genes in control L6 myotubes compared to treated with 10 mM caffeine. Scatter plot shows the treatment group 3 in y-axis against the control group in x-axis. The dotted line indicate 3 fold-regulation. Green dots are downregulated genes and red dots are upregulated genes.

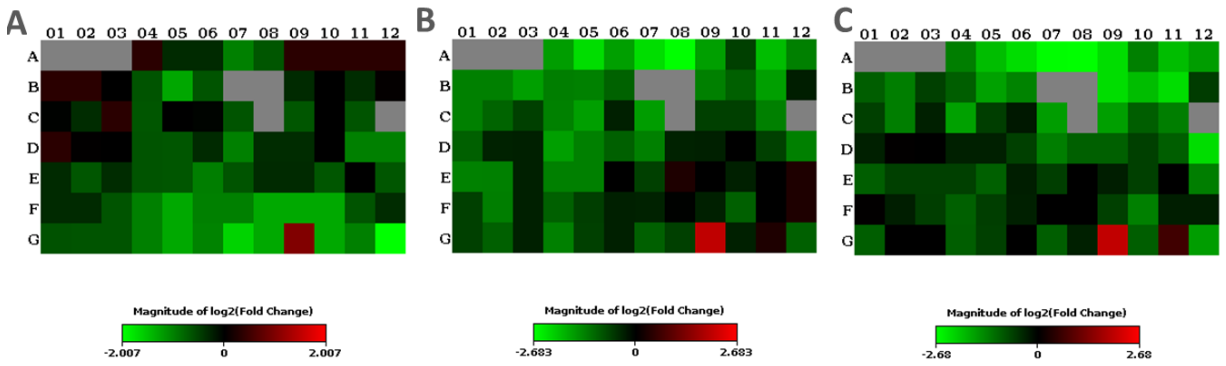

	1	2	3	4	5	6	7	8	9	10	11	12
A	Atp12a	Atp4a	Atp4b	Atp5a1	Atp5b	Atp5c1	Atp5d	Atp5f1	Atp5g1	Atp5g2	Atp5g3	Atp5h
B	Atp5j	Atp5j2	Atp5o	Atp6v0a2	Atp6v0d2	Atp6v1c2	Atp6v1e2	Atp6v1g3	Bcs1l	Cox11	Cox4i1	Cox4i2
C	Cox5a	Cox5b	Cox6a1	Cox6a2	Cox6b1	Cox6b2	Cox6c	Cox7a2	Cox7a2l	Cox7b	Cox8a	Cox8c
D	Cyc1	Lhpp	Ndufa1	Ndufa10	Ndufa11	Ndufa2	Ndufa3	Ndufa4	Ndufa5	Ndufa6	Ndufa7	Ndufa8
E	Ndufab1	Ndufb10	Ndufb2	Ndufb3	Ndufb4	Ndufb5	Ndufb6	Ndufb7	Ndufb8	Ndufb9	Ndufc1	Ndufc2
F	Ndufs1	Ndufs2	Ndufs3	Ndufs4	Ndufs5	Ndufs6	Ndufs7	Ndufs8	Ndufv1	Ndufv2	Ndufv3	Oxa1l
G	Ppa1	Ppa2	Sdha	Sdhb	Sdhc	Sdhd	Uqcr11	Uqcrc1	Uqcrc2	Uqcrfs1	Uqcrh	Uqcrq

Figure 40: Effect of 4-HNE on the gene expression of mitochondrial energy metabolism genes in C2C12 myotubes. Heat map showing downregulated genes in green, unchanged in black and upregulated in red. The symbol and location of each gene in the heat map is shown under the heat maps, which is the plate layout. The effect of caffeine **A.** 1 mM vs. control, **B.** 5 mM vs. control and **C.** 10 mM vs. control on the regulation of genes expression. (Results are in averages of triplicates)

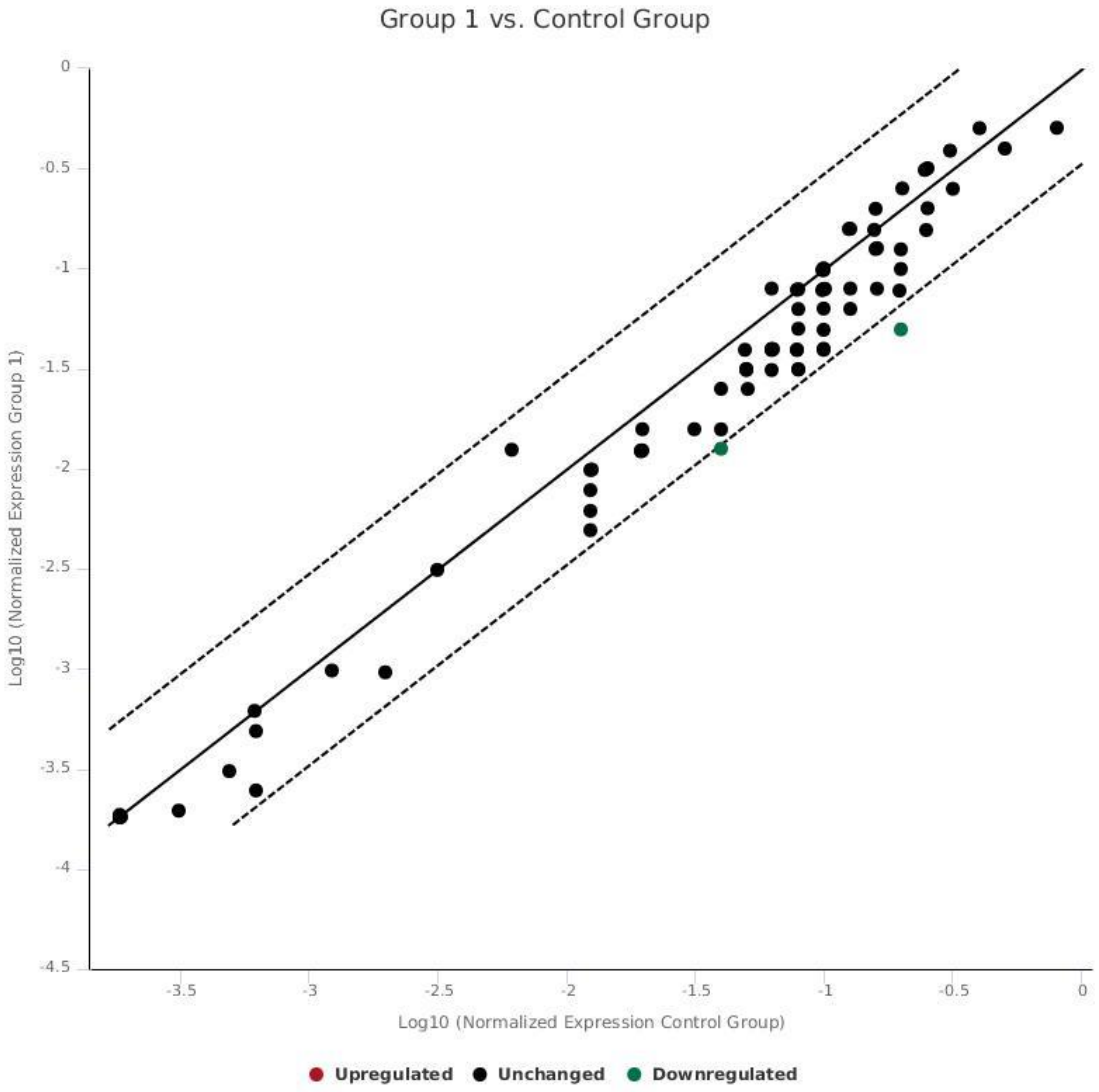

Figure 41: Expression of mitochondrial energy metabolism genes in control C2C12 myotubes compared to myotubes treated with 1 mM caffeine. Scatter plot shows the treatment group 1 in y-axis against the control group in x-axis. The dotted line indicate 3 fold-regulation. Green dots are downregulated genes.

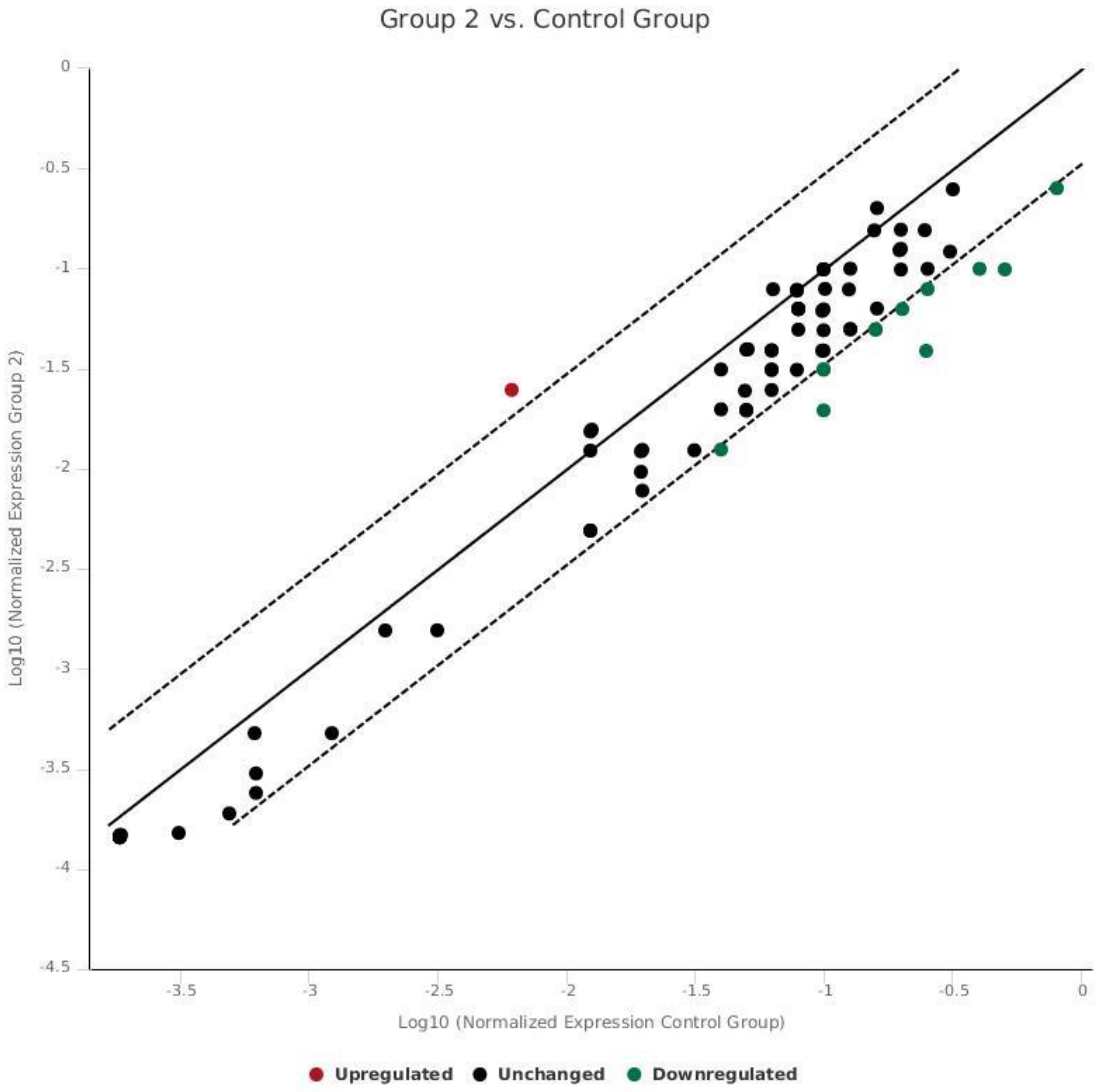

Figure 42: Expression of mitochondrial energy metabolism genes in control C2C12 myotubes compared to myotubes treated with 5 mM caffeine. Scatter plot shows the treatment group 2 in y-axis against the control group in x-axis. The dotted line indicate 3 fold-regulation. Green dots are downregulated genes and red dots are upregulated genes.

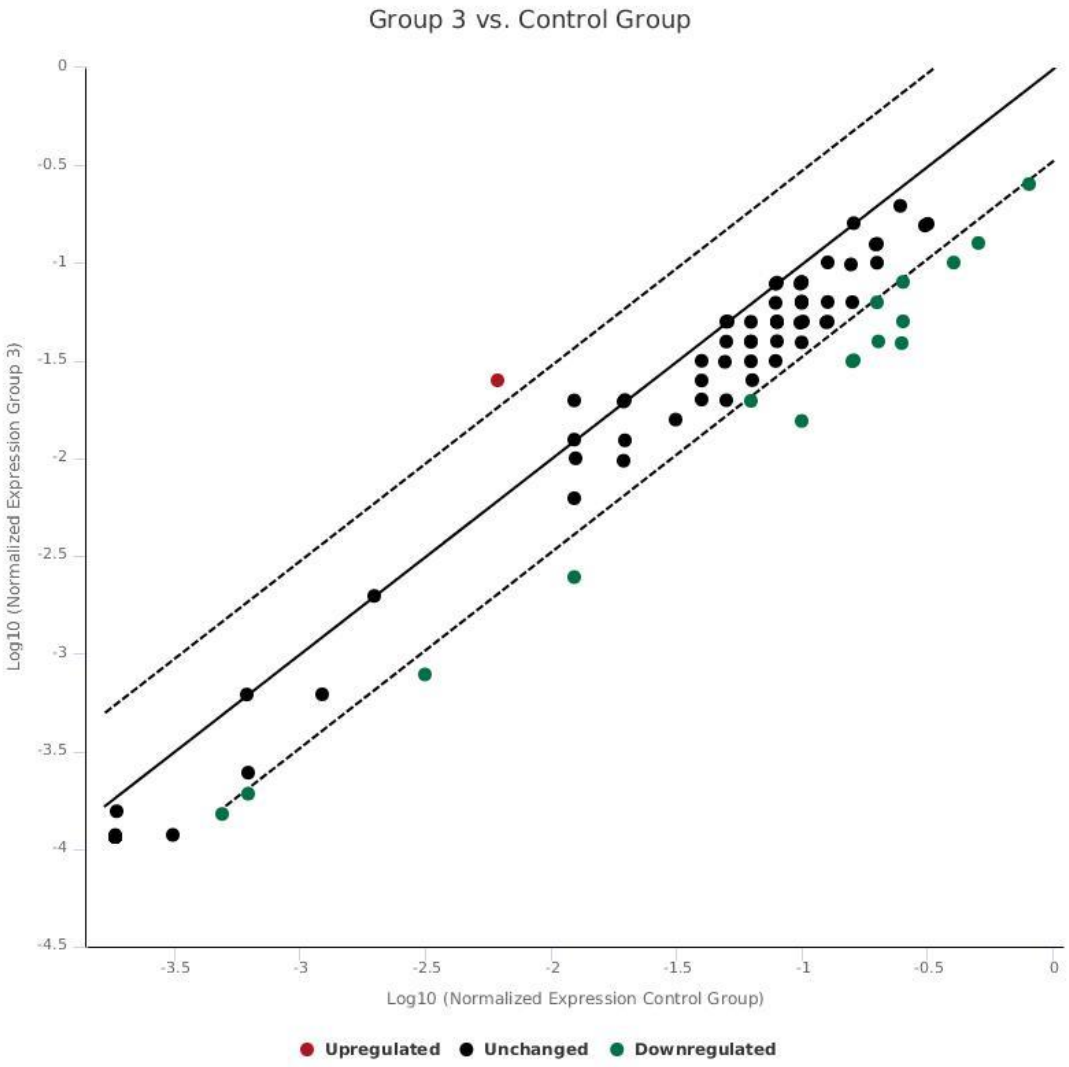

Figure 43: Expression of mitochondrial energy metabolism genes in control C2C12 myotubes compared to myotubes treated with 10 mM caffeine. Scatter plot shows the treatment group 3 in y-axis against the control group in x-axis. The dotted line indicate 3 fold-regulation. Green dots are downregulated genes and red dots are upregulated genes.

3.4. Discussion

Caffeine stimulates an increase of cytosolic calcium by evoking calcium transient (Usachev *et al.*, 1993), resulting in the increase of some of the key factors of mitochondrial biogenesis including increased NRF-1 and NRF-2, TFAM and PGC-1α contents, same factors which are stimulated by contractile activity (Ljubicic *et al.*, 2010). Thus, in the current work caffeine was used to mimic physical exercise. It is important that caffeine concentrations used are stimulating the physiological calcium signaling without turning into pathological stimuli. Studies have shown that caffeine concentrations between 1 mM to 10 mM can induce enough Ca^{2+} release from reticulum to trigger contractions of muscles isolated from frog (Weber and Herz, 1968) or to induce contracture of rat ventricular muscles (Konishi *et. al.*, 1984). In the current work, different caffeine concentrations were tested to find adequate contractility response of *in-vitro* differentiated skeletal muscle myotubes. The Ca^{2+} signaling experiment results demonstrated that 1 mM caused only one slight oscillatory response over 18 min. Similarly, an early study by Endo *et al.* (1970), showed that low caffeine concentrations in rage of 0.5 – 2 mM evoked a transient contraction that is below the threshold for contraction. Higher caffeine concentration (5 mM) induced several small oscillations. The increased Ca^{2+} signal with both 1 mM and 5 mM was immediately regulated by calcium pumps to restore basal calcium level. Controlling calcium release and removal is essential for muscle contraction and relaxation. Calcium release in skeletal muscle is mainly regulated by the activity of RyR channels, where Ca^{2+} ions are released from the SR upon activation (Gehlert, *et. al.*, 2015), while Ca^{2+} ions removal is mainly regulated by three pumps: SERCA, plasma membrane ATPase (PMCA) and the Na^{+}/Ca^{2+}-exchanger (NCX1) (Gehlert, *et al.*, 2015). On the other hand 10 mM caffeine induced massive Ca^{2+} influx that is beyond the regulation capacity of calcium pumps, where

Ca^{2+} signal was not recovered after the massive increase. Inability to regulate the Ca^{2+} level, or destruction in the calcium pumps are associated with plethora of muscle diseases (Missiaen *et al.*, 2000). To investigate pathophysiological responses of skeletal muscle to low, moderate and intense exercise, based on the caffeine induced oscillatory changes in $[Ca^{2+}]_c$, caffeine concentrations of 1, 5 and 10 mM were selected to mimic contraction of muscle by exercise. Viability results ensure that the selected concentrations are not affecting the viability of cells over the time course of the experiments. The Ca^{2+} signaling results are in agreement with myotube bioenergetic results. For example, treatment of C2C12 myotubes with 5 mM of caffeine significantly decreased ATP production, as ATP is consumed by SERCA to uptake Ca^{2+} into SR during the contractions (Fill, and Copello, 2002). Contrary, other caffeine concentrations did not show significant impact on mitochondrial respiration and ATP production, as 1 mM caffeine was unable to induce contractions and 10 mM stimulated massive Ca^{2+} release and disabled myotubes to produce Ca^{2+} oscillation or ATP. In agreement with our findings are the results of another study where the effect of 24 h exposure of C2C12 myotubes to 1 mM caffeine led to significantly decreased maximum respiration as measured by extracellular flux analyzer (Gottwalt and Kinsey, 2016). As expected, this study further showed that higher concentrations of caffeine significantly reduce the glycolytic capacity. Namely, caffeine induces Ca^{2+} signaling thus promoting the transcription of PGC-1α. The overexpression of PGC-1α leads to over than 50% reduction in glycolysis flux, as well as suppression of glycolysis (Wende, *et al.*, 2007). The obtained data indeed showed that with the increased Ca^{2+} release, a dose-dependent decrease in glycolytic capacity and glycolytic reserve occurs. This can be explained by the increased efficiency of oxidative phosphorylation. It is known that Ca^{2+} plays a crucial role as a secondary messenger in many cellular processes, such as contraction and energy metabolism. Indeed,

calcium was found to activate substrate oxidation reactions as well as phosphorylation subsystems. (Kavanagh, *et. al.*, 2000).

The health benefits of regular exercise is well established. However, intense and prolonged contractile activity leads to increased ROS production that results in oxidative stress damage altering physiological conditions of the tissue (Powers, *et. al.*, 2011). Testing the effect of caffeine on the production of ROS, shows that different skeletal muscle cell lines respond differently. For example, the effect of three days does of caffeine on ROS production shows that L6 were found to be the most susceptible to caffeine treatment, while HSMM were affected only by 1 mM but not with higher caffeine concentrations. Moreover, caffeine treatment over four hours increased $^{\bullet}O_2^-$ production in all cell lines. This can be explained by caffeine-induced contraction activity that generates ROS through different sources as listed in section 1.5.1. Indeed, myotube contraction is known to promote ROS formation that can results in a beneficial adaptation effect to exercise or in the case of ROS overproduction detrimental effects in skeletal muscle cells (Cheng, *et. al.*, 2016). Controlling ROS levels during muscle contraction is essential for cells to maintain regular functions. As RyR are found to be sensitive to ROS levels, where it increases channel opening with increased ROS production, leading to increased release of calcium from SR (Abramson and Salama, 1989). Moreover, excessive ROS production is found to inhibit SERCA activity (Xu, *et. al.*, 1997). In addition, excessive ROS can induce peroxidation of lipids, sequentially yielding the formation of reactive aldehyde among which is 4-HNE. This was supported by the results, which show that caffeine induces lipid peroxidation and subsequent modification of proteins by 4-HNE as verified by measuring 4-HNE protein adducts.

Adaptation of skeletal muscle to regular exercise or even one bout of exercise is associated with many cellular mechanisms, including regulation of genes. Treating myotubes for

three days with caffeine showed some regulation of mitochondrial genes that are also regulated by exercise. For example, Cav2 gene, which is significantly upregulated with 5 mM and 10 mM, is a positive regulator of MAPK signaling pathway. As it is known that MAPK is activated by the contractile activity of skeletal muscle and it is involved in mitochondrial biogenesis (Ljubicic *et al.*, 2010). Results also showed that caffeine treatment significantly downregulated genes including: Grpel1, and Aip, which are involved in mitochondrial protein import process. Regulation of mitochondrial protein import is tightly linked with many cellular activities such as stress, signaling, cellular metabolism and others (Harbauer, *et. al*., 2014). Moreover, caffeine treatment is involved in regulation of mitochondrial metabolism genes, mainly in the downregulation of cytochrome C oxidase genes and ATP synthase genes.

4. ROLE OF 4-HNE IN SKELETAL MUSCLE REDOX HOMEOSTASIS AND MITOCHONDRIAL BIOENERGETICS, TRANSCRIPTOME AND DENSITY

4.2. Introduction

Physical activity results in the generation of ROS. Uncontrolled production of ROS impairs the redox homeostasis in cells leading to oxidative stress. At an oxidative stress condition, the ROS production increases higher than the antioxidants capacity leading to oxidative damage to macromolecules. Lipids in particular, due to their chemical structure, are vulnerable to oxidative damage, resulting in the generation of reactive α,β-unsaturated aldehydes among which is 4-HNE. In the previous chapter, results showed that caffeine, used to induce calcium oscillations to mimic exercise, induces lipid peroxidation and 4-HNE adducts formation. Our aim was to study the role of physiological and pathological concentrations of 4-HNE in redox homeostasis, and mitochondrial bioenergetics and functions.

4.3. Methodology

4.3.2. Effect of 4-HNE on mitochondrial biochemical activities

4.3.2.1. Preparation of 4-hydroxynonenal

4-HNE is activated according to manufacturer protocol. Briefly, 4-HNE (Enzo Life Sciences) is dried using turbovap nitrogen evaporator. Then, 1 mL of cold 1mM hydrochloric acid was added, stirred for 45 minutes at 4ºC and used either immediately or stored at -20ºC and

used within 2 weeks from the date of activation. Prepared 4-HNE stock, with a concentration of 25.7 mM, is diluted approximately 2570 times when used for treatment of cells.

4.3.2.2. Effect of 4-HNE on viability of myotubes

C2C12, L6 and HSMM myoblasts were seeded in 96-well plates with density of 6×10^3 cells per well and differentiated into myotubes as described in the section 2.1.2. Fully differentiated myotubes were treated with ranging micromolar 4-HNE concentrations (1.25, 2.5, 5 and 10 μM) or left untreated overnight. The impact of overnight 4-HNE treatment on myotube viability was assessed using AlamarBlue (Molecular Probes) assay as described in section 3.2.1.1.

4.3.2.3. Effect of 4-HNE on cellular redox homeostasis

The effects of 4-HNE on the production of intracellular ROS and superoxide anion were measured using DCFH-DA and DHE redox sensitive probes, respectively, as described in section3.2.1.3. Briefly, cells were seeded and differentiated into myotubes as in section 2.1.2. Myotubes were then loaded with DCFH-DA or DHE for 30 min, excess probe was washed with PBS twice, and myotubes treated with transparent DMEM media supplemented with 2% HS and ranging 4-HNE concentrations (0, 1.25, 10, 20, 40, 80, 100 and 160 μM for DCFH-DA or 0, 2.5, 5 and 10 μM for DHE assay). Due to the high reactivity of 4-HNE, it is expected that within 4 hours all 4-HNE will be metabolized by the cells. Thus, DCFH-DA assay and DHE assay were carried out for 4 or 8 hours, respectively.

A kinetic measurement every 10 minutes was carried out to study the immediate effect of 4-HNE on intracellular ROS level using DCFH over 4 hours. In addition, DHE signal was recorded at time points 2, 4 and 8 h.

4.3.3. Measuring mitochondrial bioenergetics using XFe24 Seahorse analyzer

4.3.3.1. Effect of 4-HNE on mitochondrial respiration ability

The effect of immediate and overnight treatment of 4-HNE on mitochondrial respiration was measured. It is expected that free 4-HNE is completely metabolized within few hours after treating the cells. Therefore, the effect of 4-HNE immediately after addition and after complete dissociation are both tested. Cells were seeded in XF24 cell culture microplates at a density of 8000 cells/well, and differentiated. For the immediate treatment, 4-HNE (0, 2.5, 5 and 10 µM) was added in the first injection port and changes in OCR measured continuously for 1 hour, followed by mitochondrial stress test injections as in section 2.2.2. To measure the effect of overnight 4-HNE treatment, one day prior to the experiment cells were treated with 4-HNE (0, 5, 10, 20 and 40 µM) overnight. Cellular respiration was measured using mitochondrial stress test kit and analyzed by Seahorse XFe24 Analyzer (Agilent, USA). In the case of the assessment of overnight 4-HNE effect on myotubes only 3 injections ports were used and the same were loaded with: oligomycin (1.0 µM), FCCP (0.5 µM), and mixture of rotenone and antimycin (0.5 µM). Each treatment condition is analyzed in quadruplicates. All results are expressed in OCR (pmol (O_2)/min).

4.3.3.2. Effect of 4-HNE on myotube glycolysis

Cells were seeded in XF24 cell culture microplates at a density of 8000 cells/well, and differentiated. Effect of 4-HNE on glycolysis was performed in order to assess the effect of 4-HNE on the ability of myotubes to use other respiration method than mitochondrial respiration. The immediate and overnight effect of 4-HNE on glycolysis are analyzed. Glycolysis was measured using cell glycolysis stress test as described in section 2.2.1 with modification. 4-HNE (0, 2.5, 5 and 10 µM) was used in the first injection port to measure the immediate effect 4-HNE.

After addition of 4-HNE to myotube cultures, changes in the basal ECAR were continuously recorded for 1 hour, followed by other 3 injections: glucose (10 mM), oligomycin (1.0 µM), finally 2-DG (50 mM). For overnight effect of 4-HNE, myotubes were treated overnight with (0, 2.5, 5 and 10 µM 4-HNE), then glycolysis test was carried out using three injection ports to add glucose (10 mM), oligomycin (1.0 µM) and finally 2-DG (50 mM) according to the manufacturer protocol. Results are expressed in extracellular acidification rate (ECAR, mpH/min).

4.3.3.3. NADH autofluorescence assay

NADH and its oxidized form NAD+ act as hydrogen carriers at the site of the electron transport chain during mitochondrial respiration. The fluorescent properties of NADH make it a valuable fluorescent indicator of the mitochondrial metabolic state. NADH autofluorescence was excited at 351 nm using Xennon arc lamp and monochromator and measured at 375-470 nm. The emission was recorded using cooled CCD camera. C2C12 Myotubes base fluorescence level was measured for 2 min., followed by adding 4-HNE (0, 2.5, 5 and 10 µM) for 18 min., then, FCCP (0.5 µM) is added and measured for 5 min.

4.3.4. Effect of 4-HNE on mitochondrial density

MitoTracker is used to measure mitochondrial density. Myotubes were treated with HNE (0, 2.5, 5, 10 and 50 µM) overnight and stained with MitoTracker™ Green FM (Molecular Probes, 200 nM) and Hoechst (Molecular Probes, 2 µg/mL) and imaged using ArrayScan (filter 386-23 nm for Hoechst, filter 485-20 nm for MitoTracker green). The impact of 4-HNE on mitochondrial density was also recorded using Tecan Infinite M200 PRO with Ext/ Ems: 490 nm/ 516 nm for MitoTracker, and 570 nm/ 600 nm for Hoechst. Hoechst staining was used as a method to normalize the results based on the viability of cells.

4.3.5. Effect of 4-HNE on mitochondrial gene expression

The effect of 4-HNE on the mitochondrial gene expression was carried out as described in section 2.3.

4.4. Results

4.4.2. Effect of 4-HNE on viability of myotubes

The effect of 4-HNE on the viability of myotubes was examined using AlamarBlue assay to determine the physiological and pathological concentration ranges, shown in Figure 44. Results showed dose-dependent effect on viability of myotubes. Low 4-HNE concentrations, up to 5 µM, had no effect (p >0.01, N = 5) on the viability of myotubes when compared to control. Ten micromolar concentration showed significant decrease in the viability of C2C12 by 15.5% ± 2.1% and for the HSMM myotubes by 17.8% ± 3.1%, but had no effect on L6 myotubes. However, concentrations above 10 µM steadily decreased viability, and eventually altered myotubes morphology Figure 45 with C2C12. More screening ranges are attached in the appendices Figure 86. Physiological concentrations are selected for further experiments based on viability results.

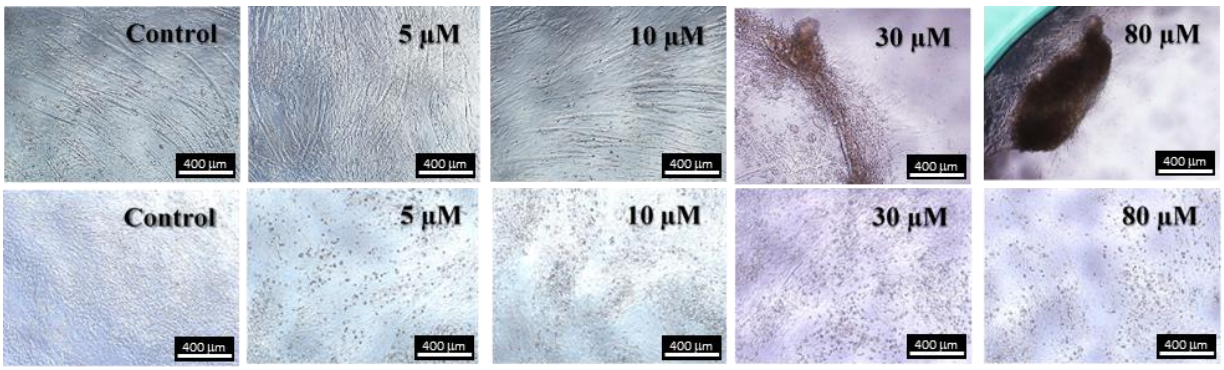

Figure 44: Determining physiological and pathological concentrations of 4-HNE on myotubes using viability test. Light microscopy images showing the effect of ranging 4-HNE concentrations on myotube viability and morphology of C2C12 myotubes (top images, magnification 40X) and L6 myotubes (below images, magnification 40X).

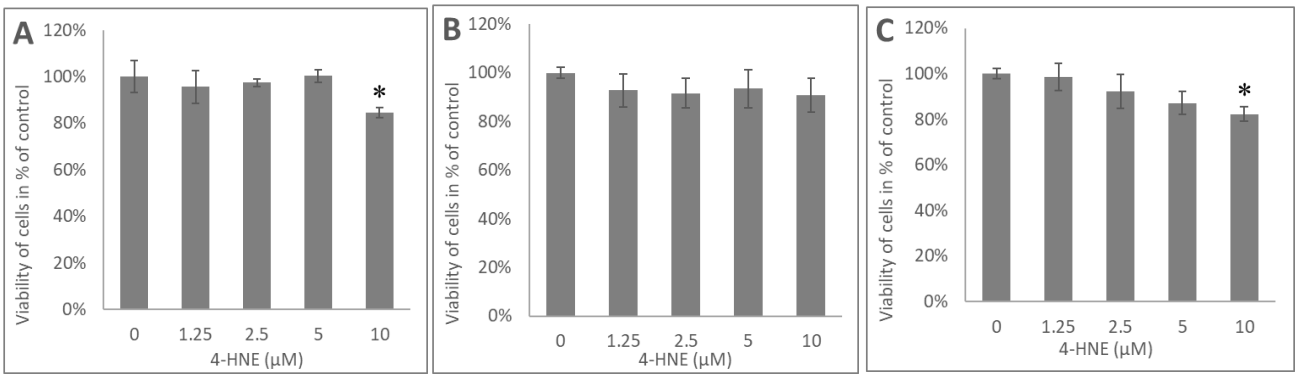

Figure 45: The effect of 4-HNE on the viability of myotubes. A. C2C12 myotubes **B.** L6 myotubes and **C.** HSMM myotubes. Treatment with 4-HNE showed a significant decrease in viability with 10 µM in C2C12 and HSMM * p <0.01 when compared to 0. (Results are presented as mean ± *SD* of N =5).

4.4.3. Effect of 4-HNE on cellular redox homeostasis

Based on the results of caffeine induced formation of 4-HNE protein adducts in myotubes and dose response effects of 4-HNE on myotube viability the concentrations 2.5 µM, 5 µM and

10 μM were selected to approximate those of low to moderate levels of physiological oxidative stress for 4-HNE functional studies on myotube metabolism. Therefore, in this thesis 2.5 μM and 5 μM of 4-HNE are defined as physiological concentrations, 10 μM as supraphysiological, and higher concentrations as pathological to myotubes based on viability results shown in 4.4.2. The impact of 4-HNE on myotube cellular redox homeostasis was assessed by measuring its ability to induce hydrogen peroxides and other oxidants production using DCFH-DA probe and superoxide anion production using DHE redox sensitive probe. 4-HNE showed dose and time-dependent effect on intracellular ROS level measured by DCFH, Figure 46, Figure 47 and Figure 48. All cell lines showed a similar response, where physiological (2.5 μM) and supraphysiological (10 μM) concentrations did not induce higher intracellular ROS production compared to control myotubes. However, higher pathological concentrations, 80 μM for C2C12 and L6 and 75 μM for HSMM and above, significantly increased (p <0.01) intracellular ROS level.

Furthermore, although it was found that 4-HNE induces superoxide production in C2C12, L6 and HSMM myotubes the cells showed different sensitivity to this reactive aldehyde. C2C12 myotubes were the most susceptible to 4-HNE induced superoxide anion production; where all three concentrations tested (2.5 μM, 5 μM and 10 μM) showed significant (p <0.01) increase in superoxide level, by more than 20% for 2.5 μM and more than 50% for 5 μM and 10 μM compared to control throughout all time points Figure 49. L6 myotubes, did not show significant change (p >0.01) in superoxide level after 2 hours. The highest 4-HNE concentration (10 μM) significantly increased superoxide level after 4 hours and that was maintained up to 8 hours after the treatment. Also 5 μM 4-HNE increased the superoxide level significantly (p <0.01) by 19.7 ± 4.2% (N = 4) after 8 hours, Figure 50. Similarly, in HSMM only higher 4-HNE

concentrations (5 μM and 10 μM) induced significant superoxide production after 2 hours of treatment that was maintained up to 8 hours, Figure 51.

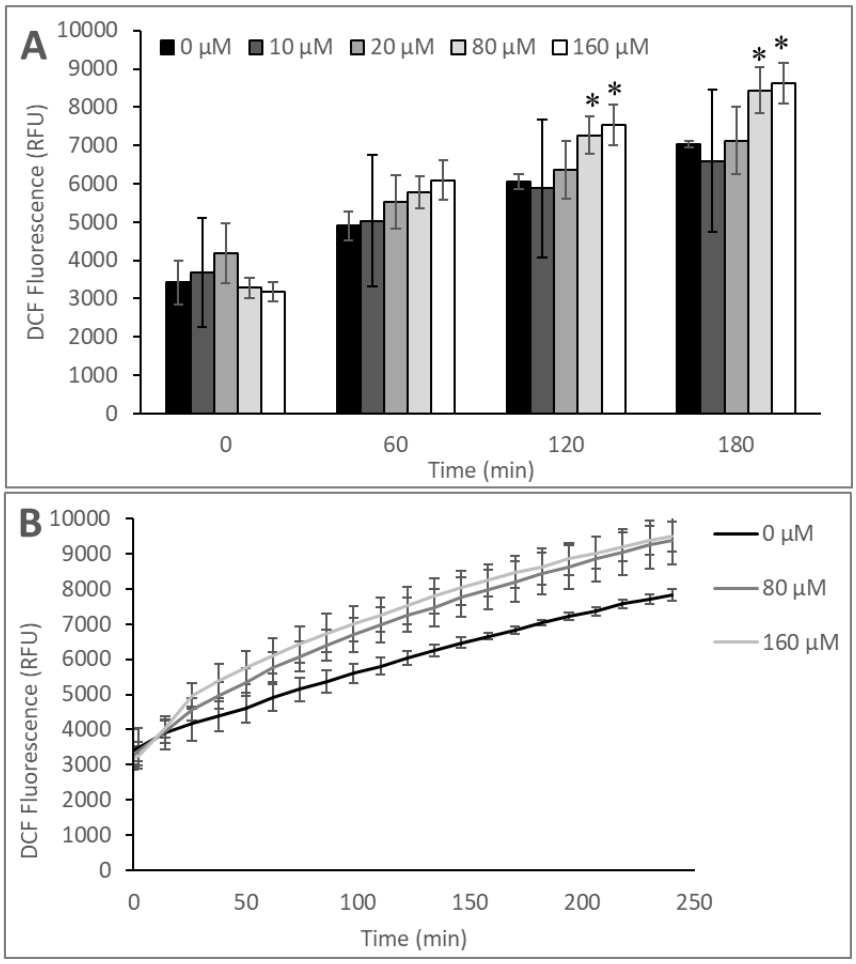

Figure 46: Kinetic measurement of the effect of 4-HNE on the intracellular ROS production in C2C12 myotubes. **A.** Bar chart showing the 4-HNE effect at selected time points. Concentrations below 80 μM 4-HNE did not induce significant changes in intracellular ROS level, while higher concentrations as are 80 μM and 160 μM 4-HNE significantly increased ROS production after 60 min of treatment **B.** Kinetic measurement of intracellular ROS production by pathological 4-HNE concentrations showed significant increase in ROS production compared to control cells. (A. and B. were both carried in the same plate). Representative experiment is given in mean values ± *SD* for $N = 4$) ($p < 0.01$ in comparison to control myotubes).

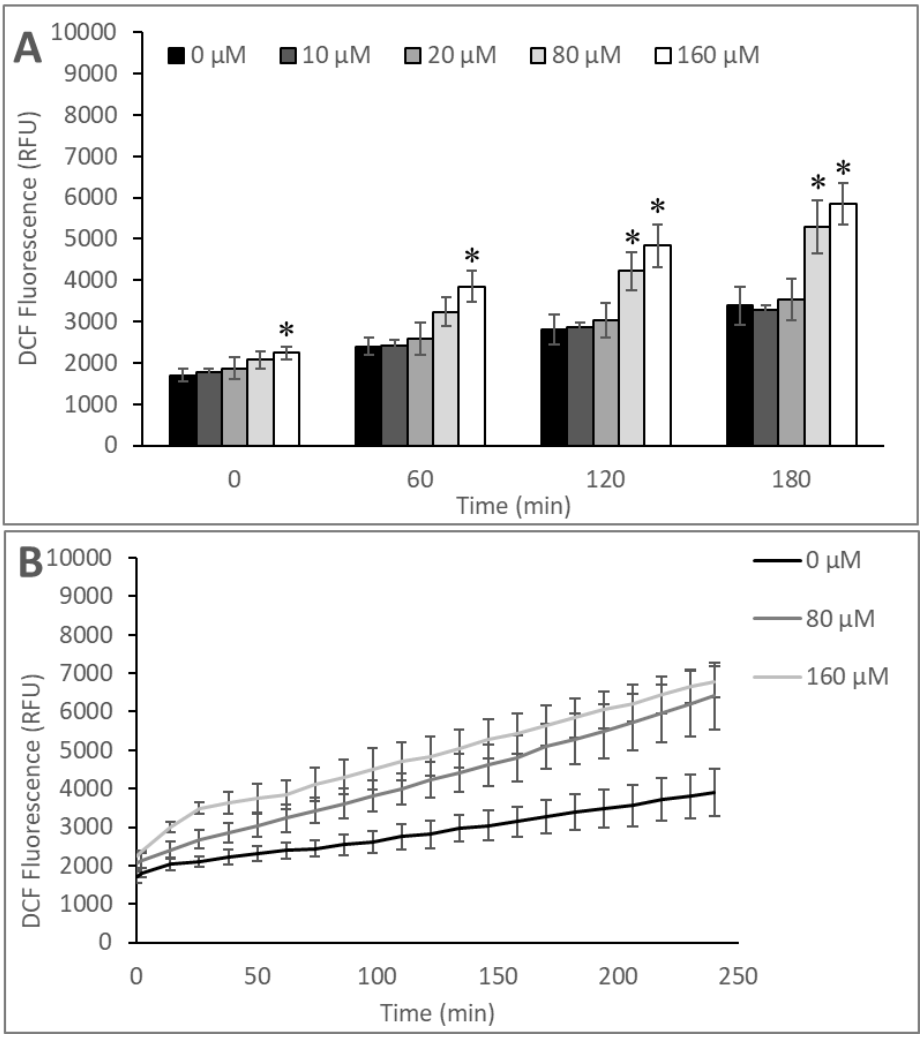

Figure 47: Kinetic measurement of the effect of 4-HNE on the intracellular ROS production in L6 myotubes. **A.** Selected time points showing concentrations below 80 µM 4-HNE did not have significant changes in intracellular ROS level, while higher concentrations 80 µM and 160 µM 4-HNE significantly increased ROS production **B.** Showing the kinetic measure of the pathological concentrations 80 µM and 160 µM 4-HNE. (A. and B. were both carried in the same plate). Results of representative experiment are presented as mean values ± *SD* for *N* = 4) ($p < 0.01$ in comparison to control myotubes).

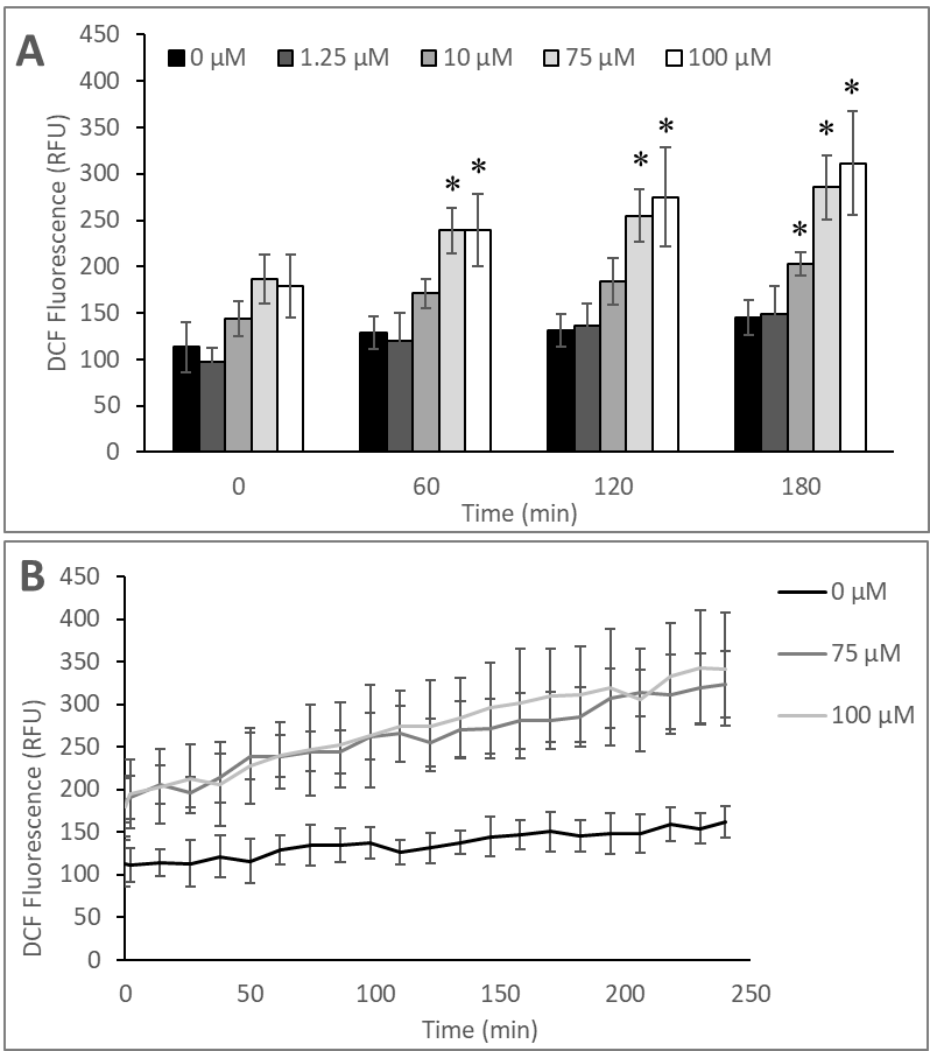

Figure 48: Kinetic measurement of the effect of 4-HNE on the intracellular ROS production in HSMM myotubes. **A.** Selected time points showing concentrations below 75 µM 4-HNE did not have significant changes in intracellular ROS level, except for 10 µM where it significantly increased ROS level at 120 min **B.** Showing the kinetic measure of the pathological concentrations 80 µM and 160 µM 4-HNE had significant increase in ROS production compared to control cells. (A. and B. were both carried in the same plate). Results of representative experiment are shown as mean values ± *SD* for $N = 4$) ($p < 0.01$ in comparison to control myotubes).

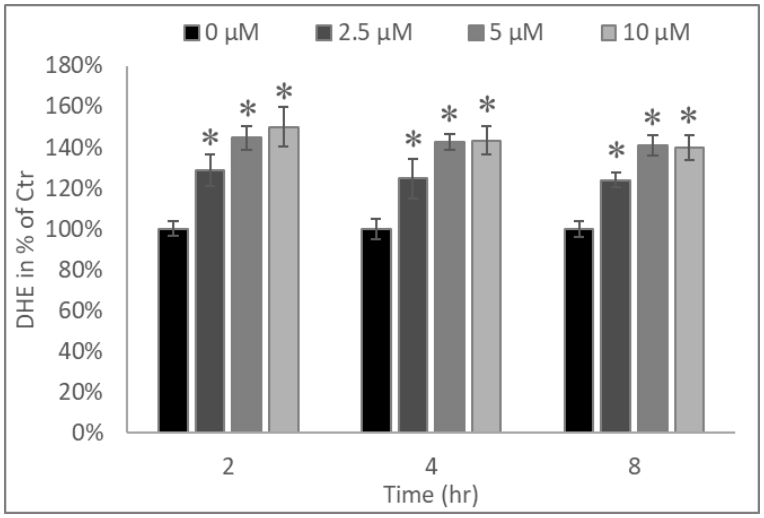

Figure 49: 4-HNE induces superoxide production in C2C12 myotubes measured by DHE. Physiological (2.5 and 5 µM) and supraphysiological (10 µM) concentrations of 4-HNE significantly increased superoxide production after 2, 4 and 8 hours. (Mean values ± *SD* for *N* = 4) (* *p* <0.01 in comparison to control myotubes).

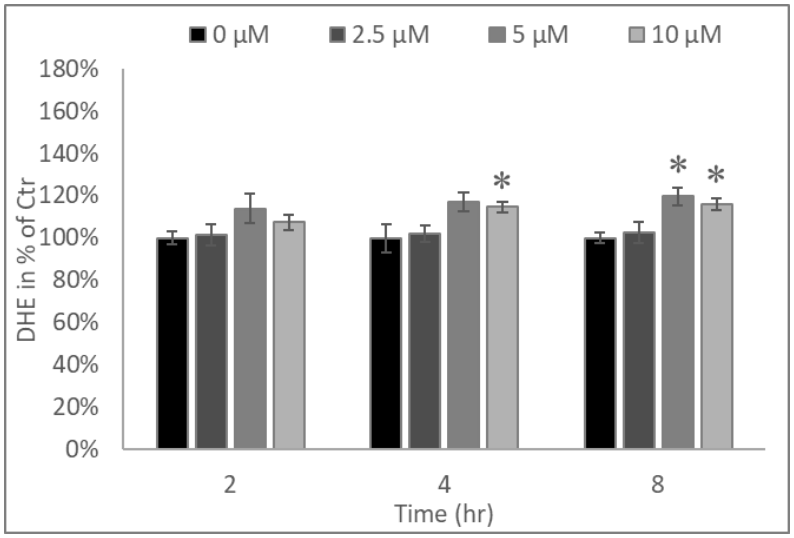

Figure 50: 4-HNE induces superoxide production in L6 myotubes measured by DHE. Supraphysiological (10 µM) concentrations of 4-HNE significantly increased superoxide production after 4 hours, and 5 µM and 10 µM increased superoxide production after 8 hours. (Mean values ± *SD* for *N* = 4) (* *p* <0.01 in comparison to control myotubes).

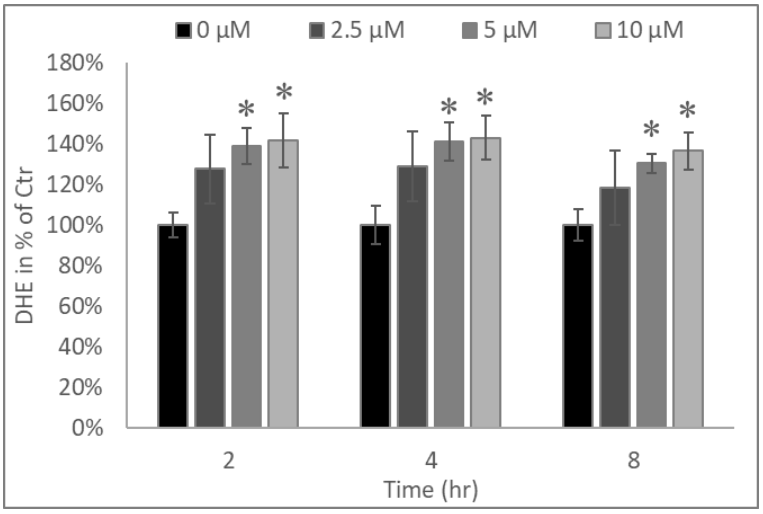

Figure 51: 4-HNE induces superoxide production in HSMM myotubes measured by DHE. Physiological (5 µM) and supraphysiological (10 µM) concentrations of 4-HNE significantly increased superoxide production after 2, 4 and 8 hours. (Mean values ± *SD* for $N = 4$) (* $p < 0.01$ in comparison to control myotubes).

4.4.4. Effect of 4-HNE on mitochondrial health and function

4.4.4.1. Regulation of mitochondrial energy metabolism

4.4.4.1.1. Effect on NADH level

The effect of 4-HNE on autofluorescence of NADH was dependent on the aldehyde concentration used. The lowest, 2.5 µM 4-HNE induced increase of mitochondrial NADH level, Figure 52-B. Contrary treatment of C2C12 myotubes with 5 µM 4-HNE induce mild and 10 µM high decrease in NADH level, as shown in Figure 52-C and -D. Application of 1 µM FCCP at the end of experiment, maximally activated respiration with consumption of all mitochondrial NADH. The addition of inhibitor (1 mM NaCN) blocked consumption of NADH in mitochondria confirming increased mitochondrial pool of NADH by 2.5 µM and decrease by 5 and 10 µM 4-HNE.

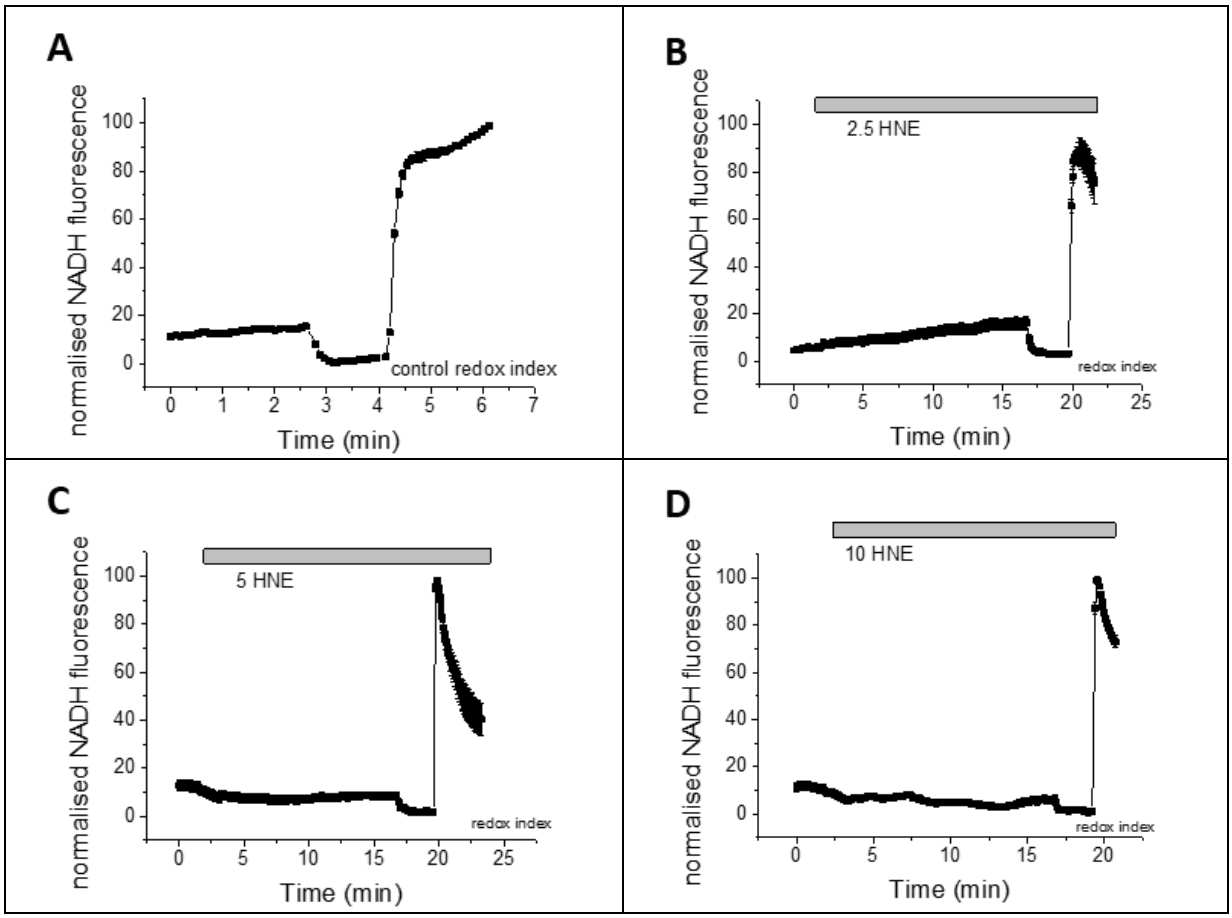

Figure 52: Effect of 4-HNE on mitochondrial NADH of C2C12 myotubes measured by autofluorescence of NADH. **A.** Control, shows the NADH in control myotubes. **B.** Myotubes treated with 2.5 μM 4-HNE. **C.** Myotubes treated with 5 μM 4-HNE. **D.** Myotubes treated with 10 μM 4-HNE.

4.4.4.1.2. Effect of 4-HNE on myotube energy metabolism

Mitochondrial respiration and glycolysis, the two major energy-producing pathways, were studied after immediate and overnight addition of 4-HNE. The immediate response of C2C12 myotubes, following 1 hour treatment with ranging 4-HNE concentrations (2.5 µM, 5 µM and 10 µM) significantly (p <0.01) reduced ATP production. Moreover, 2.5 µM and 5 µM 4-HNE significantly inhibited proton leak and maximal respiration (Figure 55). In L6 myotubes, only the highest 4-HNE concentration (10 µM) decreased the maximum respiration and ATP production (Figure 56, p <0.01). The overnight treatment of myotubes with 4-HNE significantly reduced the maximum respiration of C2C12 with 10 µM, 20 µM and 40 µM (Figure 53). While it did not have any significant changes (p >0.01) on the mitochondrial respiration of L6 myotubes (Figure 54). Contrary, 4-HNE significantly increased non-mitochondrial respiration when myotubes were treated with 5 µM 4-HNE (p<0.01 by both *t*-test and one-way ANOVA).

The immediate and overnight effect of 4-HNE on both C2C12 and L6 myotubes had no significant effect on glycolysis compared to control (Figure 57, Figure 58, Figure 59, and Figure 60 p >0.01). Exception was the C2C12 overnight treatment with 2.5 µM 4-HNE, which surprisingly significantly reduced glycolytic capacity by 20 mpH/min. Significant reduction is also observed with 2.5 µM and 5 µM 4-HNE in glycolytic reserve by 19 and 17 mpH/min respectively (Figure 57, p <0.01). Same reduction was observed in L6 but was not significant (Figure 58) (p<0.01 by both *t*-test and one-way ANOVA).

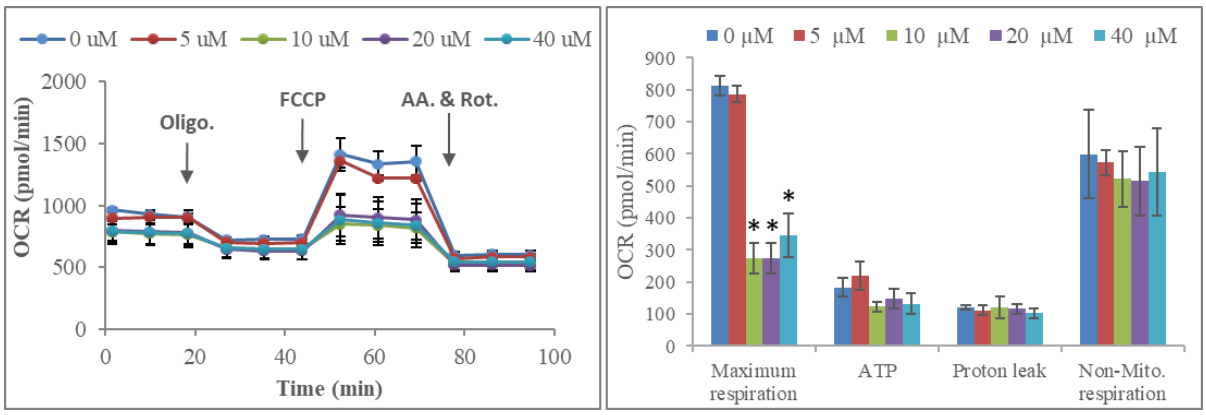

Figure 53: Effect of overnight 4-HNE treatment on mitochondrial respiration of C2C12 myotubes. A. A representative experiment graph output from XF24 showing OCR (pmol/min) response to oligomycin, FCCP and rotenone and antimycin A; **B.** The effect of overnight 4-HNE treatment on maximum respiration, ATP production, proton leak and non-mito. respiration. Maximum respiration was significantly reduced with 10 µM, 20 µM and 40 µM 4-HNE. (* p <0.01 compared to 0, results are mean ± *SD* of N =4).

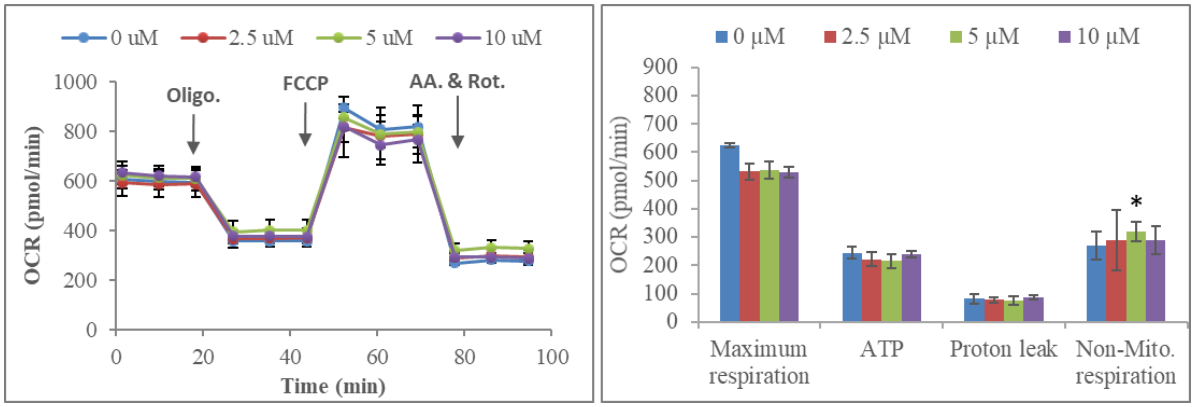

Figure 54: Overnight effect of 4-HNE on mitochondrial respiration of L6 myotubes. A. A representative experiment graph output from XF24 showing OCR (pmol/min) response to oligomycin, FCCP and rotenone and antimycin A; **B.** Overnight effect of 4-HNE treatment on maximum respiration, ATP production, proton leak and non-mito. respiration. 4-HNE had no significant effect on mitochondrial respiration of L6. (Results are presented in mean ± *SD* of N =5).

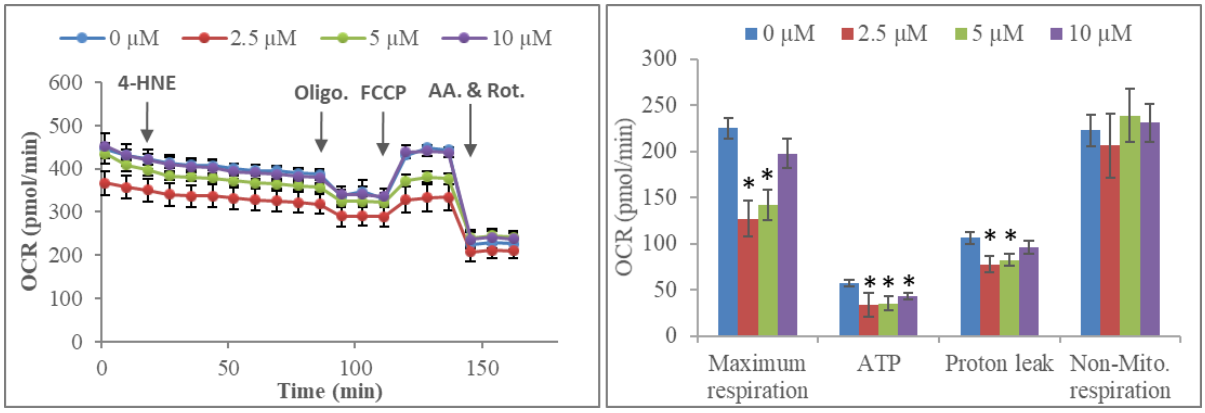

Figure 55: Immediate effect of 4-HNE treatment on mitochondrial respiration of C2C12 myotubes. A. A representative experiment graph output from XF24 showing OCR (pmol/min) response to 4-HNE, oligomycin, FCCP and rotenone and antimycin A; **B.** The effect of 4-HNE on maximum respiration, ATP production, proton leak and non-mito. respiration. Maximum respiration, ATP production and proton leak were significantly reduced with 2.5 µM and 5 µM 4-HNE. (* p <0.01 compared to 0, results are presented in mean ± *SD* of N =5).

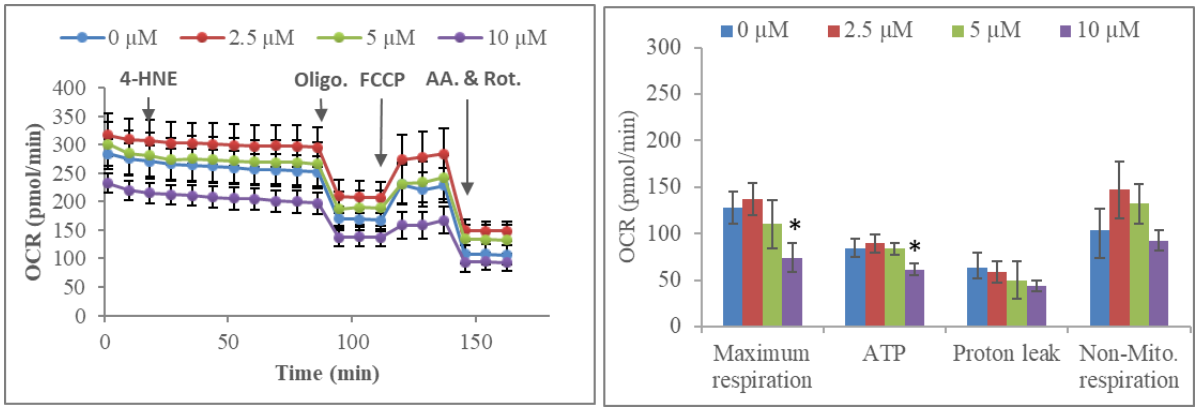

Figure 56: Immediate effect of 4-HNE on mitochondrial respiration of L6 myotubes. A. A representative experiment showing OCR (pmol/min) response to 4-HNE, oligomycin, FCCP and rotenone and antimycin A; **B.** The effect of 4-HNE on maximum respiration, ATP production, proton leak and non-mito. respiration. Max. respiration and ATP production were significantly reduced with 10 µM 4-HNE. (* p <0.01 compared to 0, results are in mean ± *SD* of N =5).

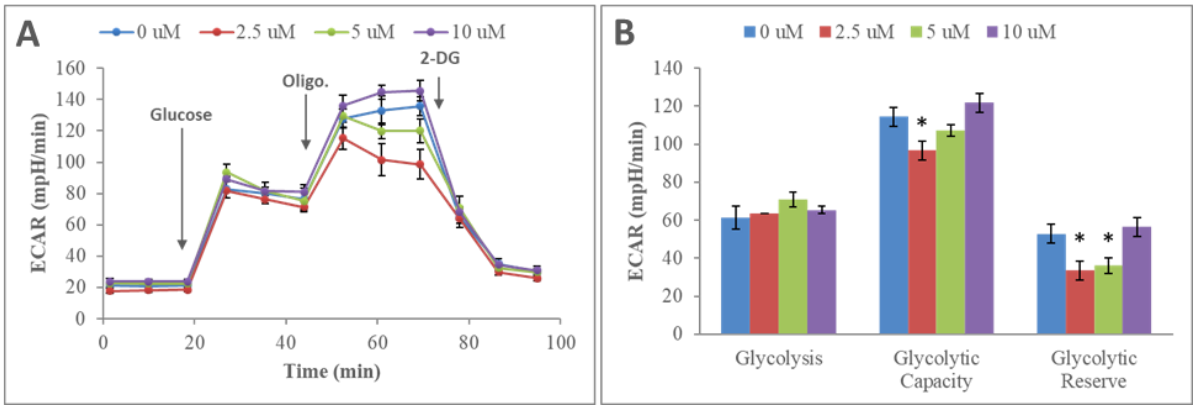

Figure 57: Effect of overnight 4-HNE treatment on glycolysis of C2C12 myotubes. A. A representative graph from XF24 showing the ECAR (mpH/min) response to glucose, oligomycin and 2-DG; **B.** Effect of overnight 4-HNE treatment on glycolysis, glycolytic capacity and glycolytic reserve. Glycolytic capacity was significantly reduced with 2.5 µM. (* p <0.01 compared to 0, results are presented in mean ± *SD* of N =5).

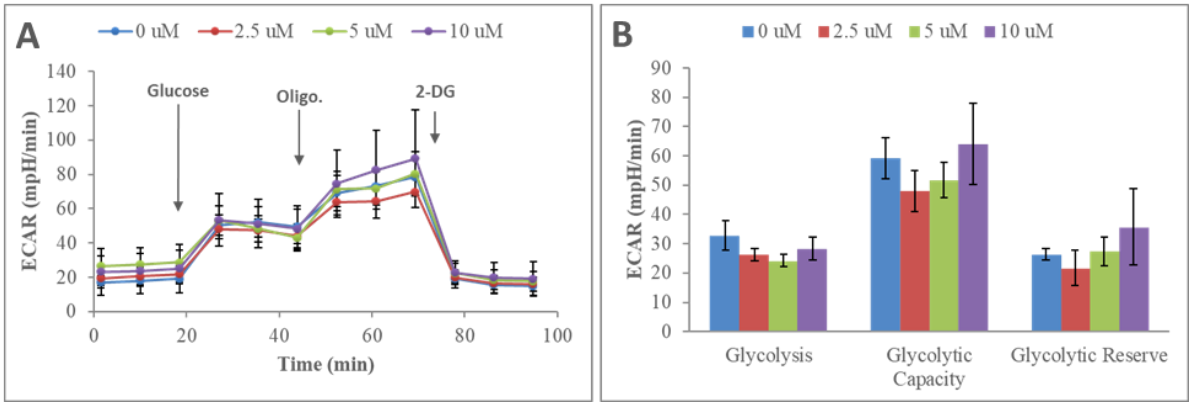

Figure 58: Overnight effect of 4-HNE on glycolysis of L6 myotubes. A. A representative graph from XF24 showing the ECAR (mpH/min) response to glucose, oligomycin and 2-DG; **B.** Effect of overnight 4-HNE treatment on glycolysis, glycolytic capacity and glycolytic reserve. 4-HNE had no significant effect on L6. (Results are presented in mean ± *SD* of N =5).

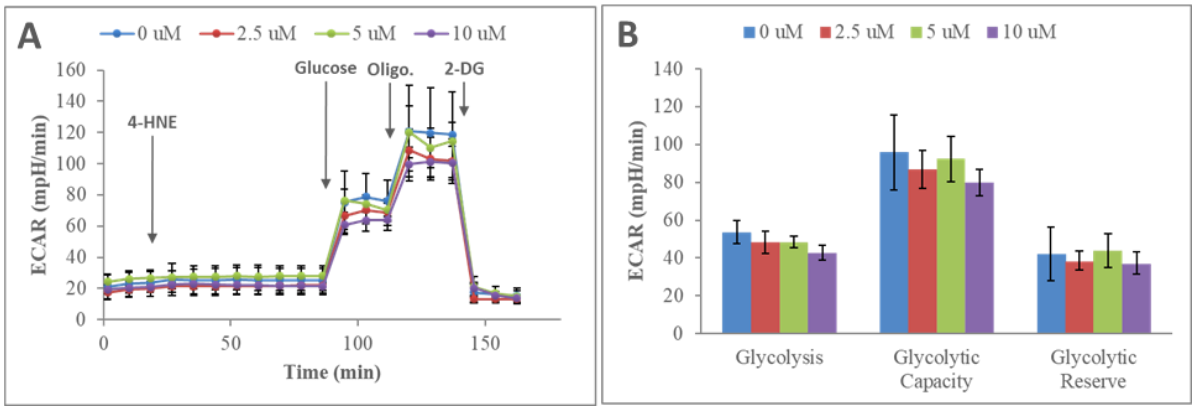

Figure 59: Immediate effect of 4-HNE on glycolysis of C2C12 myotubes. A. A representative graph from XF24 showing the ECAR (mpH/min) response to 4-HNE, glucose, oligomycin and 2-DG; **B.** The effect of 4-HNE on glycolysis, glycolytic capacity and glycolytic reserve. 4-HNE had no significant effect on C2C12. (Results are presented in mean ± *SD* of *N* =5).

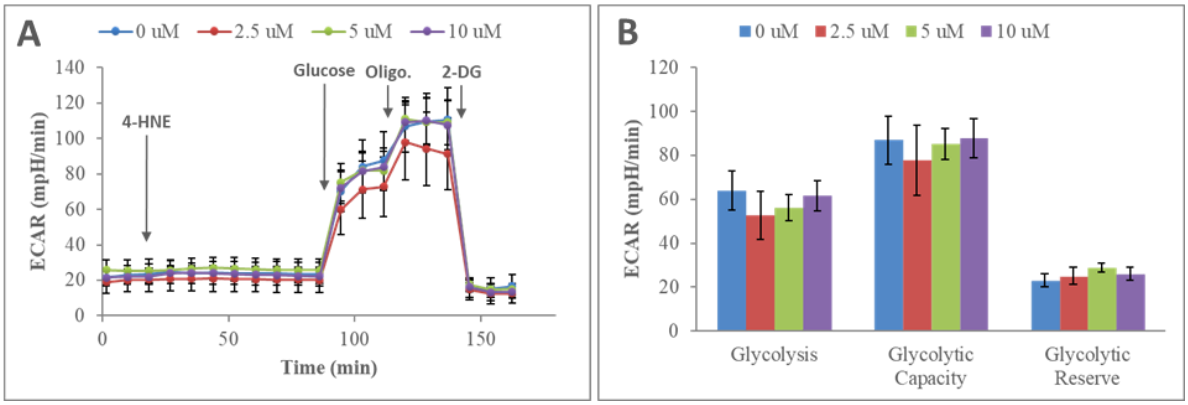

Figure 60: Immediate effect of 4-HNE on glycolysis of L6 myotubes. A. A representative graph from XF24 showing the ECAR (mpH/min) response to 4-HNE, glucose, oligomycin and 2-DG; **B.** The effect of 4-HNE on glycolysis, glycolytic capacity and glycolytic reserve. 4-HNE had no significant effect on L6. (Results are presented in mean ± *SD* of *N* =5).

4.4.5. 4-HNE treatment alters the expression of mitochondrial genes

The effect of physiological and supraphysiological concentrations of 4-HNE (2.5, 5 and 10 µM) on the expression of mitochondrial genes is shown on Figure 61. L6 myotubes with 5 µM 4-HNE has the most significantly downregulated genes with total of 72 genes (Figure 63). Compared to 29 downregulated genes of group 1 (Figure 62) and 29 genes of group 3 (Figure 64). All three 4-HNE treatments downregulated three genes that are coding for membrane polarization and potential (Gclm, Sod1 and Bak1), six genes involved in mitochondrial transport (Aip, Bcl2, Cpt2, Hsp90aa1, Bcl2l1 and Timm10b), three genes involved in small molecules transport (Slc25a17, Slc25a5 and Slc25a19), one gene involved in targeting proteins to mitochondria (Grpel1), genes involved in mitochondrial protein import (Cln8, Cox18, Gpx1 and Hspd1), one gene involved in mitochondrial fission and fusion (Fis1), and genes involved in apoptosis (Pmaip1, Akt1, Aifm2 and Sod2). No genes were upregulated among all groups compared to control.

Furthermore, overnight treatment of C2C12 myotubes with physiological (2.5 µM) 4-HNE downregulated the expression of 20 genes and upregulated the expression of only one gene (Figure 66). Interestingly, only minor changes have been observed for the 5 µM treatment with only 3 genes downregulated and 3 upregulated genes (Figure 67). However, treatment of C2C12 myotubes with supraphysiological 4-HNE 10 µM led to upregulation of 13 genes and did not have any downregulation genes (Figure 68). Uqcrh, a complex III gene, was found to be upregulated in all groups, while the expression of Atp6v0d2 (complex V gene) and Ndufv3 (Complex I gene) were significantly upregulated when myotubes were treated with higher concentrations (5 µM and 10 µM).

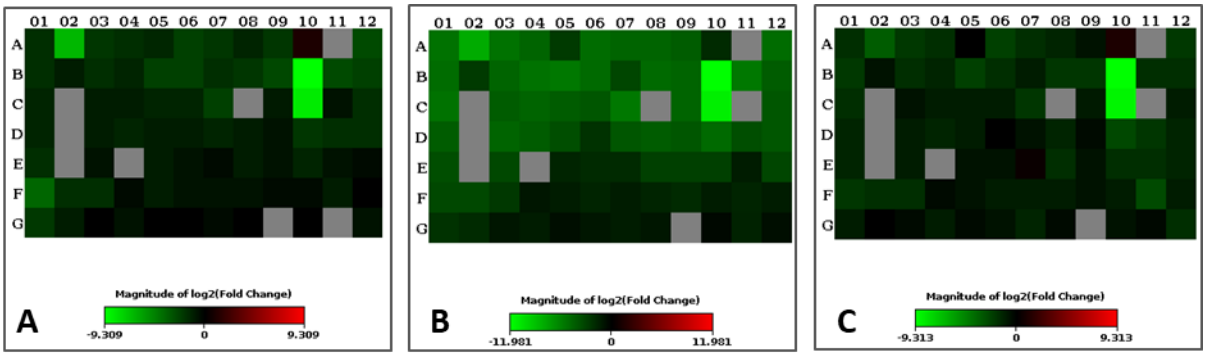

	1	2	3	4	5	6	7	8	9	10	11	12
A	Aifm2	Aip	Akt1	Bak1	Bbc3	Bcl2	Bcl2l1	Bid	Bnip3	Cav2	Cdkn2a	Cln8
B	Cox18	Cpt1b	Cpt2	Dnm1l	Fis1	Timm10b	Gclc	Gclm	Gpx1	Grpel1	Hsp90aa1	Hspd1
C	Immp1l	LOC6918	Mfn1	Mfn2	Mipep	Msto1	Mtx2	Nefl	Opa1	Pmaip1	Ppargc1a	Rhot2
D	Rnf135	Sfn	Sh3glb1	Slc25a10	Slc25a12	Slc25a13	Slc25a14	Slc25a15	Slc25a16	Slc25a17	Slc25a19	Slc25a2
E	Slc25a20	Slc25a21	Slc25a22	Slc25a23	Slc25a24	Slc25a25	Slc25a27	Slc25a3	Slc25a30	Slc25a36	Slc25a37	Slc25a4
F	Slc25a5	Sod1	Sod2	Stard3	Taz	Timm10	Timm17a	Timm17b	Timm22	Timm44	Timm8a1	Timm8b
G	Timm9	Tomm22	Tomm34	Tomm40	Tomm40l	Tomm70a	Tp53	Tspo	Ucp1	Ucp2	Ucp3	Uxt

Figure 61: Effect of 4-HNE on the gene expression of mitochondria genes in L6 myotubes. Heat map showing downregulated genes in green, unchanged in black and upregulated in red. The symbol and location of each gene in the heat map is shown under the heat maps. The effect of 4-HNE A) 2.5 µM vs. control, B) 5 µM vs. control and C) 10 µM vs. control on the regulation of genes expression. (Results are in averages of triplicates)

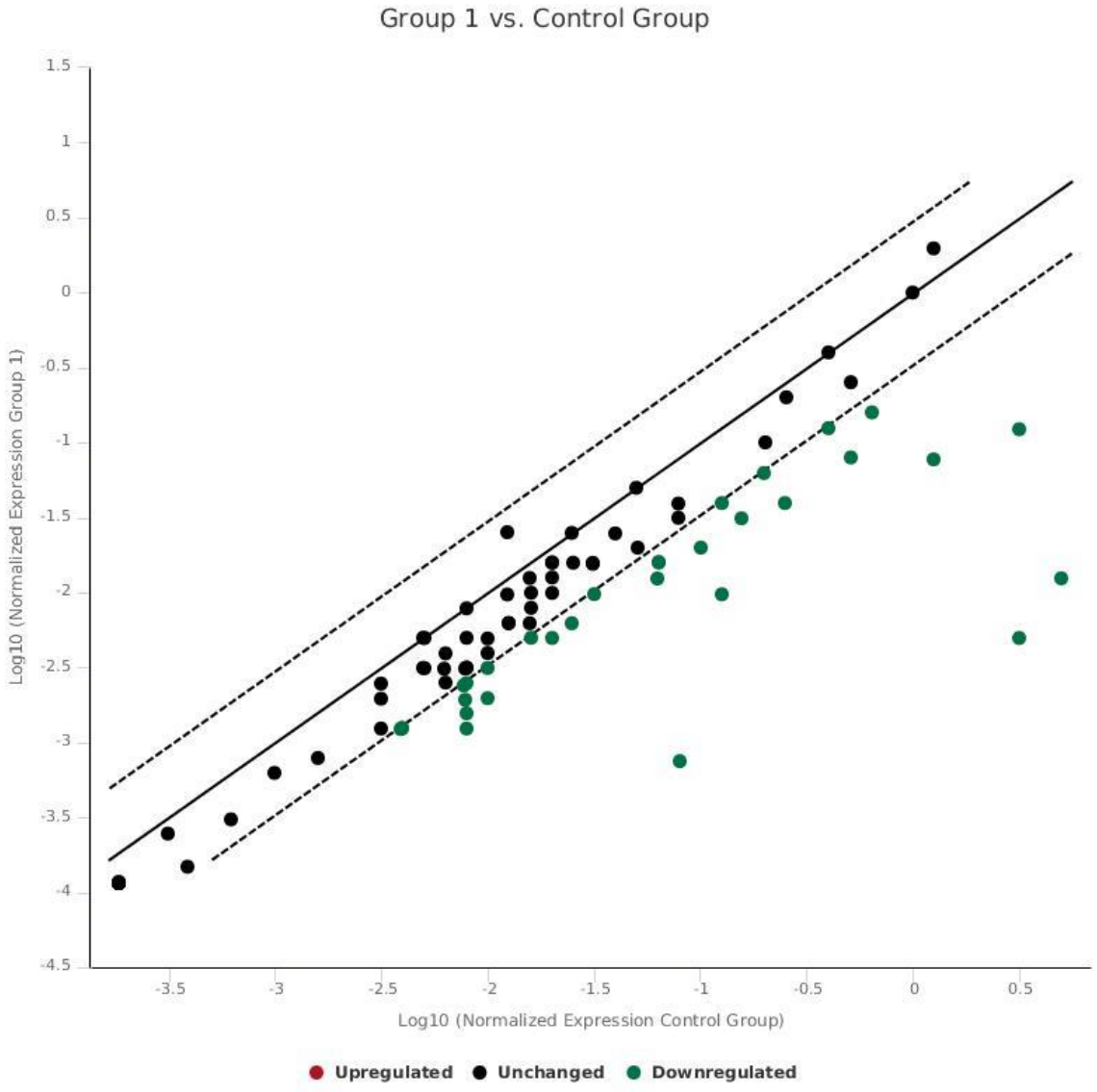

Figure 62: Expression of mitochondria genes in control L6 myotubes compared to treated with 2.5 µM 4-HNE. Scatter plot shows the treatment group1 in y-axis against the control group in x-axis. The dotted line indicate 3 fold-regulation.

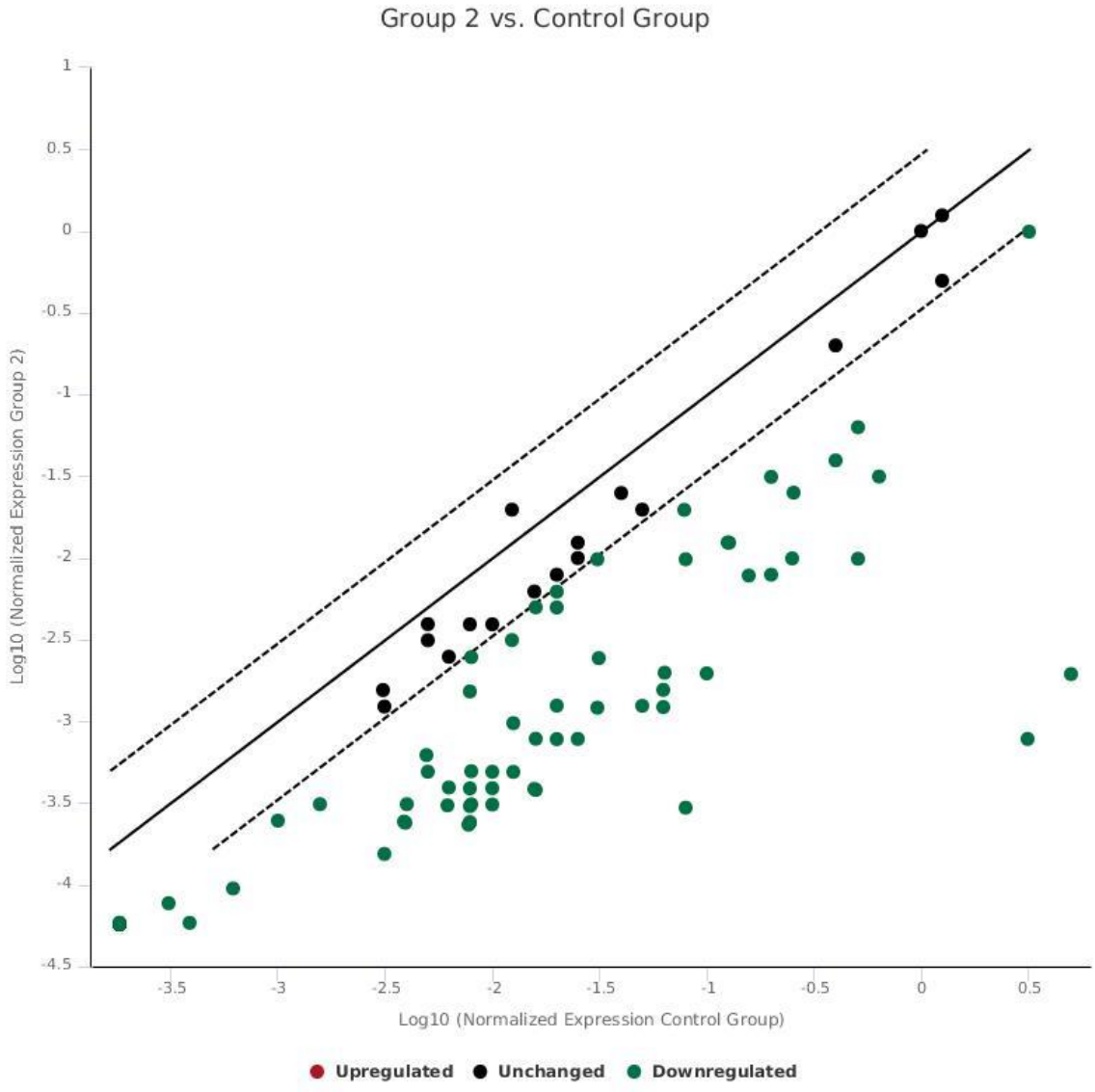

Figure 63: Expression of mitochondria genes in control L6 myotubes compared to treated with 5 µM 4-HNE. Scatter plot shows the treatment group 2 in y-axis against the control group in x-axis. The dotted line indicate 3 fold-regulation.

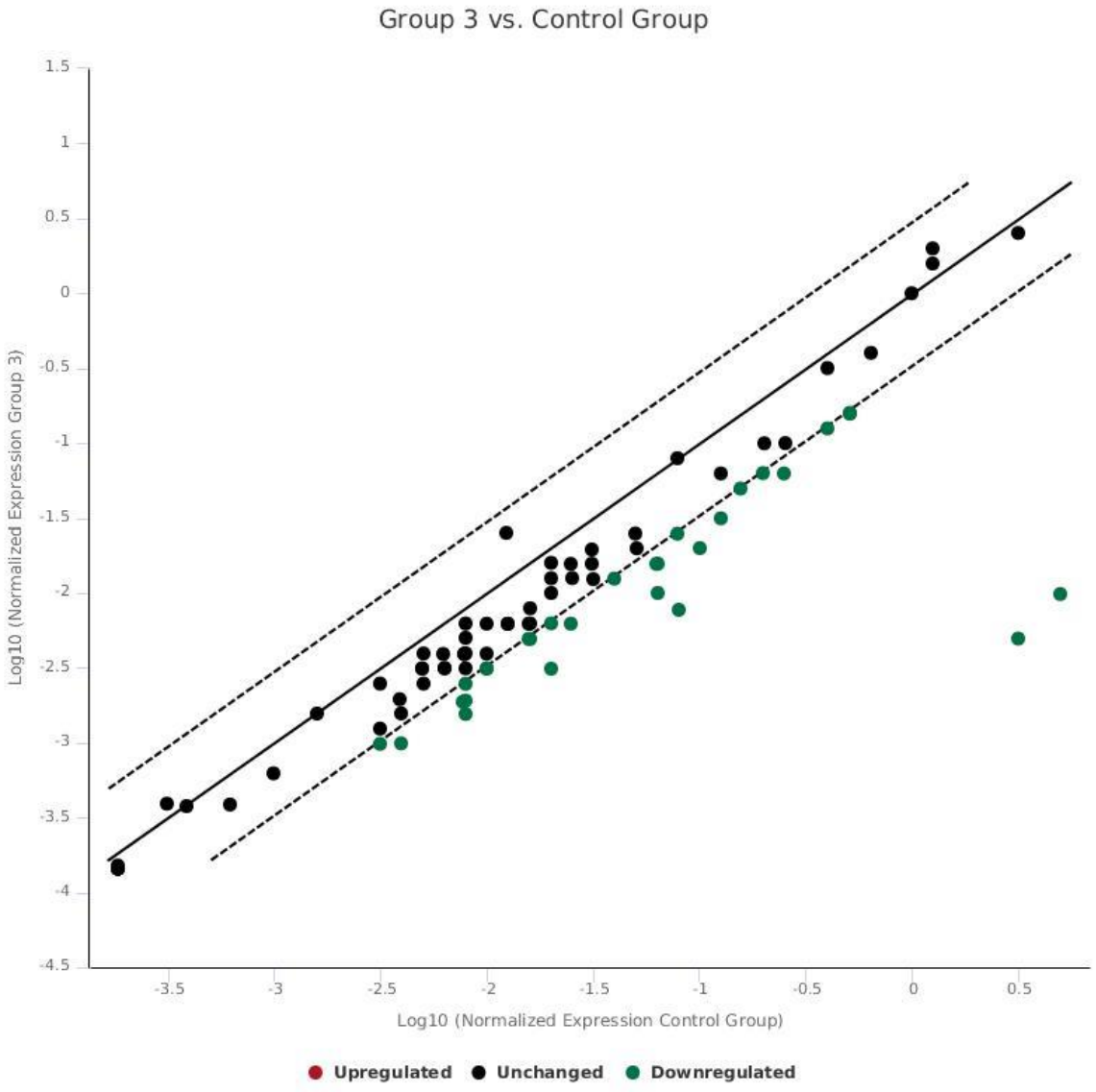

Figure 64: Expression of mitochondria genes in control L6 myotubes compared to treated with 10 µM 4-HNE. Scatter plot shows the treatment group 3 in y-axis against the control group in x-axis. The dotted line indicate 3 fold-regulation.

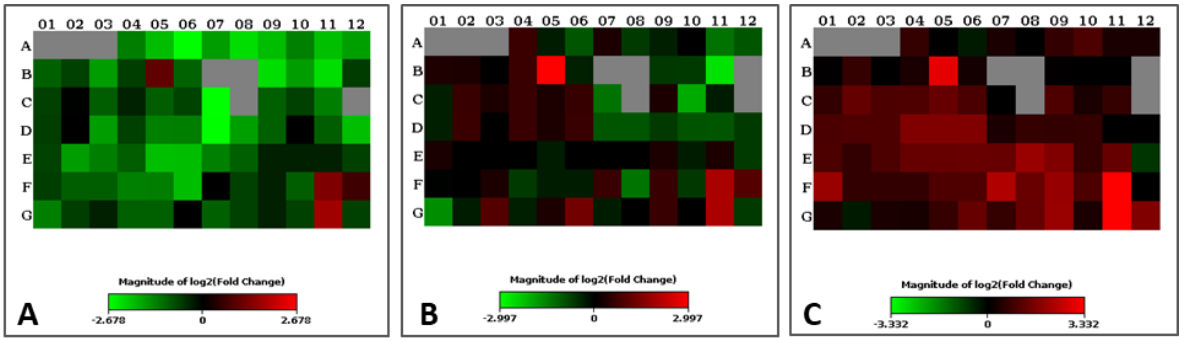

	1	2	3	4	5	6	7	8	9	10	11	12
A	Atp12a	Atp4a	Atp4b	Atp5a1	Atp5b	Atp5c1	Atp5d	Atp5f1	Atp5g1	Atp5g2	Atp5g3	Atp5h
B	Atp5j	Atp5j2	Atp5o	Atp6v0a2	Atp6v0d2	Atp6v1c2	Atp6v1e2	Atp6v1g3	Bcs1l	Cox11	Cox4i1	Cox4i2
C	Cox5a	Cox5b	Cox6a1	Cox6a2	Cox6b1	Cox6b2	Cox6c	Cox7a2	Cox7a2l	Cox7b	Cox8a	Cox8c
D	Cyc1	Lhpp	Ndufa1	Ndufa10	Ndufa11	Ndufa2	Ndufa3	Ndufa4	Ndufa5	Ndufa6	Ndufa7	Ndufa8
E	Ndufab1	Ndufb10	Ndufb2	Ndufb3	Ndufb4	Ndufb5	Ndufb6	Ndufb7	Ndufb8	Ndufb9	Ndufc1	Ndufc2
F	Ndufs1	Ndufs2	Ndufs3	Ndufs4	Ndufs5	Ndufs6	Ndufs7	Ndufs8	Ndufv1	Ndufv2	Ndufv3	Oxa1l
G	Ppa1	Ppa2	Sdha	Sdhb	Sdhc	Sdhd	Uqcr11	Uqcrc1	Uqcrc2	Uqcrfs1	Uqcrh	Uqcrq

Figure 65: Effect of 4-HNE on the gene expression of mitochondrial energy metabolism genes in C2C12 myotubes. Heat map showing downregulated genes in green, unchanged in black and upregulated in red. The symbol and location of each gene in the heat map is shown under the heat maps. The effect of 4-HNE A) 2.5 µM vs. control, B) 5 µM vs. control and C) 10 µM vs. control on the regulation of genes expression. (Results are in averages of triplicates)

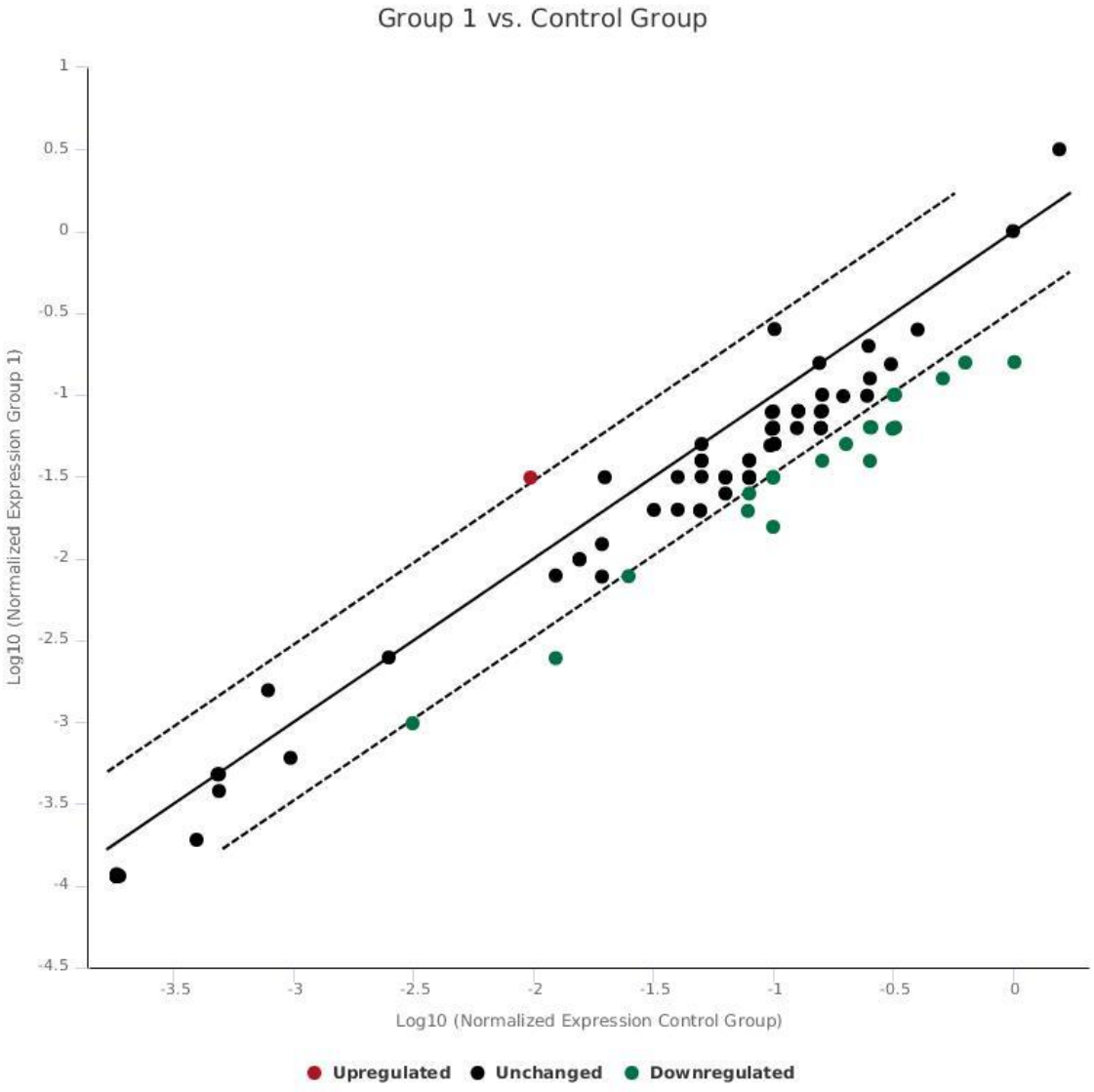

Figure 66: Expression of mitochondrial energy metabolism genes in control C2C12 myotubes compared to myotubes treated with 2.5 µM 4-HNE. Scatter plot shows the treatment group 1 in y-axis against the control group in x-axis. The dotted line indicate 3 fold-regulation.

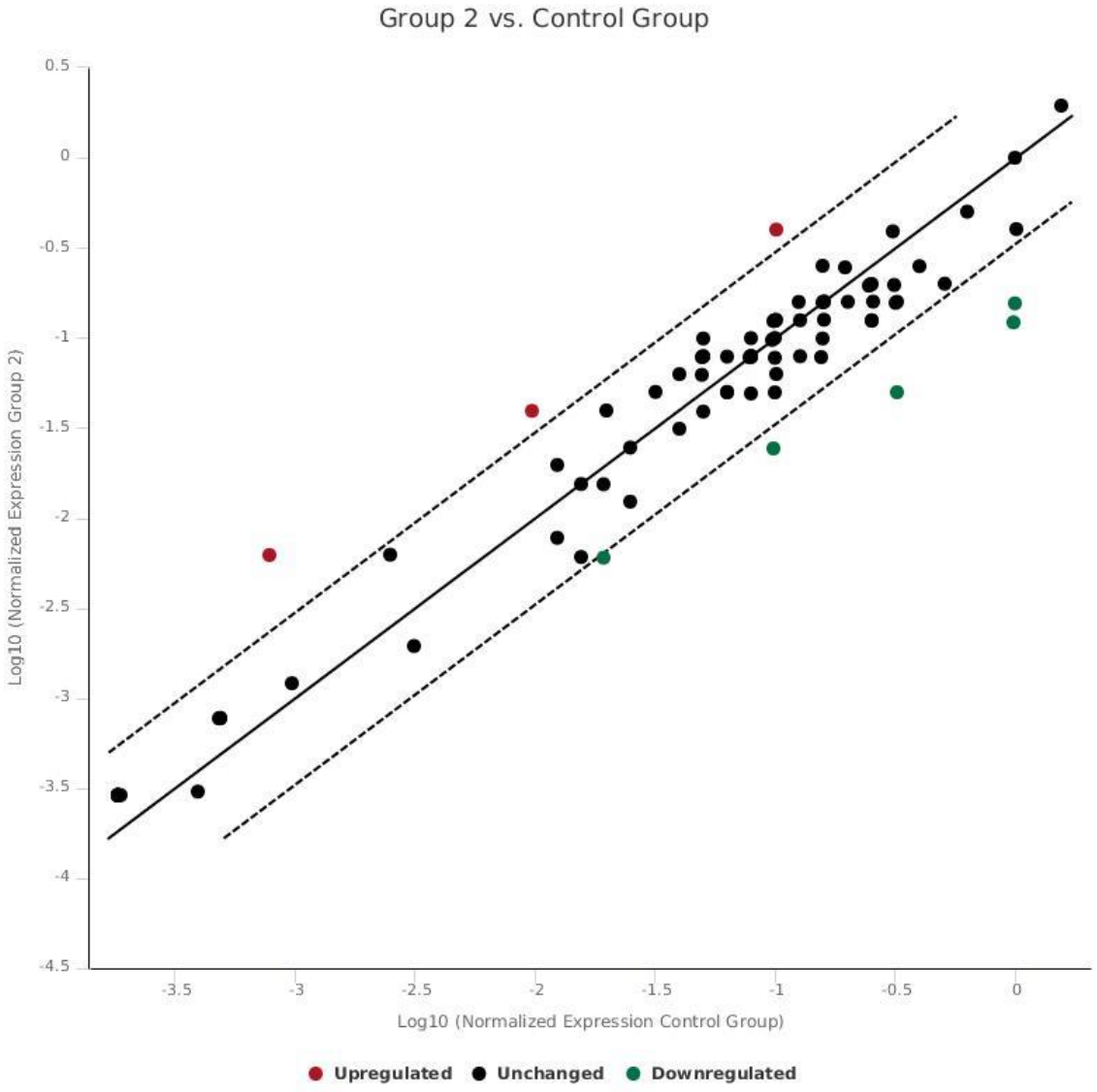

Figure 67: Expression of mitochondrial energy metabolism genes in control C2C12 myotubes compared to myotubes treated with 5 µM 4-HNE. Scatter plot shows the treatment group 2 in y-axis against the control group in x-axis. The dotted line indicate 3 fold-regulation.

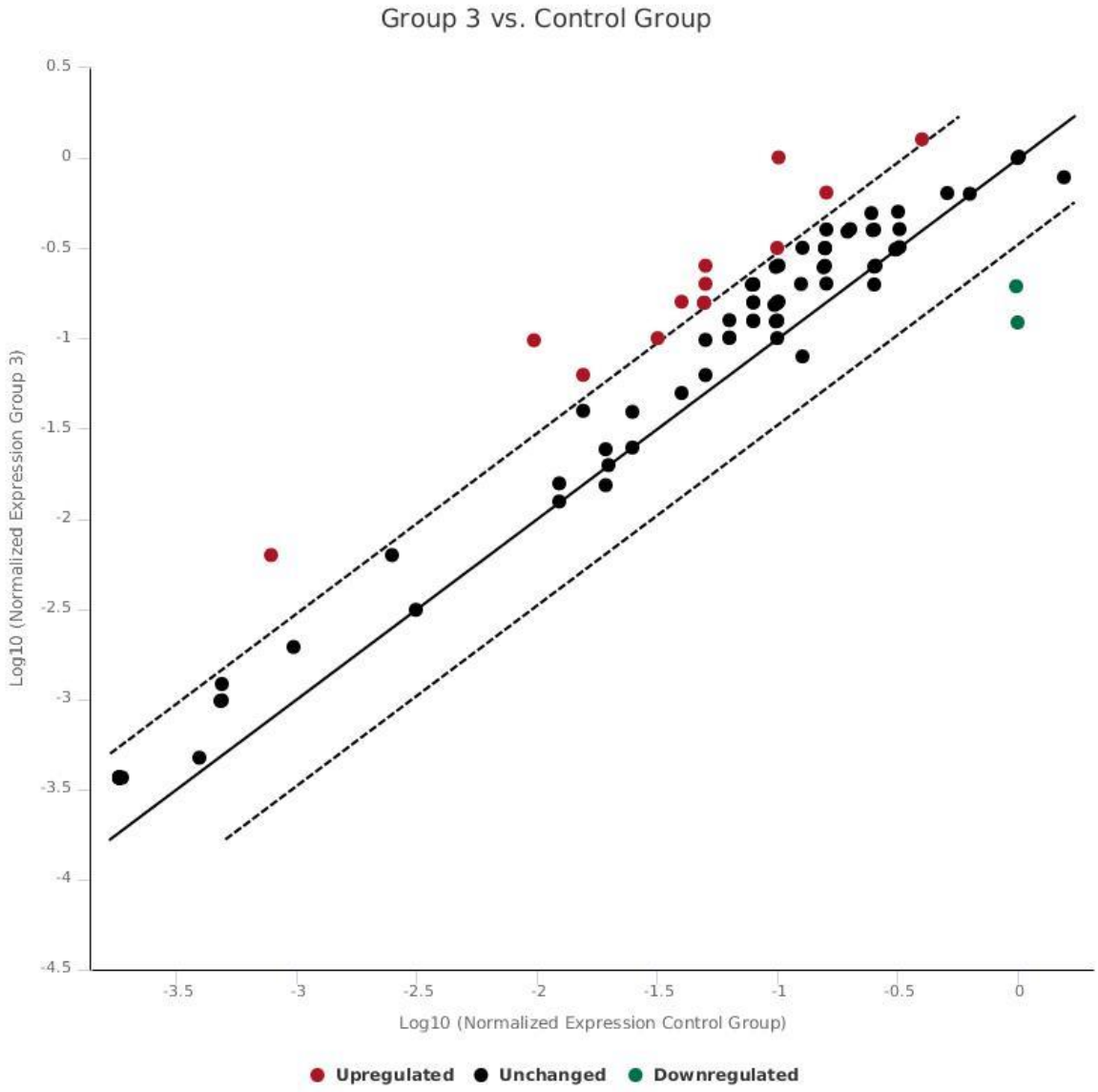

Figure 68: Expression of mitochondrial energy metabolism genes in control C2C12 myotubes compared to myotubes treated with 10 µM 4-HNE. Scatter plot shows the treatment group 3 in y-axis against the control group in x-axis. The dotted line indicate 3 fold-regulation.

4.4.6. 4-HNE induces mitochondrial biogenesis

The overnight treatment of myotubes with 4-HNE significantly (p <0.01) increased mitochondrial density in C2C12 myotubes when treated with 4-HNE concentrations higher than 2.5 µM or higher than 5 µM for L6 myotubes. Fluorescence images of C2C12 myotubes treated with 4-HNE (0, 2.5, 5 and 10 µM) show a clear dose-dependent response of mitochondrial signal (Figure 69).

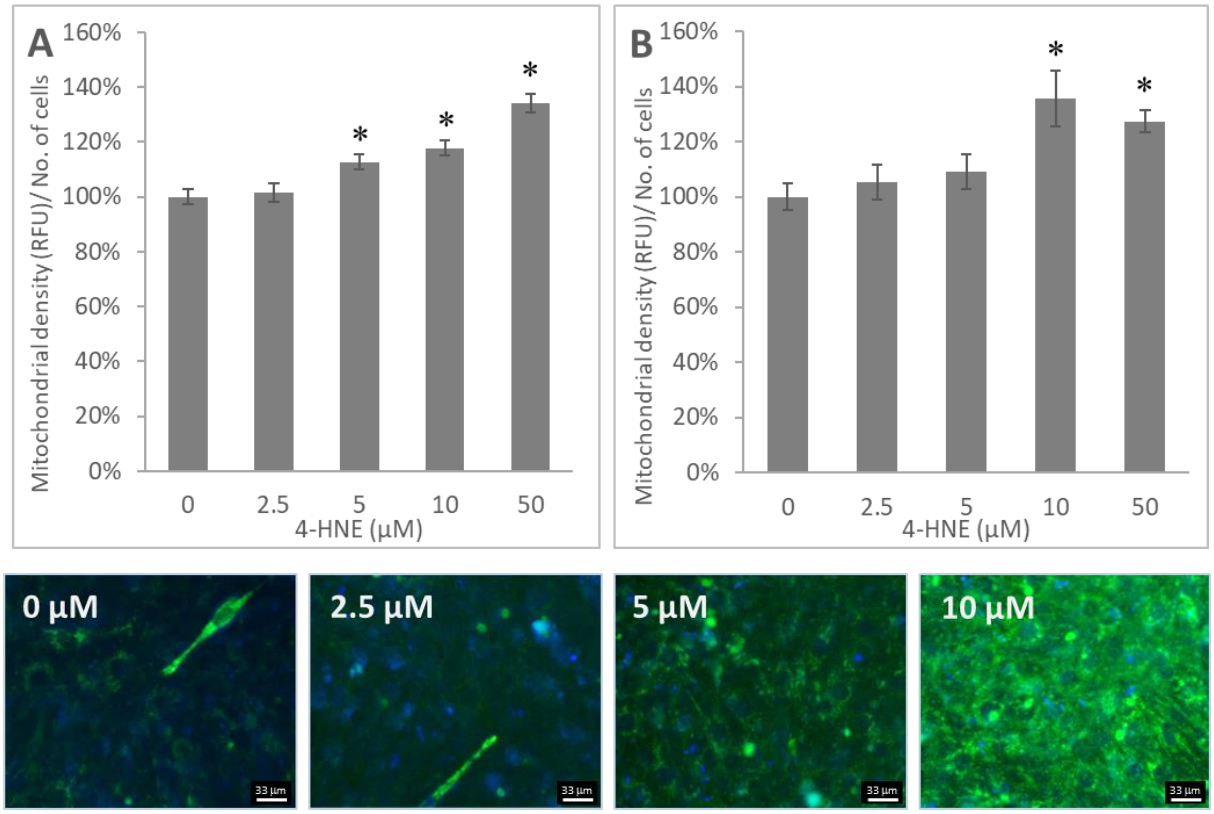

Figure 69: Overnight 4-HNE treatment induced mitochondrial biogenesis. Results shows significant increase in mitochondrial density with 4-HNE treatments for **A.** C2C12 myotubes, and for **B.** L6 myotubes compared to control in a dose-dependent manner. (Results are calculated in percent of control and presented in mean ± *SD* of *N* =3) (* p >0.01). Below is representative images using ArrayScan (20x) of C2C12 stained with MitoTracker for mitochondrial density (Green) and Hoechst for nucleus (Blue).

4.5. Discussion

4-HNE protein modification can alter protein structure and function affecting protein processing, trafficking and normal cellular function (Zarkovic, *et. al.*, 2012; Jaganjac, *et. al.*, 2013) but can also trigger further changes in the myotube viability and cellular redox balance. Indeed, our data show that 4-HNE alters cellular redox homeostasis in time and dose dependent manner. Physiological 4-HNE concentrations did not affect cellular viability and induced neither intracellular H_2O_2 nor $^{\bullet}O_2^-$ production. Contrarily, higher 4-HNE concentrations exerted pathological effects on myotubes, strongly affecting the viability of myotubes and altering cellular redox homeostasis. Interestingly, although pathological concentrations (above 10 µM) significantly induced cellular $^{\bullet}O_2^-$ production in a time dependent manner the same was not observed in the case of H_2O_2 production rendering myotubes less susceptible to 4-HNE induced H_2O_2 formation compared to other cells, such are adipocytes (Elrayess, *et. al.*, 2017). Although physiological 4-HNE concentrations did not seem to affect the myotube viability and cellular redox homeostasis the immediate effect of all concentrations tested impaired ATP synthesis. Furthermore, the immediate effect of physiological 4-HNE also reduced maximal respiration suggesting that immediate 4-HNE stress mediates mitochondrial dysfunction in myotubes. An increased ATP demand can cause mitochondrial overburden impairing mitochondrial functions like oxygen consumption and ATP synthesis promoting further ROS production that can trigger an adaptive cellular response or eventually induce autophagy (Filomeni, *et. al.*, 2015). Though, excessive ROS generation by mitochondria will trigger mitophagy as a cell defense mechanism (Filomeni, *et. al.*, 2015). A study by Galam and coworkers confirmed the specificity of the ROS generation to the mitochondrial NADH dehydrogenase mitochondrial complex (Galam, *et. al.*, 2015), thus, the observed complex I inhibitory effect by 4-HNE suggests possible myotube

hormesis in response to stress. Indeed, results show that the myotubes demonstrated transient adaptation to the acute stress with physiological 4-HNE concentrations but not in the case with supraphysiological concentrations. The 4-HNE induced hormesis was further supported by upregulation of 13 mitochondrial metabolism genes (Figure 70) and downregulation of 76 mitochondrial genes 24 hours after exposure. The observed effect of 4-HNE on several mitochondrial genes support the ability of 4-HNE to induce mitochondrial biogenesis. Indeed, a dose dependent increase in mitochondrial density was noticed 24 hours after acute exposure to 4-HNE. It is possible that 4-HNE could be one of the mechanisms that evokes mitochondrial biogenesis process as a physiological adaptation to endurance exercise (Hyatt, *et. al.*, 2015).

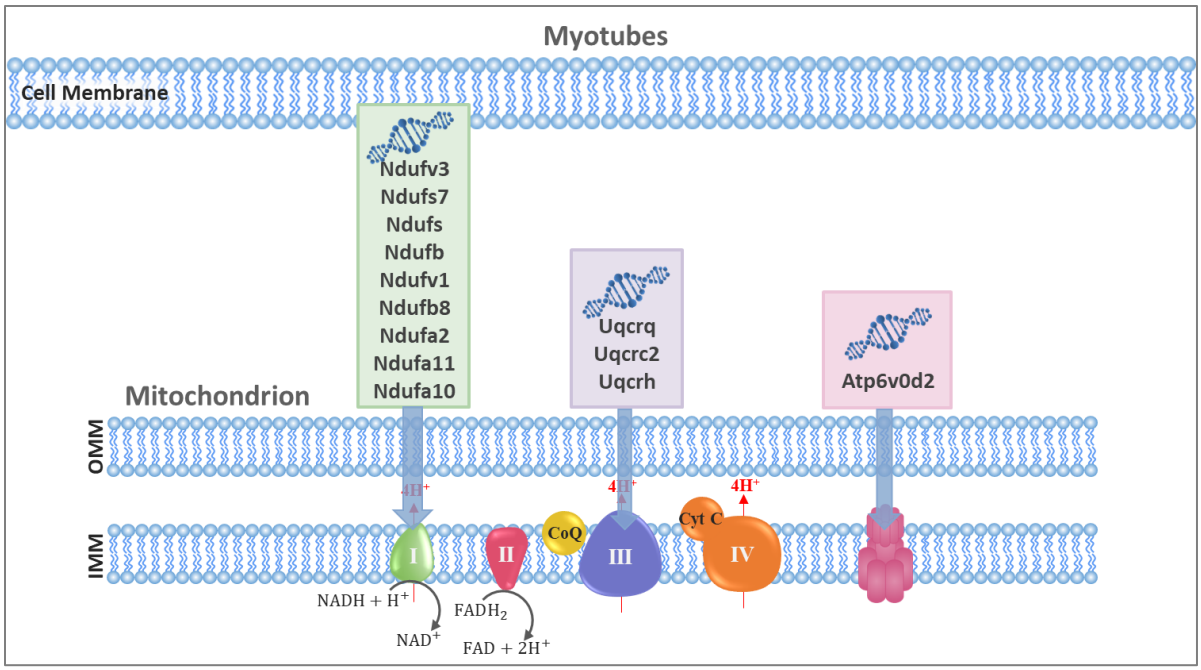

Figure 70: 4-HNE induces upregulation of mitochondrial metabolism genes. Summary of genes upregulated by 4-HNE treatment on C2C12 myotubes. Upregulated genes are involved in complex I (NADH-coenzyme Q reductase), complex III (coenzyme Q-cytochrome c reductase) and complex V (ATP synthase).

Furthermore, comparing the effects of caffeine with those of 4-HNE can give indication on the possible cellular regulations that are triggered by 4-HNE induced by caffeine through calcium oscillations or other signaling mechanisms. For example, results showed that both caffeine and 4-HNE caused upregulation of Uqcrc2 gene, which is involved in mitochondrial complex III. Moreover, both treatments downregulated several genes listed in Table 4.

Table 4: List of genes that are downregulated by both caffeine and 4-HNE treatment. Downregulated genes are listed with their main function in mitochondrial respiration.

Main Function	Genes Symbols
Complex IV (Cytochrome c Oxidase)	Cox4i1, Cox6c, Cox11
Complex V (ATP Synthase)	Atp5b, Atp5d, Atp5g3, Atp5h, Atp5o
Membrane Polarization & Potential	Bcl2, Bcl2l1 (Bcl-xl), Gclm, Sod1
Mitochondrial Transport	Aip, Bak1, Bcl2, Bcl2l1 (Bcl-xl), Cpt2, Grpel1, Hsp90aa1 (Hspca), Hspd1
Small Molecule Transport	Slc25a19, Slc25a5
Targeting Proteins to Mitochondria	Aip, Akt1, Cln8, Cox18, Gpx1, Grpel1, Hspd1
Mitochondrial Fission & Fusion	Cox18, Fis1
Apoptosis	Aifm2, Akt1, Bak1, Bcl2, Bcl2l1 (Bcl-xl), Gpx1, Pmaip1 (Noxa)

5. *IN-VIVO* EXERCISE-INDUCED 4-HNE PROTEIN ADDUCTS FORMATION IN SKELETAL MUSCLES IDENTIFIED USING NANO-LC MS/MS

5.1. Introduction

4-HNE usually binds to the nucleophilic functional groups of membrane lipids, nucleic acids, and proteins through formation of covalent adduct (Zhong and Yin, 2015). The 4-HNE modification of proteins can take place by two mechanisms: Michael addition or Schiff-bases (Rauniyar and Prokai, 2009). In Michael addition, the addition of 4-HNE to the nucleoplilic groups of amino acid results in addition of 156 Da to the molecular mass of the protein for each 4-HNE added. On the other hand, Schiff-bases form a covalent adducts to the –NH2 groups of amino acid. However, due to the loss of water molecule in the reaction, only 138 Da is added to the molecular mass of the protein for each 4-HNE added (Rauniyar and Prokai, 2009). The aim was to study the effect of exercise on the formation of 4-HNE post-translational modifications of proteins in animal model using most advanced mass spectrometry techniques to detect site specific 4-HNE protein modification.

5.2. Methodology

5.2.1. Development of liquid chromatography-mass spectrometry (LC-MS) method to measure site specific 4-HNE modifications of proteins

5.2.1.1. Sample preparation

For the development of a rapid and sensitive method for the identification of protein site specific 4-HNE-modifications, fatty acid free bovine serum albumin (BSA, SIGMA) was used. For the preparation of HNE-BSA samples, 2 mg/mL BSA was treated with different 4-HNE concentrations (0, 6.25, 12.5, 25, 50, 100, 200 and 400 µM) and incubated for one hour at room temperature. Standard HNE-BSA samples were then prepared for the proteomics analysis as described in (Al-Thani, *et. al.*, 2018 and Ludtmann, et. al., 2018). Briefly, samples prepared in non-reducing sample buffer were electophoretically separated by the sodium dodecyl sulfate-polyacrylamide gel electrophoresis (SDS-PAGE) (ExcelGel SDS Homogeneous 12.5%, GE Healthcare), with the following running condition: 600 V, 50 mA, 30 W for 80 min. The SDS-PAGE was performed using a Multiphor II electrophoresis system (Amersham biocsiences). Then, each sample in the gel was excised into eight pieces, reduced with 10 mM dithiothreitol (DTT, SIGMA) in 100 mM ammonium bicarbonate, followed by alkylation of samples by 100 mM iodoacetamide (SIGMA) in 100 mM ammonium bicarbonate, and overnight digestion at 37°C with 20 ng/µL Trypsin Gold MS grade (Promega) in 50 mM ammonium bicarbonate. Mixture of 45% water, 50% acetonitrile and 5% formic acid was used to extract peptides. Peptides were further analyzed by Orbitrap FUSION tribrid mass spectrometer (Thermo Scientific) coupled with Easy n-LC II (Thermo Scientific) for nano LC-MS/MS analysis.

5.2.1.2. LC-Orbitrap MS/MS analysis

All peptide fractions, 8/sample, were analyzed separately using the Orbitrap FUSION tribrid mass spectrometer (Thermo Scientific, San Jose, California, USA) coupled with Easy n-LC II for nano LC gradient separation. Column used is Acclaim RSLC C18 (25 cm, 75 µm, 2 µm) attached to a pre-trapping column Acclaim C18 (2 cm, 75 µm, 3 µm) (Thermo Scientific, San Jose, California, USA). Thermo Xcalibur (version 3.0) software was used to control instrument setup. Nanoelectrospray ionization (NSI) mode was used, which is the preferred ionization mode for peptides and proteins. The LC-MS/MS parameters were adjusted as recommended by the manufacturer guide for the NSI mode, which included a spray voltage of 1.2 kV for the positive mode. The ion transfer tube temperature was assigned to be 275ºC. Peptide mixtures were separated on a 25 cm reverse-phase C18 column and elution was carried out at a constant flow rate of 300 nL/min over 108 min step gradient. Solvents used for separation were solvent A (HPLC-grade water with 0.1% (v/v) formic acid) and solvent B (HPLC-grade Acetonitrile with 0.1% (v/v) formic acid). The separation gradient was set to: 5% B for 5 min, 5-37% B for 90 min, 37-80% B for 4 min, hold at 80% B for 2 min, 80-5% B for 2 min and hold at 5% B for 5 min. Figure 71 presents the gradient used.

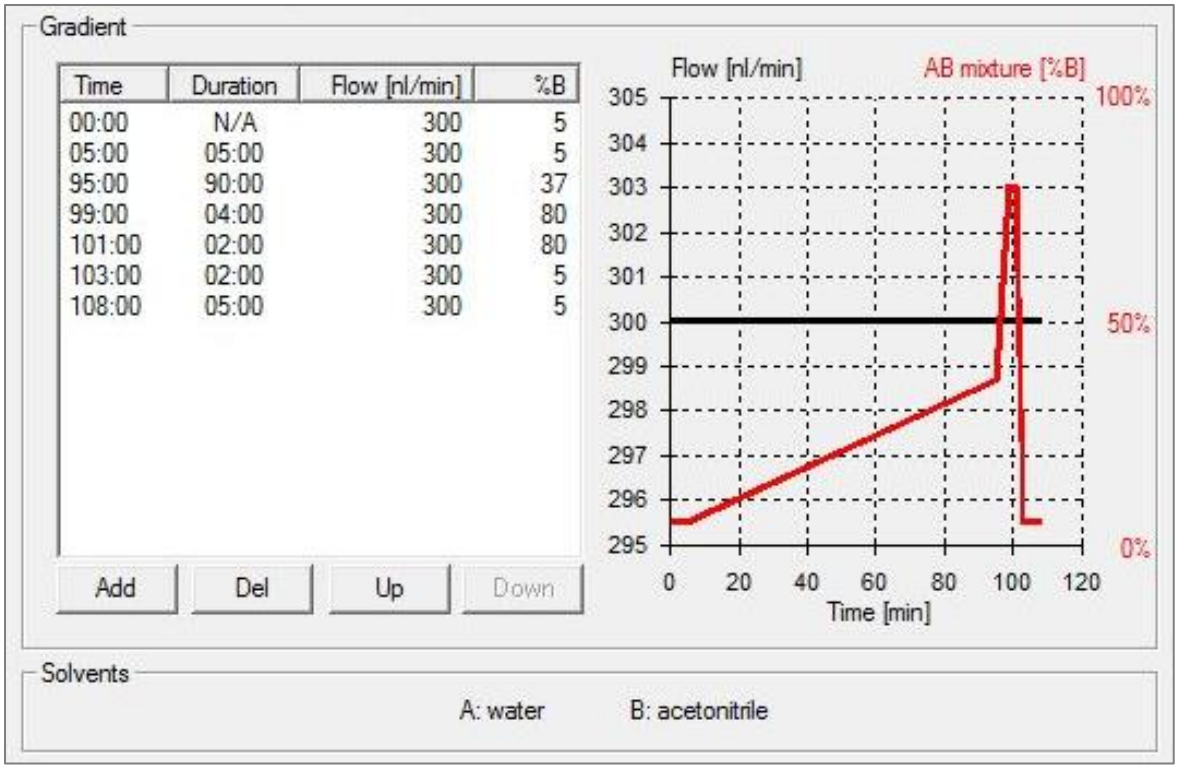

Figure 71: LC gradient setup in Thermo Xcalibur (version 3.0) software used to develop an LC-MS method to measure site specific 4-HNE modifications of proteins. The elution was carried out at a constant flow rate of 300 nL/min over 108 min gradient.

The Orbitrap FUSION Tribrid analysis was set to data-dependent acquisition (DDA) using orbitrap mass analyzer to acquire full MS spectra and the ion trap to acquire MS/MS fragment ion spectra. First full scan mode acquisition was performed with 120,000 orbitrap resolution, and scan range of 400-1600 m/z. Automatic gain control (AGC) was set at 200,000 with 100 ms injection time. This scan mode was carried out with enabling monoisotopic precursor selection (MIPS) filter and dynamic exclusion with 30 seconds duration and 10 ppm mass tolerance. This is followed by two different second scan modes based on decisions of two scan event types. Scan event type 1 uses higher energy collision-induced dissociation (HCD) fragmentation at Quadrupole isolation mode, which generates b and y ions, with 2 m/z isolation

width, 30% collision energy, at 10,000 AGC, and 70 ms maximum injection time. Neutral loss ion is triggered with masses of: 52 or 78 m/z from the 156 Da 4-HNE- modified peptide by Michael addition, or masses of: 46 or 69 m/z from the 138 Da 4-HNE- modified peptide by Schiff-bases (Carini, *et. al.*, 2004). Selected peptides are further fragmented by electron transfer dissociation (ETD), which generates c and z ions and cleaves the amide group leaving the side chain intact, using Quadrupole isolation mode with 2 m/z isolation width, 30% collision energy, at 10,000 AGC, and 70 ms maximum injection time. While scan event type 2 is HCD fragmentation at Quadrupole isolation mode with 1.6 m/z isolation width, 30% collision energy, at 10,000 AGC, and 70 ms maximum injection time. Figure 72 shows the flow of scan type used.

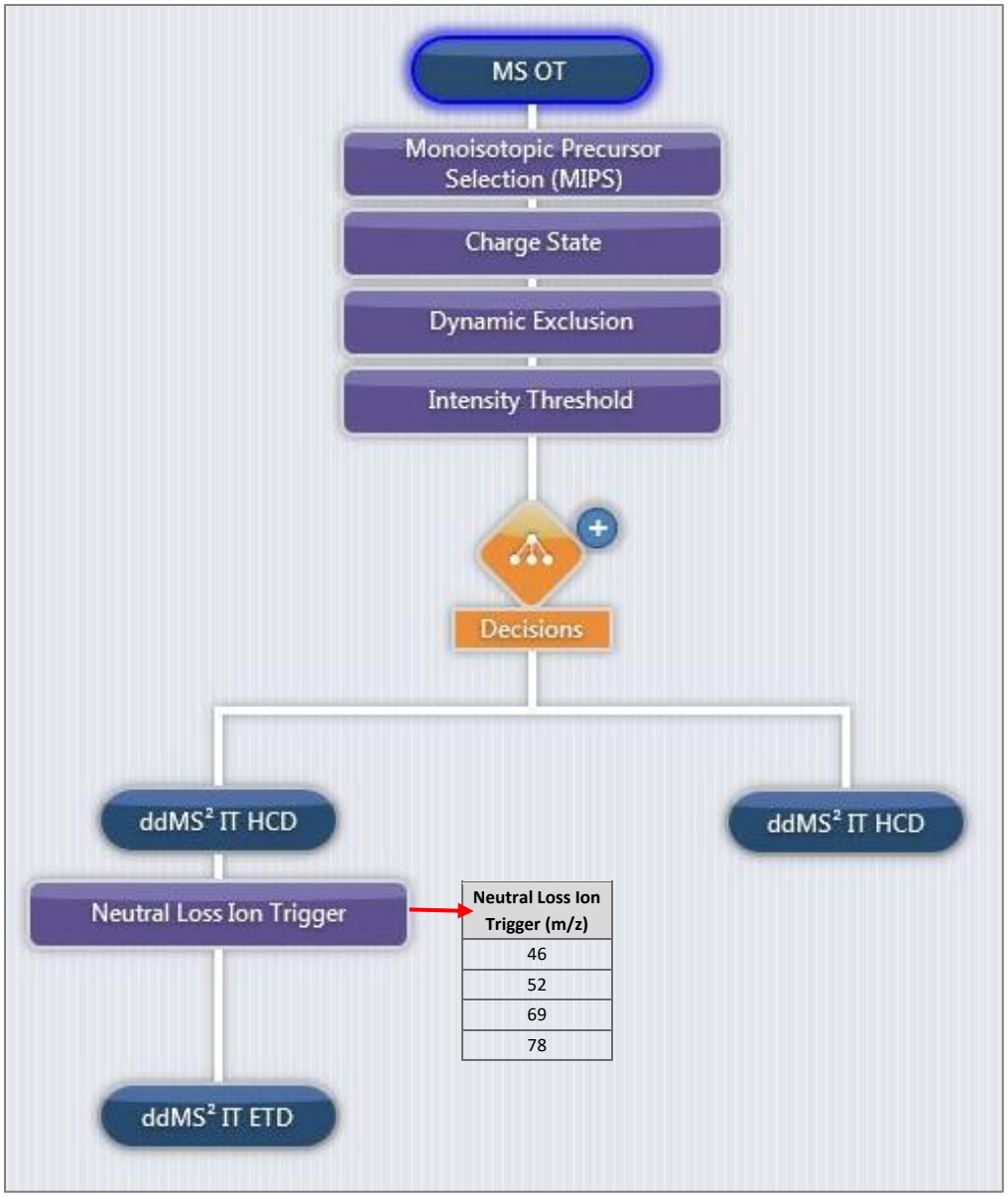

Figure 72: Scheme of the mass spectrometry created in Thermo Xcalibur (3.0) that uses DDA HCD and ETD fragmentation of peptides. The method shows full scan run followed by fragmentation using HCD. Then, trigger neutral loss ion search with masses of: 52 or 78 m/z from the 156 Da 4-HNE- modified peptide by Michael addition, or masses of: 46 or 69 m/z from the 138 Da 4-HNE- modified peptide by Schiff-bases, followed by ETD fragmentation to insure that fragmentation will leave the 4-HNE modification intact.

5.2.1.3. Data analysis

The raw data generated by the Orbitrap FUSION were processed using Proteome Discoverer 1.4 (Thermo Scientific, San Jose, California, USA), workflow is shown in Figure 73. The MS/MS spectra search was carried using SEQUEST HT search engine against Uniprot *Bos taurus* protein database (downloaded on 25th Dec. 2014). The parameters used are following: full trypsin digestion, maximum of 2 cleavages allowed, min. of 350 Da precursor mass, max. of 5000 Da precursor mass, tolerance of 20 ppm for precursor mass and 0.6 Da for fragment mass. Two scan events were used: first scan event using HCD activation type with dynamic modification of methionine oxidation (+15.995 Da) and static modifications of carbamidomethylation of cysteine (+57.021 Da), second scan event using ETD activation type with SEQUEST HT dynamic modification of methionine oxidation (+15.995 Da), carbamidomethylation of cysteine (+57.021 Da), 4-HNE of cysteine, histidine, lysine (+156.115 Da), 4-HNE + H_2 for the Michael adducts in cysteine, histidine, and lysine (+158.131 Da), and 4-HNE - H_2O for the Schiff-bases in cysteine, histidine, and lysine (+138.104 Da). The SEQUEST HT was followed by target decoy PSM validator used for peptide validation with false discovery rate (FDR) of 0.01. The values set for the XCorr confidence threshold of low and high resolution data are listed on Table 5. The resulting reports were searched using high confidence peptides filter. Data were quantified using precursor ion area detector.

Table 5: The XCorr confidence of high and low resolution limits for assigning PSMs

XCorr Confidence Threshold (low-resolution data)	
z=1: High confidence XCorr	1.8
z=1: Medium confidence XCorr	0.7
z=2: High confidence XCorr	2.4
z=2: Medium confidence XCorr	0.9
z=3: High confidence XCorr	2.5
z=3: Medium confidence XCorr	1.2
z>=4: High confidence XCorr	3
z>=4: Medium confidence XCorr	1.5

XCorr Confidence Threshold (high-resolution data)	
z=1: High confidence XCorr	1.8
z=1: Medium confidence XCorr	0.7
z=2: High confidence XCorr	2.4
z=2: Medium confidence XCorr	0.8
z=3: High confidence XCorr	2.5
z=3: Medium confidence XCorr	1
z>=4: High confidence XCorr	2.6
z>=4: Medium confidence XCorr	1.2

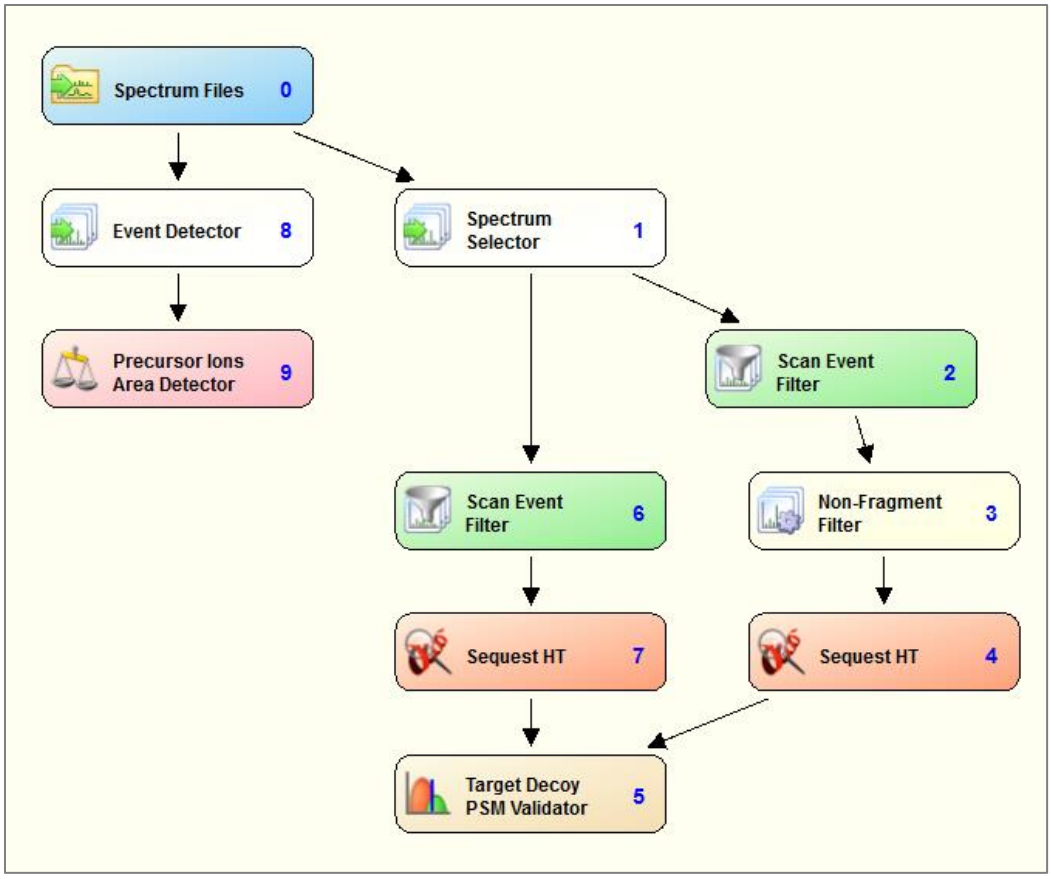

Figure 73: Proteome Discoverer 1.4 workflow for the analysis of raw data generated by Orbitrap FUSION. It includes two scan events filter for HCD and ETD activation types.

5.2.2. Effect of intensive physical exercise on 4-HNE post translational modifications of proteins of skeletal muscle tissues

5.2.2.1. Animal model

Tissue samples were prepared and provided by Prof. Alexander Gourine (Div. of Biosciences, University College London, UK). Male mice (8-10 weeks old) C57BL/6J were divided into two groups (N =7 each): a control group with a sedentary lifestyle, and an exercised group with intensive training through swimming for 5 months, 60 min per day for 5 days per week. After that, skeletal muscle tissues from right quadriceps femoris were dissected from both groups and prepared as described in 5.2.2.2. At the time of sample collection mice were 7 to 7.5 months old.

5.2.2.2.Tissues preparation and analysis

Tissues were ground into powder in ice cold lysis buffer (20 mM HEPES, 20 mM NaCl, 5 mM EDTA, 1% w/v CHAPS and protease inhibitors) 7 mL of buffer was added per 1 g of tissue. Then, samples were sonicated for 10 min., centrifugation at 14,000×g for 10 min to pellet any un-extracted materials. Finally, protein concentration was determined using BCA Protein Assay Kit (Pierce) to normalize all samples. Proteins were electophoretically separated in SDS-PAGE using non-reducing sample buffer (Invitrogen 84788), run on Mini Gel Tank system (Life Technologies) with the following conditions: 100 V, 69 mA for 2 hours. Then, samples were digested with Trypsin Gold MS grade, according to the method described in section 5.2.1.1. Peptides were further analyzed by Orbitrap FUSION coupled with Easy n-LC II for nano LC-MS/MS analysis. Thermo Xcalibur (version 3.0) software was used to control the instrument setup. DDA was performed using FTMS master scan preview mode, mass range 400 – 1600 m/z at 120000 resolution, for triggering MS/MS events. The mass spectra analyzed in DDA were set

as described in the section above (5.2.1.2). The obtained raw data were processed using Proteome Discoverer 1.4 and 2.2 (Thermo Scientific, San Jose, California, USA). Figure 74 shows the scheme of full protocol for samples preparation.

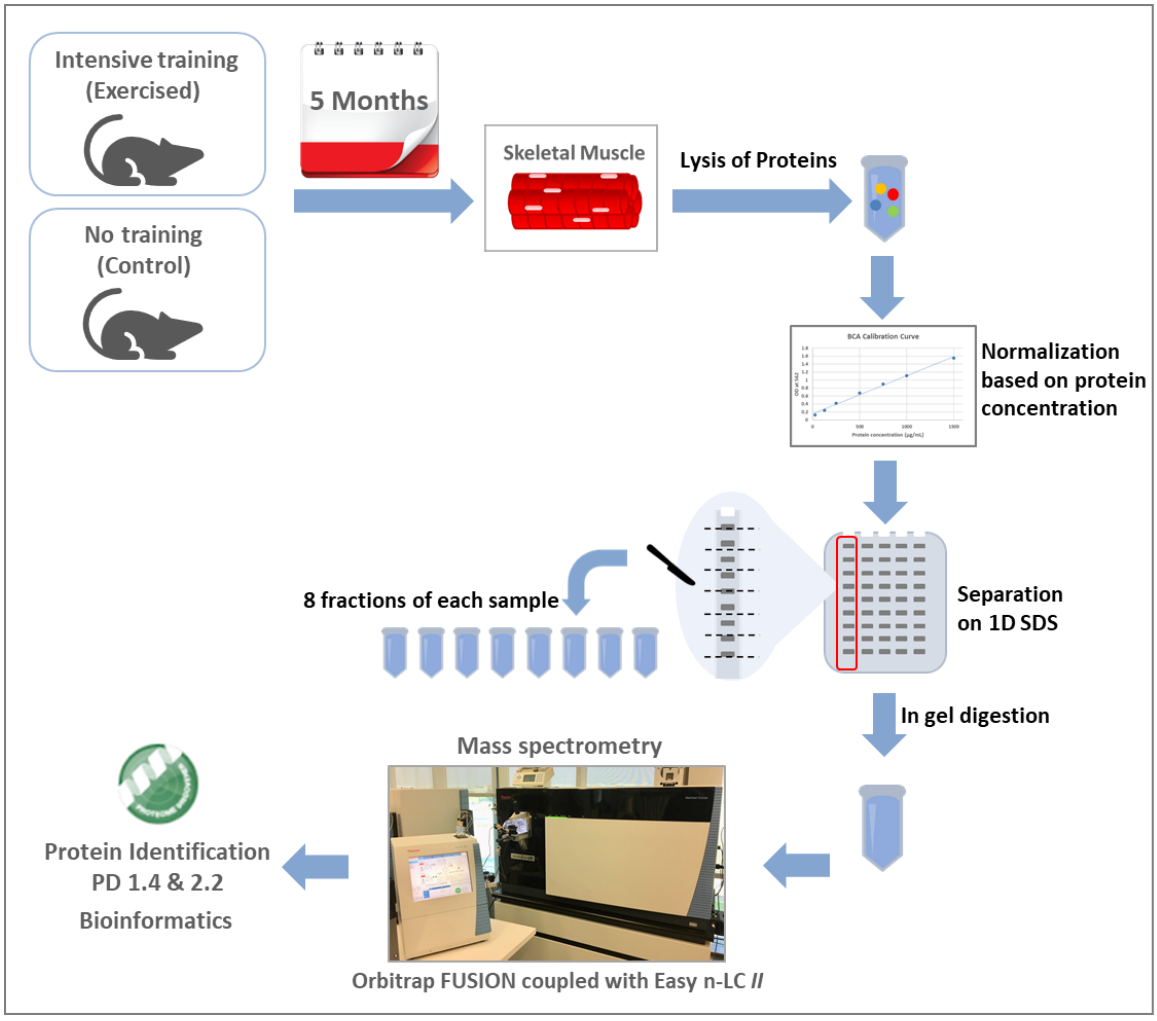

Figure 74: Scheme of samples preparation for proteomic analysis. Two groups of mice (7 each): trained group intensively for 5 months and untrained group as control. Skeletal tissue samples were collected followed by lysis of proteins, normalization based on concentration, separation on 1D SDS-PAGE, in gel digestion and fractionation into 8 equal fractions. Samples were then analyzed on LC/MS coupled with Easy n-LC II. Results were processed using PD software.

5.2.2.3. Data analysis

The raw data generated by the Orbitrap FUSION were processed using Proteome Discoverer 1.4 and 2.2. Figure 75 shows the processing workflow and the consensus workflow set in the Proteome Discoverer 2.2. Spectrum selector filter was assigned with 350 Da as minimum precursor mass, and 5000 Da as the maximum precursor mass. The MS/MS spectra search were carried using SEQUEST HT search algorithms against Uniprot *Mus musculus* (Mouse) protein database, FASTA file was retrieved on 09th of October, 2017. Two scan event filters were used: one with HCD activation type followed by SEQUEST HT search with the following parameters: full trypsin digestion, maximum of 2 missed cleavages sites, minimum of 6 peptides, tolerance of 20 ppm for precursor mass and 0.6 Da for fragment mass, dynamic modification of oxidation of methionine (+15.995 Da) and static modification of carbamidomethyl of cysteine (+57.021 Da). The second scan event filter with ETD activation type and 1000 was set as maximum collision energy. Followed by second SEQUEST HT where parameters used were the same as HCD, except for the selection of modifications: dynamic modification of oxidation of methionine (+15.995 Da), carbamidomethyl of cysteine (+57.021 Da), 4-HNE of cysteine, histidine, lysine, leucine, methionine and arginine (+156.115 Da), 4-HNE + H_2 for the Michael adducts in cysteine, histidine, lysine, leucine, methionine and arginine (+158.131 Da), and 4-HNE - H_2O for the Schiff-bases in cysteine, histidine, lysine, leucine, methionine and arginine (+138.104 Da). Target decoy PSM Validator node was used for peptide validation with FDR of 0.01. The values set for the XCorr confidence threshold of low and high resolution data are listed on Table 5. For precursor ion quantification minora feature detector was used. On the other hand, the consensus workflow parameters used: peptide validator with automatic validation mode of 0.01 FDR, peptides and proteins were searched using high

confidence peptides filter and precursor ion quantifier calculated abundance based on the intensity. Prior proteomics analysis, data were preprocessed based on the following criteria: identified protein or peptide must be common for 5 or more tissue samples of the same group of animals. Furthermore, identified proteins were searched for their annotation using STRAP software (version 1.5.0.0, free online software Tool for Rapid Annotation of Proteins developed by Cardiovascular Proteomics Center, Center for Biomedical Mass Spectrometry at Boston University School of Medicine)

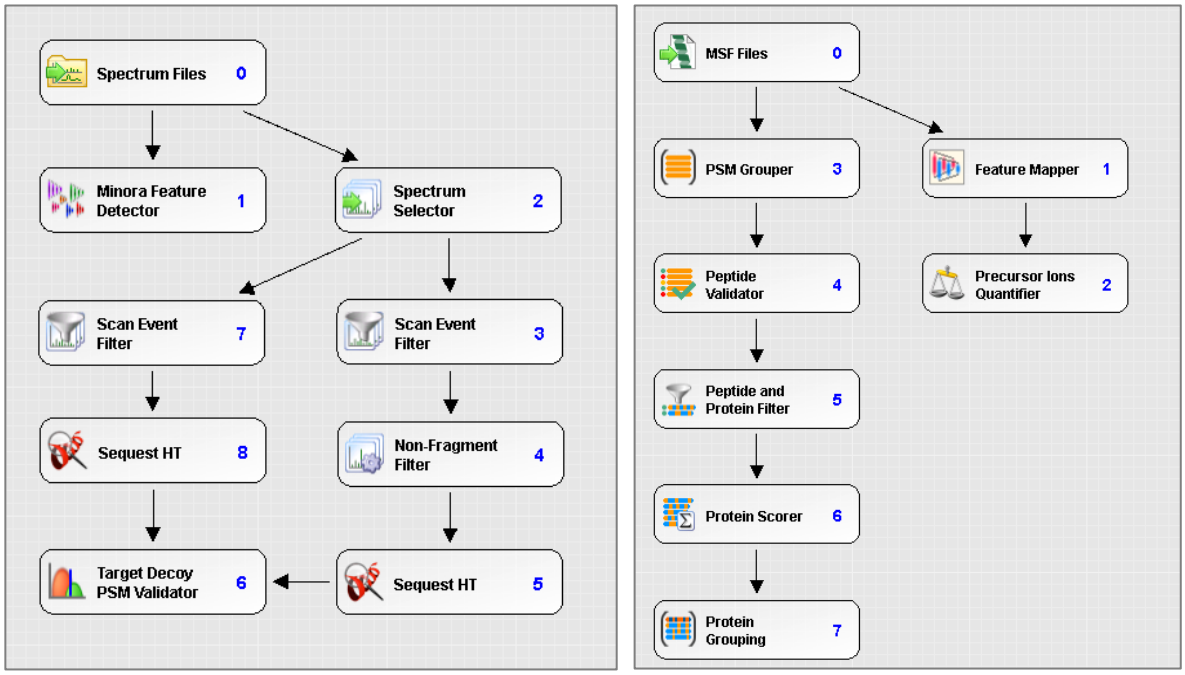

Figure 75: Proteome Discoverer (2.2) workflows. Processing workflow on left and consensus workflow on right. The nodes are setup for analysis of both HCD and ETD activation types in two scan events.

5.3. Results

5.3.1. Nano-Liquid chromatography-tandem mass spectrometry (nLC-MS/MS) method to measure site specific 4-HNE modifications of proteins

4-HNE covalently binds with the nucleophilic functional group of proteins to form a covalent adducts that could affect many signaling processes in cells. A rapid and sensitive method for identification of 4-HNE-modified proteins was developed using a set of HNE-BSA standards. Table 6 shows that all samples gave very good coverage determined by the identification of high confidence level peptides and few medium confidence peptides when compared to the database search.

Table 6: Peptides identification confidence level of all samples gave very high coverage with high and medium confidence level.

4-HNE	Percentage of coverage with high and medium confidence level
400µM	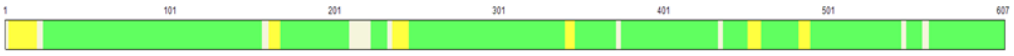
200 µM	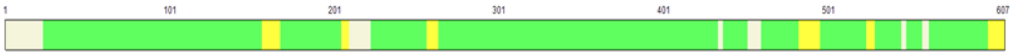
100 µM	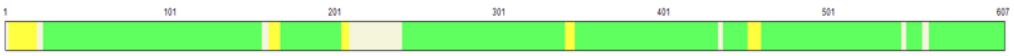
50 µM	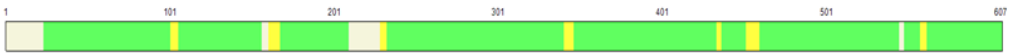
25 µM	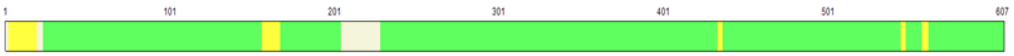
12.5 µM	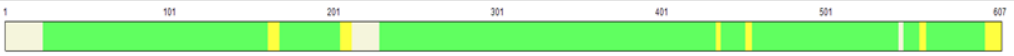
6.25 µM	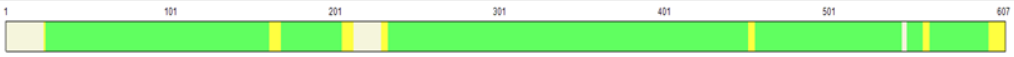
0 µM	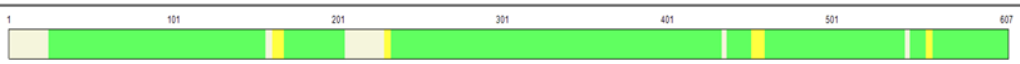

High confidence level Medium confidence level

Majority of identified peptides occurred from HCD fragmentation method compared to the ETD fragmentation in both control and treated samples (Figure 76). In the control sample >75% identified peptides originated from the HCD activation type while only 1% originated from the ETD only activation (Figure 76A). The number of peptides identified with HCD gradually decreased with the increasing 4-HNE concentrations reaching <55% in 400 µM treated BSA. Contrary, the number of peptides identified with ETD followed the increase in 4-HNE concentration up to >20% in 400 µM treated BSA (Figure 76B).

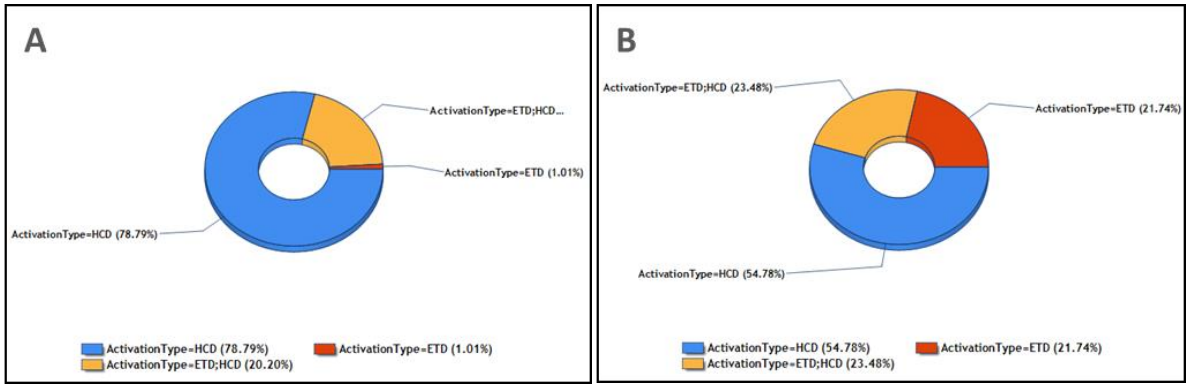

Figure 76: Fragmentation methods selected from the activation types were: HCD, ETD and both HCD and ETD. HCD produces a highly abundant series of reporter ions, while ETD cleaves peptide backbone, but side chains and modifications are left intact. **A.** is the control sample; **B**. is sample with highest 4-HNE treatment (400 µM).

The representative ETD spectra of 4-HNE modified peptide is shown on Figure 77 a total of 10 inter-residue bonds have been cleaved. The mass difference between fragment ions c_2 (m/z 259.21287) and c_3 (m/z 552.38681) is 156 Da higher due to adduction of 4-HNE to His amino acid. The modification of His has been confirmed in the z-series of ions with the 156 Da higher mass difference between z_{10} (m/z 1153.46637) and z_{11} (m/z 1446.82031) ions leading to unequivocal mapping of the 4-HNE to His-3 of this peptide.

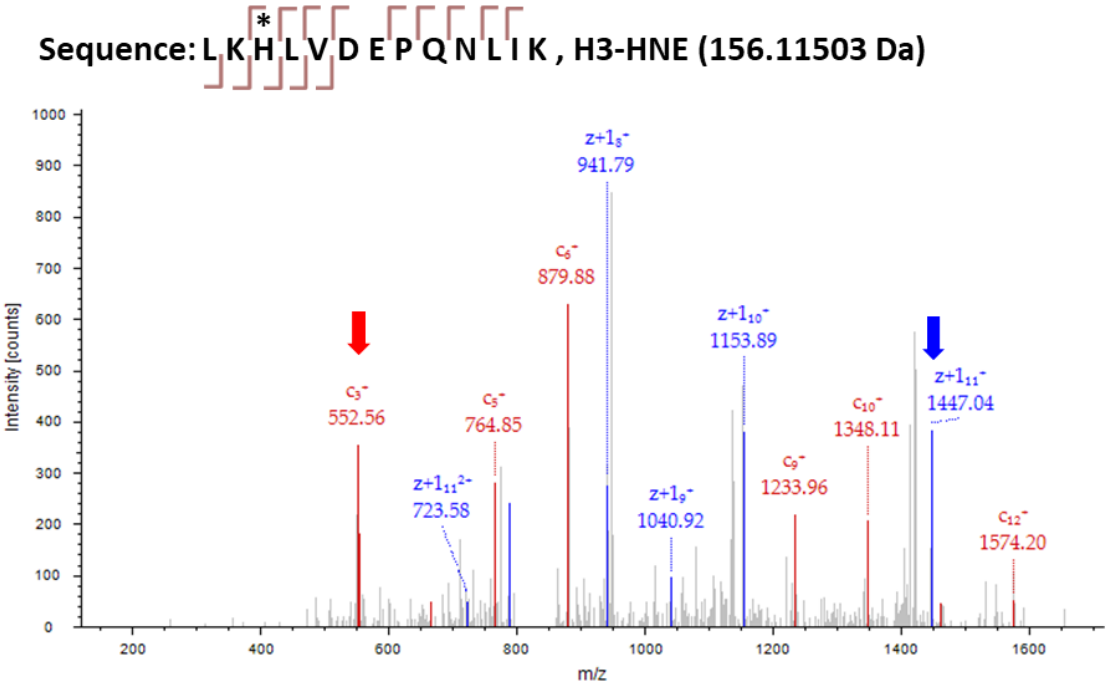

Figure 77: Peptide fragmentation result with 4-HNE modification. ETD tandem MS spectra of the BSA derived tryptic peptides, confirming the 4-HNE modification of BSA. The mass difference between fragment ions c_2 (m/z 259.21287) and c_3 (m/z 552.38681) is 156 Da higher due to adduction of 4-HNE to His amino acid (marked with red arrow). Similarly, mass difference between z_{10} (m/z 1153.46637) and z_{11} (m/z 1446.82031) ions is 156 Da higher (marked with blue arrow). * 4-HNE modification of amino acid

Furthermore, comparison of amino acid sites modified in respect to 4-HNE has been performed (Table 7). The obtain results show concentration dependent changes in the number of modified amino acids which resembled the increase in the number of 4-HNE-modified peptides. Treatment of BSA with the highest 4-HNE concentration (400 µM) resulted in the highest number of modified amino acids (Figure 78) while BSA treated with the lowest concentration of HNE (6.25 µM) had only few amino acids modified, such as 42-H and 44-K. The average coverage of 4-HNE treated BSA samples was 92.26% (min 90.44% and max 95.06%).

Table 7: Summary of percentage of coverage of BSA peptides fragmented by ETD method with number of identified 4-HNE modification with each concentration

HNE (µM)	% Coverage (Full)	No. of modified peptides ETD (Full)	No. of modification ETD (Full)
400	93.57	25	38
200	91.10	22	32
100	91.43	13	22
50	91.93	12	19
25	95.06	7	12
12.5	92.92	6	9
6.25	92.92	4	8
0	90.44	1	1

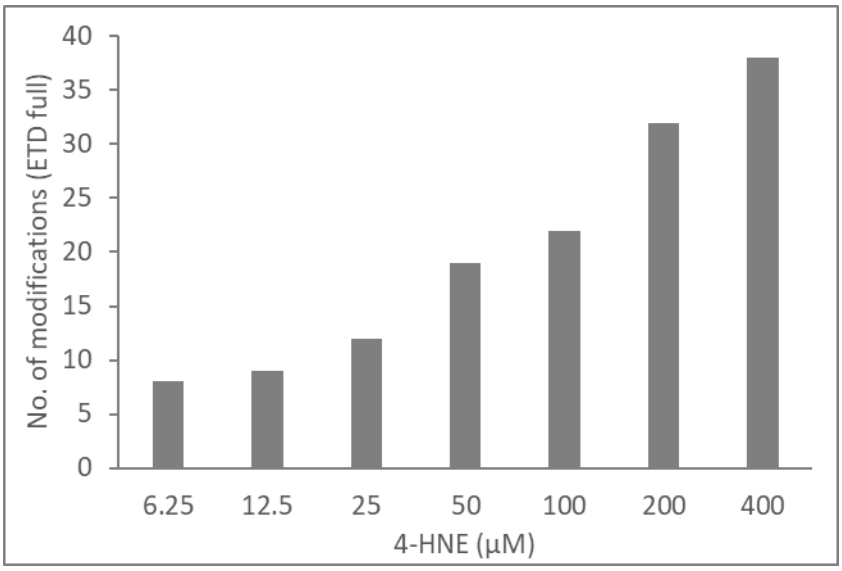

Figure 78: Number of modified peptides fragmented by ETD fragmentation with increasing 4-HNE concentration.

5.3.2. Exercise induced 4-HNE modification of proteins in skeletal muscle

The effect of exercise on 4-HNE post-translational modifications of proteins was assessed using newly developed nLC-MS/MS method. Proteins were isolated from the skeletal muscle tissues of extensively exercised and non-exercised mice. Samples were divided into two main groups:

- **Control:** contains the collection of identified proteins isolated from the skeletal muscle tissues of 7 non-exercised mice.
- **Exercised:** contains the collection of identified proteins isolated from the skeletal muscle tissues of 7 exercised mice.

The representative ETD spectra of 4-HNE modified peptide is shown on Figure 79 with a total of 10 inter-residue bonds have been cleaved. In this peptide, the modified 4-HNE amino acid is Arg. The mass difference between fragment ions c_1 (m/z 133.06077) and c_2 (m/z 445.27691) is 156.11503 Da higher due to adduction of 4-HNE to Arg amino acid. The modification of Arg has been confirmed in the z-series of ion where the mass difference between z_{11} (m/z 1256.62295) and z_{12} (m/z 1568.83910) ions is 156.11503 Da higher confirming the adduction of 4-HNE to Arg-2 of this peptide.

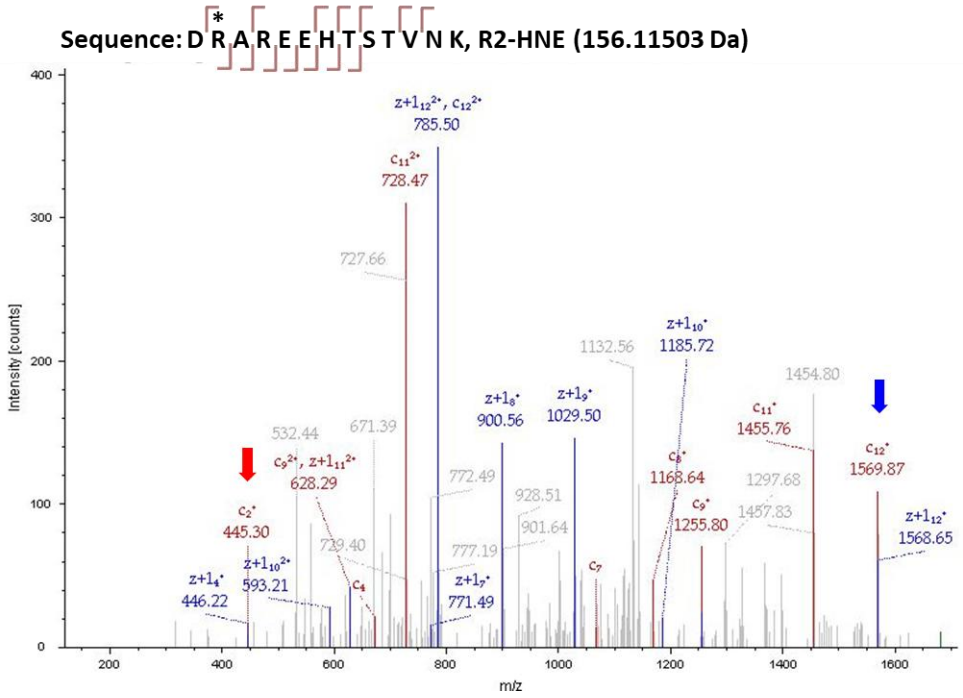

Figure 79: 4-HNE modified peptide sequence fragmented by ETD. ETD tandem MS spectra of protein isolated from the skeletal muscle of exercised sample derived tryptic peptides, confirming the 4-HNE modification of the sample. The mass difference between fragment ions c_1 (m/z 133.06077) and c_2 (m/z 445.27691) is 156.11503 Da higher due to adduction of 4-HNE to Arg amino acid (marked with red arrow). Similarly, mass difference between z_{11} (m/z 1256.62295) and z_{12} (m/z 1568.83910) ions is 156.11503 Da higher (marked with blue arrow). * 4-HNE modification of amino acid

Based on the designated criteria, i.e. that protein / peptide must be common for 5 or more tissue samples of the same group of animals, a total of 1264 proteins were identified in the control group with 4687 total number of peptides, while 832 proteins were found in the exercised group with a total of 3382 peptides. The mean percentage of peptide coverage in the control group was 20.9% ± 16.5% ranging from 87% to 1% while the mean percentage coverage of exercised group was 20.1% ± 16.5% ranging from 88% to 1%. The total number of 4-HNE modified peptides in the control group (22 modified peptides) was found to be almost double compare to those found in the exercised group (9 modified peptides) (Table 8)

Table 8: Summary comparing main results of control group and exercised group. All results are based on criteria that identification is found in ≥ 5 samples.

Tissue Group	No. of Identified Proteins	No. of Identified Peptides	No. of 4-HNE Modified Proteins
Control	1264	4687	22
Exercised	832	3382	9

Selection of 4-HNE modified proteins that were identified in control group are listed in Table 9 and those found in exercised group are listed in Table 10. All 4-HNE modified proteins had only one peptide modified with 4-HNE per protein. Furthermore, the identified 4-HNE modified proteins were searched for their known biological processes using STRAP (Software Tool for Rapid Annotation of Proteins, version 1.5). All 4-HNE modified proteins in control group or exercised group are searched as one set, respectively (Figure 80 and Figure 81). 4-HNE modified proteins in the control group are involved in different biological process including: response to stimulus, regulation, metabolic process, localization, interaction with cells and organisms, development process, cellular process and others. Similarly, identified 4-HNE modified proteins of exercised group, are involved in: response to stimulus, regulation, metabolic process, localization, interaction with cells and organisms, immune system, development process, cellular process and others. Interestingly, 8% of 4-HNE modified proteins in the exercised group are found to be involved in the immune system, where 4-HNE modified proteins in the control group are not involved in immune system at all (Figure 82). Furthermore, the involvement of 4-HNE modified proteins isolated from the control group and exercised group are searched for some of the main molecular functions, including: binding, catalytic activity, molecular transducer activity, structural molecule activity and other. Results indicate that all proteins modified by 4-HNE in exercised group are involved in binding, and the number of 4-HNE modified proteins involved in catalytic activity in the exercised group is approximately 51% higher than that of control group (Figure 83). Moreover, control group are involved by 5% in the molecular transducer activity, while exercised group is not involved in this function.

Table 9: 4-HNE-modified proteins in the skeletal muscle samples of control group. The table shows the Uniprot name of protein, main description, gene coding the protein, number of unique peptides, number of amino acids (AAs), molecular weight (MW), isoelectric point (Cal. pI) and number of samples in the control group having the same protein.

UniProt Accession	Description	Gene	# Unique Peptides	# AAs	MW [kDa]	Calc. pI	No. of positive samples
A2RT67	DENN domain-containing protein 3	Dennd3	1	1274	143.8	7.53	7
P32848	Parvalbumin alpha	Pvalb	21	110	11.9	5.19	7
Q6P8K3	Predicted gene 7978	BC061212	1	481	55.5	8.32	7
Q8R429	Sarcoplasmic/endoplasmic reticulum calcium ATPase 1	Atp2a1	50	994	109.4	5.22	7
A0A0R4J1B0	Troponin T, fast skeletal muscle	Tnnt3	14	272	32.3	5.31	7
Q07231	Zinc finger and SCAN domain-containing protein 21	Zscan21	1	555	63	7.17	7
Q9R0Y5	Adenylate kinase isoenzyme 1	Akt1	16	194	21.5	5.81	6
Q9DBS8	Centrosomal protein POC5	Poc5	1	558	60.9	8.09	6
Q810N9	Coiled-coil domain-containing protein 172	Ccdc172	1	267	31.5	5.25	6
Q61753	D-3-phosphoglycerate dehydrogenase	Phgdh	2	533	56.5	6.54	6
G3UW68	MCG1042663	Gm9376	1	176	21	8.84	6
Q5SWZ5	Myosin phosphatase Rho-interacting protein	Mprip	2	2269	257.1	5.59	6
E9PX68	Solute carrier family 4 (anion exchanger), adaptor protein	Slc4a1ap	1	744	82.8	5.03	6
Q3UHK6	Teneurin-4	Tenm4	1	2771	308.2	6.57	6
O35643	AP-1 complex subunit beta-1	Ap1b1	2	943	103.9	5.17	5

***Continued*: Details of all identified 4-HNE-modified proteins in the control group.**

UniProt Accession	Description	Gene	# Unique Peptides	# AAs	MW [kDa]	Calc. pI	No. of positive samples
P14211	Calreticulin	Calr	14	416	48	4.49	5
J3QN85	Fibroblast growth factor receptor	Fgfr1	1	833	92.9	6.21	5
P19137	Laminin subunit alpha-1	Lama1	1	3084	338	6.7	5
Q6DIB5	Multiple epidermal growth factor-like domains protein 10	Megf10	1	1147	122.9	7.05	5
O70250	Phosphoglycerate mutase 2	Pgam2	15	253	28.8	8.5	5
A2ASS6	Titin	Ttn	39	35213	3904.1	6.2	5
Q9Z2U2	Zinc finger protein 292	Zfp292	1	2698	300.9	7.53	5

Table 10: 4-HNE-modified proteins in the skeletal muscle samples of exercised group. The table shows the Uniprot name of protein, main description, gene coding the protein, number of unique peptides, number of amino acids (AAs), molecular weight (MW), isoelectric point (Cal. pI) and number of samples in the exercised group having the same protein.

UniProt Accession	Description	Gene	# Unique Peptides	# AAs	MW [kDa]	Calc. pI	No. of positive samples
Q8R429	Sarcoplasmic/endoplasmic reticulum calcium ATPase 1	Atp2a1	39	994	109.4	5.22	7
Q8C9W3	A disintegrin and metalloproteinase with thrombospondin motifs 2	Adamts2	1	1213	135.2	7.21	7
E9Q8I0	Complement factor H	Cfh	5	1252	141.2	7.11	7
P43404	Tyrosine-protein kinase ZAP-70	Zap70	1	618	70.1	7.83	6
P32848	Parvalbumin alpha	Pvalb	20	110	11.9	5.19	6
I3ITR1	MCG50313	AK157302	1	129	14.2	8.85	6
A6ZI44	Fructose-bisphosphate aldolase	Aldoa	8	418	45.1	7.91	6
Q6P8K3	Predicted gene 7978	BC061212	1	481	55.5	8.32	5
F8VQ72	Mitogen-activated protein kinase kinase kinase 1	Map3k1	1	1493	161.3	7.88	5

As shown in the previous tables, majority of identified 4-HNE modified proteins were either found in the control group only or exercised group only. However, from the identified 4-HNE-modified proteins, a total of 5 proteins were commonly found in both the control and exercised group. A suitable comparison would be based on the abundances of identified proteins. Table 11 shows the list of the modified proteins with the occurrence of modified peptides compared to the total in skeletal muscle samples (shown as percent of modification). As shown in the table 11, only one protein (Q9R0Y5) had higher percentage of modification in the exercised group. Two proteins (Q8R429 and Q6P8K3) had 100% modification, which means all Q8R429 and Q6P8K3 identified proteins were modified by 4-HNE. Two proteins had higher percent of modification in control group (P32848 and E9Q8I0). However, none of the differences reached significance.

Table 11: List of 4-HNE-modified proteins that are commonly found in skeletal muscle samples of control and exercised group. Percent modification measured by calculating the abundance of modified peptides over the total abundance of same protein in each sample.

Uniprot Accession	Description	% Modification		
		Control Group	Eexercsied Group	P-Value
Q9R0Y5	Adenylate kinase isoenzyme 1	0.3 ± 0.16	0.4 ± 0.32	0.670700294
Q8R429	Sarcoplasmic/endoplasmic reticulum calcium ATPase 1	100 ± 0	100 ± 0	-
Q6P8K3	Predicted gene 7978	100 ± 0	100 ± 0	-
P32848	Parvalbumin alpha	7.4 ± 4.70	6.3 ± 9.97	0.810613268
E9Q8I0	Complement factor H	39.2 ± 35.33	35.1 ± 22.84	0.840015098

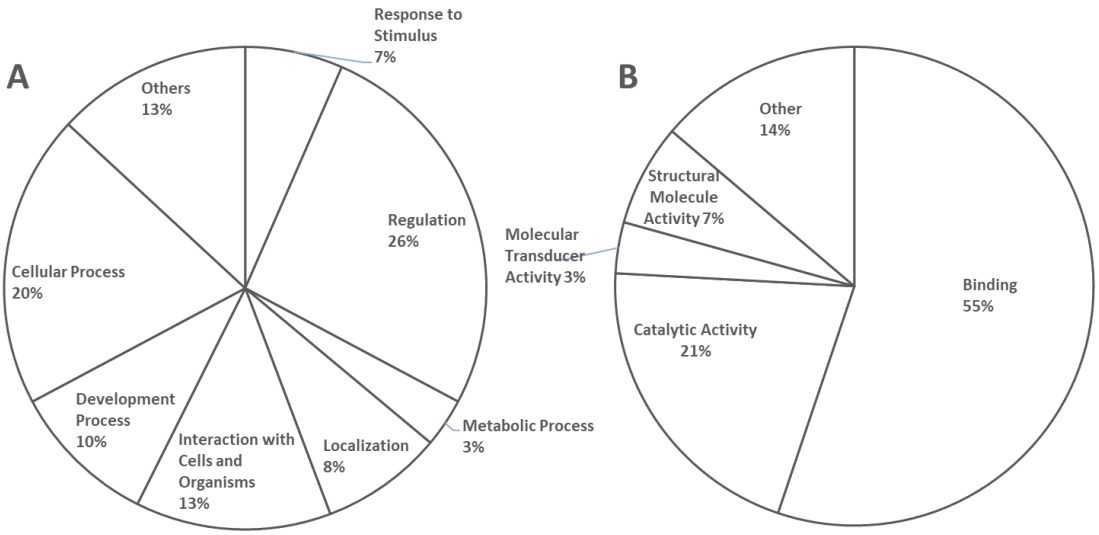

Figure 80: STRAP analysis of 4-HNE-modified proteins in skeletal muscle of control animals. Percentage of involvements of 4-HNE modified proteins in the control group in some of the main **A.** Biological processes and **B.** Molecular Functions, where one protein can be annotated to more than one category.

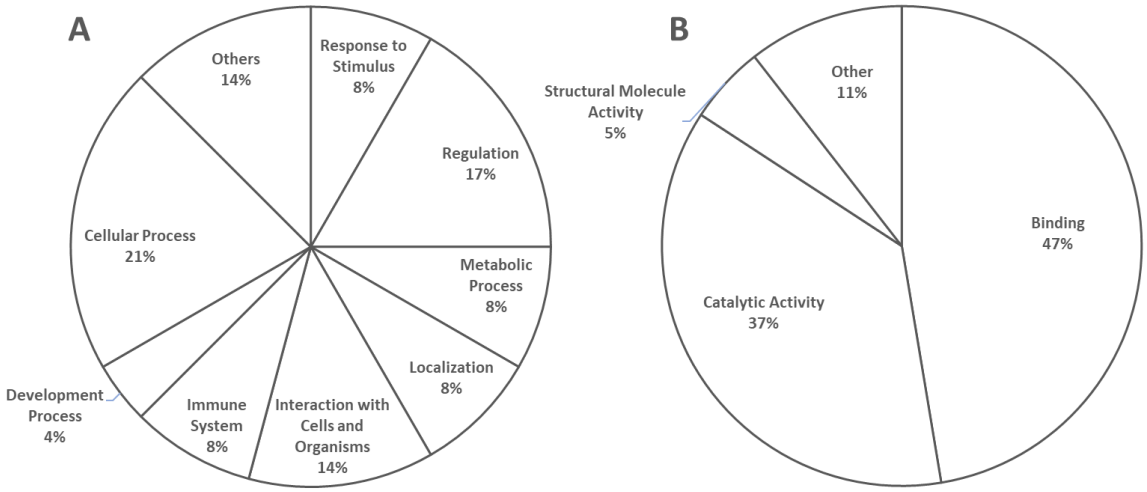

Figure 81: STRAP analysis of 4-HNE-modified proteins in skeletal muscle of exercised group. Percentage of involvements of 4-HNE modified proteins in the exercised group in some of the main **A.** Biological processes and **B.** Molecular Functions, where one protein can be annotated to more than one category.

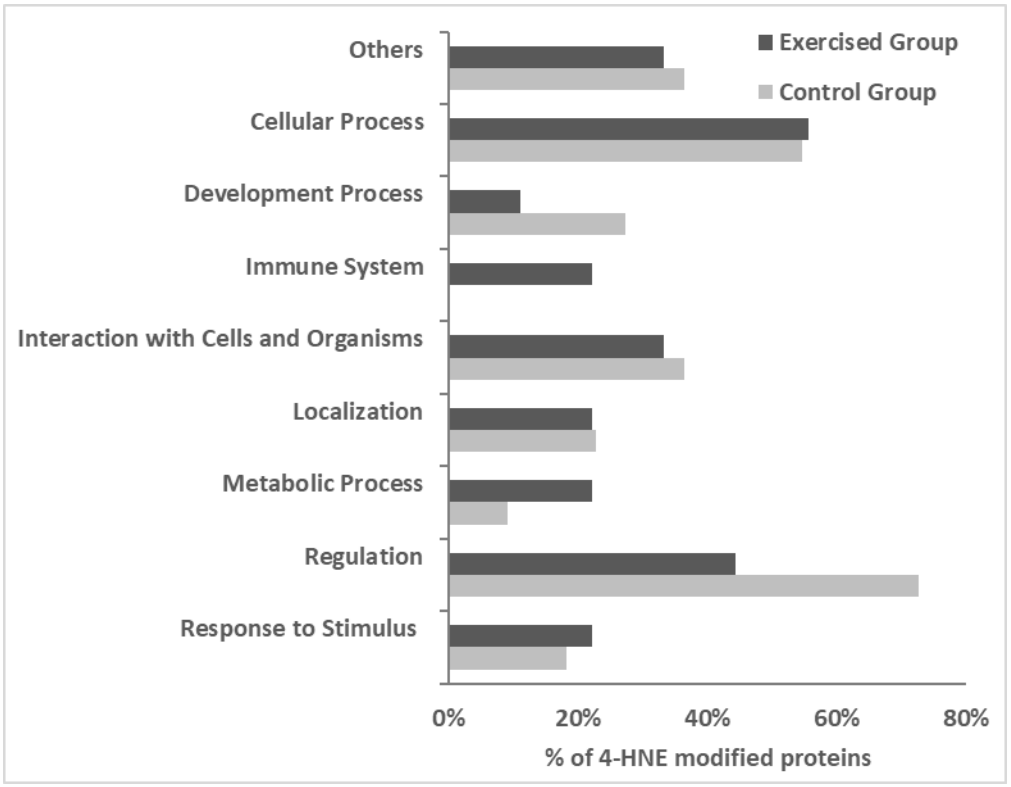

Figure 82: Comparing between control and exercised group in some of the biological processes. Percentage of involvements of 4-HNE modified proteins from control and exercised groups in some of the main biological processes.

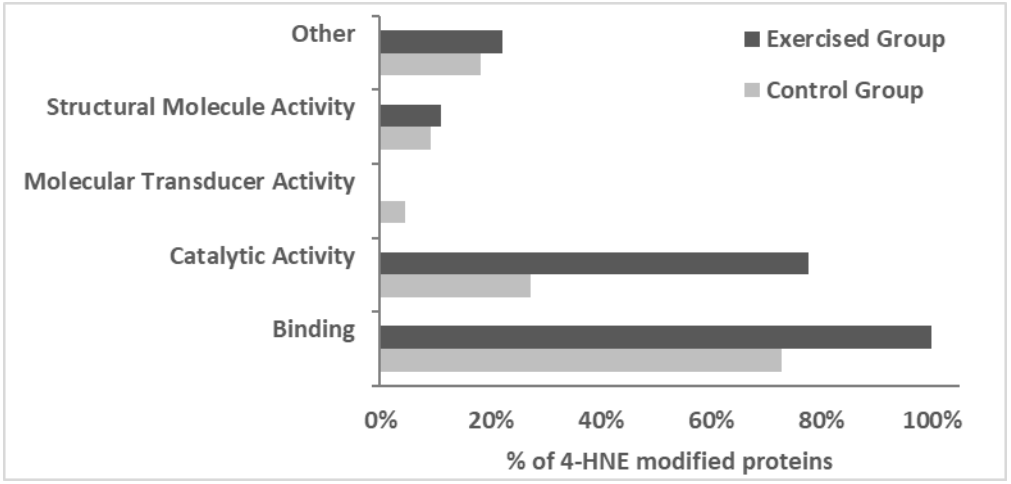

Figure 83: Comparing between control and exercised group in some of the molecular functions. Percentage of involvements of 4-HNE modified proteins from control and exercised groups in some of the main molecular functions.

Sites of modifications can be: cysteine, histidine, lysine, and arginine. The results show that the most commonly site modified by 4- HNE in the control is lysine by 43%, and in the exercised groups is arginine reaching 33% followed by lysine (32%) of the total number of 4-HNE modification (Figure 84). The exact type of 4-HNE modification and the site modified within the peptide sequence for each identified protein is listed in the appendices in Table 17-20

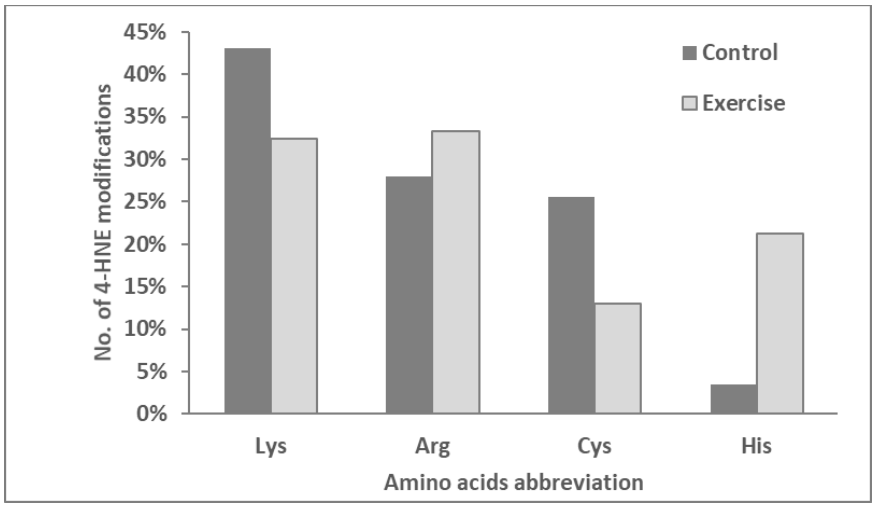

Figure 84: The abundance of site specific 4-HNE modifications of skeletal muscle proteins. Comparison of 4-HNE modified amino acid sites in the control skeletal and exercised skeletal muscle proteins. Lysine and arginine are the most susceptible to 4-HNE adduction in both groups. Results include 4-HNE modifications that are commonly found in ≥ 5 samples.

Finally, the comparative analysis of proteins differentially expressed in exercised animals compared to control animals gave a total of 88 proteins expressed in at least 5 samples of the exercised group but not in the control group. Complete list is attached in the appendices (Table 21). Results were further filtered for proteins that are directly involved in mitochondrial function. Exercised group had 2 identified proteins that are involved directly with mitochondrial function (Table 12)

Table 12: Proteins identified in exercised group only that are directly involved with mitochondrial function

Uniport Accession	Gene	Description
O88986	Gcat	2-amino-3-ketobutyrate coenzyme A ligase, mitochondrial
P40630	Tfam	Transcription factor A, mitochondrial

5.4. Discussion

In the past, much attention was given to the high production level of ROS during physical exercise, and how it can alter redox homeostasis and lead to massive damaging effects on skeletal muscle. Beside the harmful biological effects of ROS, recently, the important role of exercise-induced ROS as signaling molecule and in enhancing the endogenous antioxidant system is unequivocal. ROS can be produced in skeletal muscle cells during both rest and exercise. Post-translational modifications of proteins can change protein structure, which results in gain-of-function or loss-of-function. Thus, formation of 4-HNE protein adducts can either lead to pathological effects or regulatory effects. In order to identify proteins susceptible to exercise induced 4-HNE adduction a novel nLC-MS/MS method that uses three fragmentation methods, HCD, ETD and CID has been developed. Although the CID is a traditional method of fragmentation and most commonly used for peptide sequencing and quantitation, the use of a more recent type of fragmentations HCD and ETD receives more and more attention in the analysis of protein PTMs. Namely, due to the nature of collision of peptides with CID fragmentation method, it can result in the losses of liable PTMs, such as ubiquitylation (Porras-Yakushi, *et. al.*, 2015), phosphorylation (Collins, *et. al.*, 2014) or 4-HNE modification (Fritz, *et. al.*, 2012). Furthermore, for peptides with a charge state more than 2 ETD is a more informative

fragmentation method than CID while HCD due to the higher coverage of peptide sequences (Frese, *et. al.*, 2011) could further improve the identification of PTMs. Indeed the use of HCD, ETD, CID and data dependent decision tree fragmentation resulted in the identification of a high number of 4-HNE modified peptides.

Our results showed that sedentary group of animals had almost double the number of 4-HNE modified proteins compared to the exercised group. It is important to point that the total number of identified proteins with high confidence in the control group was higher than those identified in the exercised group. However, one explanation for the lower number of 4-HNE-modified proteins in the exercised group could be due to the influence of exercise on antioxidant system activity and adaptation. The primary antioxidant enzymes in skeletal muscle including SOD1, SOD2 and GPX activities are elevated with exercise in muscle tissue (Powers, *et. al.*, 1994). Results showed eight 4-HNE modified proteins that are identified in the exercised group but in none of the control group, which most likely indicates that those post-translational modifications are triggered by the exercise. Moreover, annotation results showed that 4-HNE modified proteins in the exercised group are involved in immune system, while control group is not. Indeed, the ability of exercise to be involved in the regulation of the immune system is well established, as the type of exercise is crucial on determining the health benefits for the immune system. Where moderate exercise is found to have different health benefits, while prolonged intensive exercise can depress immunity (Simpson, *et. al.*, 2015).

Further comparison of the proteomics results obtained from the whole muscle protein lysates with the effects of *in-vitro* exercise on transcriptome did not reveal common targets for 4-HNE. The 4-HNE is a known signaling molecule and it can either directly or indirectly alter expression of its targets genes. Continuous exposure of cells to non-pathological concentrations

of 4-HNE can induce different hormetic effects that can affect future cellular responses (Chapple *et. al.,* 2013). Daily exercise over the period of five months is likely to induce hormetic effects of skeletal muscle. Thus, as 4-HNE is degraded rapidly in cells it is possible that acute 4-HNE effects on the gene expression will not correlate with chronic effects measured as 4-HNE adduction to proteins.

Beside the above, there are numerous other factors that could affect this variation. The use of different model is one of them, as the transcriptomic results are derived from *in-vitro* model using pure cell line, while the proteomic results originate from the *in-vivo* experimental set-up and involves using a whole tissue where transport and import of proteins from different tissues are likely to occur. In fact, it might be inappropriate for a direct comparison between proteins and mRNA abundances, even from the same cell type and location. An interesting detailed review explains the limitation of predicting protein levels based on transcript level only. As multiple processes can contribute to the protein expression, such as translation rate, translation rate modulation, modulation of protein's half-life, protein synthesis delay and protein transport (Liu, *et al.,* 2016).

6. CONCLUSION

In summary, our results demonstrated that caffeine-induced calcium signaling in skeletal muscle alters the myotubes bioenergetic system and regulates mitochondrial genes. Furthermore, caffeine was found to triggers ROS production, leading to peroxidation of lipids that eventually generates the byproduct reactive aldehyde 4-HNE. This was demonstrated by the dose-dependent significant increase in caffeine-induced 4-HNE adducts formation. After obtaining those evidences, the role of 4-HNE on cellular redox homeostasis and mitochondrial function and genes were studied in depth. Our results make evident for the first time that pathological 4-HNE levels elicit damaging effects on skeletal muscle cells while acute exposure to physiological 4-HNE induces transient adaptation. Our ongoing research findings further signify the importance of skeletal muscle cells hormesis in response to acute stress in order to maintain essential biological functions. Finally, rapid and sensitive method for the identification of protein site specific 4-HNE-modifications was developed using liquid chromatography tandem mass spectrometry, summary of main findings shown in Figure 85. In addition, the effect of exercise-induced 4-HNE modifications of proteins was investigated using skeletal muscle tissues of intensively exercised mice for 5 months compared to non-exercised sedentary mice group. The obtained results showed reduction in the total number of 4-HNE modified proteins in the exercised group when compared to control group. However, analysis of the biological function of the 4-HNE modified proteins in the exercised group showed that exercise triggers the 4-HNE adducts formation of proteins that are involved in the immune system, while control group did not show this effect. This thesis highlighted the significant role of exercise-induced 4-HNE on the regulation of several cellular activities, ranging from genetic regulation to adducts formation.

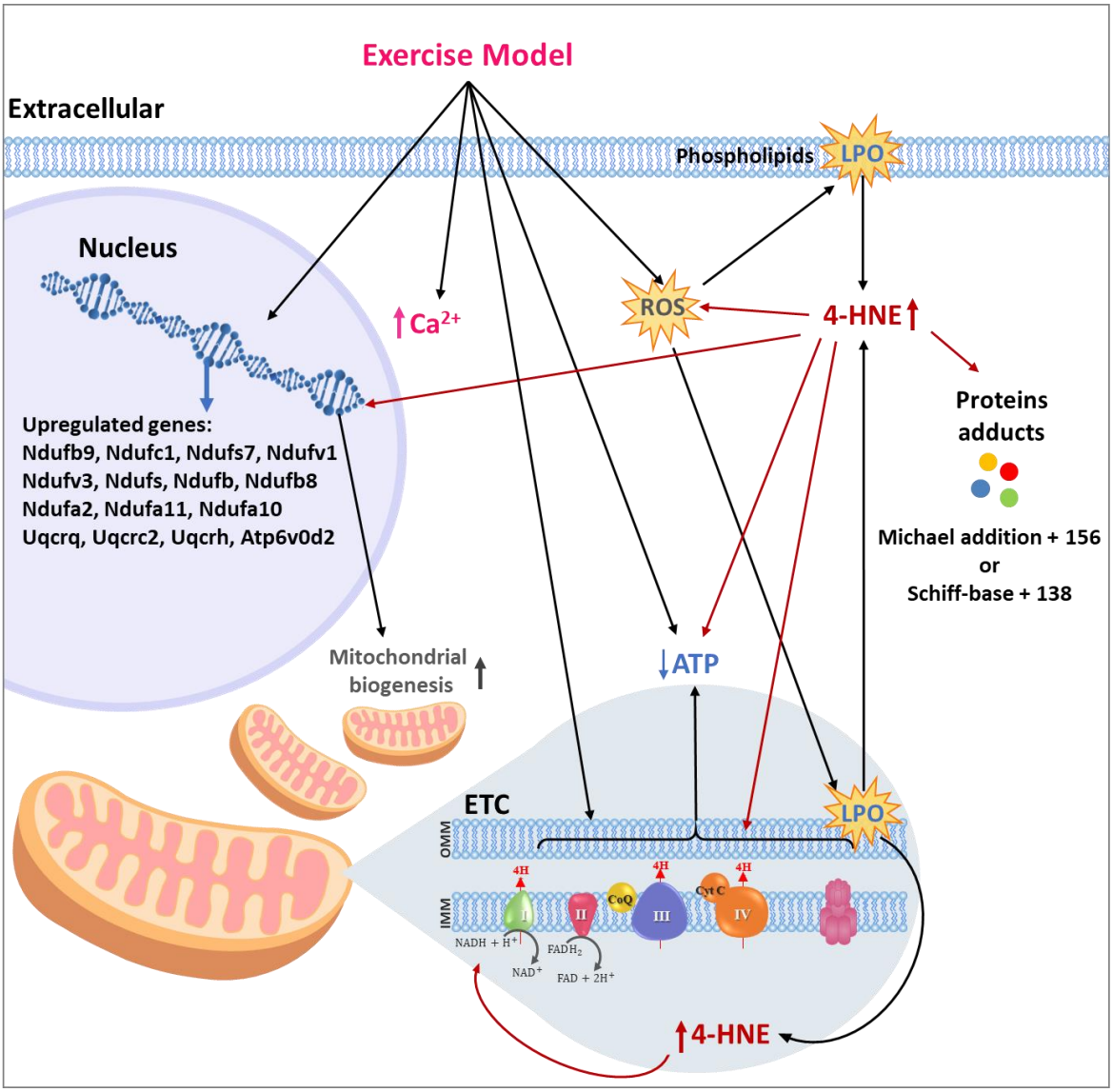

Figure 85: Scheme summarizing the main findings of the thesis. Caffeine induces calcium signaling, increases ROS production and alters mitochondrial metabolism. Increased ROS production leads to peroxidation of lipids that eventually generates the byproduct reactive aldehyde 4-HNE and formation of 4-HNE protein adducts by Michael addition (+ 156 Da for each 4-HNE added) or Schiff-base (+ 138 Da for each 4-HNE added). 4-HNE alters cellular redox homeostasis promoting ROS production. Furthermore, 4-HNE increases NAD^+ level suggesting an increase in mitochondrial respiration. 4-HNE also affects mitochondrial functions and genes and promote mitochondrial biogenesis.

6.1. Limitations

In this thesis, studying the role of 4-HNE on skeletal muscle redox homeostasis and mitochondrial bioenergetics, transcriptome and density are all carried out using *in-vitro* experimental models. The obtained results from *in-vitro* experiments are essential to acquire knowledge basis on the 4-HNE role in a controlled environment and to study the reactions of skeletal muscle explicitly. However, this should be followed by *in-vivo* experiments for confirmation of the results and to study the overall effects of 4-HNE. Furthermore, caffeine concentrations are selected based on calcium-induced contraction of myotubes to mimic mild, moderate and intensive contractions of muscle during physical exercise. But those concentrations (1 mM, 5 mM and 10 mM) are considered to be supraphysiological concentrations. Also studying the effect of exercise on mitochondria isolated from exercised animals would more closely reflect the impact of exercise on mitochondrial respiration and gene expression, but due to limited resources this option was not possible for us.

Moreover, studying ROS homeostasis with the current scientific tools is a challenging topic. Although, DCFH-DA and DHE assays, used in this thesis, are among the most commonly used methods to measure intracellular ROS they have limited selectivity and sensitivity. DCFH-DA probe is mainly used to measure H2O2, but it can also get oxidized by other free radicals (Winterbourn, 2014). Furthermore, a catalyst is required for the probe to react with. It is preferable to use additional probes to measure intracellular ROS produced, and in this study we used DCFH along with DHE. Both probes used also need to compete with the ROS scavenging antioxidants, thus, interpreting the data is critical.

In our experiments to study the effect of exercise-induced 4-HNE protein adducts formation in skeletal muscles, tissue samples were isolated after 5 months of continuous exercise. The obtained results showed reduction in total number of 4-HNE modified proteins in exercised group compared to control group. However, collecting tissue samples at different time points throughout training schedule can give information of possible adaptation mechanisms used to reduce 4-HNE adducts formation. This can be incorporated with measuring glutathione-S-transferases, alcohol dehydrogenases and aldehyde dehydrogenases to study the exercise-induced antioxidant system involved in the metabolism of 4-HNE.

In this thesis, a "bottom-up" proteomics approach has been used, that required for the sample to be electrophoretically separated and digested. Both steps can readily introduce artefacts by oxidizing methionine, cysteine or tryptophan (Verrastro, *et. al.*, 2015) and caution is therefore needed when interpreting the results. Also, although trypsin is the most commonly used proteolytic enzyme, for the better coverage of protein sequence another protease in addition to trypsin should be used. The proteomics results returned small number of proteins modified with 4-HNE and the data could be masked with the presence of more abundant proteins. Therefore, the enrichment and separation of 4-HNE modified proteins would reduce the complexity of the samples allowing better identification of 4-HNE modified peptides.

Moreover, there are some limitation associated with Proteome Discoverer analysis and settings. Identifications of 4-HNE modification is limited to those specified in the search method. Even though, in our dynamic modifications selection we tried to identify all possible 4-HNE modifications that are available in literature, including modification of 4-HNE of cysteine, histidine, lysine, leucine, methionine and arginine (+156.115 Da), 4-HNE + H2 for the Michael adducts in cysteine, histidine, lysine, leucine, methionine and arginine (+158.131 Da), and 4-

HNE - H2O for the Schiff-bases in cysteine, histidine, lysine, leucine, methionine and arginine (+138.104 Da). Moreover, the post-translational modifications were limited to only 3 modifications sites per peptide. Other limiting specification include: maximum peptide length is limited to 144, maximum missed cleavages site is 2 and maximum precursor mass is 5000 Da. Therefore, any 4-HNE post-translational modifications of proteins outside those limiting factors will not be identified in the search result. Finally, it is possible that some 4-HNE protein modifications are missed because the protein databases are not complete and some proteins are not properly annotated (Kim, *et. al.*, 2016).

6.2. Future work

Our results showed interesting effects of physiological and supraphysiological concentrations of 4-HNE on the expression of mitochondrial genes. This can be confirmed performing a comprehensive mechanistic studies focusing on specific pathways that seem to be affected by 4-HNE. It is well known that exercise activates signaling mechanisms that promotes the antioxidant system in skeletal muscle. Our results showed a reduction in total number of 4-HNE modified proteins in the exercised group when compared to the control, which can be explained by enhanced clearance of the antioxidant system induced by exercise activity. Thus, it is important to study the effect of exercise-induced 4-HNE on the antioxidant system, to underpin the cause of the reduction in exercise-induced 4-HNE modification of proteins. Moreover, the focus of this research was on the impact exercise-induced 4-HNE proteins adducts formation on skeletal muscle. However, this will be expanded by studying the effect of exercise in the formation of 4-HNE protein adducts in cardiac muscle. In fact, the cardiac muscle tissues were collected from the same experimental model, where all results will be processed and analyzed for future work.

This thesis investigated the effect of exercise-induced ROS production that can lead to oxidative damage and LPO, focusing on the mitochondrial gene transcription and bioenergetics. The obtained results will be used as platform for future follow-up research that focus on investigating the effect of excess ROS production during physical activity in promoting mitochondrial dysfunction. Studying mitochondrial dysfunction mechanisms can lead to novel therapeutic strategies to treat metabolic diseases associated with mitochondrial dysfunction.

7. REFERENCES

Abramson, J.J. and Salama, G. (1989). Critical sulfhydryls regulate calcium release from sarcoplasmic reticulum. *J. Bioenerg. Biomembr*. 21:283–294.

Al Amiri, E., Abdullatif, M., Abdulle, A., Al Bitar, N., Afandi, E.Z., Parish, M. & Darwiche, G. (2015). The prevalence, risk factors, and screening measure for prediabetes and diabetes among Emirati overweight/obese children and adolescents. *BMC Public Health*. 15:1298. doi: 10.1186/s12889-015-2649-6.

Alessio, H.M. & Goldfarb, A.H. (1988). Lipid peroxidation and scavenger enzymes during exercise: Adaptive response to training. *J. Appl. Physiol*. 64:1333–1336

Al-Thani, A.M., Voss, S.C., Al-Menhali, A.S., Barcaru, A., Horvatovich, P.L., Al Jaber, H., Nikolovski, Z., Latiff, A., Georgakopoulos, C., Merenkov, Z., Segura, J., Alsayrafi, M. and Jaganjac, M. (2018). Whole blood storage in CPDA1 blood bags alters erythrocyte membrane proteome. *Oxidative Medicine and Cellular Longevity*.

Andringa, K.K., Udoh, U.S., Landar, A. & Bailey, S.M. (2014). Proteomic analysis of 4-hydroxynonenal (4-HNE) modified proteins in liver mitochondria from chronic ethanol-fed rats. *Redox Biol.* 2014;2C:1038-1047.

Angelova, P.R. & Abramov, A.Y. (2016). Functional role of mitochondrial reactive oxygen species in physiology. *Free Radical Biology and Medicine*. doi.org/10.1016/j.freeradbiomed.2016.06.005i

Atia, N., York, P., and Clark, B.J. (2009). Development and validation of a rapid and efficient method for simultaneous determination of methylxanthines and their metabolites in urine using monolithic HPLC columns. *Journal of Separation Science*. 32: 931–938.

Ayala, A., Muñoz, M. F., & Argüelles, S. (2014). Lipid Peroxidation: Production, Metabolism, and Signaling Mechanisms of Malondialdehyde and 4-Hydroxy-2-Nonenal. *Oxidative Medicine and Cellular Longevity*. *2014*: 31. doi.org/10.1155/2014/360438

Balboa, M. A. and Balsinde, J. (2002). Involvement of Calcium-independent Phospholipase A2 in Hydrogen Peroxide-induced Accumulation of Free Fatty Acids in Human U937 Cells. *The Journal of Biological Chemistry*. 277 (43): 40384–40389. doi: 10.1074/jbc.M206155200

Barrès, R.1., Yan, J., Egan, B., Treebak, J.T., Rasmussen, M., Fritz, T., Caidahl, K., Krook, A., O'Gorman, D.J. & Zierath, J.R. (2012). Acute exercise remodels promoter methylation in human skeletal muscle. *Cell Metab*. 2012 Mar 7;15 (3):405-11.

Bedard, K. and Krause, K.H. (2007). The NOX family of ROS-generating NADPH oxidases: physiology and pathophysiology. *Physiological Reviews*. 87(1):245-313.

Begas, E., Kouvaras, E., Tsakalof, A., Papakosta, S. and Asprodini, E.K. (2007). In vivo evaluation of CYP1A2, CYP2A6, NAT-2 and xanthine oxidase activities in a Greek population sample by the RP-HPLC monitoring of caffeine metabolic ratios. *Biomedical Chromatography*. 21:190–200.

Benedetti, A., Comporti, M., & Esterbauer, H. (1980). Identification of 4-hydroxynonenal as a cytotoxic product originating from the peroxidation of liver microsomal lipids. *Biochimica et Biophysica Acta*. *620*(2): 281–296.

Bensinger, S.J. & Christofk, H.R. (2012). New aspects of the Warburg effect in cancer cell biology. *Semin Cell Dev Biol*. 23(4):352-61. doi: 10.1016/j.semcdb.2012.02.003.

Bhatia, V.N., Perlman, D.H., Costello, C.E. and McComb, M.E. (2009). Software tool for researching annotations of proteins: open-source protein annotation software with data visualization. *Anal Chem*. 81:9819-9823

Birben, E., Sahiner, U. M., Sackesen, C., Erzurum, S., & Kalayci, O. (2012). Oxidative Stress and Antioxidant Defense. *World Allergy Organization*. *5*(1):9-19. doi: 10.1097/WOX.0b013e3182439613

Booth, F.W. and Thomason, D.B. (1991). Molecular and cellular adaptation of muscle in response to exercise: perspectives of various models. Physiological Reviews. 71(2):541-585

Borovic, S., Rabuzin, F., Waeg, G. and Zarkovic, N. (2006). Enzyme-linked immunosorbent assay for 4-hydroxynonenal-histidine conjugates. *Free Radic Res*. 40(8):809-20.

Bose, A. and Beal, M.F. (2016). Mitochondrial dysfunction in Parkinson's disease. *J Neurochem*. 139(S1):216-231. doi: 10.1111/jnc.13731.

Boveris, A., Oschino, N. and Chance, B. (1972). The cellular production of hydrogen peroxide. *Biochem J*. 128: 617–630.

Brand, M.D. (2016). Mitochondrial generation of superoxide and hydrogen peroxide as the source of mitochondrial redox signaling. *Free Radical Biology and Medicine*. 100: 14-31. doi.org/10.1016/j.freeradbiomed.2016.04.001

Bridge, C.A. and Jones, M.A. (2006). The effect of caffeine ingestion on 8 km run performance in a field setting. *J Sports Sci.* 24: 433–439

Cappelletti, S., Piacentino, D., Sani, G. and Aromatario, M. (2015). Caffeine: cognitive and physical performance enhancer or psychoactive drug?. *Curr Neuropharmacol*. 13(1):71-88. doi: 10.2174/1570159X13666141210215655.

Carini, M., Aldini, G. and Facino, R.M. (2004). Mass spectrometry for detection of 4-hydroxy-trans-2-nonenal (HNE) adducts with peptides and proteins. *Mass Spectrometry Reviews*. 23(4):281-305.

Carter, H.N., Chen, C.C. and Hood DA. (2015). Mitochondria, muscle health, and exercise with advancing age. *Physiology (Bethesda)*. 30(3):208-23. doi:10.1152/physiol.00039.2014.

Chapple, S. J., Cheng, X., & Mann, G. E. (2013). Effects of 4-hydroxynonenal on vascular endothelial and smooth muscle cell redox signaling and function in health and disease. *Redox Biology*. *1*(1), 319–331. Doi.org/10.1016/j.redox.2013.04.001

Chavez, J.D., Wu, J., Bisson, W. & Maier, C.S.. (2011). Site-specific proteomic analysis of lipoxidation adducts in cardiac mitochondria reveals chemical diversity of 2-alkenal adduction. *J Proteomics*. 74(11):2417–2429.

Cheng, A.J., Yamada, T., Rassier, D.E., Andersson, D.C., Westerblad, H. and Lanner, J.T. (2016). Reactive oxygen/nitrogen species and contractile function in skeletal muscle during fatigue and recovery. *J Physiol*. 594(18): 5149-60.

Cherednichenko, G., Zima, A.V., Feng, W., Schaefer, S., Blatter, L.A. and Pessah, I.N. (2004). NADH oxidase activity of rat cardiac sarcoplasmic reticulum regulates calcium-induced calcium release. *Circ. Res*. 94:478–486.

Ciaraldi, T.P., Mudaliar, S., Barzin, A., Macievic, J.A., Edelman, S.V., Park, K.S. and Henry R.R. (2005). Skeletal muscle GLUT1 transporter protein expression and basal leg glucose uptake are reduced in type 2 diabetes. *J Clin Endocrinol Metab*. 90(1):352-8.

Cipak, A., Hasslacher, M., Tehlivets, O., Collinson, E.J., Zivkovic, M., Matijevic, T., Wonisch, W., Waeg, G., Dawes, I.W., Zarkovic, N., Kohlwein, S.D. (2005). Saccharomyces cerevisiae strain expressing a plant fatty acid desaturase produces polyunsaturated fatty acids and is susceptible to oxidative stress induced by lipid peroxidation. *Free Radic Biol Med*. 40(5):897-906.

Close, G.L., et al., (2005). The emerging role of free radicals in delayed onset muscle soreness and contraction-induced muscle injury. *Comp Biochem Physiol A Mol Integr Physiol*. 142(3):257-66.

Collins, M.O., Wright, J.C., Jones, M., Rayner, J.C. and Choudhary, J.S. (2014). Confident and sensitive phosphoproteomics using combinations of collision induced dissociation and electron transfer dissociation. *J Proteomics*. 103:1-14.

Cosgrove, J.P., Church, D.F., & Pryor, W.A. (1987). The kinetics of the autoxidation of polyunsaturated fatty acids. *Lipids*. *22*: 299–304.

Craig, D.M., Ashcroft, S.P., Belew, M.Y., Stocks, B., Currell, K., Baar, K. & Philp, A. (2015). Utilizing small nutrient compounds as enhancers of exercise-induced mitochondrial biogenesis. *Front. Physiol*. 6:296. doi: 10.3389/fphys.2015.00296

Davies, K.J., Quintanilhat, A.T., Brooks, G.A. & Packer, L. (1982). Free radicals and tissue damage produced by exercise. *Biochemical and biophysical research communications*. 107(4): 1198-1205. Doi:10.1016/S0006-291X(82)80124-1

Davis, J.K. & Green, J.M. (2009). Caffeine and anaerobic performance: ergogenic value and mechanisms of action. *J Sports Med*. 39: 813–832

DeFronzo, R.A. (1988). Lilly lecture 1987. The triumvirate: beta-cell, muscle, liver. A collusion responsible for NIDDM. *Diabetes*. 37: 667-687

Del Coso, J., Muñoz, G. and Muñoz-Guerra, J. (2011). Prevalence of caffeine use in elite athletes following its removal from the World Anti-Doping Agency list of banned substances. *Appl Physiol Nutr Metab*. 36(4):555-61. doi: 10.1139/h11-052.

Di Meo, S. and Venditti, P. (2001). Mitochondria in Exercise-Induced Oxidative Stress. *Biol Signals Recept*. 10:125–140

Díaz-Vegas, A., Campos, C. A., Contreras-Ferrat, A., Casas, M., Buvinic, S., Jaimovich, E. and Espinosa, A. (2015). ROS Production via P2Y1-PKC-NOX2 is triggered by extracellular atp after electrical stimulation of skeletal muscle cells. *PLoS ONE*. 10(6), e0129882. doi.org/10.1371/journal.pone.0129882

Ding S, Riddoch-Contreras J, Abramov AY, Qi Z, Duchen MR. Mild stress of caffeine increased mtDNA content in skeletal muscle cells: the interplay between Ca2+ transients and nitric oxide. J Muscle Res Cell Motil. 2012;33(5):327-37.

Dinkova-Kostova, A.T. and Abramov, A.Y. (2015). The emerging role of Nrf2 in mitochondrial function. *Free Radic Biol Med*. 88(Pt B):179-188. doi: 10.1016/j.freeradbiomed.2015.04.036.

Dobretsov, G.E., Borschevskaya, T.A., Petrov, V.A., & Vladimirov, Y.A. (1977). The increase of phospholipid bilayer rigidity after lipid peroxidation. *FEBS Lett*. *84* (1): 125-128

Domijan AM, Abramov AY. Fumonisin B1 inhibits mitochondrial respiration and deregulates calcium homeostasis--implication to mechanism of cell toxicity. Int J Biochem Cell Biol. 2011 Jun;43(6):897-904..

Domijan AM, Kovac S, Abramov AY. Lipid peroxidation is essential for phospholipase C activity and the inositol-trisphosphate-related Ca^{2+} signal. J Cell Sci. 2014;127(Pt 1):21-6.

du Plessis, S.S., Agarwal, A., Mohanty, G., and van der Linde, M. (2014). Oxidative phosphorylation versus glycolysis: what fuel do spermatozoa use?. *Asian journal of andrology*. 17(2):230-5.

Egan, B. & Zierath, J.R. (2013). Exercise metabolism and the molecular regulation of skeletal muscle adaptation. *Cell Metab*. 17:162-84.

Elrayess, M.A., Almuraikhy, S., Kafienah, W., Al-Menhali, A., Al-Khelaifi, F., Bashah, M., Zarkovic, K., Zarkovic, N., Waeg, G., Alsayrafi, M. and Jaganjac, M. (2017). 4-hydroxynonenal causes impairment of human subcutaneous adipogenesis and induction of adipocyte insulin resistance. *Free Radic Biol Med*. 104:129-137.

Endo, M., Tanaka, M. and Ogawa, Y. (1970). Calcium induced release of calcium from the sarcoplasmic reticulum of skinned skeletal muscle fibres. *Nature.* 228: 34–36.

Esterbauer, H., Eckl, P., & Ortner, A. (1990). Possible mutagens derived from lipids and lipid precursors. *Mutation Research*. *238*(3): 223–233

Esterbauer, H., Schaur, R.J., & Zollner, H. (1991). Chemistry and biochemistry of 4-hydroxynonenal, malonaldehyde and related aldehydes. *Free Radical Biology & Medicine. 11*: 81-128

Fan, W. and Evans, R. M. (2016). Exercise Mimetics: Impact on Health and Performance. *Cell metabolism.* 25(2), 242-247.

Federspil, G., Baggio, B., De Palo, C., De Carlo, E., Borsatti, A. and Vettor, R. (1987). Effect of prolonged physical exercise on muscular phospholipase A2 activity in rats. *Diabete Metab*. 13 (3): 171-5.

Filip-Ciubotaru F, Manciuc C, Stoleriu G and Foia L. (2016). NADPH oxidase: structure and activation mechanisms (review). note I. *Rev Med Chir Soc Med Nat Iasi*. 120(1): 29- 33.

Fill, M. and Copello, J.A. (2002). Ryanodine Receptor Calcium Release Channels. *Physiological Reviews*. 82(4): 893-922. doi.org/10.1152/physrev.00013.2002

Filomeni, G., De Zio, D. and Cecconi, F. (2015). Oxidative stress and autophagy: the clash between damage and metabolic needs. *Cell Death Differ*. 22(3):377-88.

Finsterer, J. (2012) Biomarkers of peripheral muscle fatigue during exercise. *BMC Musculoskelet Disord*. 13:218.

Frese, C.K., Altelaar, A.F., Hennrich, M.L., Nolting, D., Zeller, M., Griep-Raming, J., Heck, A.J. and Mohammed, S. (2011). Improved peptide identification by targeted fragmentation using CID, HCD and ETD on an LTQ-Orbitrap Velos. *J Proteome Res*. 10(5):2377-2388.

Fritz, K.S., Kellersberger, K.A., Gomez, J.D. and Petersen, D.R. (2012). 4-HNE adduct stability characterized by collision-induced dissociation and electron transfer dissociation mass spectrometry. *Chem Res Toxicol*. 25(4):965-70. doi: 10.1021/tx300100w.

Gailly, P. (2002). New aspects of calcium signaling in skeletal muscle cells: implications in Duchenne muscular dystrophy. *Biochim Biophys Acta*. 1600(1-2):38-44.

Galam, L., Failla, A., Soundararajan, R., Lockey, R.F. and Kolliputi, N. (2015). 4-hydroxynonenal regulates mitochondrial function in human small airway epithelial cells. *Oncotarget*. 6(39):41508-21

Gali Ramamoorthy, T., Laverny, G., Schlagowski, A.-I., Zoll, J., Messaddeq, N., Bornert, J.-M., Panza, S., Ferry, A., Geny, B. and Metzger, D. (2015). The transcriptional coregulator PGC-1β controls mitochondrial function and anti-oxidant defence in skeletal muscles. *Nature Communications*. 6: 10210. doi.org/10.1038/ncomms10210

Galter, D., Mihm, S., and Dröge, W. (1994). Distinct effects of glutathione disulphide on the nuclear transcription factor kappa B and the activator protein-1. *Eur. J. Biochem*. 221: 639–648.

Galvalisi, M., Prieto, J.P., Martínez, M., Abin-Carriquiry, J.A. and Scorza, C. (2017). Caffeine Induces a Stimulant Effect and Increases Dopamine Release in the Nucleus Accumbens Shell Through the Pulmonary Inhalation Route of Administration in Rats. *Neurotoxicity Research*. 31(1): 90-98. doi: 10.1007/s12640-016-9667-8.

Gatineau, M., Hancock, C., Holman, N., Outhwaite, H., Oldridge, L., Christie, A. & Ells, L. (2014) Adult obesity and type 2 diabetes. *Oxford: Public Health England*

Gehlert, S., Bloch, W. and Suhr, F. (2015). Ca^{2+}-Dependent Regulations and Signaling in Skeletal Muscle: From Electro-Mechanical Coupling to Adaptation. *International Journal of Molecular Sciences*. *16*(1): 1066–1095. http://doi.org/10.3390/ijms16011066

Gil, L., Siems, W., Mazurek, B., Gross, J., Schroeder, P., Voss, P., & Grune, T. (2006). Age-associated analysis of oxidative stress parameters in human plasma and erythrocytes. Free Radic. Res. *40*: 495–505.

Gollnick, P. D., & King, D. W. (1969). Effect of exercise and training on mitochondria of rat skeletal muscle. *American Journal of Physiology*. *216* (6): 1502-1509

Gomez-Cabrera, M., Martínez, A., Santangelo, G., Pallardó, F.,V., Sastre, J., and Viña, J. (2006). Oxidative stress in marathon runners: Interest of antioxidant supplementation. *The British Journal of Nutrition*. 96: S31-S33. doi:http://dx.doi.org/10.1079/BJN20061696

Gomez-Cabrera, M.-C., Borrás, C., Pallardó, F. V., Sastre, J., Ji, L. L., and Viña, J. (2005). Decreasing xanthine oxidase-mediated oxidative stress prevents useful cellular adaptations to exercise in rats. *The Journal of Physiology*. 567(Pt 1), 113–120. doi.org/10.1113/jphysiol.2004.080564

Gomez-Cabrera, M.C., Domenech, E., Romagnoli, M., Arduini, A., Borras, C., Pallardo, F.V., Sastre, J. & Vina, J. (2008). Oral administration of vitamin C decreases muscle mitochondrial biogenesis and hampers training-induced adaptations in endurance performance. *Am. J. Clin. Nutr*. 87(1):142–149.

Goncalves, R. L., Quinlan, C. L., Perevoshchikova, I. V., Hey-Mogensen, M. and Brand, M. D. (2015). Sites of Superoxide and Hydrogen Peroxide Production by Muscle Mitochondria Assessed *ex Vivo* under Conditions Mimicking Rest and Exercise. *The Journal of Biological Chemistry*.290(1): 209-227. doi: 10.1074/jbc.M114.619072

Gottwalt, B. and Kinsey, S. (2016). Caffeine's Effects On Skeletal Muscle Bioenergetics *In Vitro. The Journal of Undergraduate Research and Creative Activities for the State of North Carolina: Natural Sciences and Engineering.* XI: 122-134.

Graham, T.E. (2001). Caffeine and exercise. Metabolism, endurance and performance. *J Sports Med*. 31: 785–807

Grimsrud, P.A., Xie, H., Griffin, T.J. & Bernlohr, D.A. (2008). Oxidative stress and covalent modification of protein with bioactive aldehydes. *J Biol Chem*. 283:21837-21840

Guerrieri, D., and van Praag, H. (2015). Exercise-mimetic AICAR transiently benefits brain function. *Oncotarget*. *6* (21), 18293–18313.

Halliwell B., & Gutteridge J. M. C. (2007). Free Radicals in Biology and Medicine, 4th ed. *Oxford University Press*: Oxford, UK

Hansen, J.M., Watson, W.H. and Jones, D.P. (2004). Compartmentation of Nrf-2 Redox Control: Regulation of Cytoplasmic Activation by Glutathione and DNA Binding by Thioredoxin-1. *Toxicological Sciences*. 82 (1): 308–317. Doi org.libproxy.ucl.ac.uk/10.1093/toxsci/kfh231

Harbauer, A.B., Zahedi, R.P., Sickmann, A., Pfanner, N. and Meisinger, C. (2014). The protein import machinery of mitochondria-a regulatory hub in metabolism, stress, and disease. *Cell Metabolism*. 19(3):357-372. doi: 10.1016/j.cmet.2014.01.010.

Heckman, M.A., Weil, J. and De Mejia, E.G. (2010). Caffeine (1, 3, 7-trimethylxanthine) in Foods: A Comprehensive Review on Consumption, Functionality, Safety, and Regulatory Matters. *Journal of Food Science*. 75(3): R77-R87

Herman, A. and Herman, A.P. (2013). Caffeine's Mechanisms of Action and Its Cosmetic Use. *Skin Pharmacology and Physiology*. 26: 8–14. doi: 10.1159/000343174

Herrmann-Frank, A., Lüttgau, H.C. and Stephenson, D.G. (1999). Caffeine and excitation-contraction coupling in skeletal muscle: a stimulating story. *J Muscle Res Cell Motil*. 20(2):223-37

Hill, B.G., Haberzettl, P., Ahmed, Y., Srivastava, S., & Bhatnagar, A. (2008). Unsaturated lipid peroxidation-derived aldehydes activate autophagy in vascular smooth-muscle cells. *Biochemical Journal*. *10*(3):525-534. Doi:10.1042/BJ20071063

Hollander, J., Fiebig, R., Gore, M., Ookawara, T., Ohno, H. and Ji L. (2001). Superoxide dismutase gene expression is activated by a single bout of exercise in rat skeletal muscle. *Pflügers Arch - Eur J Physiol*. 442 (3): 426–434. doi.org/10.1007/s004240100539.

Holloszy, J.O. & Narahara, H.T. (1967). Nitrate ions: Potentiation of increased permeability to sugar associated with muscle contraction. *Science.* 155: 573-575

Holloszy, J.O. (2014). Adaptations of skeletal muscle mitochondria to endurance exercise: a personal perspective. *Exercise and Sport Sciences Reviews*. 32(2):41-43

Hoppel, C.L., Lesnefsky, E.J., Chen, Q. and Tandler, B. (2017). Mitochondrial Dysfunction in Cardiovascular Aging. *Adv Exp Med Biol*. 982:451-464. doi: 10.1007/978-3-319-55330-6_24.

Hoppeler, H. (2016). Molecular networks in skeletal muscle plasticity. *J Exp Biol*. 219(Pt 2):205-13. doi: 10.1242/jeb.128207.

Hoppeler, H., Howald, H., Conley, K., Lindstedt, S. L., Claassen, H., Vock, P., & Weibel, E.R. (1985). Endurance training in humans: aerobic capacity and structure of skeletal muscle. *J. Appl. Physiol*. 59:320–327.

Huang, F., Liu, Q., Xie, S., Xu, J., Huang, B., Wu, Y., & Xia, D. (2016). Cypermethrin Induces Macrophages Death through Cell Cycle Arrest and Oxidative Stress-Mediated JNK/ERK Signaling Regulated Apoptosis. *International Journal of Molecular Science*. *17*(6): 885. doi: 10.3390/ijms17060885

Hyatt, H.W., Toedebusch, R.G., Ruegsegger, G., Mobley, C.B., Fox, C.D., McGinnis, G.R., Quindry, J.C., Booth, F.W., Roberts, M.D. and Kavazis, A.N. (2015). Comparative adaptations in oxidative and glycolytic muscle fibers in a low voluntary wheel running rat model performing three levels of physical activity. *Physiol Rep*. 3(11). e12619.

Ibrahim B and Stoward PJ. (1978). The histochemical localization of xanthine oxidase. *Histochem J*. 10: 615–617.

Irrcher I., Adhihetty P.J., Sheehan T., Joseph A.M. and Hood D.A. (2003) PPARgamma coactivator-1alpha expression during thyroid hormone-and contractile activity-induced mitochondrial adaptations. *Am. J. Physiol. Cell Physiol*. 284: C1669-C1677. doi: 10.1152/ajpcell.00409.2002

Irrcher, I., Ljubicic, V. & Hood, D.A. (2009). Interactions between ROS and AMP kinase activity in the regulation of PGc-1α transcription in skeletal muscle cells. *Am J Physiol Cell Physiol.* 296: C116–C123. Doi:10.1152/ajpcell.00267.2007

Jaganjac M. (2010). Possible involvement of granulocyte oxidative burst in Nrf2 signaling in cancer. *Indian J Med Res*. 131: 609-616

Jaganjac, M., Cacev, T., Cipak, A., Kapitanovic, S., Gall Troselj, K. and Zarkovic, N. (2012). Even stressed cells are individuals: second messengers of free radicals in pathophysiology of cancer. *Croat Med J*. 53(4):304-9.

Jaganjac, M., Cipak, A., Schaur, R.J. & Zarkovic, N. (2016). Pathophysiology of neutrophil-mediated extracellular redox reactions. *Front Biosci (Landmark Ed)*. 1(21):839-55

Jaganjac, M., Tirosh, O.,Cohen, G., Sasson, S., & Zarkovic, N. (2013). Reactive aldehydes – second messengers of free radicals in diabetes mellitus. *Free Radical Research*. *47*(1): 39-48. Doi: 10.3109/10715762.2013.789136

James, R.S., Kohlsdorf, T., Cox, V.M. & Navas, C.A. (2005). 70 μM caffeine treatments enhances in vitro force and power output during cyclic activities in mouse extensor digitorum longus muscle. *Eur J Appl Physiol.* 95: 74–82

Janssen, I. and Leblanc, A. (2010). Systematic Review of the Health Benefits of Physical Activity in School-Aged Children and Youth. *International Journal of Behavioural Nutrition and Physical Activity*. doi: 10.1186/1479-5868-7-40

Jensen, T.E. and E.A. Richter (2012). Regulation of glucose and glycogen metabolism during and after exercise. *J Physiol*. 590(Pt 5):1069-76.

Jensen, T.E., Angin, Y., Sylow, L. and Richter, E.A. (2014). Is contraction-stimulated glucose transport feedforward regulated by Ca2+? *Exp Physiol*. 99(12):1562-8. doi: 10.1113/expphysiol.2014.081679.

JI, L. L., GOMEZ-CABRERA, M.-C. and VINA, J. (2006). Exercise and Hormesis. *Annals of the New York Academy of Sciences*. 1067: 425–435. doi:10.1196/annals.1354.061

Johnson, I. M., Prakash, H., Prathiba, J., Raghunathan, R., & Malathi, R. (2012). Spectral Analysis of Naturally Occurring Methylxanthines (Theophylline, Theobromine and

Caffeine) Binding with DNA. *PLoS ONE*. 7(12), e50019. http://doi.org/10.1371/journal.pone.0050019

Judge, A. R. and Dodd, S. L. (2004). Xanthine oxidase and activated neutrophils cause oxidative damage to skeletal muscle after contractile claudication. *Am. J. Physiol. Heart Circ. Physiol*. 286: H252–H256. doi: 10.1152/ajpheart.00684.2003

Kavanagh, N.I., Ainscow, E.K. and Brand, M.D. (2000). Calcium regulation of oxidative phosphorylation in rat skeletal muscle mitochondria. *Biochimica et Biophysica Acta*. 1457(1-2):57-70

Kerrigan, S. and Lindsey, T. (2005). Fatal caffeine overdose: Two case reports. *Forensic Science International*. 153: 67–69

Kim, M.S., Zhong, J. and Pandey, A. (2016). Common errors in mass spectrometry-based analysis of post-translational modifications. *Proteomics*. 16(5):700-14. doi: 10.1002/pmic.201500355.

Knight, J.A. (2012). Physical Inactivity: Associated Diseases and Disorders. *Annals of Clinical & Laboratory Science*. 42 (3): 320-337

Konishi, M., Kurihara, S., & Sakai, T. (1984). The effects of caffeine on tension development and intracellular calcium transients in rat ventricular muscle. *The Journal of Physiology*. 355:605–618.

Kostić, D. A., Dimitrijević, D. S., Stojanović, G. S., Palić, I. R., Đorđević, A. S. and Ickovski, J. D. (2015). Xanthine oxidase: isolation, assays of activity, and inhibition. *Journal of Chemistry*. 2015. doi:10.1155/2015/294858

Lane, S.C., Hawley, J.A. Desbrow, B., Jones, A.M., Blackwell, J.R., Ross, M.L., Zemski, A.J. and Burke, L.M. (2014)..5Single and combined effects of beetroot juice and caffeine supplementation on cycling time trial performance1. *Applied Physiology, Nutrition & Metabolism*. 39 (9): 1050-8.

Lara, B., Ruiz-Vicente, D., Areces, F., Abián-Vicén, J., Salinero, J.J., Gonzalez-Millán, C., Gallo-Salazar, C. and Del Coso, J. (2015). Acute consumption of a caffeinated energy drink enhances aspects of performance in sprint swimmers. *The British Journal of Nutrition*. 114 (6): 908-14. doi: 10.1017/S0007114515002573.

Lee, J. and Clarkson, P.M. (2003) Plasma creatine kinase activity and glutathione after eccentric exercise. *Med Sci Sports Exerc*, 35(6): 930-6.

Lee, J., et al. (2002). Eccentric exercise effect on blood oxidative-stress markers and delayed onset of muscle soreness. *Med Sci Sports Exerc*. 34(3):443-8.

Liu, Y., Beyer, A. and Aebersold, R. (2016). On the Dependency of Cellular Protein Levels on mRNA Abundance. *Cell*. 165(3):535-50. doi: 10.1016/j.cell.2016.03.014

Ljubicic, V., Joseph, AM., Saleem, A., Uguccioni, G., Collu-Marchese, M., Lai, R., Nguyen, L., & Hood, D.A. (2010). Transcriptional and post-transcriptional regulation of mitochondrial biogenesis in skeletal muscle: Effects of exercise and aging. *Biochimica et Biophysica Acta*. 1800(3): 223–234. Doi:10.1016/j.bbagen.2009.07.031

Ludtmann M.H., Angelova P.R., Horrocks M.H., Choi M.L., Rodrigues M., Baev A.Y., Berezhnov A.V., Yao Z., Little D., Banushi B., Al-Menhali A.S., Ranasinghe R.T., Whiten D.R., Yapom R., Dolt K.S., Devine M.J., Gissen P., Kunath T., Jaganjac M., Pavlov E.V., Klenerman D., Abramov A.Y., Gandhi S. (2018). α-synuclein oligomers interact with ATP synthase and open the permeability transition pore in Parkinson's disease. *Nature Communications*. 9(1):2293. doi: 10.1038/s41467-018-04422-2.

Lumb A. (2014). Diabetes and exercise. *Clin Med (Lond)*. 14(6):673-6. doi: 10.7861/clinmedicine.

Magkos, F. & Kavouras, S.A. (2005). Caffeine use in sports, pharmacokinetics in man, and cellular mechanisms of action. *Crit Rev Food Sci Nutr*. 45: 535–562

Martinez-Lopez, S., Sarria, B., Baeza, G., Mateos, R. and Bravo-Clemente, L. (2014). Pharmacokinetics of caffeine and its metabolites in plasma and urine after consuming a

soluble green/roasted coffee blend by healthy subjects. *Food Research International*. 64:125–133. doi: 10.1016/j.foodres.2014.05.043.

Meeusen, R. and Decroix L. (2018). Nutritional Supplements and the Brain. Int J Sport Nutr Exerc Metab. 28(2):200-211. doi: 10.1123/ijsnem.2017-0314.

Mejia, E.G.d. and Ramirez-Mares, M.V. (2014). Impact of caffeine and coffee on our health. *Trends in Endocrinology and Metabolism*. 25: 10. doi: 10.1016/j.tem.2014.07.003.

Meng, S.-J. and Yu, L.-J. (2010). Oxidative Stress, Molecular Inflammation and Sarcopenia. *International Journal of Molecular Sciences*. 11(4): 1509–1526. doi.org/10.3390/ijms11041509

Merrill, G.F., Kurth, E.J., Hardie, D.G. and Winder, W.W. (1997). AICA riboside increases AMP-activated protein kinase, fatty acid oxidation, and glucose uptake in rat muscle. *The American journal of physiology*. 273:E1107–1112.

Michaelson, L. P., Shi, G., Ward, C. W. and Rodney, G. G. (2010). Mitochondrial redox potential during contraction in single intact muscle fibers. *Muscle Nerve*. 42: 522–529. doi:10.1002/mus.21724

Missiaen, L., Robberecht, W., Bosch, L., Callewaert, G., Parys, J.B., Wuytack, F., Raeymaekers, L., Nilius, B., Eggermont, J. and De Smedt, H. (2000). Abnormal intracellular Ca2+ homeostasis and disease. Cell Calcium. 28 (1): 1–2. doi: 10.1054/ceca.2000.0131

Mohamed, S., Lamya, N. and Hamda, M. (2016). Effect of Maximal Versus Supra-Maximal Exhausting Race on Lipid Peroxidation, Antioxidant Activity and Muscle-Damage Biomarkers in Long-Distance and Middle-Distance Runners. *Asian J Sports Med*. 7(1):e27902. doi: 10.5812/asjsm.27902.

Mooren, F.C. and Krüger, K. (2015). Exercise, Autophagy, and Apoptosis. *Progress in Molecular Biology and Translational Science*. 135: 1877-1173. doi.org/10.1016/bs.pmbts.2015.07.023

Morris, J.N., Heady, J.A., Raffle, P.A., Roberts, C.G. and Parks, J.W. (1953). Coronary heart-disease and physical activity of work. *Lancet.* 265:1111-20.

Morton, S., Davis, R. J., Cohen, P. (2004), Signalling pathways involved in multisite phosphorylation of the transcription factor ATF-2. *FEBS Letters*. 572:177-183. doi: 10.1016/j.febslet.2004.07.031

Mounier, R., Théret, M., Lantier, L., Foretz, M. and Viollet, B. (2015). Expanding roles for AMPK in skeletal muscle plasticity. *Trends Endocrinol Metab*. 26(6):275-86. doi: 10.1016/j.tem.2015.02.009.

Muthusamy, V.R., Kannan, S., Sadhaasivam, K., Gounder, S.S., Davidson, C.J., Boeheme, C., Hoidal, J.R., Wang, L., & Rajasekaran, N.S. (2012). Acute exercise stress activates Nrf2/ARE signaling and promotes antioxidant mechanisms in the myocardium. *Free Radical Biology and Medicine*. *52*(2):366-76.

Narkar, V.A., Downes, M., Yu, R.T., Embler, E., Wang, Y.-X., Banayo, E., Maria M. Mihaylova, M.M., Nelson, M.C., Zou, Y., Henry Juguilon, H., Kang, H., Shaw, R. and Evans, R.M. (2008). AMPK and PPARδ agonists are exercise mimetics. *Cell*. 134(3): 405–415. http://doi.org/10.1016/j.cell.2008.06.051

Negre-Salvayre, A., Auge, N., Ayala, V., Basaga, H., Boada, J., Brenke, R., Chapple, S., Cohen, G., Feher, J., Grune, T., Lengyel, G., Mann, G. E., Pamplona, R., Poli, G., Portero-Otin, M., Riahi, Y., Salvayre, R., Sasson, S., Serrano, J., Shamni, O., Siems, W., Siow, R.C.M., Wiswedel, I., Zarkovic, K., & Zarkovic, N. (2010). Pathological aspects of lipid peroxidation". *Free Radical Research.* *44* (10): 1125–1171. Doi: 10.3109/10715762.2010.498478

Negre-Salvayre, A., Coatrieux, C., Ingueneau, C., & Salvayre, R. (2008). Advanced lipid peroxidation end products in oxidative damage to proteins. Potential role in diseases and therapeutic prospects for the inhibitors. *British Journal of Pharmacology*. *153*(1): 6–20. Doi.org/10.1038/sj.bjp.0707395

Nègre-Salvayre, A., Hirtz, C., Carrera, G., Cazenave, R., Troly, M., Salvaure, R., Péenicaud, L. and Casteilla, L. (1999). A role for uncoupling protein-2 as a regulator of mitochondrial hydrogen peroxide generation. *FASEB J*. 11:809–815

Nehlig A. (2018). Interindividual Differences in Caffeine Metabolism and Factors Driving Caffeine Consumption. *Pharmacol Rev*. 70 (2): 384-411

Nethery, D., Callahan, L. A., Stofan, D., Mattera, R., DiMarco, A., Supinski G. (2000). PLA2 dependence of diaphragm mitochondrial formation of reactive oxygen species. *Journal of Applied Physiology*. 89 (1): 72-80

Nikolaidis, M.G., et al. (2007). Decreased blood oxidative stress after repeated muscle-damaging exercise. *Med Sci Sports Exerc*. 39(7):1080-9.

Nikolaidis, M.G., *et al.* (2008). The effect of muscle-damaging exercise on blood and skeletal muscle oxidative stress: magnitude and time-course considerations. *Sports Med*. 38(7):579-606.

O'Connell, S.E. and Zurzola, F.J. (1984). Rapid quantitative liquid chromatographic determination of caffeine levels in plasma after oral dosing. *J. Pharm. Sci.* 73 (7): 1009–1011.

O'Brien, J., Wilson, I., Orton, T. and Pognan, F. (2000). Investigation of the Alamar Blue (resazurin) fluorescent dye for the assessment of mammalian cell cytotoxicity. *European Journal of Biochemistry*. 267(17): 5421-6.

Page, S., Fischer, C., Baumgartner, B., Haas, M., Kreusel, U., Loidl, G., Hayni, M., Ziegler-Heitbrock, H.W.L., Neumeier, D. and Brand, K. (1999). 4-Hydroxynonenal Prevents NF-kB Activation and Tumor Necrosis Factor Expression by Inhibiting IkB Phosphorylation and Subsequent Proteolysis. *The Journal of Biological Chemistry*. 274 (17): 11611–11618.

Paterson, D.H., Jones, G.R. and Rice, C.L. (2007). Ageing and physical activity: evidence to develop exercise recommendations for older adults. *Applied Physiology, Nutrition and Metabolism*. 32: S69–S108. doi:10.1139/H07-111

Pattanakuhar, S., Pongchaidecha, A., Chattipakorn, N. and Chattipakorn, S.C. (2017). The effect of exercise on skeletal muscle fibre type distribution in obesity: From cellular levels to clinical application. *Obesity Research & Clinical Practice*. 11(5): 112-132

Pedersen, B.K. and Febbraio, M.A. (2008). Muscle as an endocrine organ: focus on muscle-derived interleukin-6. *Physiol. Rev*. 88 1379–1406.

Perry, C.G.1., Lally, J., Holloway, G.P., Heigenhauser, G.J., Bonen, A. & Spriet, L.L. (2010). Repeated transient mRNA bursts precede increases in transcriptional and mitochondrial proteins during training in human skeletal muscle. *J Physiol*. 588(Pt 23):4795-810.

Physical Activity Guidelines Advisory Committee (PAGAC). (2008). *Physical Activity Guidelines Advisory Committee Report, 2008*. Washington, DC, US Department of Health and Human Services, 2008

Poljak-Blazi, M., Jaganjac, M., Mustapic, M., Pivac, N., Muck-Seler, D. (2009). Acute immunomodulatory effects of iron polyisomaltosate in rats. *Immunobiology*. 214(2):121-8. doi: 10.1016/j.imbio.2008.07.005.

Poljak-Blazi, M., Jaganjac, M., Sabol, I., Mihaljevic, B., Matovina, M. & Grce, M. (2011). Effect of ferric ions on reactive oxygen species formation, cervical cancer cell lines growth and E6/E7 oncogene expression. *Toxicol In Vitro*. 25(1):160-166

Poljsak, B., Šuput, D., & Milisav, I. (2013). Achieving the Balance between ROS and Antioxidants: When to Use the Synthetic Antioxidants. *Oxidative Medicine and Cellular Longevity*. *2013*: 11. doi:10.1155/2013/956792

Porras-Yakushi, T.R., Sweredoski, M.J. and Hess, S. (2015). ETD Outperforms CID and HCD in the Analysis of the Ubiquitylated Proteome. *J Am Soc Mass Spectrom*. 26(9):1580-1587

Powers, S.K. and Jackson, M.J. (2008). Exercise-Induced Oxidative Stress: Cellular Mechanisms and Impact on Muscle Force Production. *Physiol Rev*. 88(4): 1243–1276. doi:10.1152/physrev.00031.2007

Powers, S.K., Criswell, D., Lawler, J., Ji, L.L., Martin, D., Herb, R.A. and Dudley, G. (1994). Influence of exercise and fiber type on antioxidant enzyme activity in rat skeletal muscle. *Am J Physiol*. 266(2 Pt 2):R375-80

Powers, S.K., Nelson, W.B. and Hudson, M.B. (2011). Exercise-induced oxidative stress in humans: cause and consequences. *Free Radical Biology and Medicine*. 51(5):942-50. doi: 10.1016/j.freeradbiomed.2010.12.009. Epub 2010 Dec 16.

Radak, Z., Taylor, A., Ohno, H. and Goto, S. (2001). Adaptation to exercise-induced oxidative stress: From muscle to brain. *Exercise Immunology*. 7: 90-107.

Rauniyar, N. and Prokai, L. (2009). Detection and identification of 4-hydroxy-2-nonenal Schiff-base adducts along with products of Michael addition using data-dependent neutral loss-driven MS3acquisition: method evaluation through an in vitro study on cytochrome c oxidase modifications. *Proteomics*. 9(22): 5188–5193. doi: 10.1002/pmic.200900116

Rauniyar, N., Stevens, S.M., Prokai-Tatrai, K. and Prokai, L. (2009). Characterization of 4-hydroxy-2-nonenal-modified peptides by liquid chromatography-tandem mass spectrometry using data-dependent acquisition: neutral loss-driven MS3 versus neutral loss-driven electron capture dissociation. *Anal Chem*. 81(2):782-9. doi: 10.1021/ac802015m.

Remels, A.H., Langen, R.C., Schrauwen, P., Schaart, G., Schols, A.M., & Gosker, H.R. (2010). Regulation of mitochondrial biogenesis during myogenesis. *Molecular and Cellular Endocrinology*. 315(1–2): 113–120. Doi: 10.1016/j.mce.2009.09.029.

Richter, E.A., Garetto, L.P., Goodman, M.N. & Ruderman, N.B. (1982). Muscle glucose metabolism following exercise in the rat: increased sensitivity to insulin. *J. Clin. Invest*. 69: 785-793

Rossi a, S. P., Windschüttl, S., Matzkin, M. E., Rey-Ares, V., Terradas, C., Ponzio, R., Puigdomenech, E., Levalle, O., Calandra, R. S., Mayerhofer, A., & Frungieri, M. (2016). Reactive oxygen species (ROS) production triggered by prostaglandin D2 (PGD2) regulates lactate dehydrogenase (LDH) expression/activity in TM4 Sertoli cells. *Molecular and Cellular Endocrinology*. *434*:154–165. doi:10.1016/j.mce.2016.06.021

Rousseau, E., LaDine, J., Liu, Q. and Meissner, G. (1988) Activation of the Ca^{2+} release channel of skeletal muscle sarcoplasmic reticulum by caffeine and related compounds. *Arch Biochem Biophys* 267:75-86

Rovira-Llopis, S., Bañuls, C., Diaz-Morales, N., Hernandez-Mijares, A., Rocha, M., and Victor, V.M. (2017). Mitochondrial dynamics in type 2 diabetes: Pathophysiological implications. *Redox biology*. 11:637-645.

Saini, A., Faulkner, S., Al-Shanti, N. and Stewart, C. (2009). Powerful signals for weak muscles. *Aging Research Reviews*. 8 (4): 251-67. doi: 10.1016/j.arr.2009.02.001.

Sakellariou, G. K., Vasilaki, A., Palomero, J., Kayani, A., Zibrik, L., McArdle, A. and Jackson, M. J. (2013). Studies of mitochondrial and nonmitochondrial sources implicate nicotinamide adenine dinucleotide phosphate oxidase(s) in the increased skeletal muscle superoxide generation that occurs during contractile activity. *Antioxidants & Redox Signaling*. 18(6), 603–621. doi.org/10.1089/ars.2012.4623

Sakellariou, G.K., Jackson, M.J. and Vasilaki A. (2014). Redefining the major contributors to superoxide production in contracting skeletal muscle. The role of NAD(P)H oxidases. *Free Radical Research*. 48(1):12-29. DOI: 10.3109/10715762.2013.830718

Sayre, L.M., Lin, D., Yuan, Q., Zhu, X., & Tang X. (2006). Protein adducts generated from products of lipid oxidation: focus on HNE and one. *Drug Metab Rev.* 38 (4):651-75.

Schauenstein, E., Esterbaner, H., Jaag, G., & Taufer, M. (1964). The effect of aldehydes on normal and malignant cells. 1st report: Hydroxy-octenal on new fat-aldehyde. *Monatsh. Chem. 95*: 180-183.

Schaur, R.J., Siems, W., Bresgen, N. & Eckl, P.M. (2015). 4-Hydroxy-nonenal—A Bioactive Lipid Peroxidation Product. Biomolecules. 5: 2247-2337. Doi:10.3390/biom5042247

Schneider, C., Tallman, K.A., Porter, N.A., & Brash, A.R. (2001). Two distinct pathways of formation of 4-hydroxynonenal. Mechanisms of nonenzymatic transformation of the 9- and 13-hydroperoxides of linoleic acid to 4-hydroxyalkenals. *Journal of Biological Chemistry*. *276* (24): 20831–20838. Doi.org/10.1074/jbc.M101821200

Scott, W., Stevens, J., Binder-Macleod, S.A. (2001). Human skeletal muscle fiber type classifications. *Phys Ther*. 81: 1810–1816

Shadel, G.S. and Horvath, T.L. (2015). Mitochondrial ROS signaling in organismal homeostasis. *Cell*. 163(3):560-9.

Shevchenko, A., Tomas, H., Olsen, J.V. & Mann, M. (2007). In-gel digestion for mass spectrometric characterization of proteins and proteomes. *Nature Protocols*. 1(6): 2856-2860

Shridas, P. and Webb, N. R. (2014). Diverse functions of secretory phospholipases A_2. *Advances in Vascular Medicine*. 2014. doi:10.1155/2014/689815

Siems, W.G., Zollner, H., Grune, T., & Esterbauer, H. (1997). Metabolic fate of 4-hydroxynonenal in hepatocytes: 1,4-dihydroxynonene is not the main product. *Journal of Lipid Research*. *38*(3): 612-22

Sies, H. and Cadenas, E. (1985). Oxidative stress: damage to intact cells and organs. *Philos. Trans. R. Soc. Lond. B Biol. Sci.* 311 (1152): 617–631

Sies, H., Berndt, C. and Jones, D. (2017). Oxidative Stress. *Annual review of biochemistry*. 86: 715-748

Silva, J.R., et al. (2014). Biochemical impact of soccer: an analysis of hormonal, muscle damage, and redox markers during the season. *Appl Physiol Nutr Metab*. 39(4): 432-8.

Simpson, R.J., Kunz, H., Agha, N. and Graff, R. (2015). Exercise and the Regulation of Immune Functions. *Progress in Molecular Biology and Translational Science*. 135:355-80. doi: 10.1016/bs.pmbts.2015.08.001.

Skinner, T.L., Jenkins, D.G., Coombes, J.S., Taaffe, D.R. and Leveritt, M.D. (2010). Dose response of caffeine on 2000-m rowing performance. *Med Sci Sports Exerc*. 42 (3): 571–6.

Sloboda, D. D. and Brooks, S. V. (2013). Reactive oxygen species generation is not different during isometric and lengthening contractions of mouse muscle. *American Journal of Physiology - Regulatory, Integrative and Comparative Physiology*, 305(7), R832–R839. http://doi.org/10.1152/ajpregu.00299.2013

Sökmen, B., Armstrong, L.E., Kraemer, W.J., Casa, D.J., Dias, J.C., Judelson, D.A. and Maresh, C.M. (2008). Caffeine use in sports: considerations for the athlete. *Strength Cond Res*. 22(3):978-86. doi: 10.1519/JSC.0b013e3181660cec.

Stadheim, H.K., Spencer, M., Olsen, R. and Jensen, J. (2013). Caffeine and Performance over Consecutive Days of Simulated Competition. *Medicine & Science in Sports & Exercise*. 46(9): 1787–1796. doi: 10.1249/MSS.0000000000000288

Starkov, A.A. (2010). Measurement of Mitochondrial ROS Production. *Methods Mol Biol*. 648: 245–255. doi:10.1007/978-1-60761-756-3_16

Steinbacher, P. and Eckl, P. (2015). Impact of Oxidative Stress on Exercising Skeletal Muscle. *Biomolecules*. 5:356-377. doi:10.3390/biom5020356

Sun, Q.A., Hess, D. T., Nogueira, L., Yong, S., Bowles, D. E., Eu, J. and Stamler, J. S. (2011). Oxygen-coupled redox regulation of the skeletal muscle ryanodine receptor-Ca2+ release channel by NADPH oxidase 4. *Proceedings of the National Academy of Sciences of the United States of America*. 108(38):16098–16103

Suzuki, Y.J., Carini, M. & Butterfield, D.A. (2010). Protein carbonylation. *Antioxid Redox Signal*. 12: 323–325.

Svensson M., Lexell J., Deierborg T. (2015). Effects of Physical Exercise on Neuroinflammation, Neuroplasticity, Neurodegeneration, and Behavior: What We Can Learn From Animal Models in Clinical Settings. *Neurorehabil Neural Repair*. 29(6):577-89. doi: 10.1177/1545968314562108.

Tallis, J., James. R.S., Cox, V.M. & Duncan, M.J. (2012). The effect of physiological concentrations of caffeine on the power output of maximally and sub maximally stimulated mouse EDL (fast) and soleus (slow) muscle. *J Appl Physiol.* 112: 64–71

Tallis, J., James. R.S., Cox, V.M. & Duncan, M.J. (2013). The effect of a physiological concentration of caffeine on the endurance of maximally and submaximally stimulated mouse soleus muscle. *J Physiol Sci.* 63: 125–132

Tanito, M., Haniu, H., Elliott, M.H., Singh, A.K., Matsumoto, H. & Anderson, R.E. (2006). Identification of 4-hydroxynonenal-modified retinal proteins induced by photooxidative stress prior to retinal degeneration. *Free Radic Biol*. 41(12):1847–1859.

Tarnopolsky, M. A. (2008). Effect of caffeine on the neuromuscular system - potential as an ergogenic aid. Applied Physiology, Nutrition & Metabolism. 33(6):1284–1289.

Theilen, N.T., Kunkel, G.H., and Tyagi, S.C. (2017). The Role of Exercise and TFAM in Preventing Skeletal Muscle Atrophy. *Journal of cellular physiology*. 232(9):2348-2358.

Tipton, C.M. (2008). Susruta of India, an unrecognized contributor to the history of exercise physiology. *J. Appl. Physiol*. 104: 1553-1556

Turner, J. E., Bosch, J. A., Drayson, M. T. and Aldred, S. (2011). Assessment of oxidative stress in lymphocytes with exercise. *Journal of Applied Physiology*, 111 (1) 206-211. doi:10.1152/japplphysiol.00051.

Uchida, K.1., Szweda, L.I., Chae, H.Z. & Stadtman, E.R. (1993) Immunochemical detection of 4-hydroxynonenal protein adducts in oxidized hepatocytes. *Proc Natl Acad Sci U S A*. 90(18): 8742-8746

Uma, S.V., Raman, V.K. & Nochikattil, S.K. (2016). Life Course Socioeconomic Transition and its Association with Early Onset Type 2 Diabetes: Protocol for a Sequential Exploratory Mixed Method Study. *J Clin Diagn Res*. 10(6):LO01-5. doi: 10.7860/JCDR/2016/17800.8020.

Usachev, Y., Shmigol, A., Pronchuk, N., Kostyuk, P. & Verkhratsky, A. (1993). Caffeine induced calcium release from internal stores in cultured rat sensory neurons. 57(3): 845–859

Vaarmann A, Gandhi S, Abramov AY. Dopamine induces Ca2+ signaling in astrocytes through reactive oxygen species generated by monoamine oxidase. J Biol Chem. 2010;285(32):25018-23.

Verrastro, I., Pasha, S., Jensen, K.T., Pitt, A.R. and Spickett, C.M. (2015). Mass spectrometry-based methods for identifying oxidized proteins in disease: advances and challenges. *Biomolecules*. 5(2):378-411. doi: 10.3390/biom5020378.

Veskoukis, A.S., Nikolaidis, M.G., Kyparos, A., Kokkinos, D., Nepka, C., Barbanis, S. and Kouretas, D. (2008). Effects of xanthine oxidase inhibition on oxidative stress and swimming performance in rats. *Appl Physiol Nutr Metab*. 33(6): 1140–1154. doi.10.1139/H08-102.

Villella, M. and Villella, A. (2014). Exercise and cardiovascular diseases. *Kidney Blood Press Res.* 39(2-3):147-53. doi: 10.1159/000355790

Viña, J., Gomez-Cabrera, M.C., Borras, C., Froio, T., Sanchis-Gomar, F., Martinez-Bello, V.E., & F.V. Pallardo (2009). Mitochondrial biogenesis in exercise and in ageing. *Advanced Drug Delivery Reviews*. 61(14): 1369–1374. Doi:10.1016/j.addr.2009.06.006

Vincent, H.K., Powers, S.K., Demirel, H.A., Coombes, J.S. & Naito, H. (1999). Exercise training protects against contraction-induced lipid peroxidation in the diaphragm. *Eur J Appl Physiol*. 79: 268 - 273

Wadley, G. D., Nicolas, M. A., Hiam, D. S. and McConell, G. K. (2013). Xanthine oxidase inhibition attenuates skeletal muscle signaling following acute exercise but does not impair mitochondrial adaptations to endurance training. *American Journal of Physiology*. 304 (8): E853 E862. doi:10.1152/ajpendo.00568.2012

Wallberg-Henriksson, H., Constable, S.H., Young, D.A. & Holloszy, J.O. (1988). Glucose transport into rat skeletal muscle: interaction between exercise and insulin. *J. Appl. Physiol*. 65: 909-913

Wang, C.H. and Wei, Y.H. (2017). Role of mitochondrial dysfunction and dysregulation of Ca2+ homeostasis in the pathophysiology of insulin resistance and type 2 diabetes. *J Biomed Sci*. 24(1):70. doi: 10.1186/s12929-017-0375-3.

Weber, A. and Herz, R. (1968). The relationship between caffeine contracture of intact muscle and the effect of caffeine on reticulum. *The Journal of General Physiology*. 52(5):750-9.

Wende, A.R., Schaeffer, P.J., Parker, G.J., Zechner, C., Han, D.H., Chen, M.M., Hancock, C.R., Lehman, J.J., Huss, J.M., McClain, D.A., Holloszy, J.O. and Kelly, D.P. (2007). A role for the transcriptional coactivator PGC-1alpha in muscle refueling. *The Journal of Biological Chemistry*. 282(50): 36642–36651.

Whitsett, J., Picklo, M.J. Sr., &Vasquez-Vivar, J. (2007). 4-Hydroxy-2-nonenal increases superoxide anion radical in endothelial cells via stimulated gtp cyclohydrolase proteasomal degradation. *Arterioscler Thromb Vasc Biol*. *27*(11):2340-2347. Doi: 10.1161/ATVBAHA.107.153742

Wild, S., Roglic, G., Green, A., Sicree, R. & King, H. (2014). Global Prevalence of Diabetes Estimates for the year 2000 and projections for 2030. *Diabetes Care.* 27(5): 1047-1053

Winterbourn, C.C. (2014). The challenges of using fluorescent probes to detect and quantify specific reactive oxygen species in living cells. *Biochim Biophys Acta*. 1840(2):730-8. doi: 10.1016/j.bbagen.2013.05.004.

World Anti-Doping Agency (WADA). (2018). Prohibited list: January 2018. *WADA*. The World Anti-Doping Code International Standard.

World Health Organization. (2018). *WHO launches Global Action Plan on Physical Activity*. Retrieved from http://www.who.int/news-room/detail/04-06-2018-who-launches-global-action-plan-on-physical-activity

Wright, D.C.1., Han, D.H., Garcia-Roves, P.M., Geiger, P.C., Jones, T.E. & Holloszy, J.O. (2007). Exercise-induced mitochondrial biogenesis begins before the increase in muscle PGC-1alpha expression. *J Biol Chem.* 282:194-9.

Xu, K.Y., Zweier, J.L. and Becker, L.C. (1997). Hydroxyl radical inhibits sarcoplasmic reticulum Ca2+-ATPase function by direct attack on the ATP binding site. *Circ. Res.* 80:76–81.

Yoboue, E. D., & Devin, A. (2012). Reactive Oxygen Species-Mediated Control of Mitochondrial Biogenesis. *International Journal of Cell Biology*. *2012*: 8. doi:10.1155/2012/403870

Yu, M., Blomstrand, E., Chibalin, A. V., Krook, A., and Zierath, J. R. (2001). Marathon running increases ERK1/2 and p38 MAP kinase signalling to downstream targets in human skeletal muscle. *The Journal of Physiology*. 536(Pt 1): 273–282. doi.org/10.1111/j.1469-7793.2001.00273.x

Zarkovic, N., Cipak, A., Jaganjac, M., Borovic, S. and Zarkovic, K. (2013). Pathophysiological relevance of aldehydic protein modifications. *J Proteomics*. 92:239-47.

Zhao, X., Bey, E. A., Wientjes, F. B., Cathcart, M. K. (2002). Cytosolic Phospholipase A2 (cPLA2) Regulation of Human Monocyte NADPH Oxidase Activity: cPLA2 AFFECTS TRANSLOCATION BUT NOT PHOSPHORYLATION OF p67*phox* AND p47*phox*. *The Journal of Biological Chemistry*. 277: 25385-25392. doi: 10.1074/jbc.M203630200

Zhao, Y., Miriyala, S., Miao, L., Mitov, M., Schnell, D., Dhar, S.K., Cai, J., Klein, J.B., Sultana, R., Butterfield, D.A., Vore, M., Batinic-Haberle, I., Bondada, S. & St Clair, D.K. (2014). Redox proteomic identification of HNE-bound mitochondrial proteins in cardiac tissues reveals a systemic effect on energy metabolism after doxorubicin treatment. *Free Radic Biol Med.*. 72:55-65.

Zhong, H., & Yin, H. (2015). Role of lipid peroxidation derived 4-hydroxynonenal (4-HNE) in cancer: Focusing on mitochondria. *Redox Biology*. *4*: 193–199

Živković, M., Žarković, K., Škrinjar, L., Waeg, G., Poljak-Blaži, M., Šunjić, S.B., Schaur, R.J. and Žarković, N. (2005). A New Method for Detection of HNE-histidine Conjugates in Rat Inflammatory Cells. *Croatica Chemica Acta*. 78(1): 91-98

8. APPENDICES

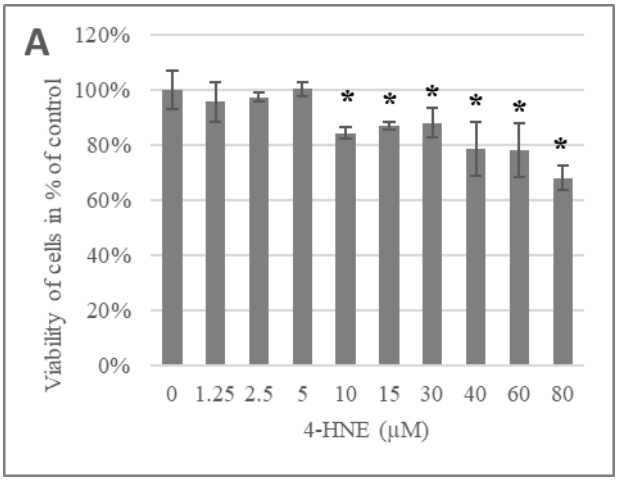

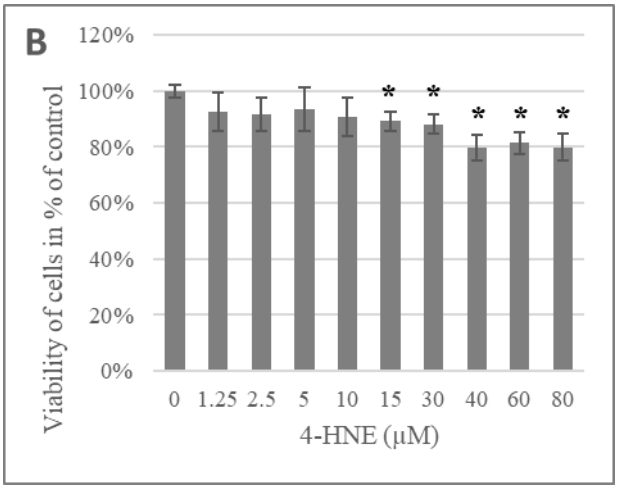

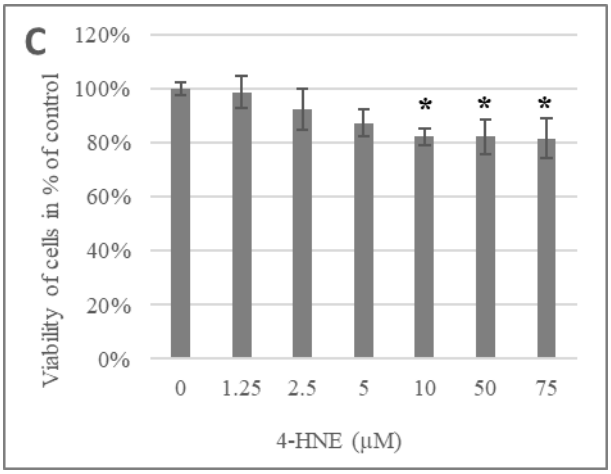

Figure 86: The effect of wide range of 4-HNE concentrations on the viability. A. C2C12, **B.** L6 and **C.** HSMM. Myotubes were treated overnight and measured using AlamarBlue assay. (p <0.01) (Mean ± *SD* of N =5)

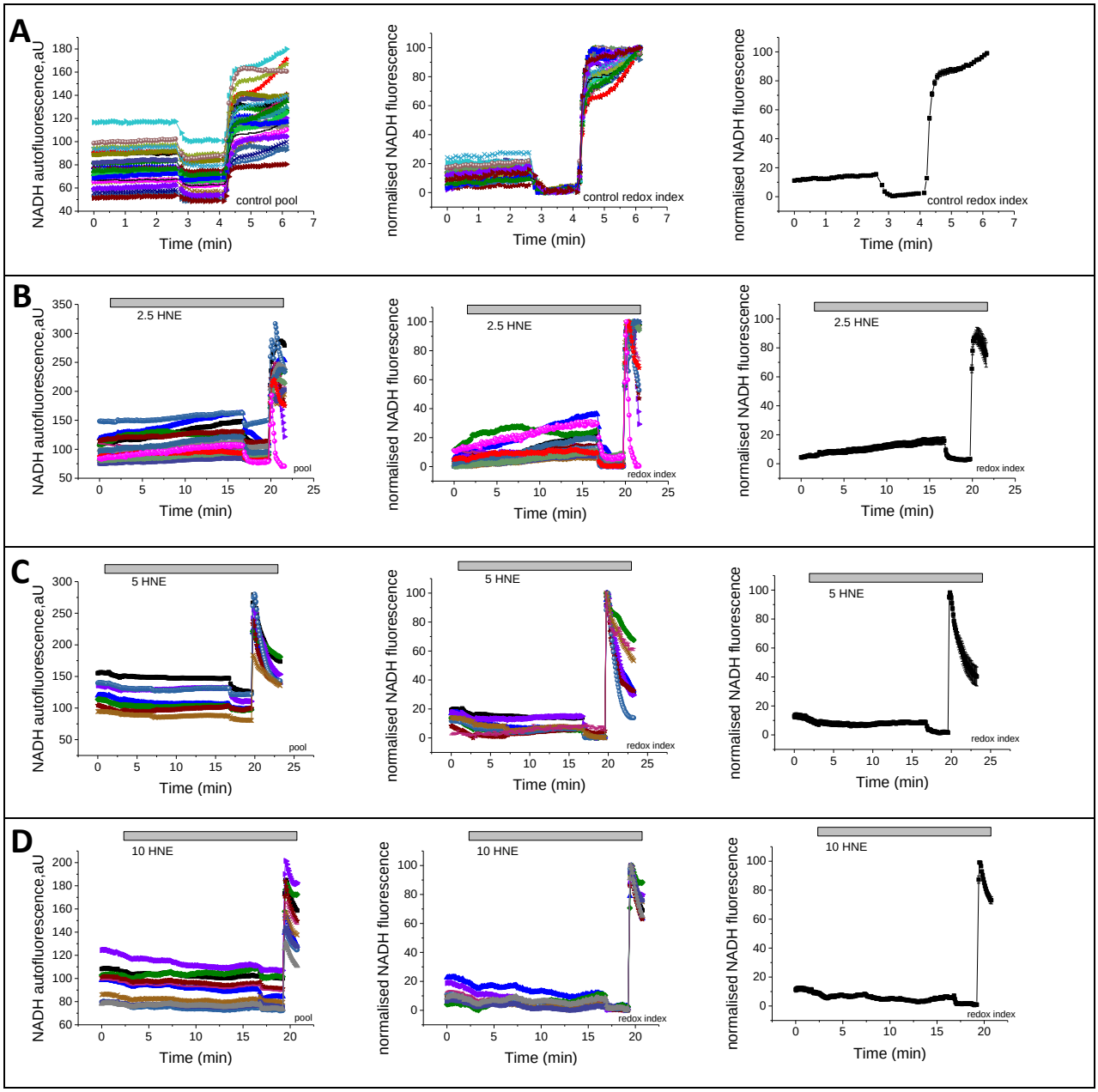

Figure 87: Effect of 4-HNE on mitochondrial NADH of C2C12 myotubes measured by autofluorescence of NADH. **A.** Control result without addition of 4-HNE, **B.** NADH signal with 2.5 µM 4-HNE, **C.** NADH signal with 5 µM 4-HNE, and **D.** NADH signal with 10 µM 4-HNE.

Table 13: Housekeeping genes selected for normalization of each experiment for the RT² Profiler PCR Array

PCR Array	Experiment	Selected Housekeeping Genes
Mouse Mitochondrial Energy Metabolism RT² Profiler PCR Array (PAMM008Z)	Effect of 4-HNE treatment on the expression of mitochondrial respiration genes	Hsp90ab1
	Effect of caffeine on the expression of mitochondrial respiration genes	B2m
Rat Mitochondria RT² Profiler PCR Array (PARN087Z)	Effect of 4-HNE on the expression of mitochondrial biogenesis genes	Rplp1
	Effect of caffeine on the expression of mitochondrial biogenesis genes	Ldha, Rplp1

Table 14: List of genes of Mouse Mitochondria RT² Profiler PCR Array with their main function

Main Function	Genes Symbols
Complex I (NADH-Coenzyme Q Reductase)	Ndufa1, Ndufa10, Ndufa11, Ndufa2, Ndufa3, Ndufa4, Ndufa5, Ndufa6, Ndufa7, Ndufa8, Ndufab1, Ndufb10, Ndufb2, Ndufb3, Ndufb4, Ndufb5, Ndufb6, Ndufb7, Ndufb8, Ndufb9, Ndufc1, Ndufc2, Ndufs1, Ndufs2, Ndufs3, Ndufs4, Ndufs5, Ndufs6, Ndufs7, Ndufs8, Ndufv1, Ndufv2, Ndufv3.
Complex II (Succinate-Coenzyme Q Reductase)	Sdha, Sdhb, Sdhc, Sdhd.
Complex III (Coenzyme Q-Cytochrome c Reductase)	Bcs1l, Cyc1, Uqcr11, Uqcrc1, Uqcrc2, Uqcrfs1, Uqcrh, Uqcrq.
Complex IV (Cytochrome c Oxidase)	Cox4i1, Cox4i2, Cox5a, Cox5b, Cox6a1, Cox6a2, Cox6b1, Cox6b2, Cox6c, Cox7a2, Cox7a2l, Cox7b, Cox8a, Cox8c, Cox11.
Complex V (ATP Synthase)	Lhpp, Atp12a, Atp4a, Atp4b, Atp5a1, Atp5b, Atp5c1, Atp5d, Atp5f1, Atp5g1, Atp5g2, Atp5g3, Atp5h, Atp5j, Atp5j2, Atp5o, Atp6v0a2, Atp6v0d2, Atp6v1c2, Atp6v1e2, Atp6v1g3, Oxa1l, Ppa1, Ppa2.

Table 15: List of genes of and Rat Mitochondria RT² Profiler PCR Array with their main function

Main Function	Genes Symbols
Membrane Polarization & Potential	Bak1, Bcl2, Bcl2l1 (Bcl-xl), Bnip3, Gclc, Gclm, Sod1, Tp53 (p53), Ucp1, Ucp2, Ucp3.
Mitochondrial Transport	Aip, Bak1, Bcl2, Bcl2l1 (Bcl-xl), Bnip3, Cpt1b, Cpt2, Timm10b (Fxc1), Grpel1, Hsp90aa1 (Hspca), Hspd1, Mfn2, Mipep, Mtx2, Stard3, Tp53 (p53), Tspo (Bzrp), Ucp1, Ucp2, Ucp3.
Small Molecule Transport	Slc25a10, Slc25a12, Slc25a13, Slc25a14, Slc25a15, Slc25a16, Slc25a17, Slc25a19, Slc25a2, Slc25a20, Slc25a21, Slc25a22, Slc25a23, Slc25a24, Slc25a25, Slc25a27, Slc25a3, Slc25a30, Slc25a36, Slc25a37, Slc25a4, Slc25a5.
Targeting Proteins to Mitochondria	Aip, Timm10b (Fxc1), Grpel1, Hspd1, Mfn2, Mipep, Tspo (Bzrp).
Mitochondrion Protein Import	Aip, Akt1, Cav2, Cln8, Cox18, Timm10b (Fxc1), Gpx1, Grpel1, Hspd1, LOC691853 (Cox10), Mipep, Ppargc1a (Ppargc1), Sh3glb1.
Outer Membrane Translocation	Tomm22, Tomm34, Tomm40, Tomm40l, Tomm70a.
Inner Membrane Translocation	Timm10b (Fxc1), Immp1l, Opa1, Taz, Timm10, Timm17a, Timm17b, Timm22, Timm44, Timm8a1, Timm8b, Timm9.
Mitochondrial Fission & Fusion	Cox18, Fis1, LOC691853 (Cox10), Mfn1, Mfn2, Opa1
Mitochondrial Localization	Dnm1l, Mfn2, Msto1, Nefl, Opa1, Rhot2, Rnf135 (Rhot1), Uxt.
Apoptosis	Aifm2, Akt1, Bak1, Bbc3, Bcl2, Bcl2l1 (Bcl-xl), Bid, Bnip3, Cdkn2a (INK4A, p16, p19ARF), Dnm1l, Gpx1, Pmaip1 (Noxa), Sfn (14-3-3σ), Sh3glb1, Sod2, Tp53 (p53).

Table 16: The 20 common naturally occurring amino acids. The chemical formula given here is for the bound amino acid. The monoisotopic mass given here is the mass calculated based on most abundant isotope of each element in the amino acid. The average mass calculated based on the average masses of all isotopes of each element in the amino acid.

Name	Code	Symbol	Chemical Formula *	Molecular Weight (g/mol)	Monoisotopic Mass (Da)	Average Mass (Da)
Alanine	A	Ala	C_3H_5ON	89.0935	71.03711	71.0788
Arginine	R	Arg	$C_6H_{12}ON_4$	174.2017	156.10111	156.1875
Asparagine	N	Asn	$C_4H_6O_2N_2$	132.1184	114.04293	114.1038
Aspartate	D	Asp	$C_4H_5O_3N$	133.1032	115.02694	115.0886
Cysteine	C	Cys	C_3H_5ONS	121.159	103.00919	103.1388
Glutamate	E	Glu	$C_5H_7O_3N$	147.1299	129.04259	129.1155
Glutamine	Q	Gln	$C_5H_8O_2N_2$	146.1451	128.05858	128.1307
Glycine	G	Gly	C_2H_3ON	75.0669	57.02146	57.0519
Histidine	H	His	$C_6H_7ON_3$	155.1552	137.05891	137.1411
Isoleucine	I	Ile	$C_6H_{11}ON$	131.1736	113.08406	113.1594
Leucine	L	Leu	$C_6H_{11}ON$	131.1736	113.08406	113.1594
Lysine	K	Lys	$C_6H_{12}ON_2$	146.1882	128.09496	128.1741
Methionine	M	Met	C_5H_9ONS	149.2124	131.04049	131.1926
Phenylalanine	F	Phe	C_9H_9ON	165.19	147.06841	147.1766
Proline	P	Pro	C_5H_7ON	115.131	97.05276	97.1167
Serine	S	Ser	$C_3H_5O_2N$	105.093	87.03203	87.0782
Threonine	T	Thr	$C_4H_7O_2N$	119.1197	101.04768	101.1051
Tryptophan	W	Trp	$C_{11}H_{10}ON_2$	204.2262	186.07931	186.2132
Tyrosine	Y	Tyr	$C_9H_9O_2N$	181.1894	163.06333	163.176
Valine	V	Val	C_5H_9ON	117.1469	99.06841	99.1326

* For the molecular formula of free amino acid add H_2O

Table 17: Peptides with one site of 4-HNE modification identified in proteins isolated from skeletal muscle of the control groups.

UniProt Accessions	Peptide Sequence	4-HNE Modifications and Site of Modification in the Peptide	No. of positive samples
P32848	AIGAFAAADSFDHK	HNE [H/K]	7
Q6P8K3	AIMAAWTFPCLPVGALMK	HNE [M/L/K]	7
Q6DIB5	CAEACRCVNGGK	HNE-Delta:H(2)O [C1]	5
O35643	DIANENEAQFQIR	HNE [R13]	5
Q810N9	DTLLQACEAIKNK	HNE [L3]	6
Q8R429	IGIFSENEEVTDR	HNE [R13]	7
P14211	KEEEEAEDKEDDDDR	HNE [K1]	5
A0A0R4J1B0	KPLNIDHLSDDK	HNE [K/L]	6
A0A0R4J1B0	KPLNIDHLSDDKLR	HNE [R/K/L]	7
E9PX68	KTELQTTNAENK	HNE [K1]	6
Q9Z2U2	LTGQENISSKANQEKSK	HNE [K10]	5
Q3UHK6	NDRLSSVTMPNVAR	HNE+Delta:H(2) [L4]	6
Q5SWZ5	TGQKFSLCILTPDK	HNE-Delta:H(2)O [L/C]	6
P19137	TVGSLNEDPCIEPCLCKKNVEGK	HNE+Delta:H(2) [C14]	5
A2RT67	TYLQDCSEVTCMIR	HNE+Delta:H(2) [R/M]	7
O70250	YAGLKPEELPTCESLK	HNE [K16]	5

Table 18: Peptides with two or three sites of 4-HNE modifications identified in proteins isolated from skeletal muscle of the control groups.

UniProt Accessions	Peptide Sequence	4-HNE Modifications and Sites of Modification in the Peptide	No. of positive samples
Q6DIB5	CAEACRCVNGGK	HNE [C7; K12]	5
Q9R0Y5	LETYYNATEPVISFYDK	HNE [L1; K17]	6
A2ASS6	RLEETDESQLER	HNE [R1; R12]	5
Q07231	RTHTGEKPYVCTK	HNE [R1; K13]	7
A2RT67	TYLQDCSEVTCMIR	HNE [C6; C11]	7
Q9DBS8	CSLHVAHNDSDR	HNE [R12]; HNE-Delta:H(2)O [C1]	6
G3UW68	HFETDCYPNEETLQAFAEELK	HNE [L20]; HNE-Delta:H(2)O [C6]	6
J3QN85	DLSDLISEMEMMK	HNE+Delta:H(2) [M/K]; HNE-Delta:H(2)O [M]	5
Q61753	KGILVMNTPNGNSLSAAELTCGMIMCLAR	HNE [M/L/K/C]; HNE+Delta:H(2) [K1]	6

Table 19: Peptides with one site of 4-HNE modification identified in proteins isolated from skeletal muscle of the exercised groups.

UniProt Accessions	Peptide Sequence	4-HNE Modifications and Site of Modification in the Peptide	No. of positive samples
Q8R429	IGIFSENEEVTDR	HNE [R13]	7
Q6P8K3	AIMAAWTFPCLPVGALMK	HNE [L/M/K]	5
P32848	AIGAFAAADSFDHK	HNE [H13]	6
I3ITR1	TKGDSDEEVIQDGVR	HNE [K2]	6
A6ZI44	YASICQQNGIVPIVEPEILPDGDHDLK	HNE [L/H/K]	6

Table 20: Peptides with two or three sites of 4-HNE modifications identified in proteins isolated from skeletal muscle of the exercised groups.

UniProt Accessions	Peptide Sequence	4-HNE Modifications and Sites of Modification in the Peptide	No. of positive samples
Q8C9W3	CGVCGGDNTHCK	HNE+Delta:H(2) [H10; C11]; HNE-Delta:H(2)O [C1]	7
P43404	EEAERKLYSGQQTDGK	HNE [R/K/L]; HNE-Delta:H(2)O [L/R/K]	6
F8VQ72	KLLSLLTFALQSIDNSHSMVGK	HNE [K22]; HNE+Delta:H(2) [L3; L5]; 1xHNE-Delta:H(2)O [H17]	5
E9Q8I0	IEGHKEIHCSENGLWSNEKPR	HNE [R21]; HNE+Delta:H(2) [H/C/K]; HNE-Delta:H(2)O [K19]	7

Table 21: Proteins expressed in exercise group but not in control group

Uniport Accession	Description
A0A0A0MQF6	Glyceraldehyde-3-phosphate dehydrogenase OS=Mus musculus GN=Gapdh PE=1 SV=1
A0A0N4SW73	Rab11 family-interacting protein 5 OS=Mus musculus GN=Rab11fip5 PE=1 SV=1
A2A6J8	Troponin I, fast skeletal muscle (Fragment) OS=Mus musculus GN=Tnni2 PE=1 SV=1
E9PWQ3	Collagen, type VI, alpha 3 OS=Mus musculus GN=Col6a3 PE=1 SV=2
E9PZC3	Flavin reductase (NADPH) OS=Mus musculus GN=Blvrb PE=1 SV=1
E9Q8K5	Titin OS=Mus musculus GN=Ttn PE=1 SV=1
F8VQJ3	Laminin subunit gamma-1 OS=Mus musculus GN=Lamc1 PE=1 SV=1
O35887	Calumenin OS=Mus musculus GN=Calu PE=1 SV=1
O55143	Sarcoplasmic/endoplasmic reticulum calcium ATPase 2 OS=Mus musculus GN=Atp2a2 PE=1 SV=2
P35918	Vascular endothelial growth factor receptor 2 OS=Mus musculus GN=Kdr PE=1 SV=1
Q3TUF7	YEATS domain-containing protein 2 OS=Mus musculus GN=Yeats2 PE=1 SV=2
Q3UV17	Keratin, type II cytoskeletal 2 oral OS=Mus musculus GN=Krt76 PE=1 SV=1
Q4FZE8	Major urinary protein 1 OS=Mus musculus GN=Mup1 PE=1 SV=1
Q61292	Laminin subunit beta-2 OS=Mus musculus GN=Lamb2 PE=1 SV=2
Q6S9I0	Kininogen 2 OS=Mus musculus GN=Kng2 PE=1 SV=1
Q8C9W3	A disintegrin and metalloproteinase with thrombospondin motifs 2 OS=Mus musculus GN=Adamts2 PE=1 SV=2

Uniport Accession	Description
Q8CIP4	MAP/microtubule affinity-regulating kinase 4 OS=Mus musculus GN=Mark4 PE=1 SV=1
Q9CPX4	Ferritin OS=Mus musculus GN=Ftl1 PE=1 SV=1
Q9DBP5	UMP-CMP kinase OS=Mus musculus GN=Cmpk1 PE=1 SV=1
Q9QUG9	RAS guanyl-releasing protein 2 OS=Mus musculus GN=Rasgrp2 PE=1 SV=2
A0A087WQD8	TRAF3-interacting protein 1 OS=Mus musculus GN=Traf3ip1 PE=1 SV=1
A0A0G2JDE5	Immunoglobulin kappa variable 1-35 (Fragment) OS=Mus musculus GN=Igkv1-35 PE=4 SV=4
A0A0G2JDN5	Immunoglobulin kappa variable 17-127 (Fragment) OS=Mus musculus GN=Igkv17-127 PE=4 SV=4
A0A0N4SV63	Dysferlin OS=Mus musculus GN=Dysf PE=1 SV=1
A0A0R4J255	Outer dense fiber protein 4 OS=Mus musculus GN=Odf4 PE=1 SV=1
D3YU50	Myosin-binding protein C, slow-type OS=Mus musculus GN=Mybpc1 PE=1 SV=1
D3Z5G7	Carboxylic ester hydrolase OS=Mus musculus GN=Ces1b PE=1 SV=1
E9Q390	Myoferlin OS=Mus musculus GN=Myof PE=1 SV=2
E9Q5A6	Nuclear receptor subfamily 1, group H, member 5 OS=Mus musculus GN=Nr1h5 PE=3 SV=1
E9Q6E9	SUMO-interacting motifs-containing 1 OS=Mus musculus GN=Simc1 PE=1 SV=1
E9Q8V6	DENN/MADD domain-containing 4A OS=Mus musculus GN=Dennd4a PE=1 SV=1
F7D3W5	Phosphodiesterase OS=Mus musculus GN=Gm45837 PE=1 SV=1
G3X8T7	Sodium channel protein OS=Mus musculus GN=Scn4a PE=3 SV=1
G3X914	Cullin-5 OS=Mus musculus GN=Cul5 PE=1 SV=1
G5E829	Plasma membrane calcium-transporting ATPase 1 OS=Mus musculus GN=Atp2b1 PE=1 SV=1
P05213	Tubulin alpha-1B chain OS=Mus musculus GN=Tuba1b PE=1 SV=2

Uniport Accession	Description
P30412	Peptidyl-prolyl cis-trans isomerase C OS=Mus musculus GN=Ppic PE=1 SV=1
P43404	Tyrosine-protein kinase ZAP-70 OS=Mus musculus GN=Zap70 PE=1 SV=3
Q3V3R4	Integrin alpha-1 OS=Mus musculus GN=Itga1 PE=1 SV=2
Q58A65	C-Jun-amino-terminal kinase-interacting protein 4 OS=Mus musculus GN=Spag9 PE=1 SV=2
Q8C129	Leucyl-cystinyl aminopeptidase OS=Mus musculus GN=Lnpep PE=1 SV=1
Q8R1C0	Potassium voltage-gated channel subfamily C member 4 OS=Mus musculus GN=Kcnc4 PE=2 SV=1
Q8R3B1	1-phosphatidylinositol 4,5-bisphosphate phosphodiesterase delta-1 OS=Mus musculus GN=Plcd1 PE=1 SV=2
A0A0B4J1H7	Immunoglobulin kappa variable 1-135 (Fragment) OS=Mus musculus GN=Igkv1-135 PE=4 SV=1
A0A0G2JDV4	Immunoglobulin kappa variable 5-39 (Fragment) OS=Mus musculus GN=Igkv5-39 PE=1 SV=4
A0A0R4J0I9	Low density lipoprotein receptor-related protein 1 OS=Mus musculus GN=Lrp1 PE=1 SV=1
A0A140T8M2	Immunoglobulin kappa variable 12-44 (Fragment) OS=Mus musculus GN=Igkv12-44 PE=4 SV=2
A0A1L1SQG7	Ryanodine receptor 1 OS=Mus musculus GN=Ryr1 PE=1 SV=1
A0A1N9PTV1	Probable fibrosin-1 OS=Mus musculus GN=Fbrs PE=1 SV=1
A2AIM4	Tropomyosin beta chain OS=Mus musculus GN=Tpm2 PE=1 SV=1
B0QZW4	Suppressor of Ty 3 (Fragment) OS=Mus musculus GN=Supt3 PE=1 SV=1
B1ATV0	Chloride channel protein OS=Mus musculus GN=Clcn5 PE=1 SV=1
E9PXE2	Guanine nucleotide exchange factor DBS OS=Mus musculus GN=Mcf2l PE=1 SV=1
F2Z3U4	Matrilin-4 OS=Mus musculus GN=Matn4 PE=1 SV=1

Uniport Accession	Description
F6SEU4	Ras/Rap GTPase-activating protein SynGAP OS=Mus musculus GN=Syngap1 PE=1 SV=2
F6VUT6	Predicted gene 8251 OS=Mus musculus GN=Gm8251 PE=4 SV=1
F6X9I3	Peptidylprolyl isomerase (Fragment) OS=Mus musculus GN=Fkbp1a PE=1 SV=1
F8VQ72	Mitogen-activated protein kinase kinase kinase 1 OS=Mus musculus GN=Map3k1 PE=1 SV=1
G3X972	SEC24 related gene family, member C (S. cerevisiae), isoform CRA_a OS=Mus musculus GN=Sec24c PE=1 SV=1
O55023	Inositol monophosphatase 1 OS=Mus musculus GN=Impa1 PE=1 SV=1
O70481	E3 ubiquitin-protein ligase UBR1 OS=Mus musculus GN=Ubr1 PE=1 SV=2
O88986	2-amino-3-ketobutyrate coenzyme A ligase, mitochondrial OS=Mus musculus GN=Gcat PE=1 SV=2
P17710	Hexokinase-1 OS=Mus musculus GN=Hk1 PE=1 SV=3
P18527	Ig heavy chain V region 914 OS=Mus musculus PE=1 SV=1
P23611	Interferon regulatory factor 8 OS=Mus musculus GN=Irf8 PE=1 SV=1
P34960	Macrophage metalloelastase OS=Mus musculus GN=Mmp12 PE=1 SV=3
P40630	Transcription factor A, mitochondrial OS=Mus musculus GN=Tfam PE=1 SV=2
P42227	Signal transducer and activator of transcription 3 OS=Mus musculus GN=Stat3 PE=1 SV=2
P47941	Crk-like protein OS=Mus musculus GN=Crkl PE=1 SV=2
P49452	Centromere protein C OS=Mus musculus GN=Cenpc PE=1 SV=2
P50462	Cysteine and glycine-rich protein 3 OS=Mus musculus GN=Csrp3 PE=1 SV=1
P58871	182 kDa tankyrase-1-binding protein OS=Mus musculus GN=Tnks1bp1 PE=1 SV=2

Uniport Accession	Description
P70313	Nitric oxide synthase, endothelial OS=Mus musculus GN=Nos3 PE=1 SV=4
Q00519	Xanthine dehydrogenase/oxidase OS=Mus musculus GN=Xdh PE=1 SV=5
Q02384	Son of sevenless homolog 2 OS=Mus musculus GN=Sos2 PE=1 SV=2
Q6P9K8	Caskin-1 OS=Mus musculus GN=Caskin1 PE=1 SV=2
Q6PFX9	Tankyrase-1 OS=Mus musculus GN=Tnks PE=1 SV=1
Q7TMM9	Tubulin beta-2A chain OS=Mus musculus GN=Tubb2a PE=1 SV=1
Q80TY4	Suppression of tumorigenicity 18 protein OS=Mus musculus GN=St18 PE=2 SV=2
Q810B6	Rabankyrin-5 OS=Mus musculus GN=Ankfy1 PE=1 SV=2
Q8BU30	Isoleucine--tRNA ligase, cytoplasmic OS=Mus musculus GN=Iars PE=1 SV=2
Q8C0L9	Glycerophosphocholine phosphodiesterase GPCPD1 OS=Mus musculus GN=Gpcpd1 PE=1 SV=1
Q8QZS3	Folliculin OS=Mus musculus GN=Flcn PE=1 SV=1
Q8R554	OTU domain-containing protein 7A OS=Mus musculus GN=Otud7a PE=1 SV=1
Q9ESQ8	Pro-FMRFamide-related neuropeptide VF OS=Mus musculus GN=Npvf PE=2 SV=1
Q9JJU8	SH3 domain-binding glutamic acid-rich-like protein OS=Mus musculus GN=Sh3bgrl PE=1 SV=1
Q9WVL3	Solute carrier family 12 member 7 OS=Mus musculus GN=Slc12a7 PE=1 SV=1